UNIVERSITÉ DE GRENOBLE

THÈSE

Pour obtenir le grade de

DOCTEUR DE L'UNIVERSITÉ DE GRENOBLE

Spécialite: **Ingénierie-Matériaux Mécanique Énergétique Environnement Procédés Production (510)**

Arrêté ministériel: 7/8/2006

Présentée par

Hana Santruckova – Smrzova

Thèse dirigée par **Pierre FORAY** et
coencadrée par **Philippe GOTTELAND** et
Stéphane GRANGE

préparée au sein du **Laboratoire 3S-R**
dans **l'École Doctorale IMEP2**

Inertial loading of soil reinforced by rigid inclusions associated to a flexible upper layer

Thèse soutenue publiquement le **18.06.2012**,
devant le jury composé de:

Mme. Farimah MASROURI
Professeur à l'Université de Lorraine, Présidente
M. Daniel LEVACHER
Professeur à l'Université de Caen, Rapporteur
M. Luc THOREL
Directeur de recherche à l'IFSTTAR Nantes, Rapporteur
M. Pierre FORAY
Professeur émérite à Grenoble INP, Directeur de thèse, Membre
M. Stéphane GRANGE
Maître de Conférence à l'UJF, Coencadrant de thèse, Membre
M. Jimmy WEHR
Directeur technique de Keller Holding, Membre
M. Philippe GOTTELAND
Maître de Conférence à l'UJF, Direction FNTP, Coencadrant de thèse, Membre

Acknowledgements

The presented work was carried out in the 3SR Lab under a financing divided between *CNRS* and *Keller, Fondations Spéciales* to whom I would like to thank for their financial support.

My greatest gratitude goes to my supervisor Pierre Foray without whose advice and guidance the work presented in this dissertation would not have been possible. Despite the difficult periods that life brings, he was always very encouraging and very supportive. I would also like to express my gratitude to my co-supervisor Stéphane Grange for his scientific knowledge, inspiring ideas, and enthusiasm. There are words of acknowledgement for my co-supervisor Philippe Gotteland, who offered me a great deal of support throughout my thesis.
I would also like to thank Etienne Flavigny for his support that he offered me, especially in the experimental tasks. His enthusiasm for geotechnics is a great inspiration for me.

I would also like to extend my thanks to the members of the technical department, especially Jean-Benoît Toni, without who's technical support the project could not have been accomplished.

Finally, I would like to thank my family and friends for the support they gave me during my studies. They made this 'Grenoble period' of my life a very pleasant time that I'll always remember.

Résumé

Le renforcement des sols en zone sismique par des colonnes ballastées et/ou des inclusions rigides représente une alternative prometteuse et de plus en plus répandue par rapport aux solutions lourdes de fondations sur pieux. On sait que les pieux subissent, du fait de leur rigidité, des moments très importants au niveau de la liaison chevêtre-pieu. Les inclusions rigides surmontées d'un matelas granulaire permettent de mieux dissiper les efforts inertiels transmis par la superstructure, mais peuvent nécessiter des armatures si ce matelas n'est pas suffisamment épais. On peut penser que la colonne à module mixte (CMM) offre une solution combinant l'effet « matelas » à travers sa partie supérieure en colonne ballastée plus flexible et l'effet stabilisateur de la colonne inférieure. Cette thèse présente dans une première partie l'étude expérimentale réalisée au Laboratoire 3S-R (Grenoble) sur des modèles réduits à l'échelle 1/10 afin d'analyser la réponse de ces systèmes sous différentes charges statiques et dynamiques. Le modèle physique se compose d'une semelle carrée reposant directement sur l'argile renforcée. Le chargement vertical et horizontal, statique et dynamique est appliqué par l'intermédiaire de la fondation. Une instrumentation a été placée au niveau de la semelle pour obtenir la réponse globale du système, ainsi que dans la partie rigide inférieure du modèle pour évaluer la répartition des efforts entre inclusion et partie flexible supérieure. Une attention toute particulière a été donnée à la simulation de l'effet inertiel d'un séisme. Les profils de moments, d'efforts tranchants et de déplacements en fonction de la profondeur déterminés à partir de 20 extensomètres répartis régulièrement sur toute la hauteur de la partie rigide ont permis d'étudier l'influence de la hauteur de la colonne ou du matelas. La comparaison entre les déplacements dynamiques de la semelle et les courbes P-y (pression latérale P fonction du déplacement latéral y de la tête de pieu), permet de quantifier la dissipation de l'énergie dans les différentes parties du système. Les résultats expérimentaux montrent que la partie supérieure souple absorbe l'essentiel de l'énergie inertielle sismique. Une modélisation numérique 3D confirme les tendances observées expérimentalement et souligne l'importance du rôle de la zone de transition entre partie souple et partie rigide.

Mots clés : Modélisation physique, Fondation superficelle, Chargements transverses dynamiques, Inclusions Rigides, Colonnes à Module Mixte, CMM, Interaction sol-structure, Dissipation d'énergie, Effet inertiel.

Abstract

Along with the increasing need of construction land, numerous soil reinforcement technologies are proposed in order to improve the soil mechanical properties on one hand and overall site response on the other hand. The presented study is carried out in the context of seismic soil reinforcement and its interaction with a shallow footing which undergoes inertial loading. The system is studied mainly through physical modelling when reduced scale models are constructed in order to simulate clay reinforcement, which is composed of a rigid lower part associated to a flexible upper part. The soft upper part offers shear and moment capacity and the rigid lower part gives bearing capacity. In order to design the reinforcement elements, the response of this combined system to different static and dynamic loads must be understood. This thesis presents results from a primarily experimental study performed in Laboratoire 3S-R (Grenoble).

Two reduced (1/10) physical models consisting of a group of four rigid inclusions associated to an upper flexible part are studied in clay. Combined vertical and horizontal static and dynamic loading is applied with a shallow foundation model. A parametric study is done, varying the height of the flexible part of the models in order to define its effect on the settlements of the foundation and lateral performance of the rigid inclusion. A special emphasis was given to the study of the inertial effects of seismic type loading. For this purpose, one of the rigid inclusions was instrumented with 20 levels strain gauges measuring flexural strain, used to calculate the bending moment along the pile. This gives pile deflection (y) by double integration and soil reaction (P) by double derivation. P-y curves are thus obtained. The analysis of the dynamic deflection of the rigid inclusion compared to the movement of the foundation allowed an estimation of the energy dissipated. The results indicate that a large amount of the seismic energy is dissipated within the upper flexible part of the models.

Even though the scaling laws are not strictly respected, the main objective of the physical modelling was to perform a qualitative study of the soil reinforcement, studying its behaviour under inertial loading and pointing out important mechanisms, which should be taken into account by the current practice.

Key words : Soil Reinforcement, Physical Modelling, Lateral Pile Response, Energy dissipation, Shallow foundation, Clay, Soil-Structure Interaction, Numerical modelling, Rigid Inclusions, Mixed Module Columns.

Glossary of symbols

B	Foundation width [m]
E	Young's modulus [Pa]
F	Soil inertia force [N]
G	Shear modulus [Pa]
H	Horizontal load [N]
I	Area moment of inertia [l^4]
M	Bending moment [N.m]
N	Normal force [N]
P	Soil reaction per unit length [$\frac{kN}{m}$]
T	Shear force [N]
V	Vertical load [N]
d	Pile diameter [m]
e	Void Ratio
g	Acceleration field [$\frac{m}{s^2}$]
k	Coefficient of subgrade reaction [$\frac{kN}{m^3}$]
p	Lateral soil reaction [kPa]
t	Time [s]
y	Pile Deflection [m]
z	Depth [m]
Es	Subgrade reaction modulus [kPa]
E_m	Pressuremeter modulus
Cc	Compresion index
Cs	Swell index
Nc	Bearing capacity factor
d_0	Pile reference Diameter [m]
cu	Undrained shear strength (Cohesion) [^{o}]
kh	Coefficient of lateral subgrade reaction [$\frac{kN}{m^3}$]
ks_1	Coefficient of vertical subgrade reaction [$\frac{kN}{m^3}$]
pc	Preconsolidation pressure [kPa]
t_h	Footing-soil friction coefficient
vs	Shear wave velocity [$\frac{m}{s}$]

λ	Slope of normal compression line
ϕ	Friction angle [^{o}]
ν	Poissons coefficient
σ	Stress tensor
ϵ	Strain tensor
κ	Slope of izotropic unload-reload line
ρ	Mass density [$\frac{kg}{m^3}$]
ω	Water content
Θ	Rotation

Energy Balance:	
ξ	Damping ratio
Wd	Dissipated energy [N.m]
Ws	Accumulated energy [N.m]
ω	Angular Frequency
k	Stiffness [N.m]
k_s	Stiffness of the flexible part of the physical models [N.m]
k_eq	Global stiffness of the physical models [N.m]
k_r	Stiffness of the rigid part of the physical models [N.m]
k_c	Stiffness of the system due to lateral pressure of the soil surrounding the models [N.m]

Contents

List of Figures

List of Tables

CHAPTER 1

General Introduction

Along with the increasing need of construction land, numerous soil reinforcement technologies are proposed in order to improve the soil mechanical properties on one hand and overall site response on the other hand. In seismically active areas, the construction soil has to offer not only the desired bearing capacity and limited foundation settlement but has to also provide a maximum foundation stability under the earthquake loading. The earthquake dynamic loads applied to the foundation arise from inertia forces which develop in the superstructure and from passage of seismic waves inducing shear strain within the soil. These two phenomena are often referred as inertial and kinematic loading.

The presented study, primarily experimental, is carried out in the context of seismic soil reinforcement and its interaction with a shallow footing which undergoes inertial loading. The system is studied mainly through physical modelling when reduced scale models are constructed in order to simulate two types of soil reinforcement technologies:

- Mixed Module Columns (CMM)
- Rigid Inclusions (RI)

Both technologies use a soil reinforcement which is composed of two main parts - an upper flexible part and a lower rigid inclusion.

Shallow foundations on soil reinforced by Mixed Module Columns (CMM) or Rigid Inclusions (RI) in seismically active areas represent an alternative to deep foundations. The main difficulty with rigid pile foundations is that they undergo important moments and shear forces at their heads, which imply that the piles have to be made of reinforced concrete. An advantage of shallow foundations on the soil reinforced by CMM or RI is that the reinforcement is designed in such a way that it is more resistant to inertial loading applied by the superstructure. The necessity of adding a steel reinforcement into the lower rigid part depends

on a thickness of the upper flexible part and the inertial forces imposed at the foundation level.

The addressed problematic of force and moments distribution within the rigid inclusion of both types of soil reinforcement is studied in detail in the work presented. An emphasis is given to the role of the flexible part in the transmission of inertial forces to the rigid inclusions. Two types of the upper flexible parts are studied experimentally:

- Load Transfer Column (LTC)
- Load Transfer Platform (LTP)

The response of the soil reinforced by rigid inclusions associated to Load Transfer Columns (LTCs) or a Load Transfer Platform (LTP) is studied in detail and the results obtained are presented in this work.

A difficult task was addressed in the satisfactory monitoring of the response of the flexible part to the applied inertial loading of the foundation. Stress and strain distribution within the flexible part is difficult to measure directly with pressure and displacement sensors and therefore it was decided to extrapolate these values from the foundation response and the rigid inclusion lateral performance. Although this approach provided satisfactory results in terms of vertical strain, shear strain and shear force distribution, the normal stress distribution could not be obtained.

The aim of the presented work is to extend the knowledge on the reinforced soils serving as a foundation subsoil under seismic conditions, with a particular interest in the inertial loading. Due to the complexity of the subject, the problematic is usually approached through numerical modelling, where seismic conditions are frequently implemented in the commercial numerical codes. The motivation was to address the problematic from an experimental point of view and to enable a comparison between the obtained experimental results and the numerical results. The presented experimental work can serve not only as a qualitative study of the reinforced soil behaviour under inertial loading but can also provide input data and parameters to calibrate numerical models. Even more, the experimental study performed on the reduced physical models can serve as a preliminary basis for more costly experiments carried out either in a real scale or in the centrifuge.

The dynamic behaviour of the reinforced soil-foundation system is a complex study approaching topics from number of different fields. Chapter 2 introduces hence details on the soil reinforcement technologies, the problematic of shallow footings under seismic loading as well as the behaviour of a rigid inclusion under lateral static and cyclic loading. Examples of studies carried out previously on this topic are mentioned and some important results based on their observations are mentioned.

The physical models as well as the experimental device developed in order to study the introduced problematic are described in Chapter 3. Instrumenting the reinforced soil and the foundation with different sensors enabled to monitor the behaviour of the system. The data obtained from the monitoring was treated in order to allow a subsequent analysis of the results. This data treatment is described in detail in Chapter 4.

Chapter 5 presents in detail the experimental results, making conclusions on the response of the reinforced soil to inertial loading of the shallow foundation. Carrying out the experimental study in the context of seismic loading, a special emphasis is given to analysing energy dissipation and damping provided by different parts of the soil reinforcement. The obtained experimental results served not only to deepen the understanding concerning the response of the reinforced soil to inertial loading but also to calibrate a numerical model. The numerical modelling, described in Chapter 6, can subsequently serve as a basis for numerical modelling of real-scale problems.

CHAPTER 2

Literature Review

2.1 Shallow foundation under combined loading

In addition to vertical loads V due to the weight of a structure, a shallow foundation can be subjected to horizontal loads H and moments M due to seismic, wind or wave forces (Figure 2.1). Behaviour of a shallow foundation under such combined loading is the topic of the following section.

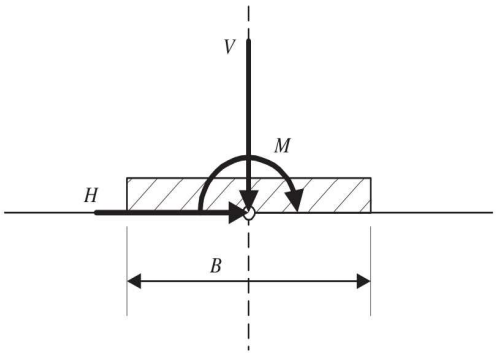

Figure 2.1: Combined loading of a shallow foundation

2.1.1 Foundation design

2.1.1.1 Bearing capacity

Bearing capacity factors that are introduced in current state of practice are a simple tool to evaluate ultimate capacity of shallow foundations undergoing horizontal and moment loading (Richards et al., 1993), (Kumar and Rao, 2002). This traditional approach is currently being replaced by the use of bearing envelopes, which define the ultimate capacity in a V-H-M space. Seismic bearing capacity of a shallow foundation is influenced by numerous factors:

- Pre-earthquake conditions of the foundation design such as initial static pressure, load eccentricity and static safety factors.

- Dynamic loads acting on the foundation, which have 6 components. Vertical force, which can be in most cases neglected since its magnitude is small enough compared to static permanent vertical laod. Two shear forces T arising from inertia forces developed in the structure and acting in orthogonal horizontal directions. Two overturning moments, also related to inertia forces, that arise from elevated position of the centre of gravity of the structure above the foundation level. These moments induce eccentricity loads acting on the foundation. Finally, a torsional moment, created if a center of mass of structure is not aligned with geometric center of the foundation, is the sixth and final component of dynamic load acting on the foundation.

- Soil strength and its dependency on rate of loading, its degradation under cyclic loading and pore pressure build-up under dynamic loading.

- Inertia forces Fx created in the soil medium, which initiate inertia forces arising from the superstructure.

An approach analysing foundation capacity, representing a current state of practice is described in the following. This approach consists of dividing a global model, including both the soil and the structure, in two separate tasks - evaluation of dynamic loads, which is in the current state of practice work of a structural engineer and evaluation of bearing capacity, which is a geotechnical engineer task. The bearing capacity can be checked using a pseudo-static approach, where a concept of bounding surface is used to find a solution to the problem. The bounding surface, defined in 2.1 (Pecker, 1997), can be evaluated once knowing the problem geometry, material strengths and 5 independent loading parameters - normal force N, shear force T, overturning moment M and two components of soil inertia force F.

$$\Phi(N, T, M, F) \leq 0 \tag{2.1}$$

Inequality in equation 2.1 expresses the fact that when the combination of parameters lies outside the surface, the problem is unstable and when the combination of parameters lies inside or on the surface, the problem is potentially stable.

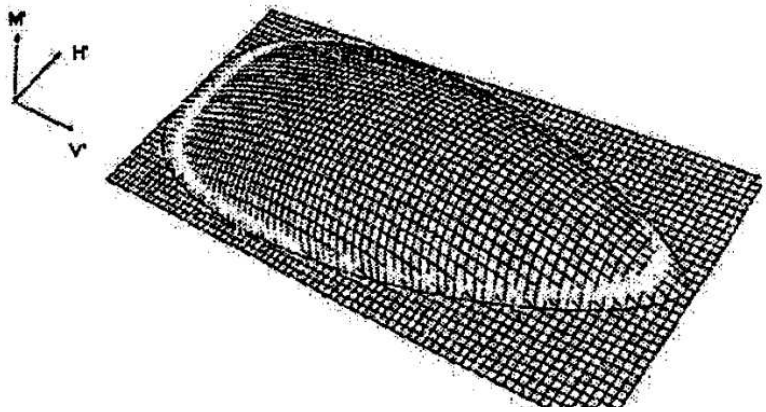

Figure 2.2: Ultimate loads surface for cohesive soils; after (Pecker, 1997)

Since the study presented in the following deals with a shallow foundation on clay, only a bounding surface for cohesive soils (Figure 2.2) is presented (Pecker, 1997):

$$\frac{[(1-eF^*)\beta T^*]^2}{(\alpha N^*)^a[1-\alpha N^*-eF^{*g}]^b}+\frac{(1-fF^*)(\gamma M^*)^2}{(\alpha N^*)^c[1-\alpha N^*-eF^{*g}]^d}-1=0 \tag{2.2}$$

where N^*, T^*, M^* and F^* are loading adimentional parameters defined as:

$$N^*=\frac{N}{cuB} \tag{2.3}$$

$$T^*=\frac{T}{cuB} \tag{2.4}$$

$$M^*=\frac{M}{cuB} \tag{2.5}$$

$$F^*=\frac{FB}{cu} \tag{2.6}$$

cu being the undrained shear strength and B the foundation width. Parameters a-g and α to γ are defined numerically. It can be noticed that when $F^*=M^*=T^*$, equation 2.2 reduces to the well known bearing capacity formula in 2D:

$$N=(\pi+2)cu.B \tag{2.7}$$

Experimental study introduced in the following deals with a shallow foundation problem where moment loading is nil. This loading combination is statically equivalent to a single load acting at a footing centre, inclined at an angle α to the vertical. A bounding surface for M=0 is shown in the following figure after (Pecker, 1997).

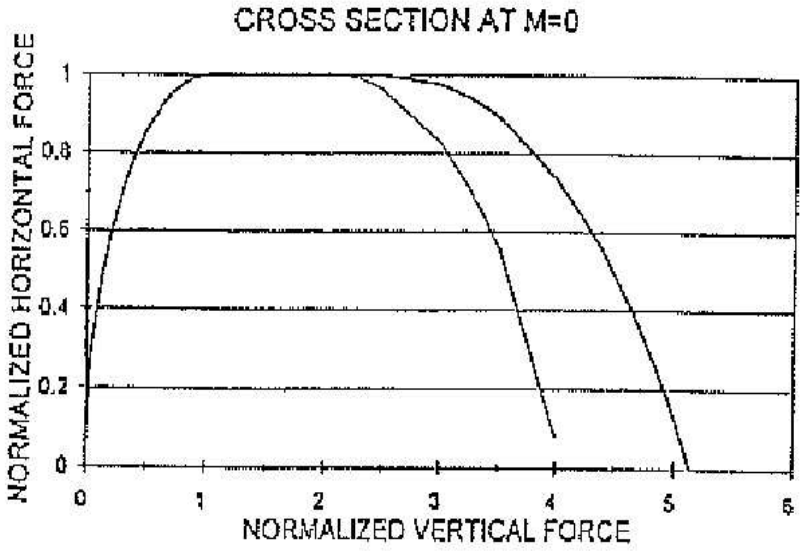

Figure 2.3: Bounding surface for M=0 (Pecker, 1997)

The presented approach evaluating the foundation bearing capacity is implemented in the current version of Eurocode 8 (Annex F) (Eurocode8, 2005).
The experimental study presented in the following was carried out respecting such loading conditions which would allow to stay inside the bounding surface.

2.2 Soil reinforcement - CMM and RI

The necessity of building on compressible soil is gradually increasing. This is due to the fact that sites suitable for construction are already exhausted within most industrial areas while the need of new constructions is still growing. This led to development of soil reinforcement methods.

2.2.1 Rigid Inclusions - RI

Soil reinforcement by rigid inclusions is an economic and time saving method of soil improvement, which improves foundation soil properties and considerably reduces settlements. A schematic picture of this technique is shown in Figure 2.4 (**?**).

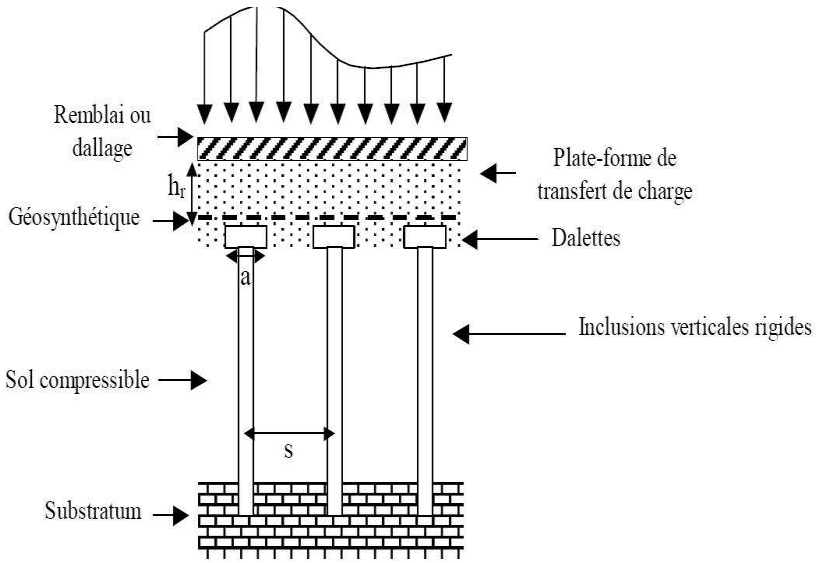

Figure 1 : Illustration du renforcement par inclusions rigides.

Figure 2.4: Soil improved by rigid inclusions, after (Briançon, 2002)

A footing is underlayed by a gravel mattress. This gravel mattress takes vertical load from the footing bottom and transfers it onto heads of rigid inclusions. Inclusions traverse through soft soil and support the vertical load either by being embedded into bedrock or by sufficient soil-inclusion friction. The RI soil reinforcement can be divided into two parts which are described in the following:

1. Gravel mattress
   Gravel mattress, lying on top of the rigid inclusions has an ability of settlement reduction and homogenisation. A well known phenomenon when gravel layer concentrates load onto more rigid underlying areas and leaves the less rigid areas with minimal stress plays an important role in the stress distribution within the reinforcement elements. The aim of concentrating load onto inclusions can be seconded by utilisation of a geotextile.

2. Rigid inclusions
   The head of rigid inclusion forms a contact with the mattress and takes over load from the superstructure. Unlike the piles, rigid inclusions do not take over all the foundation stress and leave minority of foundation load to be adopted by soil. This fact is shown in Figure 2.5 (Berthelot et al., 2003).

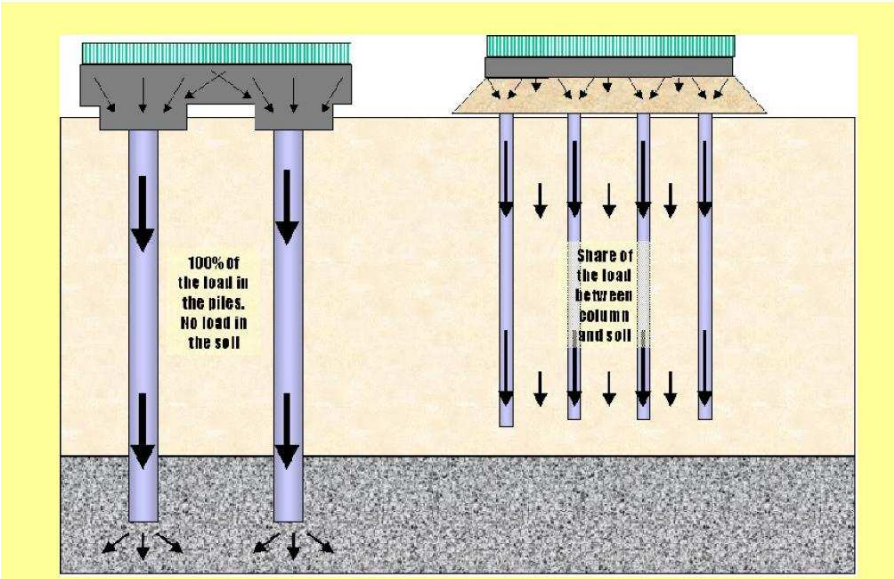

Figure 2.5: Transfer of load from a superstructure to piles or to rigid inclusions, after (Berthelot et al., 2003)

The rigid inclusions can be divided according to:

- the fabrication technology:
  - Prefabricated inclusions - these inclusions are fabricated before inserting into the ground. Inclusions are either forced or hammered into the ground.
  - In situ inclusions
- the pattern in which inclusion groups are organized:
  - Triangle pattern
  - Square pattern

Influence of mattress thickness on the efficiency of RI

Let us consider that there exists a group of rigid inclusions, which by their presence influence the behaviour of the surrounding soil. Furthermore, the area of influence of one rigid inclusion is defined as the total area of influence divided by number the rigid inclusions. Efficiency E evaluation of one rigid inclusion can be then evaluated by using the following relation (Hewlett and Randolph, 1988):

$$E = \frac{Q_p}{Q} \tag{2.8}$$

where Q_p is the vertical load overtaken by the rigid inclusion itself and Q is the vertical load applied to the area of influence of the inclusion.

An observation was made, based on previous experimental studies in a centrifuge (Baudouin et al., 2010), that for a small height of gravel mattress, plastification occurring within the

mattress causes a decrease in efficiency E. For more important heights form 0.6m to 1.5m the efficiency values climbed up to 50%, meaning that half of the load applied was overtaken by the rigid inclusions.

Influence of spacing between inclusions on their efficiency

Defining a ratio α between a cross-section of a rigid inclusion Ap and an area influenced by that inclusion A:

$$\alpha = \frac{Ap}{A} \tag{2.9}$$

It was shown (Baudouin et al., 2010) that the efficiency E (defined in the previous paragraph) is higher for bigger α, even though this is valid only for cases when inclusions are combined with higher mattress. Efficiency of rigid inclusions with lower mattress don't seem to be influenced by the α ratio.

RI in seismic conditions

Soil reinforcement by rigid inclusions presents an interesting alternative to other soil improvement technologies, because its installation process is very fast, keeping the settlement reduction efficient. The research frequently addresses the problematic of the vertical stress distribution between the rigid inclusions and the effect of the mattress height on the efficiency of the reinforcement. There is although a lack of research carried out on the behaviour of the rigid inclusions under combined vertical and horizontal loading, studying the system response under seismic loading conditions. Despite this, the soil reinforcement by rigid inclusions used in combination with a shallow foundation is often considered to be an alternative for pile foundations in seismic areas. It is considered, that the gravel mattress presents a zone of dissipation of energy transmitted from the superstructure to the rigid inclusions. This implies that there is a reduction of inertial forces transferred to the heads of the rigid inclusions. An example of such an application of the RI technology is the Rion-Antirion bridge located between the Peloponese and the continent, at the entry of the Gulf of Corinth in Western Greece.
The design of the Rion-Antirion bridge was based on an experimental study carried out in the centrifuge at the LCPC Nantes Laboratory (Garnier and Pecker, 1999). The bridge needed to withstand earthquakes up to a magnitude 7 on Richter scale and strong winds and therefore a special care was taken while designing its foundations. Each of the pylons of the bridge is supported by a caisson, which lies on a seafloor reinforced by 150 to 200 rigid inclusions. The rigid inclusions are hollow steel piles of 25 to 30m length and 2m in diameter. A 3.6m layer of ballast was introduced between the foundation and the top of the rigid inclusions. The seafloor reinforcement served to control the foundation failure mode as well as the forces transmitted to the superstructure.
Physical modelling in a reduced scale was conducted on the centrifuge at the LCPC Nantes Laboratory. The physical model consisted of a consolidated clay mass reinforced by rigid inclusions which were supporting a ballast layer. Some of the rigid inclusions were instrumented with strain gauges in order to monitor their behaviour. A circular foundation was submitted to different loading conditions with loads of increasing magnitude reaching a foundation system failure. The soil used for the experimental study was a clay deposit obtained at the

site. Results obtained from the experimental study enabled not only to verify the effective resistance of the foundation-reinforced soil system to different loading conditions but also to optimize the number and position of the reinforced inclusions.

The problematic of soil reinforced by rigid inclusions in seismic conditions was addressed in a numerical study performed by Mayoral et al. (Mayoral et al., 2006). It was shown that the RI soil reinforcement enables an acceleration reduction at the surface by 17%, where most of this reduction is due to the presence of the gravel mattress and only 1% is due to the presence of the rigid inclusion. This phenomenon is shown in Figure 2.6

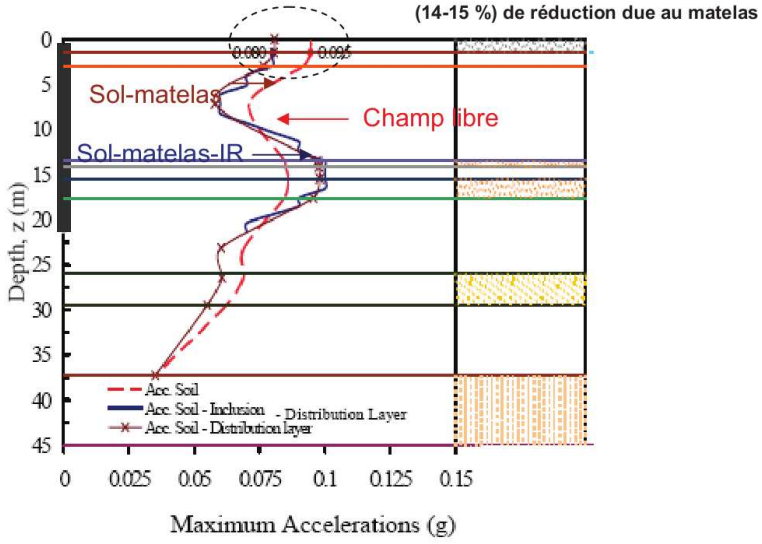

Figure 2.6: A comparison between a seismic response of non-reinforced soil and soil reinforced by a RI (Hatem, 2009), after (Mayoral et al., 2006)

A.S.I.RI. Project

The A.S.I.RI. Project, concerning the soil reinforcement by rigid inclusions is a French National project assembling the studies carried out on this subject. A special interest is given to development and validation of the design methods. The RI soil reinforcement problematic is addressed by the means of experimental studies in a real and a reduced scale (Jenck et al., 2007), (Baudouin et al., 2010), (Briançon, 2002) as well as by the means of numerical modelling (Chevalier et al., 2010).

2.2.2 Mixed Module Columns - CMM

The Mixed Module Column (CMM) technology is developed within *Keller, Fondations Spéciales*. It is an alternative solution for the widely used soil reinforcement techniques, such as

stone columns and rigid inclusions. By combining features of these two techniques, it seems to present an interest for foundation projects in seismic areas. A CMM is composed of three parts (Figure 2.7):

1. Upper part - stone column.
2. Lower part - rigid inclusion. made of concrete; absence of steel reinforcement.
3. Transition zone between the upper and the lower part consisting of a mixture of concrete and gravel.

The upper part of CMM represents a flexible link between the foundation and the rigid, lower part. Its height and diameter is in order of 1.5m and 30 to 50cm, respectively, varying according to the site conditions. Gravel used for its construction is either a crushed gravel or river run gravel with a controlled granulometry. The lower part of CMM is a rigid inclusion made of concrete, without any steel reinforcement. Link between the lower and the upper part consists of concrete mixed with gravel.

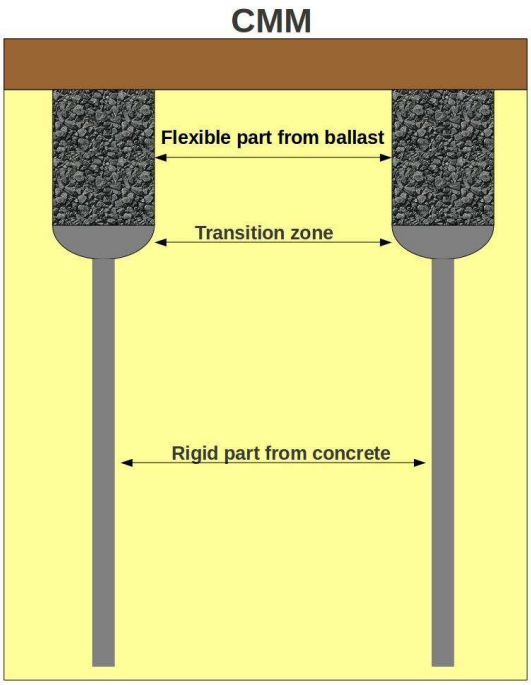

Figure 2.7: Mixed Module Columns (CMM) composed of three parts - stone column, transition zone and a rigid inclusion, technology developed by Keller, Fondations Spéciales (Keller, 2006)

CMM reinforcement influences the surrounding soil in following ways:

- Settlement reduction
- Takes over horizontal loads and moments without the need of installing a gravel mattress.
- Increase of bearing capacity.

2.2.2.1 CMM installation

The installation of CMM in the soil is described in four stages, which are graphically described in Figure 2.8. (Keller, 2006). A spiral of a continuous flight auger is supported by a hollow stem. An auger is rotated into the soil in a continuous operation until the design depth of the pile is reached. Concrete mortar is then pumped through the hollow stem under pressure which extrudes the auger and soil column from the boring. Concrete is therefore placed under high pressure, creating a concrete-soil interface. A cylindrical vibrating probe is then introduced into the hole, which is backfilled with gravel or crushed rock densified by the vibratory probe as it is withdrawn from the ground.

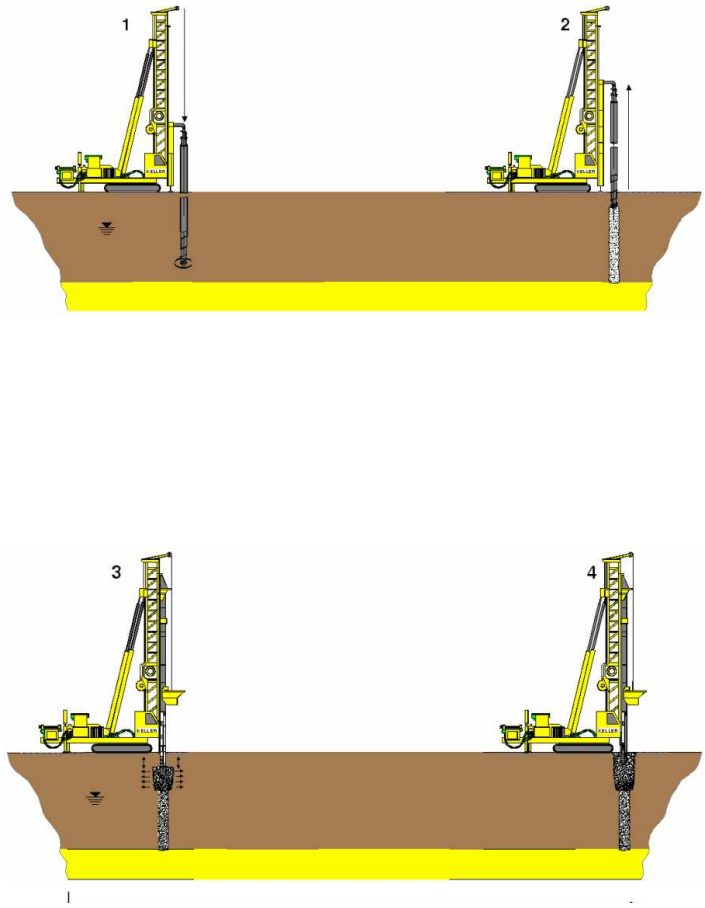

Figure 2.8: CMM installation

2.2.2.2 CMM design

Following the design instructions provided by *Keller, Fondations Spéciales*, total load qT applied by a foundation to the reinforced soil is distributed between the soil q_s and the CMMs q_{CMM} as shown in Figure 2.9b). Rigid part of the CMM follows the rigid inclusion design rules (*Combarieu method*) and effect of horizontal loads or moments applied to the inclusion can be neglected (Keller, 2006). Since the *Combarieu* method is designed for rigid inclusions, modifications have to be made in order to apply it to CMM soil reinforcement. Layer composed of stone columns and clay is homogenized and one set of material characteristics is obtained for the entire layer.

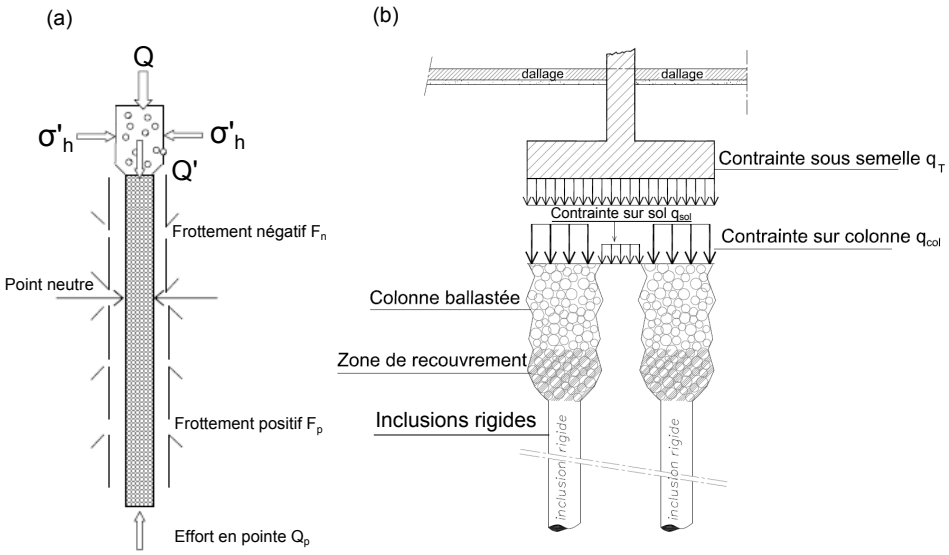

Figure 2.9: (a) Interaction between the soil and the rigid inclusion - skin friction; (b) Distribution of the total load qT applied by a foundation between the soil q_s and the CMMs q_{CMM}

The upper part of CMMs and the surrounding soil can be then treated as a gravel mattress. Settlement and load distribution within the stone column is determined using *Pribe* method (Keller, 2006). Shallow foundation characteristics are then obtained by considering results of both methods in the final evaluation. Vertical load tansfer to a CMM and its distribution is controlled by number of mechanisms:

- Load distribution between soil and CMM.
- Load transfer through a stone column.
- Interaction between the soil and rigid inclusion - skin friction 2.9a).

The design methods have to verify that :

1. **Stress applied to the stone columns and the soil does not exceed acceptable levels.**

Acceptable load for unreinforced soil q_a^s and for the stone columns Q_a^{SC} can be obtained from the following relations using the pressure-meter data:

$$q_a^s = \frac{k_p.p_{le}}{\gamma_q} \tag{2.10}$$

where
k_p: bearing capacity factor obtained according to DTU 13.2 (CSTB, 2007)
p_{le}: an average value of pressure-meter limit pressure over 1.5 times the foundation size
γ_q: partial coefficient; γ_q= 3 for serviceability limit states ; γ_q = 2 for ultimate limit states

$$Q_a^{SC} = \frac{1}{\gamma_{gR}}.\sigma_h.\frac{1+sin\phi}{1-sin\phi}.S_{CMM} \tag{2.11}$$

where:
σ_h: lateral earth pressure
ϕ: friction angle of gravel inside the stone column
S_{CMM} : cross-section of the stone column
γ_{gR}: security coefficient; γ_{gR} = 2 for serviceability limit states; γ_{gR} = 1.5 for ultimate limit states

2. **Stress applied to the rigid inclusions does not exceed acceptable levels.**
Acceptable load applied to the rigid inclusions can be calculated by the following relation:

$$Q_a^{RI} = min(\frac{R_b}{\gamma_b} + \frac{R_s}{\gamma_s}, Q_a^c) \tag{2.12}$$

where: R_b: point resistance
R_s: friction resistance calculated below the neutral point
γ_b : security coefficient on the point
γ_s : security coefficient on the friction
Once knowing acceptable load for different parts of soil reinforcement, an ultimate design load Q_a^{found} for a shallow foundation lying on the reinforced soil can be determined:

$$Q_a^{found} = n.Q_a^{CMM} + (B.L - n.S_{CMM}).q_a^s \tag{2.13}$$

where
n: number of CMMs
S_{CMM} : cross-section of the stone column
B, L : foundation dimensions
Q_a^{CMM} : acceptable load for the CMM. Its value is equal to minimum value from Q_a^{SC} and Q_a^{RI}:

$$Q_a^{CMM} = min(Q_a^{SC}, Q_a^{RI}) \tag{2.14}$$

where
Q_a^{SC}: acceptable load on upper part of CMM
Q_a^{RI}: acceptable load on lower part of CMM

3. **Settlement is acceptable for the structure concerned.**

2.2.3 Experimental and numerical study of soil reinforcement by CMM and RI previously carried out within the 3SR-Lab

Because the presented doctoral thesis is a continuation of previous works (Zhang, 2011) carried out within the 3SR Lab, a lot of attention is given to the presentation of the previous experimental and numerical results.
A 2D experimental model was designed in gravity 1g and scale 1/10 and was not strictly respecting the similarity conditions. A laterally loaded square shallow foundation was supported by very soft clay reinforced by four CMMs or four RIs associated to a granular layer (Figure 2.10). Both quasi static and dynamical horizontal cyclic loadings were applied to the foundation models in order to investigate the inertial effect on the behaviour of the ground reinforcement system. Even though the scaling laws were not strictly respected, the work served to visualize the mechanism of the ground reinforcement during a dynamic loading and to calibrate a numerical model.

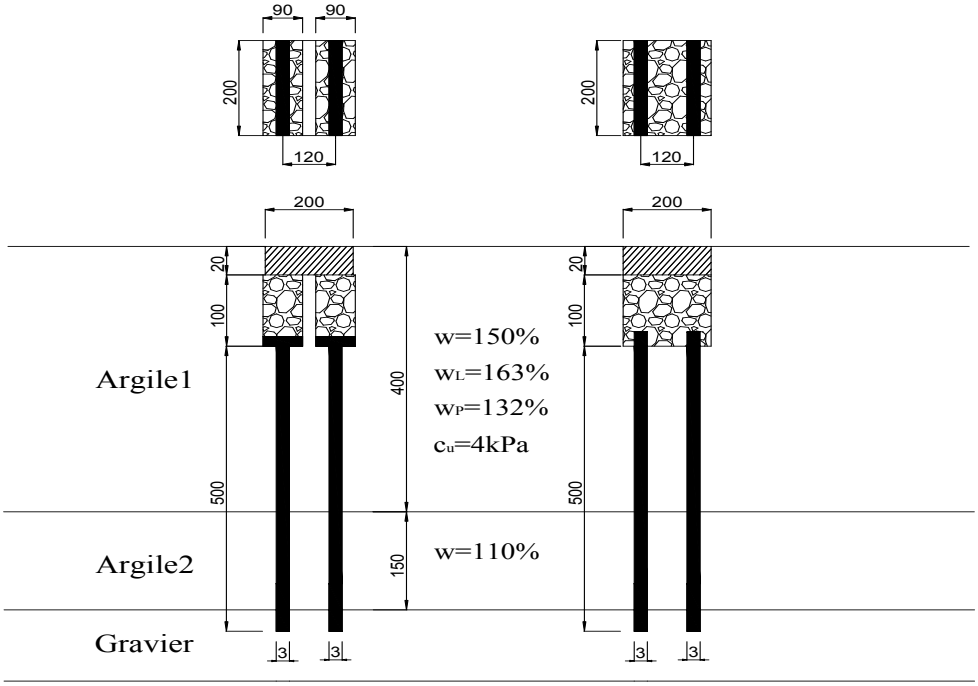

Figure 2.10: Physical models; dimensions are in mm

Experimental set-up

The experimental set-up derived from that used in a soil-pipe interaction research program (Orozco, 2009). A large rigid and impervious tank of 2m long, 1m wide and 1m deep, allowing a lateral visualization of the mechanisms (Figure 2.11), was filled with saturated soft clay underlain by a granular rigid stratum. The physical model was placed on the side near the window to visualize the deformation mechanisms during the experiment. A second identical model was built on the other side in order to allow the system to work symmetrically. The foundation model was fixed to a horizontally sliding trolley above the tank. This guidance system where the trolley could slide along two rails enabled controlled horizontal loading of the foundation model. A constant vertical load was applied by putting weights on the foundation model. The system permitted the foundation to freely settle down under the vertical

Figure 2.11: Photo of the experimental device

loading.
Horizontal and vertical forces were monitored by two load cells fixed to the loading system. Horizontal displacement of the foundation model, being the same as the horizontal displacement of the trolley, was controlled by a large displacement sensor in the quasi-static tests and a LVDT in the dynamical tests. The vertical displacement was measured by a vertical LVDT fixed on the foundation model.

The physical models

The reduced physical models consisted of a square footing made from aluminium with a width of 20cm and a thickness of 2cm, lying on the soft clay reinforced by the CMM or the RI. The reconstituted clay was prepared in the 3SR Lab by mixing two types of powder clay, Kaolin and Bentonite with water addition. The undrained shear resistance was about cu=4kPa and the liquid limit and the plastic limit were respectively wL=163% and wP=132%.
The foundation model was embedded into the surrounding clay. CMMs were modelled by two stone columns with a rectangular section (20cm by 9cm) for the upper part and two pieces of aluminium plates with a rectangular section (20cm by 0.3cm) for the lower part (rigid inclusions). The lengths of the upper and the lower part were respectively 10cm and 50cm, and the lower part was embedded into the granular layer. The axial distance between the two CMM models was 12cm. Between the upper part and the lower part, the transition zone was modelled with two plates in PVC with the same rectangular section as the stone columns. These transition zones provided a horizontal support to the gravel columns and simulated the transition zones in the real CMMs. Heads of the rigid inclusions were embedded into these PVC plates to simulate a real connection between the two parts. Geotextile socks served to avoid penetration of gravel of the stone columns into surrounding soil. In the RI model, almost the same configuration was reproduced except for replacing two stone columns with PVC plates by a granular layer1. Set-up and dimensions of the physical models are illustrated in Figure 2.10.

Loading application

Once completing the physical models and the clay installation, the foundation model was put in contact with the reinforced soil. The vertical force was applied by a total weight of about 500N. Forty cycles of horizontal cyclic loading were then applied with a constant displacement amplitude of 5mm. The frequency was 0.05Hz in the quasi-static tests and 1.2Hz in the dynamic tests (Zhang et al., 2011).

Experimental result analysis

During the quasi-static tests, the upper gravel parts of the CMM move horizontally with a displacement gradually decreasing with depth. At the same time, these gravel parts were expanding laterally, especially in their upper part, inducing a significant settlement of the foundation. Lateral movements were only observed in the upper parts of the CMM. The PVC plates and the heads of the aluminium plates were not found to move. Apparently, the transmission of the horizontal load is strongly reduced over the height of the upper gravel part and the lower rigid part of the CMM seems to undergo only vertical loads during the horizontal cyclic loading. A similar behaviour was observed in the model combining rigid inclusions and a thick gravel mattress.
During the dynamic tests, the amplitude of the horizontal movement of the two models was higher. Importantly, a horizontal displacement of the heads of the rigid inclusions (aluminium plates) could clearly be observed in both models. Therefore it is noted that a more important part of the horizontal load is transmitted to the rigid inclusions due to the inertial effects. The settlements of the foundation measured during the experiments are presented in Figure 2.12. The strong values of the settlements can be related to a plastification of the system occurring rapidly in this soft clay with a very weak undrained shear resistance of 4 kPa. The accumulation of the settlement was more significant for the first cycles, while it tends to stabilize later. For both models CMM and RI, the settlements in the quasi-static test were lower than those in the dynamic test. This difference is particularly strong for the RI model, but this fact may be due to a progressive local punching of the mattress above the head of the inclusion due to a weak compaction.

Numerical modelling of soil reinforced by CMM and RI in the reduced scale

The numerical modelling of the experimental study was carried out using a computer program FLAC3D (Fast Lagrangian Analysis of Continua in 3 Dimensions; (FLAC3D, 2006)). It is a three-dimensional explicit finite difference program for engineering mechanics computation designed by Itasca Consulting Group Inc. It simulates the behaviour of three dimensional structures built of soil, rock or other materials that undergo plastic flow when their yield limits are reached. The dynamic analysis option permits to resolve the full equations of motion, using the fully nonlinear method embodied in FLAC3D, rather than the 'equivalent-linear' method which is commonly used in earthquake engineering for modelling wave transmission in layered sites and dynamic soil-structure interaction. The fully nonlinear method follows any prescribed nonlinear constitutive relation, and irreversible displacements and other permanent changes are modelled automatically.
The numerical models were designed according to the geometry, proportions and mechanical characteristics of the physical models (Zhang, 2011). Despite this, it is noted that the tran-

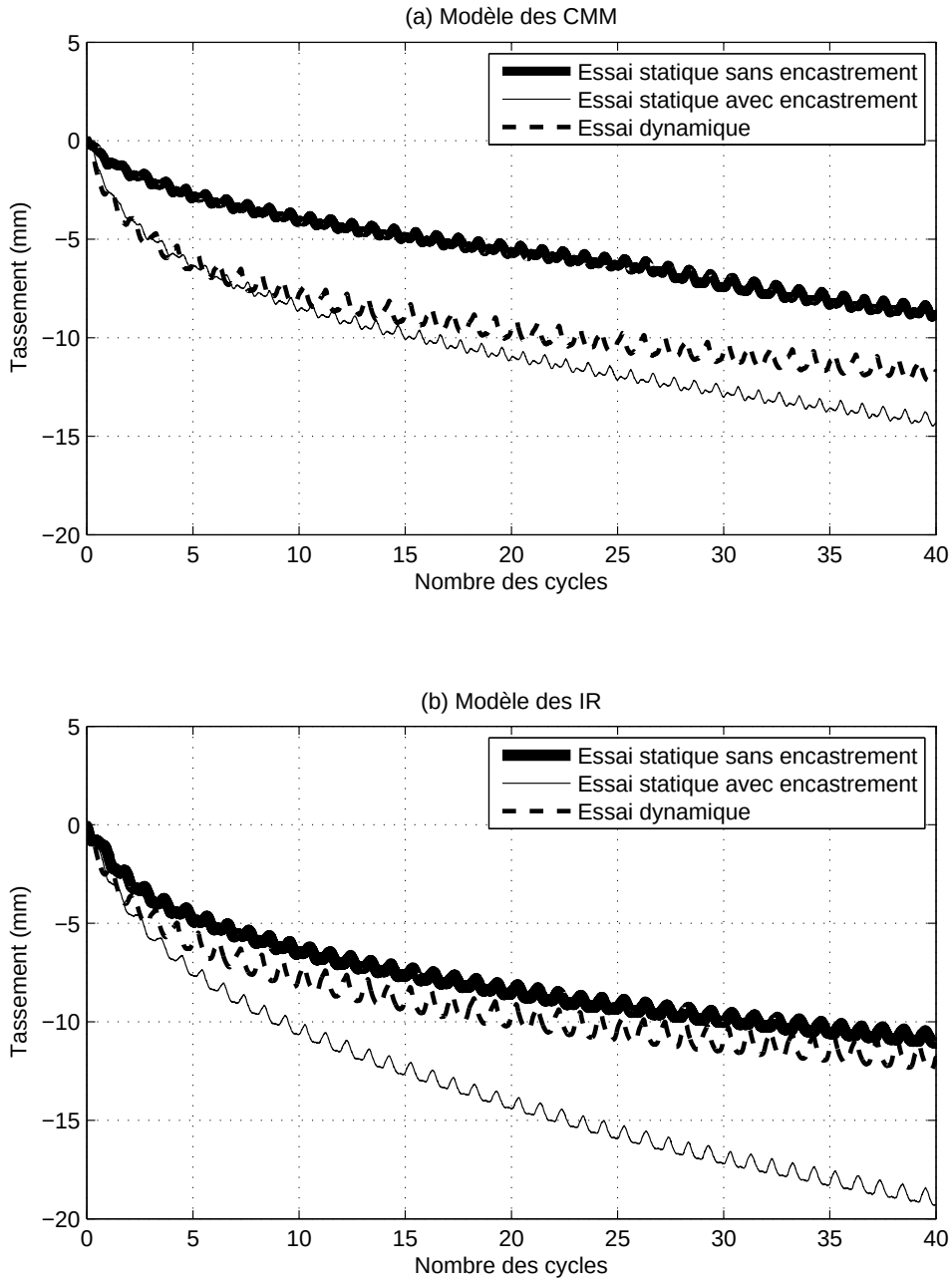

Figure 2.12: Foundation settlement with cyclic loading a) CMM, b) RI

sition zone made of PVC plates and the geotextile socks, both figuring in the experimental study, were neglected in the numerical simulations. Mohr-Coulomb constitutive laws were used for clay and gravel material with input parameters summarized in table 2.1. Rigid parts of the CMM and RI were represented by pile 'structural elements', a pre-defined possibility included in FLAC3D.

Table 2.1: Input parameters for clay and gravel materials

Material	Young's modulus E	Poissons coefficient ν	Friction angle ϕ	Cohesion c
Clay	1 MPa	0.45	0	2.1kPa
Gravel	60 MPa	0.3	38	0.3kPa

Being interested in the behaviour of the rigid inclusion acting within the CMM and RI systems, deflection, bending moment, normal and shear force were studied along the piles during the dynamic loading. Figure 2.13 shows the envelopes of the deflection and the internal forces, distinguishing cases when the foundation model was embedded or not. It was found that the deflection values and the values of internal forces are higher for piles acting within the RI system. This would suggest that the stone columns are able to absorb more of the forces applied to the foundation model.

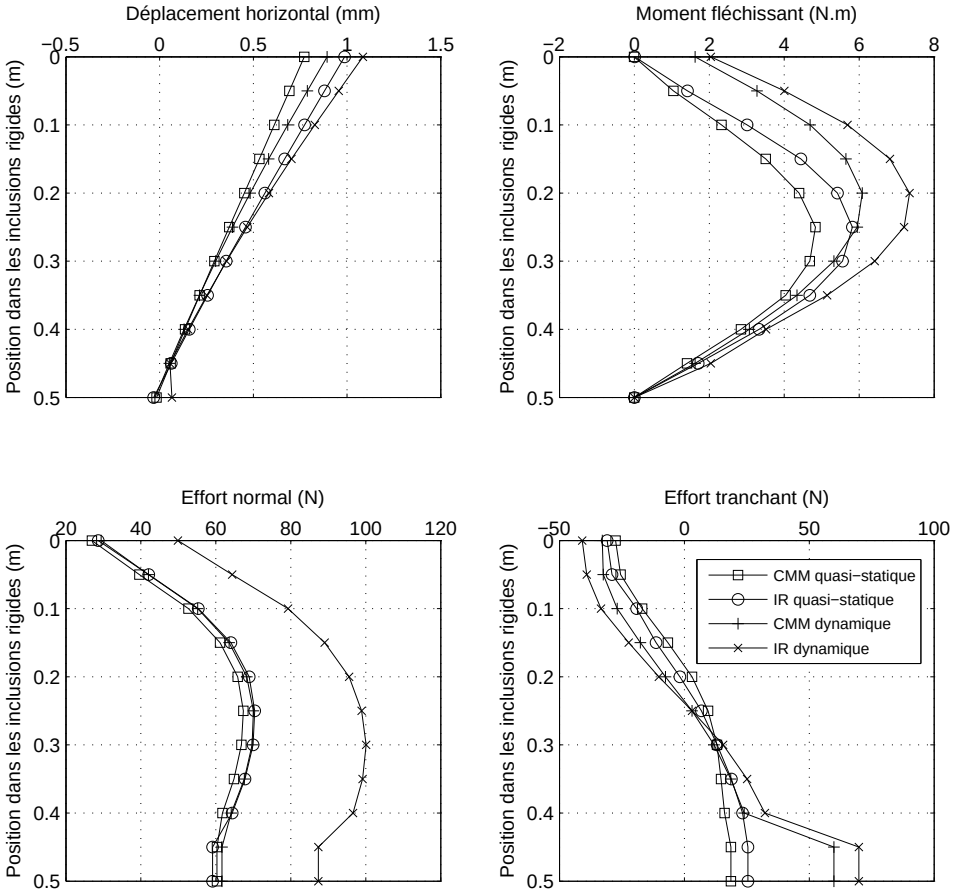

Figure 2.13: Deflection, bending moment, normal force and shear force along the pile

Numerical modelling of soil reinforced by CMM and RI in the real scale

The studied foundation system consisted of a square footing 2m wide and 0.5m thick. It was totally embedded in the soil. Four (2 x 2) CMMs or four rigid inclusions associated to a granular layer were placed in the soil under the footing. The upper part of the CMM was a stone column with 0.9m diameter and a varying length (0.3m, 1.0m and 1.5m). The lower part of the CMM was a rigid inclusion made of plain concrete with 0.34m diameter, with a length of 5m. Between the upper and the lower part of the CMM was an area called a 'transition zone' which had the same diameter as the stone column and a length of 0.5m. The RI was modelled in the same way and the CMM, but the stone columns were replaced by a gravel mattress having the same width as the foundation. There was considered no 'transition' zone. The length of the upper part of the CMMs and RIs was varied in order to examine its influence on the behaviour of the rigid inclusions in the lower part. Two soil layers were taken into account in the numerical modelling. A soft clay layer and a more resistant gravel layer to obtain the embedding of the rigid inclusions. The rigid inclusions were modelled by three-dimensional pile elements and each rigid inclusion was discretized in ten pile elements. In the case of CMM, the heads of the rigid inclusions were linked rigidly to the 'transition zones' in the three displacement directions (no relative displacement between the grid and the node) and free in the three rotational directions. To form the embedding of rigid inclusions in gravel layer, the links between the pile element nodes and the gravel layer were set rigid in all the degrees of freedom. The behaviour of stone columns, soft clay and gravel layer was described by an elastoplastic constitutive model based on the non-associated Mohr-Coulomb criterion. The input parameters are summarized in table 2.2.

Table 2.2: Input parameters

Material	Young's modulus E	Poissons coefficient ν	Friction angle ϕ	Cohesion c
	c			
Gravel columns or mattress	$60MPa$	$0,3$	38	0
Bottom gravel layer	$100MPa$	$0,3$	45	0
Clay mass	$6MPa$	$0,3$	0	$20kPa$
Transition zone	$600MPa$	$0,3$		
Foundation	$10GPa$	$0,2$		
Rigid inclusions	$5,3GPa$	$0,2$		

As horizontal cyclic loading was imposed to the foundation, the pile lateral response to this loading was registered. Figure 2.14 shows the pile lateral deflection for the case when the pile is within a CMM or a RI system. The pile deflection seems to increase with the decreasing height of the stone columm or mattress. It can be seen that the pile within the RI reinforcement system is more affected by the foundation loading.

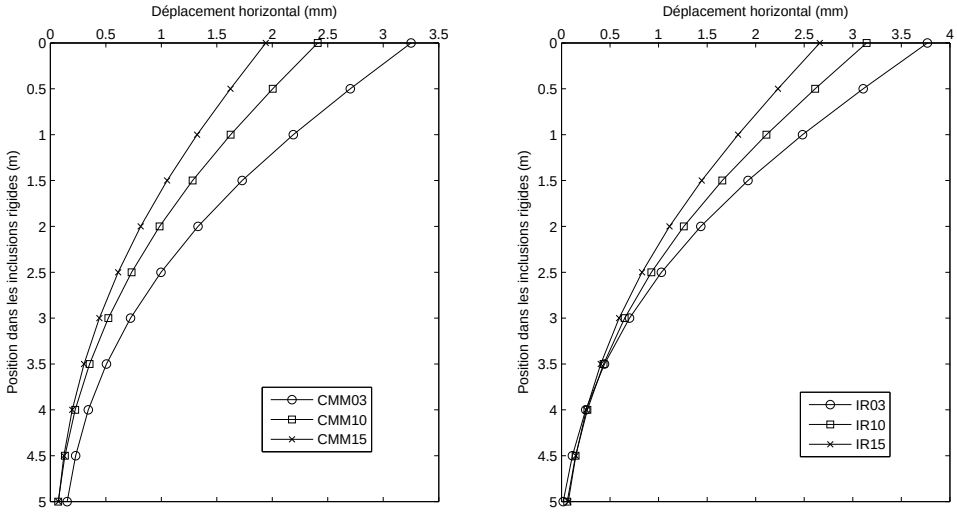

Figure 2.14: Deflection along the pile within a CMM or RI technology

2.3 Pile under static lateral loading

2.3.1 Pile design

Piles making part of a foundation can be loaded by lateral forces caused by earthquake, wind forces or wave forces. Designing the pile foundations to resist such lateral loads, the pile design criteria are based either on *ultimate lateral resistance*, but in most cases on *allowed lateral deflection*. The allowed lateral deflection of piles within a foundation depends on the structure type and the structure design - bridges or tall structures do not tolerate large deflections of pile foundations, on the contrary temporary structures or retaining walls can be designed with relatively large pile deflections allowed. The load-deflection relationship is linear at loads less than one third to one half of the ultimate lateral resistance of the pile. After exceeding such load level, the load-deflection relationship becomes nonlinear. When pile deflection at the ground surface becomes approximately 20 % of the pile diameter, the maximum lateral resistance is reached (Broms, 1964).

2.3.1.1 Ultimate lateral resistance

A conventional static approach is based on determining a horizontal force H_u and bending moment M_u at the pile head which mobilize the ultimate soil resistance p_u along the pile. This approach assumes the pile to be floating and sufficiently rigid that the failure of soil will occur before the pile failure. Considering equilibrium of horizontal forces and moments and solving the resulting equations, a general solution for a failure load H_u and moment M_u combination is obtained (Figure 2.15).

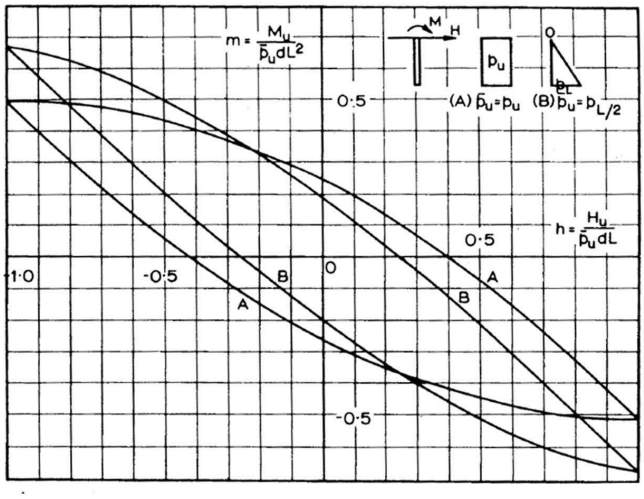

Figure 2.15: Ultimate lateral resistance of unrestrained rigid piles, (Poulos and Davis, 1980)

where envelope (A) is valid for a case of a uniform distribution of soil resistance with depth along the pile. Envelope (B) can be applied for a case of linear variation of soil resistance with depth, from p_0 at the ground surface to p_L at the pile tip.

A theory developed by (Broms, 1965) is based on the conventional static approach and deals in detail with piles in purely cohesive soil and piles in purely frictional soil. Because the work presented concerns a group of piles surrounded by clay, only ultimate soil resistance for piles in purely cohesive soil will be addressed.

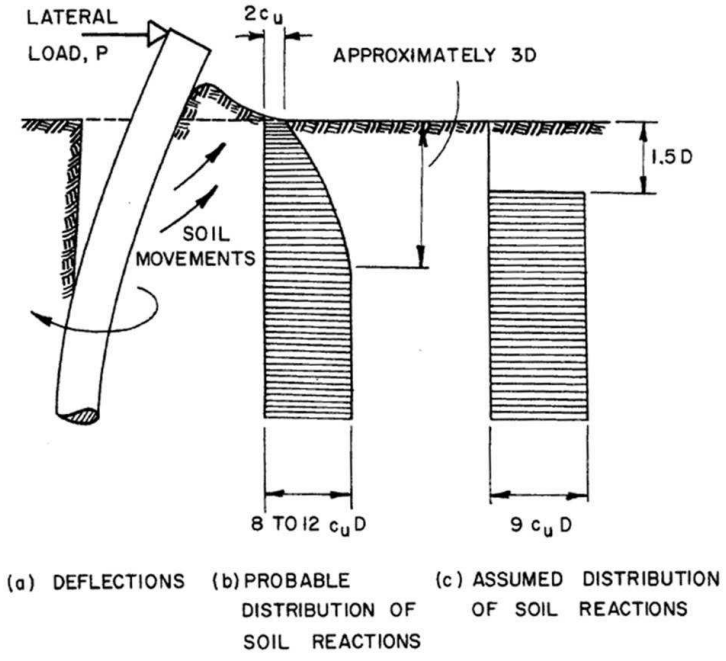

Figure 2.16: Distribution of lateral earth pressure (Broms, 1964)

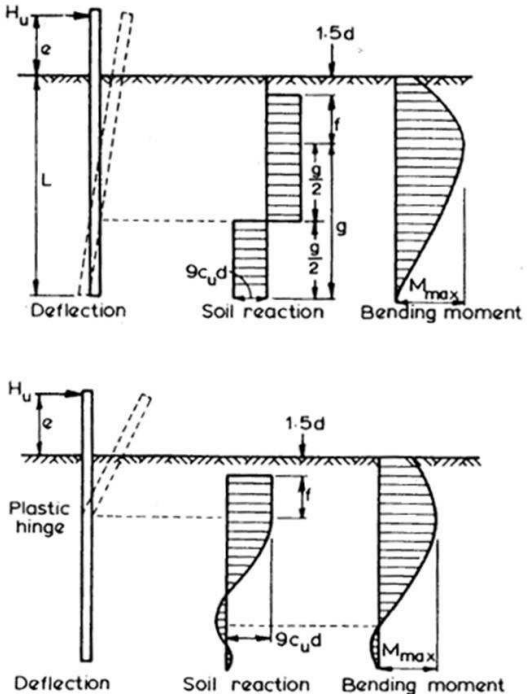

Figure 2.17: Failure mechanism for free-head piles in cohesive soil (after (Broms, 1964)); upper example - short pile, lower example - long pile

For purely cohesive soil, the ultimate lateral resistance p_u increases from surface down to a depth of three pile diameters *3d* and then stays constant (Poulos and Davis, 1980). Its values are equal to *2cu* at the surface(*cu* being the soil undrained shear strength) and *8 cu* to *12cu* at a depth of three pile diameters (Poulos and Davis, 1980) (Figure 2.16). Broms(1964) simplified this distribution by suggesting a zero soil resistance from the ground surface to a depth of *1.5 d* and a constant value of *9 cu d* below this depth (Figure 2.16(c)). In the following, a case of a free headed and a fixed headed pile in a cohesive soil is considered. The failure mechanisms for a free-head and a fixed-head pile are shown in figures 2.17 and 2.18, respectively. It can be seen that the failure mechanism differs for a short and a long pile. Long pile is termed a pile whose lateral capacity is primarily dependent on yield moment of the pile itself. Short pile, on the contrary, has a lateral capacity dependent wholly on the soil resistance.

When dealing with a pile group, the total lateral resistance of the pile group can be calculated as a sum of H_u of every individual pile. This can be done under a condition, that the pile spacing is more than four pile diameters. If it is not the case, the total ultimate lateral resistance of the pile group may be less than the ultimate lateral resistance calculated as a sum of H_u of all individual piles (Broms, 1964).

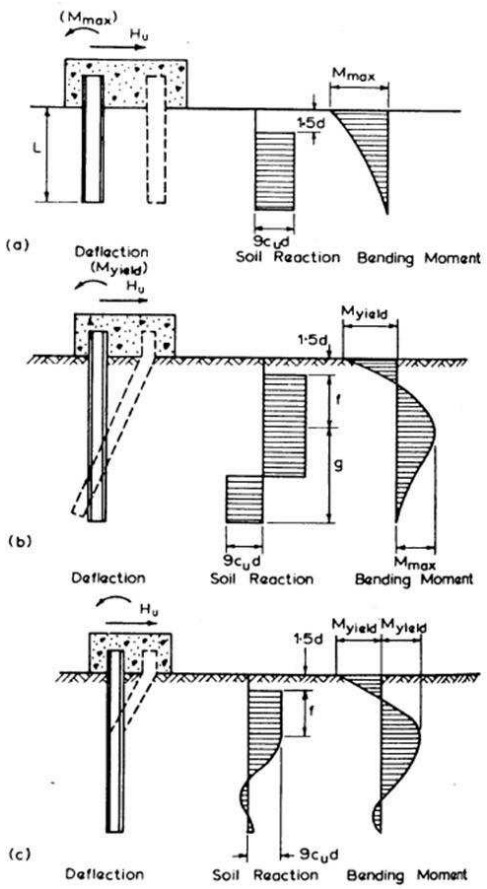

Figure 2.18: Failure mechanism for fixed-head piles in cohesive soil (after (Broms, 1964)); a) short pile, b) intermediate pile, c) long pile

Analytical calculations lead to a graphical solution (Figure 2.19) for the ultimate lateral resistance.

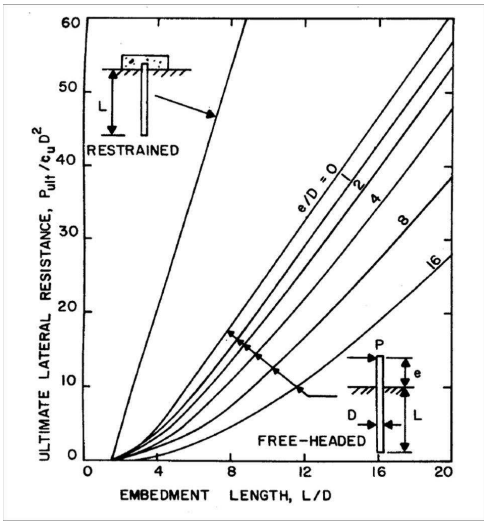

Figure 2.19: Ultimate lateral resistance in cohesive soils, (Broms, 1964)

2.3.1.2 Load-Deflection design

Two most comonly used theoretical approaches used for predicting lateral pile deflection under lateral loading are:

- Subgrade reaction approach
- Elastic approach

The subgrade-reaction approach discretizes a pile surrounded by a soil mass into a number of points and relates, at each point, a pile reaction to a deflection. The elastic approach, on the contrary, assumes the soil to be an ideal elastic continuum. The following text is devoted to the subgrade reaction approach.
Load-deflection prediction for laterally loaded piles is most commonly described by the subgrade-reaction approach, which was introduced by Winkler in 1867. This approach describes soil as a series of springs which are attached to the pile body. Subgrade-reaction theory relates soil reaction p [kPa] acting on the laterally loaded pile and pile deflection y [m] by the following equation:

$$p = k.y \tag{2.15}$$

where k $[\frac{kN}{m^3}]$ is a coefficient of subgrade reaction. Multiplying the coefficient of subgrade-reaction k by a pile diameter d, equation (2.15) can be restated as

$$P = E_s.y \tag{2.16}$$

where P [kN/m] is soil reaction per unit length and Es is the sugrade-reaction modulus [kPa]:

$$Es = k.d \tag{2.17}$$

Assuming the pile to be a flexible beam, a governing equation for the soil-pile interaction can be written in a form:

$$E_p I_p.\frac{d^4y(z)}{dz^4} + Es.y(z) = 0 \tag{2.18}$$

where E_p I_p is the pile bending stiffness and z is the depth below the surface. Solutions to the above differential equation may be obtained either analytically or numerically. Some methods used limit to considering k being constant with depth, other methods take into account a k variation with depth.

Modulus of subgrade reaction

Determination of E_s is generally carried out by one of the following methods:

- Empirical correlations with other soil properties
- Plate-load test (assuming that Es is constant with depth) (Broms, 1964)
- Triaxial test
- Full scale lateral loading test on pile
- *in-situ* pressure-meter test

The value of E_s is a function of the pile deflection. It is constant for small deflections but falls rapidly as the deflection increases.

Empirical correlations with other soil properties, giving a coefficient of horizontal subgrade reaction k_h ,were proposed for cohesive soil by the numerous authors. Some of these correlations are listed in the following:

- Broms (1964):

$$k_h = 1.67E_{50}/d \tag{2.19}$$

- Skempton (1951): Taking correlation proposed by Broms (1964) and using a value of E_{50} equal to 50 to 200 times the undrained shear strength cu, he obtained

$$k_h = (80 - 320)cu/d \tag{2.20}$$

  (Skempton, 1951)

- Davisson (1970):

$$k_h = 67cu/d \tag{2.21}$$

  (Davisson, 1970)

The use of plate loading-test has been discussed by Terzaghi in (Terzaghi, 1955). The main disadvantage of this method is that results obtained for a plate have to be extrapolated to a pile problem. For clays, (Terzaghi, 1955) proposes to consider the same value for horizontal and vertical subgrade reaction modulus, which is therefore independent on depth. Then the value of coefficient of horizontal subgrade reaction k_h for piles embedded in stiff clay can be determined by the following relation:

$$kh = \frac{1}{1.5d} ks_1 \tag{2.22}$$

where d is the pile diameter. ks_1 denotes basic value of coefficient of vertical subgrade reaction for a square plate. (Terzaghi, 1955) proposes empirical values of ks_1 for stiff, very stiff and hard clays. For normally consolidated clay, the values of ks_1 are so small, that the bending moment in loaded beam should be computed on the assumption that the load supporting structure is perfectly rigid.

The application of pressuremeter test to determine k_h is a method which is often included in the national codes and recommendations. k_h is related to the pressuremeter modulus and a factor dependent on the soil type. Menard (Menard et al., 1969) proposed to calculate the sugrade-reaction modulus Es as a function of the pressuremeter modulus E_m, rheologic coefficient α, the pile diameter d and a reference diameter d_0 which is equal to 0.6m.

for $d > d0$

$$\frac{E_s}{E_m} = \frac{3}{\frac{2}{3}(\frac{d}{d_0})(2.65\frac{d}{d_0})^{\alpha} + \frac{\alpha}{2}} \tag{2.23}$$

for $d < d0$

$$\frac{E_s}{E_m} = \frac{18}{4(2.65)^{\alpha} + 3\alpha} \tag{2.24}$$

Rheologic coefficient α depends on the soil type and is given in the following table (after (Baguelin et al., 1978)):

Soil Type	α
Peat	1
Clay	2/3
Silt	1/3
Sand	1/3

Nonlinear analysis - P-y curves

Relationship between pressure and deflection at any point along pile is nonlinear. This nonlinearity is accounted for in several approaches of which the most widely used was introduced by Reese and his co-workers (Reese and Welch, 1975). This approach is often referred as 'p-y' approach and requires an input of 'p-y' curves for various points along the pile. Design procedures for constructing the p-y relationships can be based on the results of field measurements such as pressure-meter test of type Menard. Menard (Menard et al., 1969) relates the pressure-meter probe dilatation and the interaction of pile-soil system. The p-y curve proposed in Fascicule 62 is shown in figure 2.20.

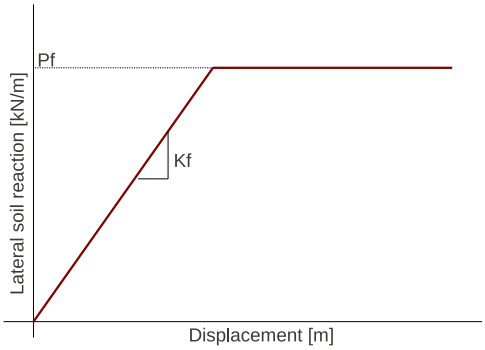

Figure 2.20: Pile-soil interaction

The pressure-deflection curve is characterized by Kf and Pf. It is considered within the Fascicule 62 that Kf is equal to 2xEs (equations (2.23) and (2.24)) and therefore:

for $d > d0$

$$Kf = \frac{12Em}{\frac{4}{3}(\frac{d}{d0})(2.65\frac{d0}{d})^{\alpha} + \alpha} \tag{2.25}$$

for $d < d0$

$$Kf = \frac{12Em}{\frac{4}{3}(2.65)^{\alpha} + \alpha} \tag{2.26}$$

Value of Pf indicates a plastic flow.

Cohesive soils show an increase of ultimate lateral soil resistance with increasing pile deflection (Rosquoët, 2004). To take this into account as well as to better fit the experimentally obtained curves, Fascicule 62 proposes, for cohesive soils, a p-y curve having the following form:

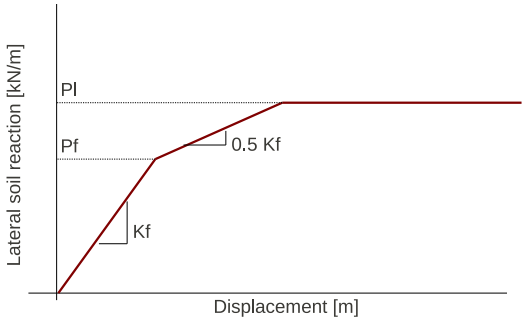

Figure 2.21: Pile-soil interaction

where $Pl = 0.8Pf$

The analysis of the p-y curves is addressed in numerous experimental studies. In general, it is shown that the initial stiffness of the p-y curves and the ultimate lateral reaction increases with the depth. This is due to the fact, that the mechanical properties of the soil change with increasing depth. This phenomenon can be seen from experimental results plotted in Figure 2.22 which were presented by M. Khemakhem (Khemakhem, 2012). Figure 2.22 shows p-y curves obtained while imposing lateral load to a pile surrounded by an overconsolidated clay. The p-y curves are plotted for different depths from the surface and it can be seen that indeed, the initial stiffness increases with increasing depth (Khemakhem, 2012). An exception are the p-y curves close to the surface of the clay mass, which are superposed. One of the reasons for this trend is that the soil mechanical properties are quasi-constant close to the surface.

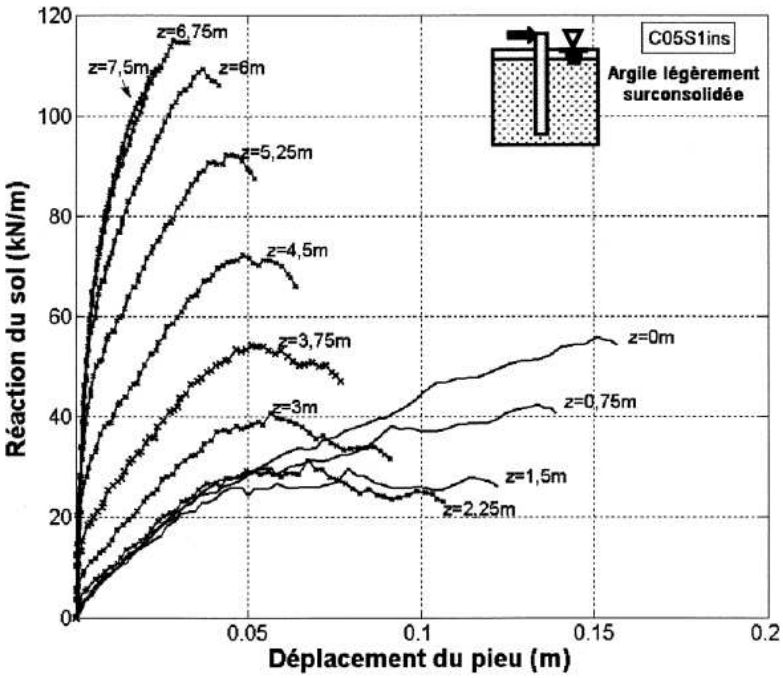

Figure 2.22: p-y curves plotted for different depths along the pile - initial stiffness increase with increasing depth (Khemakhem, 2012)

Load-deflection in view of Eurocode 8

Annex C of Eurocode 8 (EN 1998-5:2004) (Eurocode8, 2005) defines the pile-head static stiffness as the slope of the force (moment)-deflection (rotation) curve obtained for the pile head. Following correlation with soil and pile properties is proposed for horizontal stiffness K_{HH} and flexural stiffness K_{MM}:

Soil model	$\frac{K_{HH}}{dEs}$	$\frac{K_{MM}}{d^3Es}$
$E = Es.z/d$	$0.6(\frac{Ep}{Es})^{0.35}$	$0.14(\frac{Ep}{Es})^{0.8}$
$E = Es.\sqrt{z/d}$	$0.79(\frac{Ep}{Es})^{0.28}$	$0.15(\frac{Ep}{Es})^{0.77}$
$E = Es$	$1.08(\frac{Ep}{Es})^{0.21}$	$0.16(\frac{Ep}{Es})^{0.75}$

where E is the Young's modulus of the soil model; Ep is the Young's modulus of the pile material; Es is the Young's modulus of the soil at a depth equal to one pile diameter d and z is the pile depth.

Moments in pile

Poulos (Poulos and Davis, 1980) presented a moment distribution along a pile in a purely elastic soil, which is shown in Figure 2.23. Figures 2.23a and 2.23b refer to a free-head pile subjected to horizontal load only and to moment load only, respectively. For a pile subjected to horizontal load only, the maximum moment typically occurs at a depth of between 0.1L and 0.4L below the surface. For moment loading only, the maximum moment always occurs at the surface and equals to the applied moment. For a fixed head pile (Figure 2.23c), the maximum moment occurs at the pile head where the restraint is provided (Poulos and Davis, 1980).

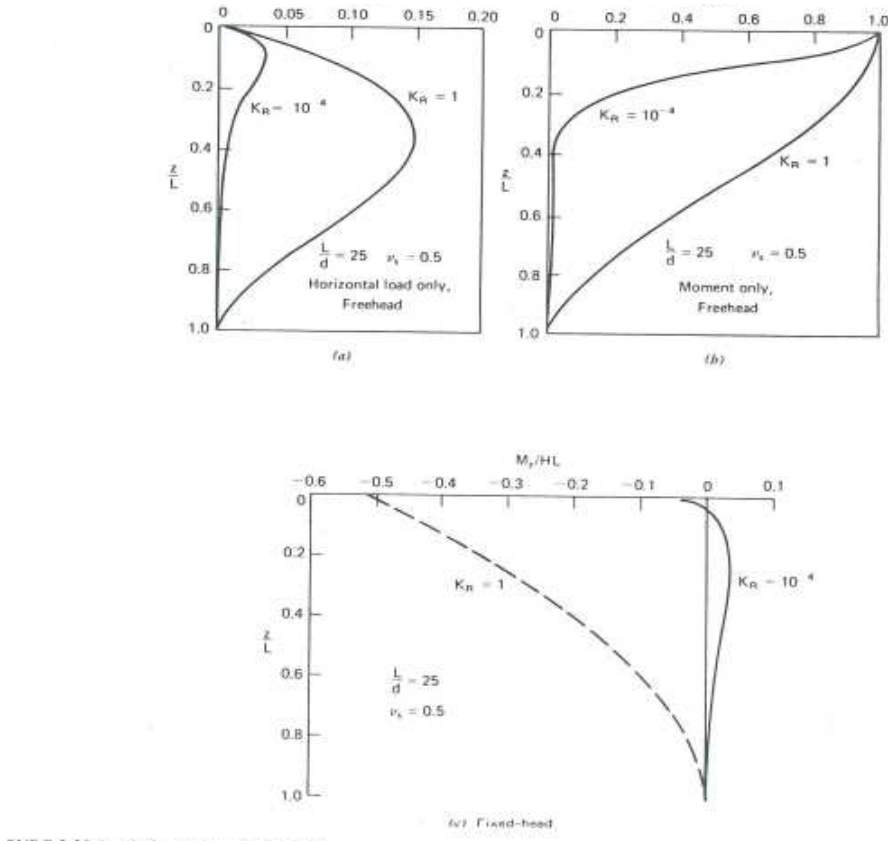

Figure 2.23: Moments in pile, citePoulos80

2.4 Pile under lateral cyclic loading

Based on observations presented in previous studies of lateral cyclic pile performance in clay, following phenomena can be listed:

- Displacement accumulation - Brown(1987) (Brown et al., 1987) has shown, comparing cyclic and static lateral pile performance, that a deflection along the pile is more important after 100 loading cycles than after 1 loading cycle. He described this phenomenon by a deflection ratio, relating pile head deflection at 100 cycles to pile head deflection at 1 cycle. This phenomenon was shown not only for a single pile but also for a case of a pile group.
  The phenomenon of the displacement accumulation with the cyclic loading was addressed in detail within the study of M. Khemakhem (Khemakhem, 2012). The experimental study was carried out in the centrifuge, analysing the behaviour of pile in clay under static and cyclic lateral loading. Results concerning displacement accumulation under cyclic loading of the pile in saturated and slightly overconsolidated clay are shown in the following.
  In the mentioned experimental study, the lateral loading applied to the pile head was controlled in force. Figure 2.24 shows the loading path, which is linear until a horizontal force H_m is reached and then changes to have a form of a sinusoid with a constant cyclic load amplitude H_c.

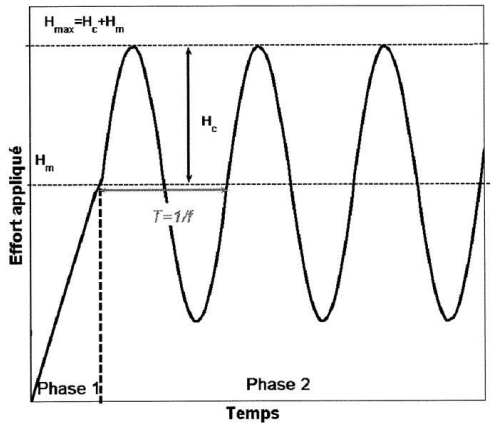

Figure 2.24: The path of a force controlled loading applied to a pile during an experimental study carried out by M. Khemakhem (Khemakhem, 2012)

It was observed that the level of lateral pile solicitation has an influence on the pile response in terms of deflection accumulation. Figure 2.25 shows three (figure a) b) and c)) different trends observed according to the level of horizontal load H_c and H_m applied. The graphic a) shows a case where the level of displacement accumulation decreases with increasing number of cycles applied, graphic b) refers to a case where the level of displacement accumulation is constant throughout the cyclic loading and the graphic c) refers to a case where the level of displacement accumulation increases with

the cyclic loading.

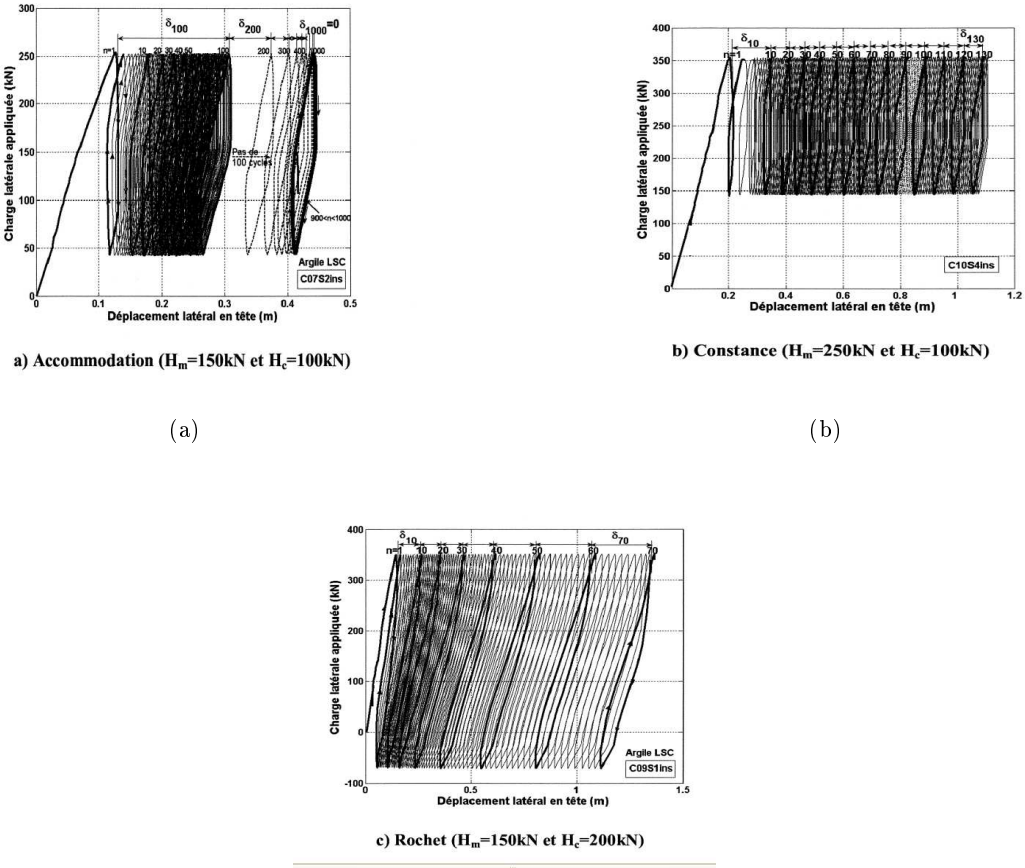

(a) (b)

(c)

Figure 2.25: Pile deflection accumulation with cyclic loading (Khemakhem, 2012) (a)Hm = 150kN, Hc = 100kN (b)Hm = 250kN, Hc = 100kN (c)Hm = 150kN, Hc = 200kN

The work of M. Khemekhem (Khemakhem, 2012) showed that there is a dependence between the pile deflection accumulation and the type, the level and the amplitude of horizontal loading applied.

- Lateral stiffness degradation - An important aspect to consider in the cyclic soil-pile interaction for soft clays is the lateral stiffness degradation. It is caused by remoulding and softening of the surrounding soil, as well as by a gap opening near the soil surface. This phenomenon is taken into account adjusting the cyclic P-y curve envelope as is shown in Figure 2.26. The cyclic P-y envelope is based on empirical observations from field tests performed by Matlock (Matlock, 1970).

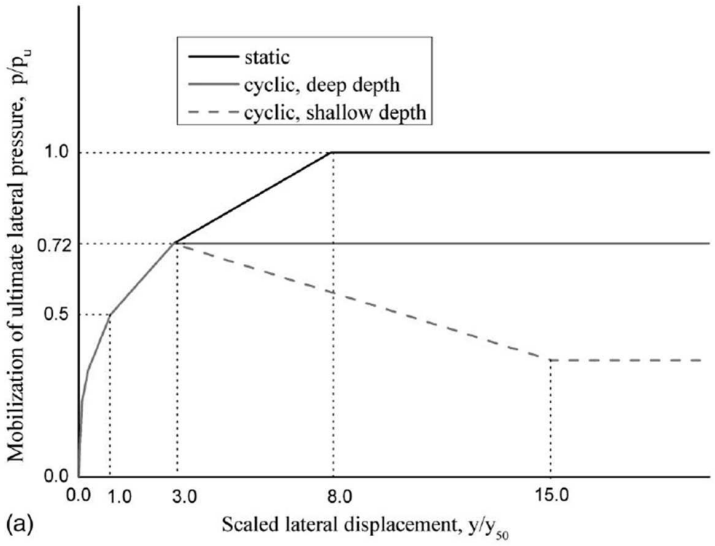

Figure 2.26: Predicted P-y curves (API, 2000)

where $y_{50} = 2.5\varepsilon_{50}D$, ε_{50} is the strain at which 50% of soil strength is mobilized

It was shown, that the above presented lateral stiffness degradation reaches a stabilisation after a certain number of cycles (Matlock, 1970).
The phenomenon of lateral soil reaction P degradation with cyclic loading has been proved by numerous experimental studies. Figure 2.27 shows an example of such experimental results showing lateral soil reaction measured at different depths on a pile as a function of the pile deflection measured at the same points (Khemakhem, 2012).

- Post cyclic behaviour addressed in (Zhang et al., 011b) and (Jeanjean, 2009) shows that cycles with small amplitudes cause an increase of global stiffness and therefore of post-cyclic ultimate lateral resistance. This phenomenon is described in Figure 2.28 (Jeanjean, 2009). The tests, marked chronologically from 1 to 4, were performed in a centrifuge. After each test, a three months long consolidation stage was carried out. It can be seen that the static ultimate lateral resistance, and therefore the stiffness, increased after applying the two stages of cyclic loading. Smaller the amplitude of cycles applied, bigger the increase in shear resistance and therefore stiffness of the soil (Jeanjean, 2009).

- The ultimate lateral resistance reached for cyclic loading is smaller than the ultimate lateral resistance reached for monotonic loading. Matlock (Matlock, 1970) proposes to consider cyclic lateral resistance being equal to 0.72 times static lateral resistance. This phenomenon was confirmed by (Brown et al., 1987) and can be seen in Figure 2.29. The experimental results shown were obtained by cyclic lateral loading of a large-scale pile group embedded in stiff clay. The p-y curves are plotted for 1.2m depth, but are representative of the trends observed at other depths of the pile. As can be seen, a soil reaction mobilised after 100 cycles is smaller than a soil reaction mobilized after 1 cycle. There is a visible loss of soil resistance during the cyclic loading. This trend is valid not only for a single pile but also for a pile within a pile group.

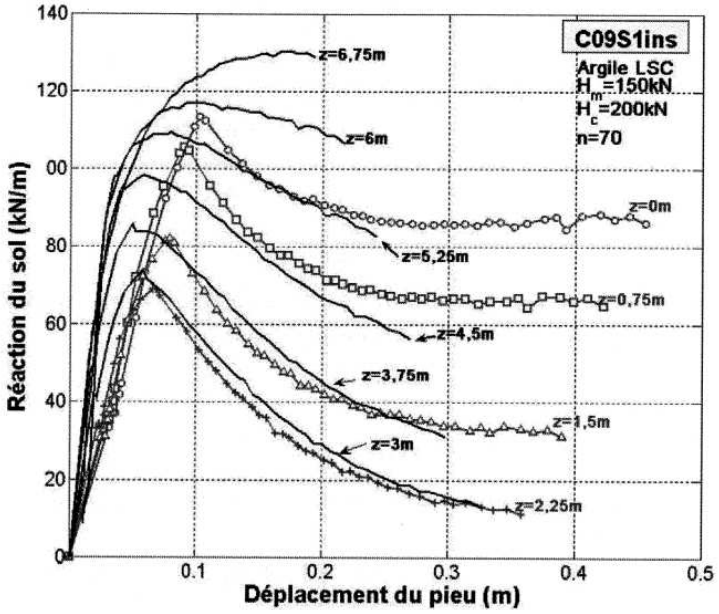

Figure 2.27: Lateral soil reaction degradation. The lateral soil reaction is plotted for different depths on a pile as a function of the pile deflection measured at the same points (Khemakhem, 2012)

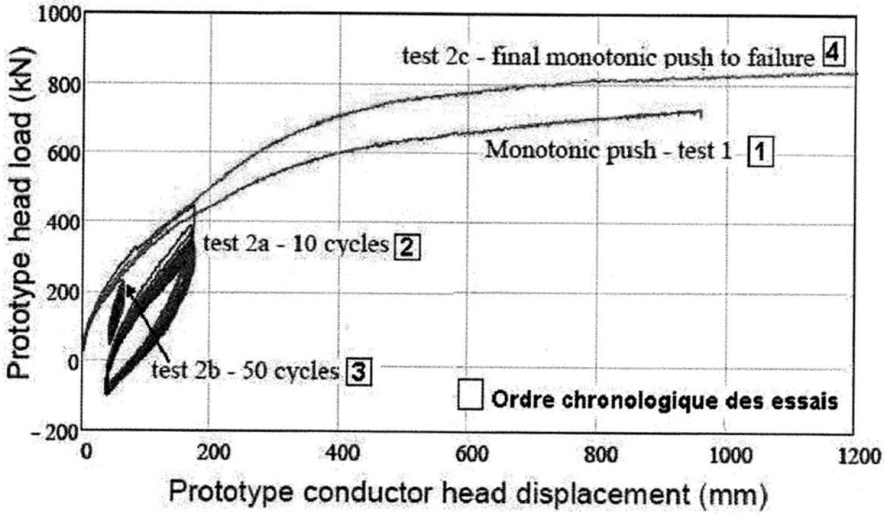

Figure 2.28: Force-displacement curves for lateral static and cyclic loading of a pile (Jeanjean, 2009)

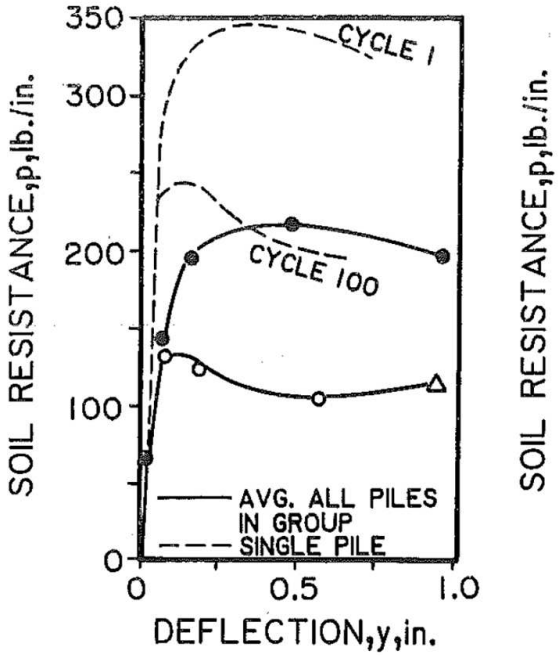

Figure 2.29: Experimental P-Y curves for monotonic and cyclic loading (Brown et al., 1987)

- Local maximum of bending moment increases in value and in depth with the cyclic loading (Reese and Welch, 1975). This phenomenon is visible in Figure 2.30 which shows a bending moment distribution along the pile for first, fifth and twentieth cycle.

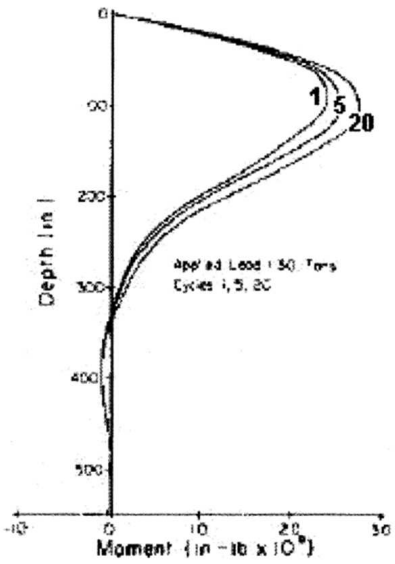

Figure 2.30: Bending moment evolution with cyclic lading (Reese and Welch, 1975)

Such effect of cyclic loading on the bending moment position was also observed by Khemakhem (Khemakhem, 2012), who also analysed the phenomenon in relation to the level of horizontal force applied to the pile H_m (see Figure 2.24) and the amplitude of the cyclic loading H_c (see Figure 2.24). Experiments on lateral pile response to a horizontal

loading in a slightly overconsolidated clay provided results shown in Figure 2.31. It was not only confirmed that under such conditions the local maximum of the bending moment increases in value and moves deeper along the pile with the cyclic loading, but it was also observed that the cyclic loading amplitude H_c has an important effect on the moment distribution. Indeed, Figure 2.31(a) shows that 70 loading cycles cause the local maximum of the bending moment to increase by 40% in its value when the cyclic loading amplitude H_c is equal to 200kN, whereas when the loading amplitude H_c is equal to 50kN, 1000 loading cycles cause the local maximum of the bending moment to increase only by 17% (Khemakhem, 2012). Based on results shown in Figures 2.31(a) and 2.31(b), it was noted that the position of the local bending moment maximum reaches a faster stabilisation for smaller cyclic loading amplitudes H_c. The position of the bending moment maximum is deeper from the surface with increasing loading amplitudes H_c. This is assumed to be due to degradation on mechanical properties of the soil which cause the load to transfer to lower, more resistant layers (Khemakhem, 2012).

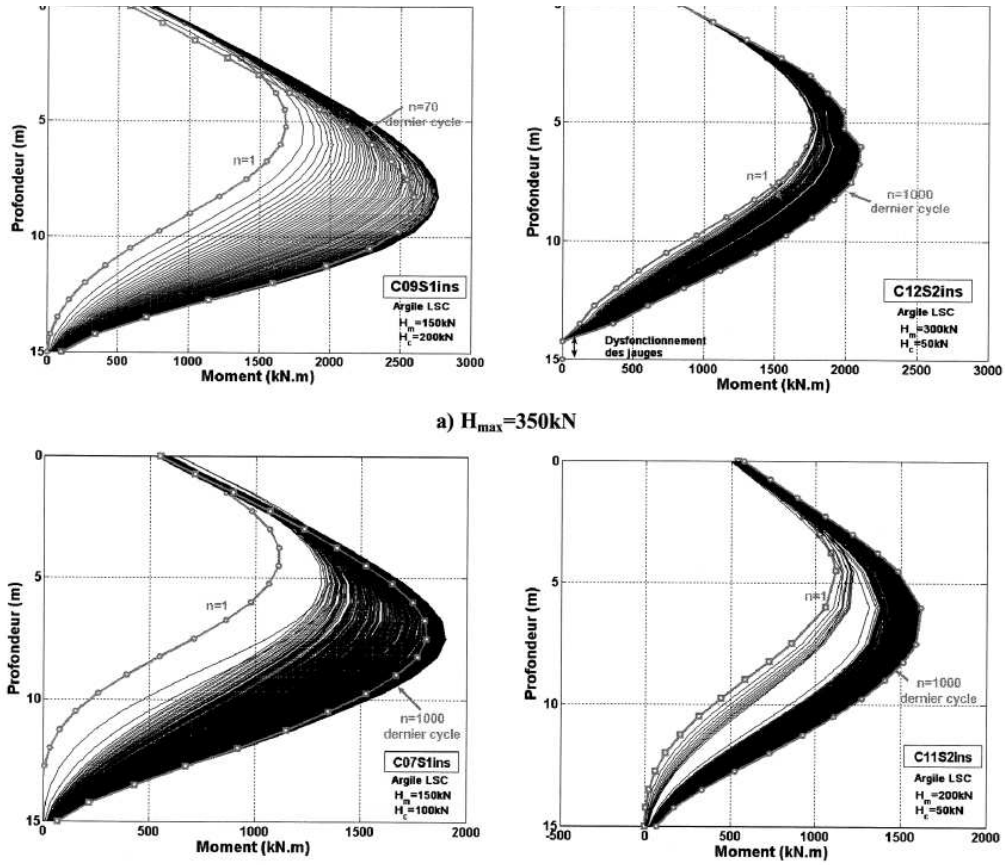

Figure 2.31: Bending moment along the pile developed under different kinds of lateral cyclic loading in a slightly overconsolidated clay (Khemakhem, 2012)

- A gap opening behind a pile after a pile lateral deflection was observed during numerous studies of pile behaviour in clay (Brown et al., 1987), (Zhang et al., 011b)
- Comparing performance of a single pile with a pile acting within a pile group, following features can be listed based on (Brown et al., 1987):
  - The maximum soil resistance for piles in a group is reduced as compared to that of a single pile. This observation was shown to be valid for both static and cyclic loading.
  - Reduction of soil resistance under cyclic loading is similar for a single pile and a pile within a pile group (figure 2.28).
  - Bending moments in a pile within a pile group are grater than bending moments in a single pile.
  - Considering that a load acting on a single pile is equal to an average load per pile acting within a pile group. Deflection and a moment of a pile within a group of piles is grater than that of a single pile. Maximum moments are shifted deeper for a pile in a pile group.
  - Variation of load to the piles in a pile group is generally 20 % or less.
  - Variation of maximum bending moment in piles in a pile group is generally 20 % or less.

2.5 Conclusion

The presented literature review addresses topics related to the problematic of the response of reinforced soil subjected to an inertial loading of a shallow foundation. In the presented experimental study, a shallow foundation model simulates seismic, wind or water loading of a superstructure applied to a reinforced soil. The topic of shallow footings under combined loading was therefore addressed in the first part of this chapter.

The physical models used in the experimental study are composed of a foundation model which is lying on clay reinforced by the rigid inclusions associated either to Load Transfer Columns (LTCs) or to a Load Transfer Platform (LTP). These models can, up to some extend, represent two types of soil improvement technologies - the Mixed Module Columns (CMM) and the Rigid Inclusions (RI). Section 2.2 of this chapter was therefore dedicated to these two technologies, describing them and summarizing results of the previous studies carried out in this field.

Both of the physical models of the soil reinforcement have their lower rigid parts made of a rigid inclusion surrounded by clay. It is one of the aims of the presented work to study the response of the rigid inclusion to the applied loading in order to analyse the nature of inertial forces transmitted through the upper flexible part to the rigid inclusion. Hence, lateral pile behaviour in clay under monotonic and cyclic loading was addressed in sections 2.3 and 2.4 of this chapter.

It is noted that even though many research projects concerning the soil reinforcement are carried out, there seems to be a lack of studies addressing this problematic in seismic conditions. Moreover, a very little number of these studies on soil reinforcement under seismic

loading are carried out in 3D. It is assumed that this is due to the complexity of the physical models in 3D and due to a difficult monitoring of the system response to the dynamic loading. The 3D numerical models are more complex with a higher time demands that the 2D numerical models.

The aim of the presented thesis was to continue in the research started by Zhang (Zhang, 2011) in order to extend the knowledge on the problematic of the response of reinforced soil to the inertial loading in 3D. The performed study provides qualitative results on the subject. These could be used not only as a reference for the current design practice, but also as a data base for the numerical modelling or as preliminary results for experiments in the real scale or a centrifuge.

CHAPTER 3

Experimental Methodology

3.1 Introduction

The aim of the presented work was to study the response of the reinforced soil to inertial loading applied by a foundation model. The soil reinforcement was composed of rigid inclusions associated to an upper flexible part consisting either of Load Transfer Columns (LTCs) surrounded by clay (Figure 3.1(a)) or a Load Transfer Platform (LTP) (Figure 3.1(b)). These reduced 1/10 physical models were studied in clay. The rigid inclusions were modelled by aluminium piles, one of which was equipped with sensors. In order to simulate the inertial loading of the reinforced soil, combined vertical static and horizontal dynamic loading was applied with a shallow foundation model, which prevents rotation. A parametric study was carried out varying the LTC or LTP height in order to define its effect on lateral performance of the rigid inclusion and the energy dissipation. Lateral response of the instrumented inclusion was monitored using 20 levels of strain gauges. The strain measured was used to calculate the bending moment along the pile, giving a pile deflection y by double integration and soil reaction P by double derivation. P-y curves were thus obtained. Furthermore, the calculation of the deflection y at the pile head yield the energy dissipation within different parts of the physical models.

3.2 Physical Modelling in reduced scale

3.2.1 Similarity Conditions

After (Roscoe, 1968), there are two main uses of model testing in soil mechanics:

1. A reduced scale model examines on a non-quantitative basis assumptions made in the-

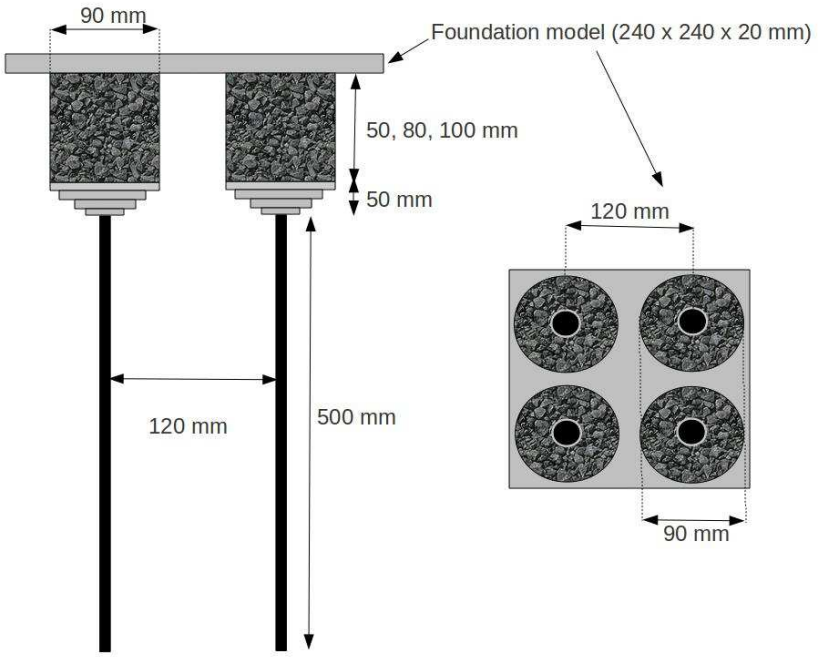

(a)

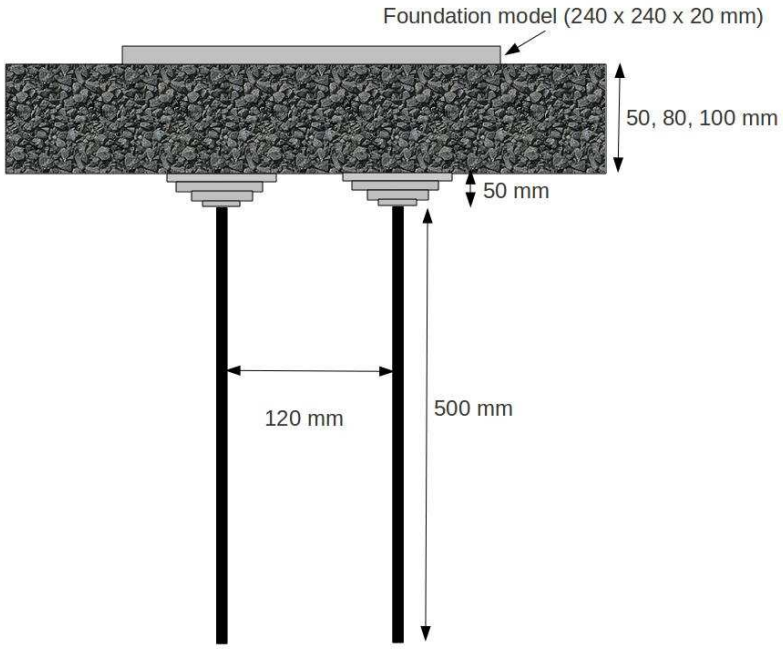

(b)

Figure 3.1: Physical models of rigid inclusions associated to Load Transfer Columns (LTCs) surrounded by clay (a) or a Load Transfer Platform (LTP) (b)

oretical analysis of prototype problems. The objective is to develop analysis and model side by side with a view of analysis improvement. This approach does not necessarily respect the similarity conditions, therefore care should be taken when analyzing the data.

2. A reduced scale model attempts to satisfy the similarity conditions so that prototype behaviour can be predicted directly from model data. These similarity conditions are derived from basic equilibrium equation of continuous media:

$$\frac{\delta\sigma_{ij}}{\delta x_j} + \rho(g_i + \frac{d^2\xi_i}{dt^2}) = 0 \tag{3.1}$$

where σ is the stress tensor, x are the coordinates, ξ is the displacement vector, ρ is the volumetric mass, g is the acceleration field of the gravity and t is the time. Introducing scale factors which relate model scale m to prototype scale p, we obtain following equations:

$$\sigma^*_{ij} = \frac{\sigma_{ij_m}}{\sigma_{ij_p}} \tag{3.2}$$

$$l^* = \frac{x_{j_m}}{x_{j_p}} \tag{3.3}$$

$$\xi^* = \frac{\xi_{i_m}}{\xi_{i_p}} \tag{3.4}$$

$$\rho^* = \frac{\rho_{i_m}}{\rho_{i_p}} \tag{3.5}$$

$$g^* = \frac{g_{i_m}}{g_{i_p}} \tag{3.6}$$

$$t^* = \frac{t_m}{t_p} \tag{3.7}$$

where index m stands for model scale and index p stands for prototype scale. l^* represents the scale reduction factor applied to the geometry of the models.

In order to obtain identical equilibrium equations for the prototype and the model, equations 3.8 and 3.9 are introduced representing the similarity conditions for physical modelling.

$$\sigma^*_{ij} = \rho^* g^* l^* \tag{3.8}$$

$$\xi^* = g^* t^{*2} \tag{3.9}$$

Since it is desired to have the same scale reduction factor l^* applied to the geometry of the model as well as to the displacement obtained, next similarity condition is presented in 3.10

$$\xi^* = l^* \tag{3.10}$$

and therefore the strain tensor ε is equal for the physical model and the real scale problem:

$$\varepsilon^* = 1 \tag{3.11}$$

Because mechanical behaviour of soils is closely related to the level of applied stress, it is essential, for preserving the similarity, to subject the model to the same level of stress as is applied to the prototype. This condition is mathematically formulated in following equation

$$\sigma^* = 1 \tag{3.12}$$

To be sure to obtain same rheological properties for soil in the prototype and the model, a final similarity condition is introduced in 3.13

$$\rho^* = 1 \tag{3.13}$$

(Garnier, 1995).

The reduced physical models in the presented experimental study belong to the first case described, providing only qualitative results. The models presented in Figure 3.1 are in scale 1/10 and work under gravity of 1g. The scaling law described in equation 3.12 is not fulfilled. As a consequence, a gradient with depth in the soil properties cannot be simulated in such a model and the laboratory soil is considered to have constant properties. Also, the frequency applied in the dynamic tests should be $\sqrt{10}$ times the prototype frequency. Hence, assuming a prototype input with a frequency around 1Hz, the model should be tested at 3.16 Hz.
Even though the scaling laws are not strictly respected, this work provides a qualitative study of the two types of soil reinforcement and of the mechanisms mobilized under the dynamic loading.

3.3 Experimental Device

3.3.1 The 'Visucuve'

The experiments were carried out in an experimental device named 'VisuCuve' (Figure 3.2, standing for a visualization tank. This device was developed in Laboratory 3S-R and previously used for studying soil-pipeline interaction (Foray et al., 2004), (Orozco, 2009), (Zhang, 2011). VisuCuve setup was adjusted to meet the required loading conditions, i.e. combined vertical and horizontal loading of shallow foundation with resulting settlement and horizontal movement of this foundation while preventing it from rotation in any possible sense. Further modifications were done in order to make the system sufficiently resistant to vibrations caused by dynamic loading. Reduced models surrounded by clay were installed within the tank in order to study their behaviour under lateral loading. Experimental setup is composed of:

•A rigid tank which holds the reinforced soil. This tank, named 'VisuCuve', is 2m long, 1m wide and 1m high. The presented study used the 'VisuCuve' as a rigid tank, dividing it in half by a reinforced wooden board. This reduced the experimental area to $1m^3$. The visualization possibility was not used since the physical models were installed in the center of the $1m^3$ area and the objective was to study 3D models (Figure 3.3).

•A trolley, a metal framework sliding horizontally on top of the tank. The framework is made of square profiles 20x20mm, which are welded together. To allow horizontal movement of the trolley, two rails were fixed on top of the tank, which enable the trolley to slide along the rails (Figure 3.4). This sliding system was developed and used for previous studies (Orozco, 2009), (Zhang, 2011).

•A foundation model, made of square aluminium plate (240mm side length; 20mm thickness). Foundation is rigidly fixed to a metal rod of 56mm in diameter and 30cm in length. This metal rod is compatible with an anti-rotational ball bearing which, being fixed to the trolley, makes the link between the foundation and the horizontal loading system (Figure 3.5).

Figure 3.2: Experimental setup 'VisuCuve'

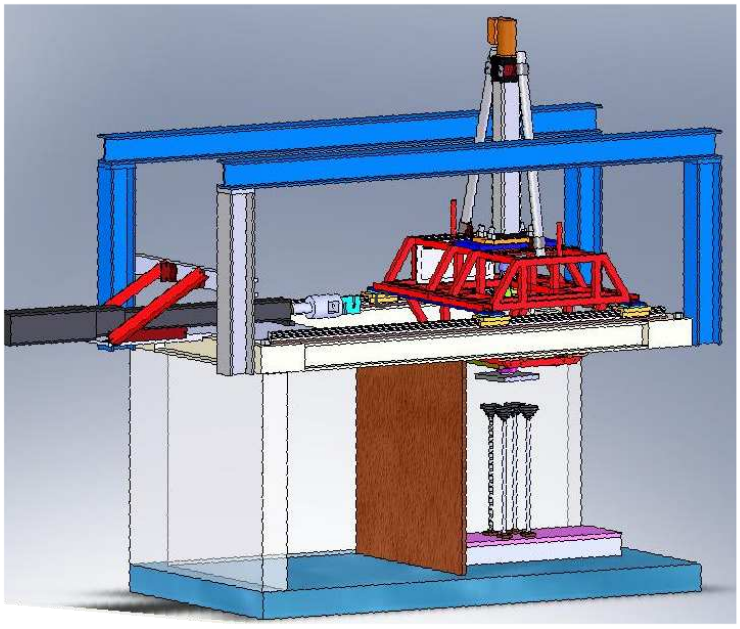

Figure 3.3: Experimental setup 'VisuCuve'

Figure 3.4: Sliding system of a trolley

The ball-bearing is supported by a system of aluminium plates, which are fixed to the trolley framework (Figure 3.6). The system was designed to sustain loads expected during the experimental procedures. Vertical load is applied to the foundation by a vertical actuator, which is linked through a force sensor to the metal rod holding the foundation and sliding freely in the anti-rotational ball bearing. This system of fixation was developed for the purpose of the presented work in order to allow vertical displacement but avoiding any rotation of the foundation model. The whole system was designed to be easily disassembled and exchanged for the previous loading system.

•Vertical loading device: Unlike in the case of the previous work carried out in the VisuCuve (Zhang, 2011), it was desired to control the vertical loading of the foundation. For this reason, a vertical actuator was installed in a vertical position on the metal trolley. This set-up was already used in previous studies ((Orozco, 2009)) and so the fixation system was reassembled in the same way. The vertical actuator used was a type Exlar IX40. It is a linear motion electromechanical actuator with a roller screw technology. It is combined with a high performance brush-less motor and a variator. The actuator can be controlled in position and velocity. The minimum velocity is 0.017 mm/s and the maximum is 12.7 mm/s. A constant force up to 17.6kN can be applied, while the peak force can rise up to 33.6kN.

•Horizontal loading device: It was desired to impose horizontal dynamic loading to the foundation model. Horizontal cycles of amplitude up to 5mm had to be controlled in displacement and have a frequency of 2-3Hz. For these purposes, a horizontal actuator Exlar FT35 was chosen (Figure 3.8). The loading device was rigidly connected to the trolley and therefore the load was applied through the trolley skeleton to the foundation model. The actuator used is a linear electric actuator using a roller screw mounted inside a telescoping tube mechanism. It is combined with a high performance brush-less motor and a numerical variator. The actuator can be controlled in position and velocity. The maximum velocity that can be applied is 750 mm/s and the actuator needs 100ms for accelerating/deaccelerating. A constant force up to 17.8 kN can be applied. This actuator served well for the purposes of applying dynamic loads.

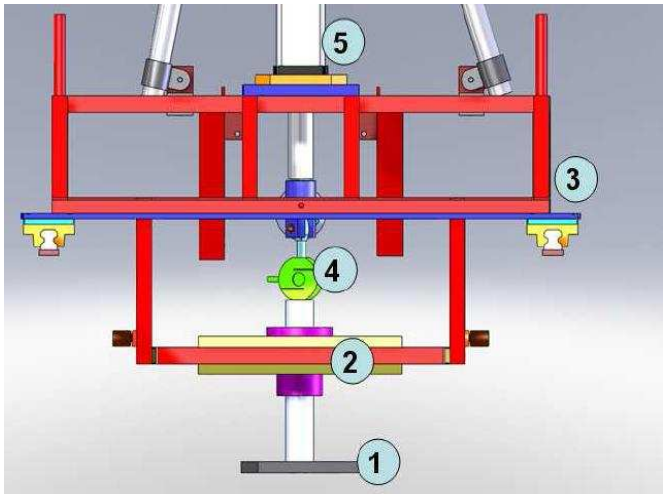

Figure 3.5: 1) Foundation; 2) System of aluminium plates supporting the ball bearing; 3) Sliding system; 4) Force sensor; 5) Vertical actuator

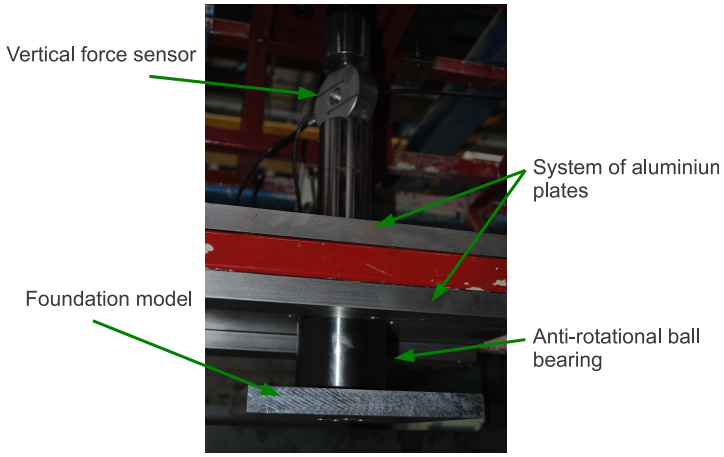

Figure 3.6: Foundation model with vertical sliding system

Figure 3.7: Vertical actuator - Exlar IX40

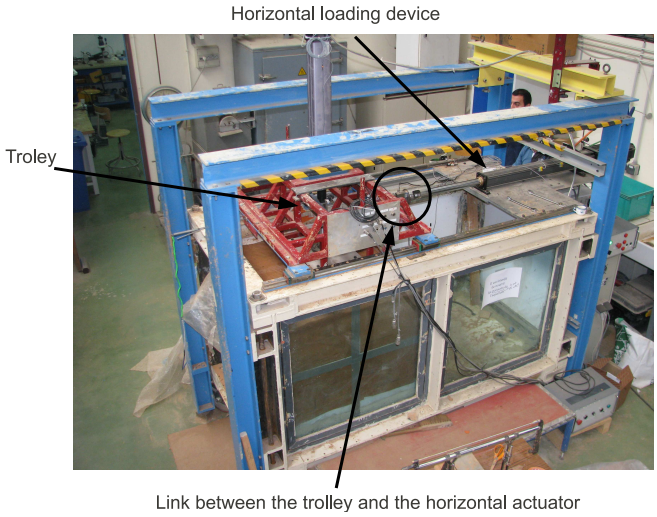

Figure 3.8: Horizontal actuator - Exlar FT35 installed on the 'VisuCuve'

•Force and displacement sensors:

- Horizontal force - The force applied by the horizontal actuator on the trolley was measured by a force sensor linking the actuator with the trolley. The sensor was of type *STS 2.5 T*, being of an *S* shape and having maximum capacity of 2.5 tons.

- Vertical force - The force applied by the vertical actuator on the foundation was measured by a force sensor linking the actuator with the metal rod fixed to the foundation. The sensor was of type *AEP TS 20 kN*, being of an *S* shape and having maximum capacity of 2 tons.

- Horizontal Displacement - Horizontal LVDT served to measure the foundation horizontal displacement. It was fixed in the horizontal axes of the 'VisuCuve' and was measuring the horizontal displacement of the sliding trolley. Since the trolley and the foundation model were rigidly linked in horizontal sense, the obtained measurements stand for the foundation horizontal displacement. The LVDT sensor used had a working range of +/-5mm or +/-100mm, depending on the experiments performed.

- Vertical Displacement - Vertical LVDT served to measure the foundation vertical displacement. It was fixed to the trolley and was directly measuring the foundation settlement. The LVDT sensor user had a working range of +/-100mm, depending on the experiments performed.

3.3.2 Modifications of the experimental device

As mentioned before, the experimental device 'VisuCuve' was developed and previously used to study soil-pipeline interaction (Foray et al., 2004), (Orozco, 2009) and then it served for the purposes of studying CMM and RI soil reinforcement in 2D (Zhang, 2011). For the presented experimental program, the 'VisuCuve' was modified in order to meet the required loading conditions and to adapt it to application of dynamic loading. List of the modifications carried out is presented:

1. Replacement of the pipe by a footing model, which was made of an aluminium plate (240mmx240mm)
2. Vertical loading system allowing controlled foundation loading and displacement. This system, as introduced in section 3.3.1, was composed of a metal rod, firmly fixed to the foundation model, which traversed an anti-rotational ball bearing to be linked to the vertical actuator (Figures 3.5 and 3.6). The ball bearing was fixed to the trolley frame by a system of aluminium plates. All design plans are listed in Annex A.
3. Dividing the 'VisuCuve' in two parts by a wooden board fixed onto a rigid metallic frame, which was connected to the 'Visucuve'. The joints had to be sufficiently rigid to avoid any vibrations.
4. Installation of the physical model inside the 'Visucuve' (the model is described in the following section). Design plans for different parts of the physical model are listed in Annex A.
5. Because dynamic loading was being applied, measures were done in order to avoid unnecessary vibrations of the horizontal actuator, which would be subsequently transferred to the 'Visucuve'. The horizontal actuator, which was applying a dynamic loading with a frequency of 2.7 Hz, was fixed to the 'VisuCuve' frame with angle irons (Annex A).
6. The horizontal actuator was a source of strong electromagnetic perturbations, which had an influence on the monitoring system. In order to limit the effect of these perturbations on different sensors, the actuator had to be electrically isolated from the 'VisuCuve' frame. It was then observed, that isolating also the instrumented pile from the 'Visucuve'

frame improved signal of the strain gauges. Therefore all joints between the 'Visucuve' and the actuator and between the physical model and the 'Visucuve', were isolated by introducing isolation discs and isolation screw coats (design plans and photos are listed in Annex A).

7. In order to have a better access to the physical models and to enable clay installation, one side of the 'VisuCuve' was taken apart and was reconstructed from wooden boards. The wooden boards were easily disassembled and when combined with a plastic foil, provided a sufficient rigidity and waterproofness.

3.3.3 Physical models

Two types of physical models in clay at scale 1/10 were used - four piles associated to the Load Transfer Columns (LTCs) or four piles associated to a Load Transfer Platform (LTP). The models consisted of three parts, where the lower rigid part and the transition zone are common for the two models:

1. Lower rigid part is made from an aluminium tube with inner diameter 8mm and external diameter 16mm. The tube is 58cm long and is embedded into the 'VisuCuve' bottom by 8cm. Therefore the rigid part taking role in the physical model is 50cm long. The tube cross-section parameters were set to the stated values in order to:

   (a) obtain equivalent pile-flexibility factor Kr (Poulos and Davis, 1980) for the reduced model and the prototype

   (b) to permit installation of strain gages with cables passing inside the pile.

   The pile flexibility factor is formulated as:

$$Kr = \frac{E_p I_p}{E_s L^4} \tag{3.14}$$

   where E_p is Young modulus of the pile, I_p is moment of inertia of the pile section, E_s is the Young modulus of the soil and L is the pile length.
   Pile length was chosen in order to respect the scale 1/10 between the prototypes and the reduced models. One of the four tubes serving as pile models was equipped with 20 levels of strain gages. In order to avoid mechanical damage of the strain gages, aluminium tube was grooved (Figure 3.9), which permitted embedding of every gauge as well as its electrical wires. A little hole was drilled after every five levels of strain gauges in order to permit passage of the wires to inside of the tube. Collecting all electrical wires inside the tube, wires were led through the tube bottom towards the amplifier. Details on the pile instrumentation are presented in section 3.3.5

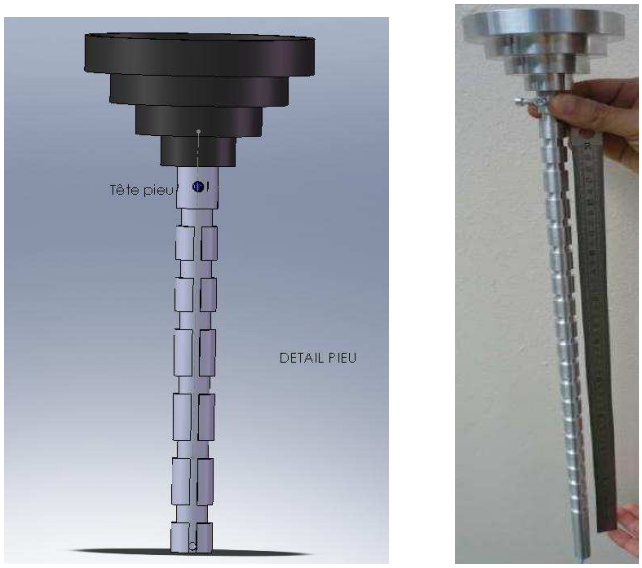

(a) (b)

Figure 3.9: Pile before instrumentation with 20 levels of strain gages

Piles were fixed to the 'Visucuve' bottom as shown in Figure 3.10. They were embedded in an aluminium plate which was fixed to two U shaped metal profiles. Each pile was fixed from both sides to the aluminium plate by two mechanical support components of type *SFWR16* (details in Annex A).

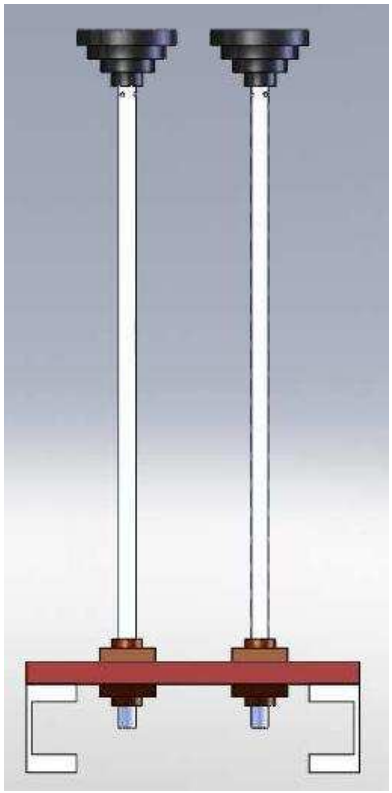

Figure 3.10: The pile installation

2. The transition zone is represented in the physical model by an aluminium funnel which

can be seen at the top of the piles in Figure 3.10. Funnel dimensions and design plans are presented in Annex A. Each funnel is filled with gravel with grain size 2-4mm. The link between the funnel and the pile is semi-rigid, where the funnel is attached to the pile from four sides by screws which are not screwed in entirely to allow some play. Funnel attached to the tube equipped with strain gages has an accelerometer fixed to its bottom. In order to protect this accelerometer from mechanical damage, it was separated from the gravel by a metal plate (shown in a Figure in Annex A). The aim was to measure acceleration obtained at the pile head. Double integration of the signal with respect to time would give pile head displacement which could be compared with the strain gauge measurements. Due to technical problems (see section 5.7), accelerometer signal was not interpretable.

3. The upper flexible part differs for the two types of physical models (see Figure 3.1. For one type of model, the flexible part is composed of four Load Transfer Columns (LTCs) which are surrounded by clay. The columns are made of gravel and are designed with a diameter around 90mm (the exact diameter is not known due to the installation process described in section 3.4.2). For the second type of the physical model, the flexible part of the model is represented by a Load Transfer Platform (LTP) composed entirely of gravel. The same type of gravel with a grain size in the order of 2-4mm is used in both models. Height of the flexible part is varied from 5cm to 10cm in order to study its effect on the response of the lower rigid part.

3.3.4 Soil

Two types of materials were used during the experimental procedure - gravel and clay. Basic characteristics of both materials are given in the following.

3.3.4.1 Gravel

The gravel material used for gravel columns and gravel mattresses was a crushed limestone with silica impurities. The grain size distribution was from 2mm to 4mm.
A shear box test was carried out on the gravel in order to find out residual and peak friction angle of the gravel. Gravel was compacted and sheared in a shear box with dimensions 30 cm by 30 cm (Figure 3.11). Obtained results for three different confining pressures are plotted in Figure 3.12 and are summarized in table 3.1. The range of confining pressure applied was chosen in order to represent the conditions in the experimental procedure.

Figure 3.11: A shear box with dimensions 30cm by 30cm

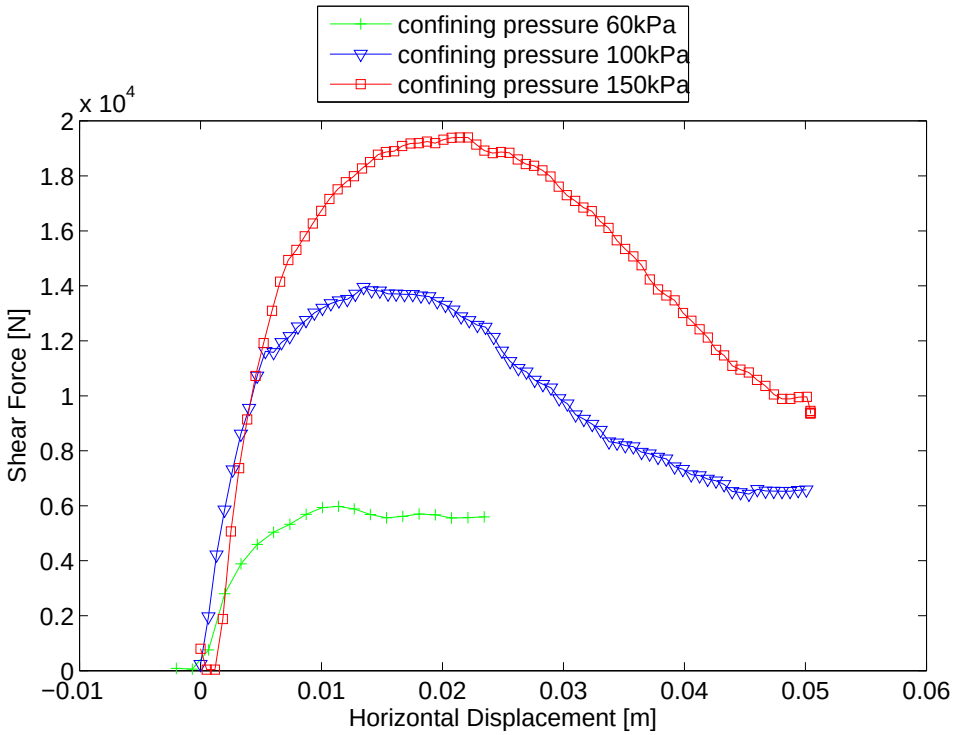

Figure 3.12: Shear box test results

Table 3.1 lists the experimental results obtained. Analysing the values of friction angle, it is noted that the experiment carried out under a 60 kPa confining pressure doesn't provide satisfactory results. It is concluded that the residual friction angle of the gravel is 37^o and its peak friction angle is 56^o.

Table 3.1: Soil characteristics based on the shear box test

	60 kPa	100 kPa	150 kPa
Residual Friction Angle	46	36	37
Peak Friction Angle	48	57	55

3.3.4.2 Clay

The aim was to create a clay mass, as homogeneous as possible, which would consequently present as a soil to which reinforcement would be applied. It was desired to obtain a clay mass having a cohesion around 20 kPa without having to consolidate the clay in the 'VisuCuve'. Such a clay was purchased in blocks of 10 kg with their origin in Provence, France. The soil was classified by number of tests, which are listed in the following text. The obtained results served not only for the experimental study, but also for a numerical model calibration.

1. **Atterberg limits** The results of the Atterberg limits, which were used to measure the nature of the clay used are listed in Table 3.2

Table 3.2: Atterberg limits

Plastic limit	21%
Liquid limit	42%
Water content	28%
Plasticity index	21%
Liquidity index	33%

2. **Isotropic compression**

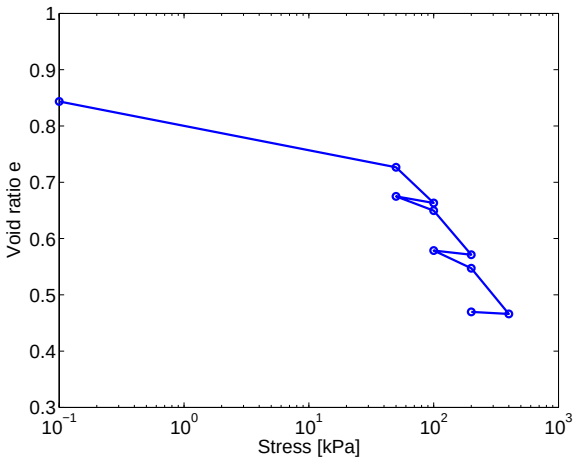

Figure 3.13: Isotropic compression stress-strain path

The obtained stress-strain path, where the strain is represented in terms of void ratio, is shown in Figure 3.13. Evaluating the results, following clay characteristics were

obtained:

$$Cc \approx 0.288 \tag{3.15}$$

$$Cs \approx 0.084 \tag{3.16}$$

$$\lambda = \frac{Cc}{ln(10)} \approx 0.1254 \tag{3.17}$$

$$\kappa = \frac{Cs}{ln(10)} \approx 0.0366 \tag{3.18}$$

$$pc \approx 60kPa \tag{3.19}$$

where Cc is the compression index, Cs is the swell index, λ is slope of normal compression line, κ is the slope of the isotropic unload-reload line and pc is the preconsolidation pressure.

3. **Bender Element Test on Clay - Identifying the Shear Wave Arrival Time** As the clay sample was subjected to different compression stages during the isotropic compression, shear wave velocity was measured using bender elements. Sample and signal characteristics are given in Table 3.3:

Table 3.3: Bender elements - sample and signal characteristics

Sample height	102mm
Sample width	70mm
Source type	S-wave; sinusoidal wave
Period of the source	0.2s
Amplitude of the source	14V
Sample frequency	100 ksamp/sec
Sampling time	5 msec
Number of stacs to obtain the final signal	25-50

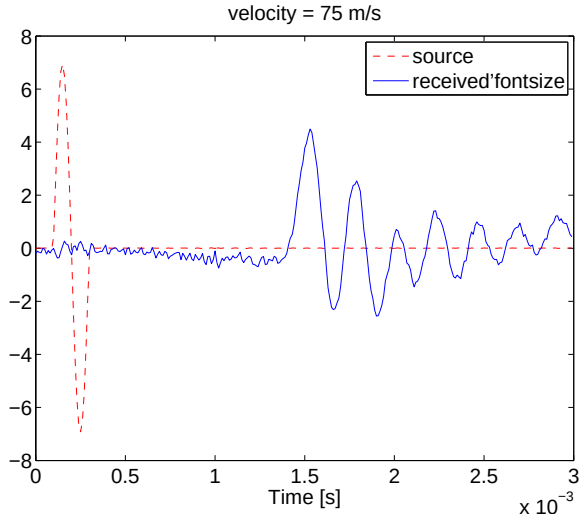

Figure 3.14: Shear wave at compression = 0 kPa

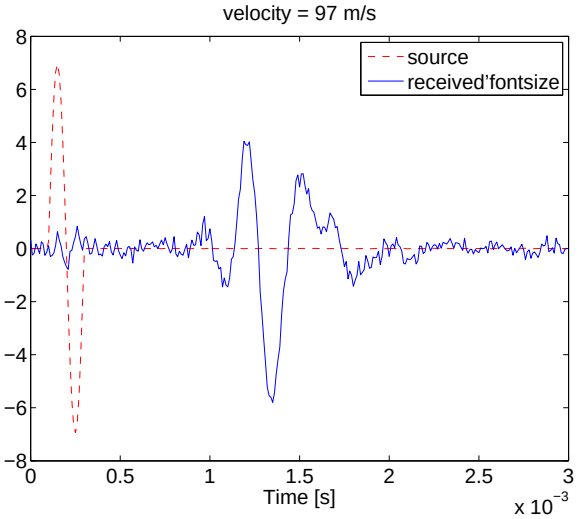

Figure 3.15: Shear wave at compression = 50 kPa

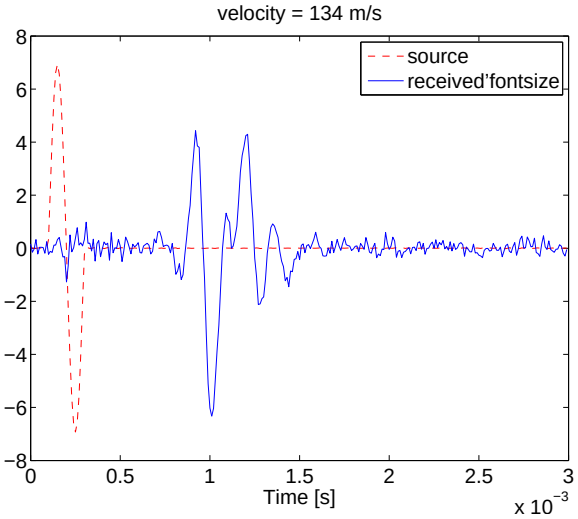

Figure 3.16: Shear wave at compression = 100 kPa

Knowing the shear wave velocity vs for different compression stages, the small-strain shear modulus G can be evaluated using the following equation:

$$vs = \sqrt{\frac{G}{\rho}} \tag{3.20}$$

where ρ is the mass density. Obtained results for confining pressure of 0kPa, 50kPa and 100kPa are summarized in Table 3.4. This confining pressure range corresponds to pressures applied during the experiment. The obtained values of the s-wave velocity are in the expected order for the tested material.

Table 3.4: Results of bender elements test on clay

Pressure [kPa]	Mass density [$\frac{kg}{m^3}$]	Velocity [m/s]	Shear Modulus [MPa]
0	2091.8	75	11.77
50	2233.5	97	21
100	2318.6	134	41.6

4. **Oedometer**

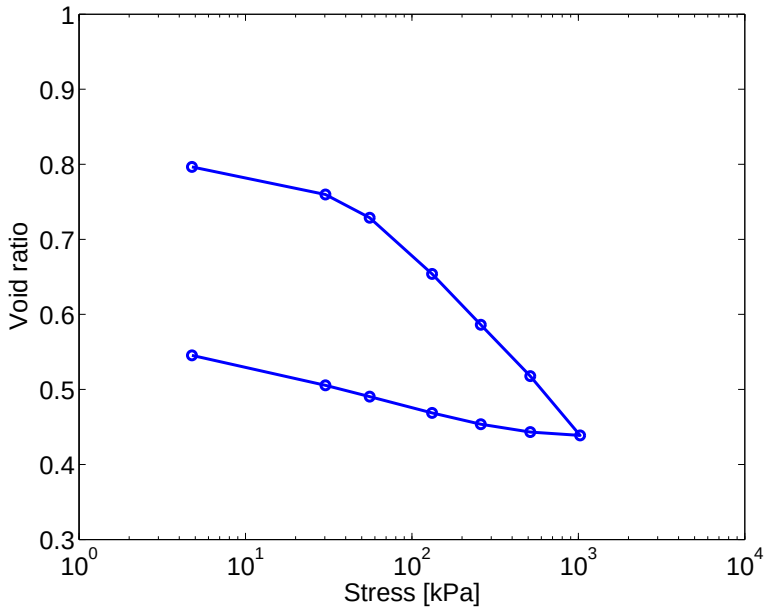

Figure 3.17: Oedometric path

Three oedometer tests were performed in a stress range visible from Figure 3.17, obtaining the following results:

$$Cc \approx 0.24 \tag{3.21}$$

$$Cs \approx 0.051 \tag{3.22}$$

$$\lambda = \frac{Cc}{ln(10)} \approx 0.105 \tag{3.23}$$

$$\kappa = \frac{Cs}{ln(10)} \approx 0.022 \tag{3.24}$$

$$pc \approx 40kPa \tag{3.25}$$

Figure 3.18 shows the oedometric stress-strain curve plotted in the same graph as the isotropic compression stress-strain curve. It is considered that the difference between the two paths is acceptable.

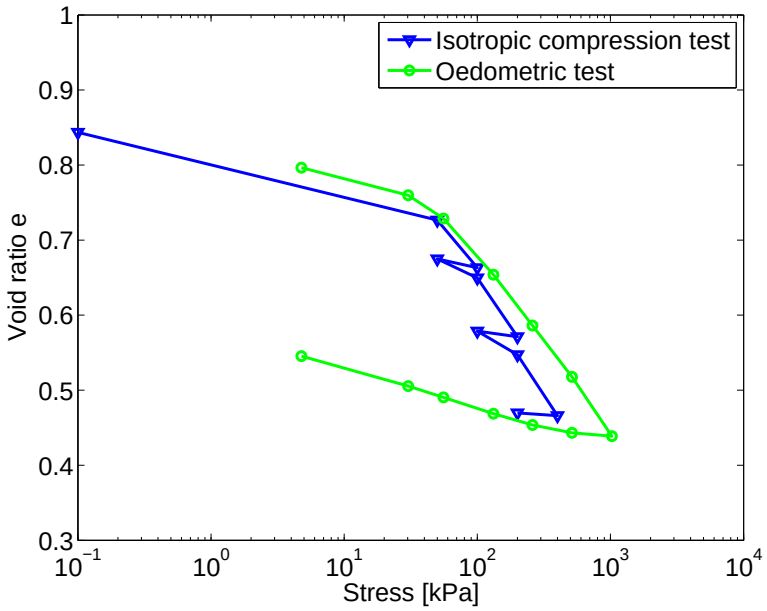

Figure 3.18: Isotropic compression and oedometric stress path

5. **Vane test, cone test**
   Vane tests and cone tests were performed on the clay samples in order to obtain undrained shear strength cu. The average water content w was evaluated.

$$cu \approx 17 - 21kPa \tag{3.26}$$

$$w \approx 0.30 \tag{3.27}$$

6. **Unconfined compression test**
   Unconfined compression test (Figure 3.19) was performed on clay samples with water content $w = 0.28$.

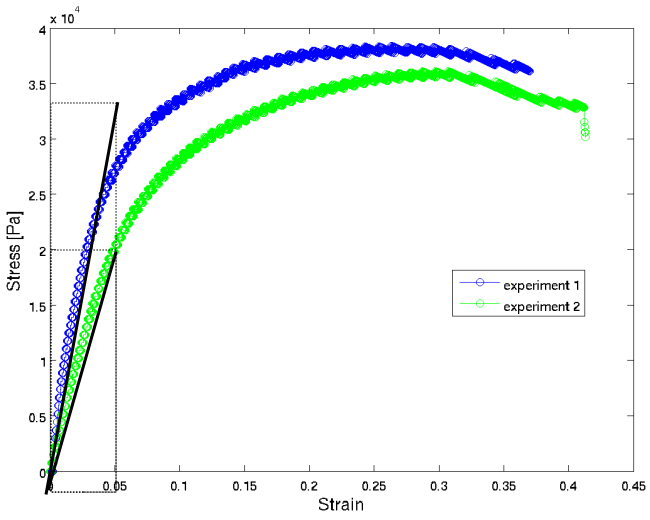

Figure 3.19: Unconfined compression of a clay sample

The obtained Young modulus E values are 0.44 MPa and 0.7 MPa. It is noted, that these values are valid for large strains and therefore no relation can be applied between the shear modulus G obtained from shear wave velocity measurements and the Young modulus E evaluated from the unconfined compression test. Undrained shear strength cu obtained based on number of unconfined compression tests is:

$$cu = \frac{1}{2}\sigma_{max} \approx 18kPa \tag{3.28}$$

7. **Shear box test - clay-aluminium interface**
In order to characterize the clay-pile and the clay-foundation interface, a specially adapted shear box apparatus was used (Figure 3.20). This apparatus consists of a shear box, containing a clay sample, which slides on a metal plate. For the purpose of the presented study, the plate was made of aluminium, because both, the pile and the foundation were designed in aluminium.

Figure 3.20: Shear box apparatus for testing clay-aluminium interface

Clay samples were sheared under different vertical stresses and different shear strain velocities. Consolidated and unconsolidated clay samples were used. A summarizing graph giving one common cohesion cu value of 3.7kPa and one friction angle ϕ value of $\phi = 6.6^o$ is shown in Figure 3.21.

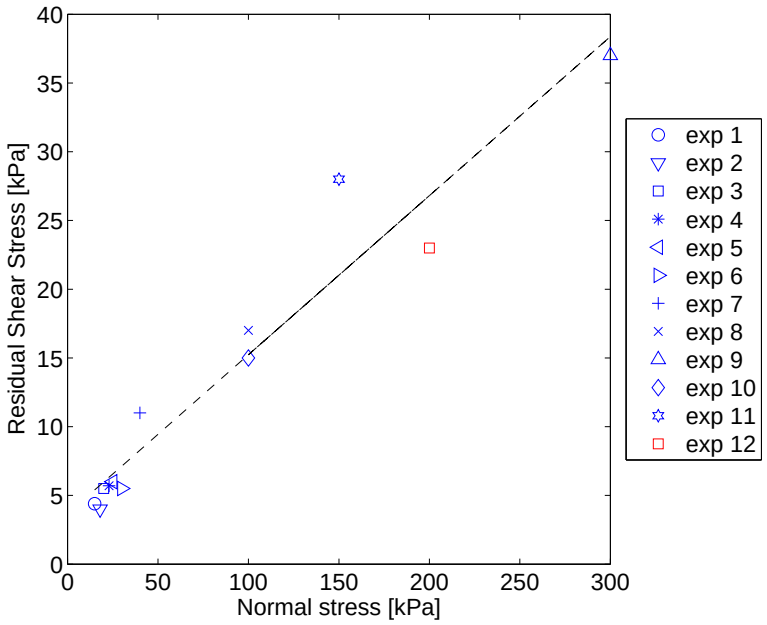

Figure 3.21: Results giving cohesion and friction angle characteristics of the clay-aluminium interface

Naming initial slope of the normal stress-displacement path k_n and initial slope of the shear stress-displacement path k_s, their values obtained from different experiments performed are listed in Table 3.5:

Table 3.5: k_s and k_n values obtained for different experiments performed

Consolidation	Velocity [mm/min]	Normal Stress [kPa]	kn [kPa/mm]	ks [kPa/mm]
No	0.2	15	85	36
No	0.2	18	77	27
No	0.2	20	70	75
No	0.2	23	161	33
No	0.2	25	59	44
No	0.2	30	207	72
No	0.002	100	241	99
No	0.002	150	507	198
No	0.002	200	434	128
Yes	0.02	300	662	389
No	0.02	40	357	108
No	0.02	100	179	212
No	0.02	300	459	375

Table 3.6 summarizes the clay and gravel characteristics.

Table 3.6: Clay and gravel characteristics based on laboratory experiments

	Clay	Gravel
Peak friction angle	-	56°
Residual friction angle	-	37°
Cohesion	18 kPa	-
Water content	0.3	-
Cc	0.27	-
Cs	0.06	-
λ	0.12	-
κ	0.03	-
pc	50 kPa	-
G at 0 confining pressure	12 MPa	-
G at 50 kPa confining pressure	21 MPa	-
G at 100 kPa confining pressure	42 MPa	-
Young's modulus	0.5 MPa	-

3.3.5 Monitoring and data acquisition system

The following section discusses main monitoring devices used. Force sensors and LVDTs are not mentioned because they were already described in section 3.3.1.

Strain gauges
Strain gauge measurements giving moments along the instrumented pile serve to obtain lateral soil reaction P, shear force T and deflection y of the pile. Because the listed strain derived physical values were obtained by derivating and integrating the moment curve along the pile, it is important to have as exact and 'smooth' strain measurements as possible. For this reason, it was decided to instrument the pile model with twenty levels of strain gauges with a measuring range of +/- 1500 μdef. Each level of gages consists of four individual gauges forming a Wheatstone configuration shown in Figure 3.22.

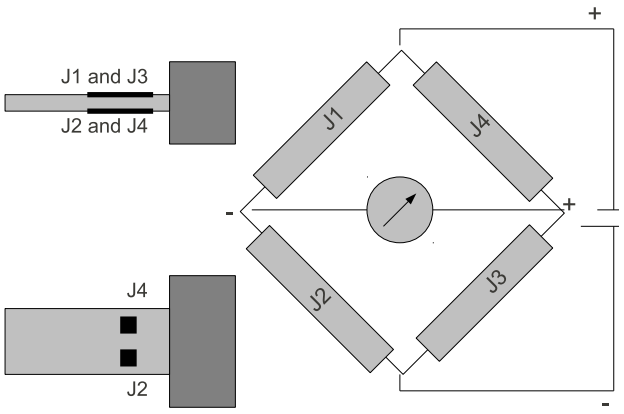

Figure 3.22: Strain gauge configuration used for the pile model

The Wheatstone bridge configuration is used to measure small variations in resistance R that the strain gauges produce, corresponding to a physical change of the surface that they are stuck on. When the gauges at the four sides of the bridge have their resistance changed to:

$$R1 + \Delta R1 \tag{3.29}$$

$$R2 + \Delta R2 \tag{3.30}$$

$$R3 + \Delta R3 \tag{3.31}$$

and

$$R4 + \Delta R4 \tag{3.32}$$

the bridge output voltage , e, becomes:

$$e = \frac{1}{4}(\frac{\Delta R1}{R1} - \frac{\Delta R2}{R2} + \frac{\Delta R3}{R3} - \frac{\Delta R4}{R4})E \tag{3.33}$$

where E is the input voltage. Introducing a strain gage factor K, equation 3.33 can be rewritten as:

$$e = \frac{1}{4}K(\epsilon 1 - \epsilon 2 + \epsilon 3 - \epsilon 4)E \tag{3.34}$$

Two strain gages from the Wheatstone bridge are mounted in the direction of bending strain on one side of the pile model; the other two are mounted on the opposite side of the pile model (i.e. in directions 'A' and 'B'; for reference see Chapter 5). This strain gauge configuration is only sensitive to bending strain but rejects axial strain. Used strain gages have an electrical resistance of 350 Ohm. More details on the technical characteristics and the set-up are listed in Annex A. Conditioners of type *Sensorex 9300 and 9350* were used.

Accelerometers
The aim was to monitor acceleration at the foundation surface and to compare it to acceleration measured at the pile head. To do that, two accelerometers were used in the experimental set-up. One was fixed to the foundation surface and the second was fixed to the pile head.

1. Accelerometer at the pile head: For space limitations, a miniature accelerometer PCB 356A01 was chosen to be used. This triaxial accelerometer monitors vibrations in three *x-y-z* perpendicular axes has a wide frequency range up to 8kHz. A compatible conditioner of type *482C15* was purchased. The exact accelerometer position at the pile head is graphically described in Annex A.

Figure 3.23: Accelerometer at the pile head

2. Accelerometer at the foundation level: An accelerometer *Bruel and Kjaer* of type *4379* was fixed from the top of the foundation. It was connected to a compatible conditioner *Isotron type 4416B*.

Force sensors
It was desired to determine vertical stress distribution inside the stone columns and at the pile head. For this reason, 3 force sensors of type BC303 (Figure 3.24a), with a capacity of 350kg and dimensions plotted in Figure 3.24b were used.

(a) (b)

Figure 3.24: Force sensors used in the experimental set-up

Mechanical adaptations were carried out in order to enable the desired force measurements:

- The force sensors are designed in a way that they measure force applied to a small round plate of 3mm in diameter which is placed in the center of the force sensor (Figure 3.24b). Because this surface was not sufficient compared to the grain size of gravel, there had to be a transition of force from a bigger surface to the small surface. This was done by

placing the sensors in a cover (Figure 3.25), where the small surface of 3mm in diameter was in a direct contact with the rigid cover. Therefore, all normal forces applied to the cover could be measured by the force sensors. The cover was, at first, made of steel. Experience showed that it become wedged in place through a drawer jamming effect and therefore gave wrong measurements. For this reason, the cap material was changed to teflon.

Figure 3.25: Metal cover in which is placed the force sensor

- Force measurements, made with the configuration described before, suggested that the transition surface of the cover is still not large enough, compared to the gravel grain size. Therefore a metal plate of a same diameter as the stone columns, was fixed on the metal cap. In this way, by introducing such a 'load transition surface', vertical force applied to the whole stone column could be measured.

It is noted that neither accelerometer measurements nor force sensor measurements were used in the final result evaluation. This is described in more detail in section 5.7.

Acquisition system and control system
The acquisition and the control system was entirely designed and prepared by a technical support of 3SR-Lab. Two high-speed data acquisition cards of type *National Instruments USB 6259* were used, allowing sufficiently fast data acquisition which was needed for performing experiments in dynamic domain. A control system was created in LabVIEW design platform with visual programming language.

3.4 Experimental Procedure

3.4.1 Clay installation

The aim was to have a clay soil mass which was as homogeneous as possible, while ensuring a good contact between the piles representing the rigid inclusions and the clay. The clay came in blocs of rectangular prism shape, which were installed, one by one, into the 'VisuCuve'. A wire was used to cut sides of the blocks in order to make them smoother and so the surfaces of two adjacent blocks would be in a better contact. Water was sprayed on the clay to ensure that the blocks stick together. A special care was taken while installing the clay around the

physical model. While installing the clay around the piles, numerous procedures were tried in order to find the best one. It was desired to create a good contact between the clay and the pile and at the same time avoid too much deformation of the pile. The final procedure consisted of careful 'pottery-like' sculpting of clay around the piles (Figure 3.26a).
Because it would have been too much time consuming emptying the whole 'VisuCuve' after each experiment, it was decided to replace only the flexible part of the model (i.e. LTP or LTCs surrounded by clay) and a top layer of clay with each experiment carried out. The clay was removed down to a depth of 20cm from the pile head (Figure 3.26d). This depth was determined according to the experimental results which showed that most of the pile deformation occurred at the upper 20cm of the pile. After removing this part of soil, the clay and gravel installation procedure was once more repeated for the missing part of soil.
Photos describing the installation procedure are shown in the following figures.

(a)

(b)

(c)

(d)

Figure 3.26: The clay installation procedure

3.4.2 Load Transfer Column (LTC) and Load Transfer Platform (LTP) installation

3.4.2.1 LTC installation

The upper flexible part made of the LTCs surrounded by clay consisted of four columns made of gravel which were installed in clay. The column installation procedure can be divided into several steps:

1. After installing the clay up to the top edge of the funnels, each funnel was covered with a geotextile. A clay layer was then added, reaching a desired thickness. This thickness corresponds to the planed stone column height (i.e. 5cm, 8cm or 10cm).
2. Taking a core drill of 70mm in diameter, a hole was made above the funnels. To arrive precisely onto the funnel tops, a PVC pattern, designed for this purpose, was used as a guide to the core drill (Figure 3.27a). The clay from the core drill was then taken out and so was the geotextile at the top of the funnels.
3. The core drill was once more introduced into the hole.
4. The core drill was filled with a predefined amount of gravel. This gravel was then compacted during a predefined amount of time, while the core drill was slowly being pulled up. As a consequence, the gravel penetrated into the surrounding clay. This stage was repeated until the stone column was formed. The final diameter was due to the gravel penetration into the clay higher than the the core drill diameter. This was planned, since it was desired to reach a stone column diameter of 90mm. The finished stone columns with the surrounding clay are shown in Figure 3.27b.

(a) (b)

Figure 3.27: Installation procedure of the Load Transfer Columns surrounded by clay

3.4.2.2 LTP installation

The upper flexible part made of the LTP consisted of a gravel mattress covering the whole surface of the clay. The gravel mattress installation procedure was not as long and difficult

as the column installation. After installing the clay up to the top edge of the funnels, a gravel layer was added on top of the clay. The gravel layer thickness was either 5cm, 8cm or 10cm, depending on the experiment planned. The gravel was then compacted with a flat, wooden tool. It was found, that the gravel compaction was difficult, having such a big surface. Therefore a metal pattern was used to compact the gravel around the physical model. Then the rest of the gravel was added on the external side of the metal pattern and compacted. The metal piece was then pulled out. Photos from the mattress installation procedure are shown in Figure 3.28.

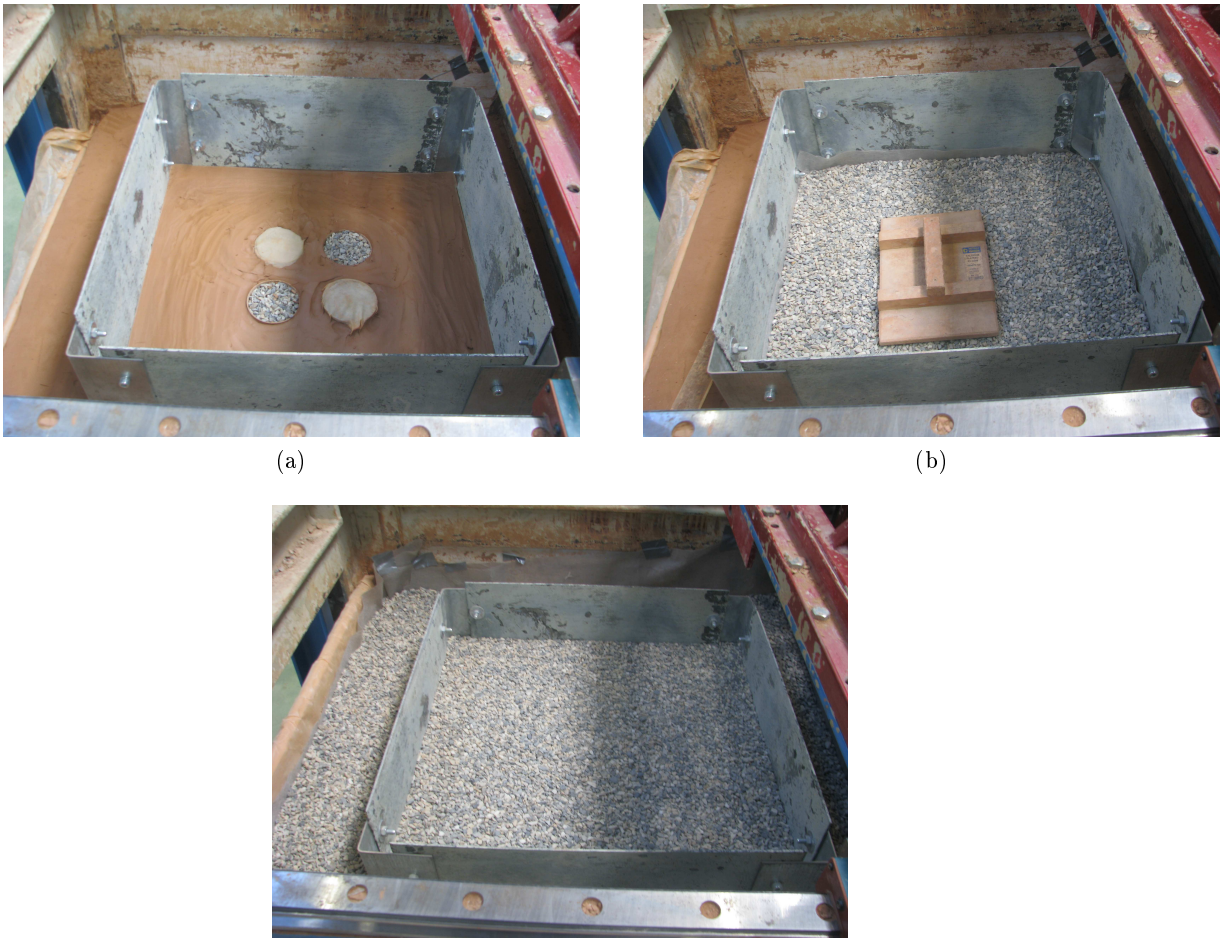

(a) (b)

(c)

Figure 3.28: Installation procedure of the Load Transfer Platform

3.5 Experimental Program

3.5.1 Preliminary experiments

1. **Experiments in the 'small tank'**
   The aim of these experiments was to obtain data characterizing the behaviour of the physical models under horizontal loading. Effort was made to simulate the conditions comparable to the conditions in the 'VisuCuve' in order to measure response of the models which would represent the range of data expected for experiments in the 'Visu-

Cuve'. Having knowledge of expected stress-strain conditions within different parts of the models helped to design a monitoring system for future experiments in the VisuCuve.

Experimental device: A physical model of a rigid inclusion associated to a LTC (Figure 3.29a) was placed in a radial tank and surrounded by clay. The clay used was identical to clay used for experiments in the 'VisuCuve'. Radial foundation, partly embedded in clay (Figure 3.29b), was installed directly on the LTC and was subjected to horizontal cyclic loading. The response of the model to this horizontal and vertical loading (vertical loading applied by weight of the foundation; 5,5kg) was measured by 10 levels of strain gauges located along the rigid inclusion (Figure 3.29c).

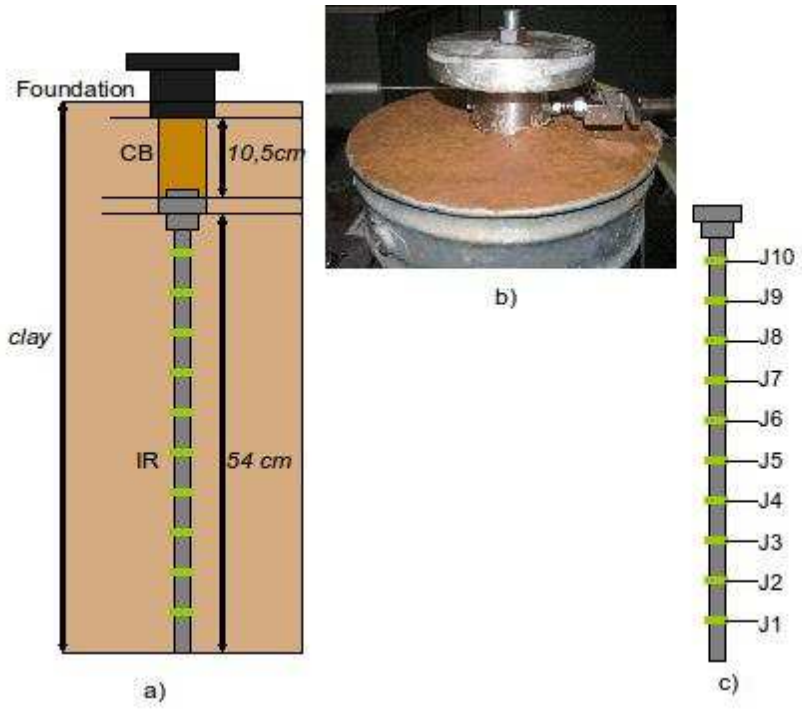

Figure 3.29: a) Experimental model of a rigid inclusion associated to a LTC; b) Foundation model embedded in clay; c) Rigid inclusion model equipped with 10 levels of strain gages numbered from 1 to 10

Loading device: To impose horizontal loading, a horizontal actuator of type SKF (Figure 3.30a) was used. This actuator was previously used in a study of soil-pipeline interaction (Orozco, 2009). Modifications of the acquisition and control system had to be made. LabVIEW (short for Laboratory Virtual Instrumentation Engineering Workbench) system was implemented.

Experimental program: Horizontal cyclic loading was applied to the foundation model in cycles with 2.5mm amplitude. Frequency and number of cycles was varied.

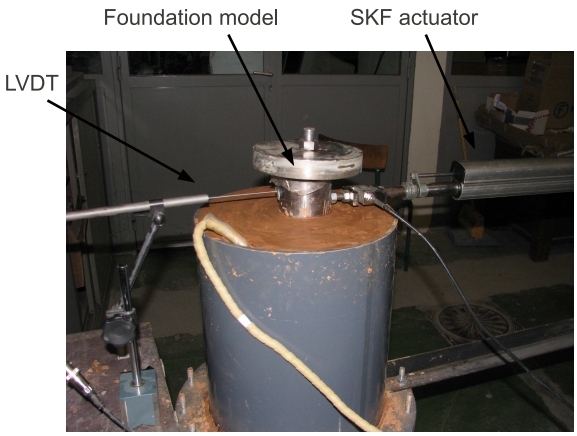

(a)

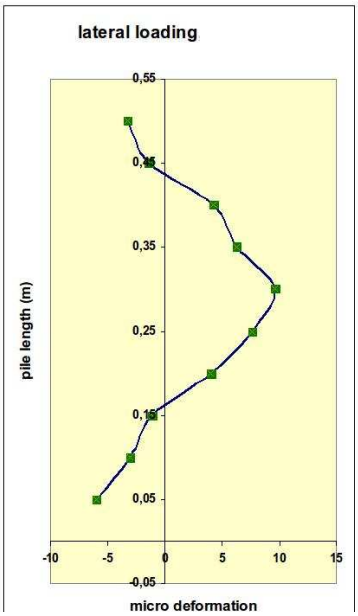

(b)

Figure 3.30: Preliminary experiments carried out in a 'small tank' (a) providing results (b) on expected range of data for future experiments in the 'VisuCuve'

Results and conclusions: For known loading conditions, lateral pile behaviour was obtained. An example of measured strain along the pile is shown in Figure 3.30b. Having such results, a method of data evaluation could be tested. Fitting the experimental data with a polynomial, integrating and derivating moment curves along the pile allowed testing of such procedures. These were then routinised, thus permitted more efficient final data evaluation.
The described series of preliminary experiments was carried out in order to obtain limited information on the system behaviour under horizontal cyclic loading. Even though these experiments did not provide valuable results, they were necessary and very important in terms of monitoring system design and definition of the final experimental program. The final pile models were designed with reference to the pile behaviour during the preliminary experiments. Since the expected range of strain within the pile was known, strain gauge types could be chosen for the final pile model. Problems experienced during these preliminary experiments allowed to prevent the same problems in the final experimental program.

2. **Experiments measuring pile response without the surrounding soil - area moment of inertia calibration.**
Once the piles were installed in the 'VisuCuve', two experiments (ESSAI PREM 1, ESSAI PREM 2) were carried out in order to study lateral pile response without interference of the surrounding soil (Figure 3.31). The measured pile response was compared to the analytically calculated pile response and served to calibrate a value of area moment of inertia. The difficulty of determining the area moment of inertia analytically was the fact, that the instrumented pile had grooving in its surface and the strain gauges were covered by a protective layer of unknown properties. While performing these experiments, influence of the horizontal actuator on different sensors was examined.

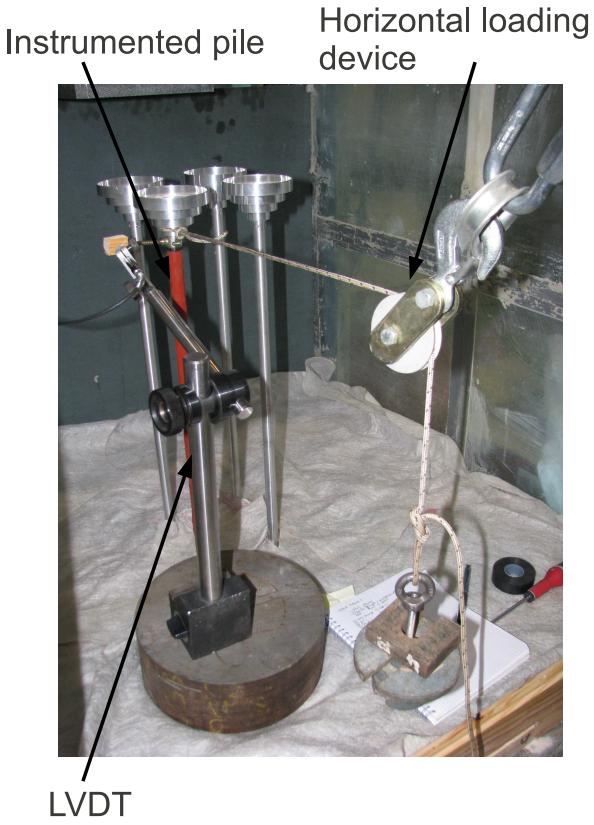

Figure 3.31: Pile lateral behaviour without interference of the surrounding soil

3. **Experiments testing the soil installation procedure:**
   In order to study lateral pile-soil interaction, care was taken while installing the clay around the pile. Numerous methods of clay installation were tested, defining a final installation procedure described in section 3.4.1. This, as well as the clay mass preparation, was done within the scope of a master thesis within the Lab 3SR (Cofone, 2010).

4. **Experiments leading to horizontal and vertical bearing capacity of clay and soil reinforced by piles associated to LTCs surrounded by clay.**
   Once the clay mass was installed in the 'VisuCuve', the foundation model was used to determine the bearing capacity. The same was done for the reinforced soil. A 'swipe test' was used to define the yield surface for the foundation on clay and on the soil reinforced by piles associated to LTCs surrounded by clay. The swipe test uses a procedure when at a given vertical load, the footing is moved horizontally while the vertical penetration is held constant (Byrne and Houlsby, 2001). This is graphically shown in Figure 3.32. Table 3.7 lists experiments carried out in order to study vertical and horizontal bearing capacity of the clay and the reinforced clay.

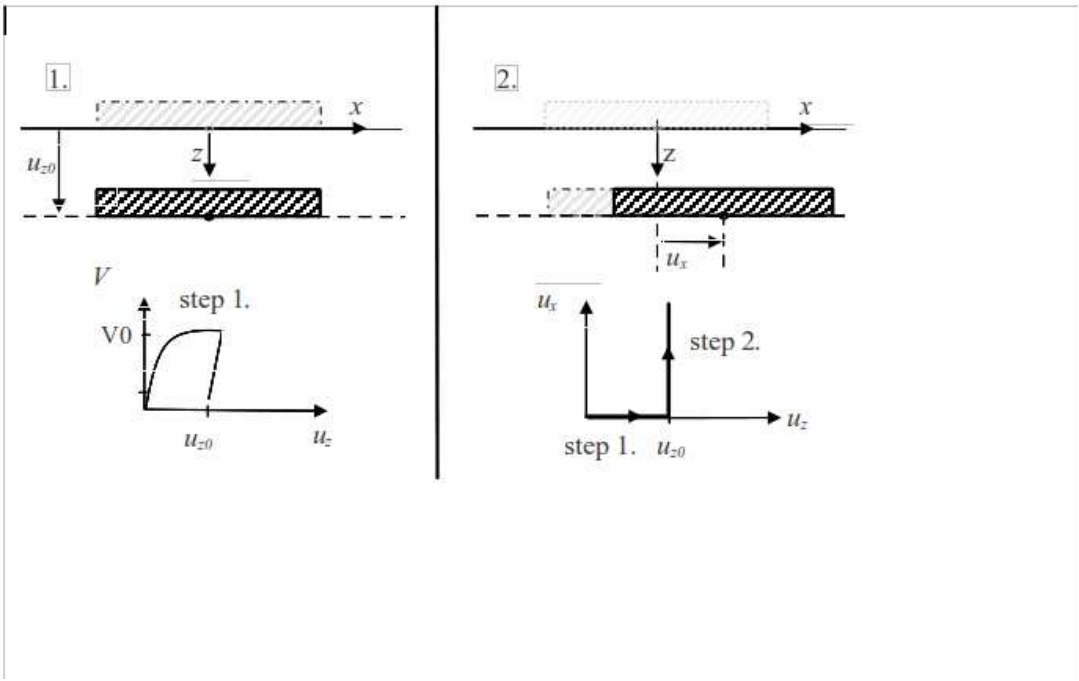

Figure 3.32: Swipe test, after (Grange, 2008)

Table 3.7: Preliminary experiments in the 'VisuCuve' - Bearing capacity determination

Experiment	Soil type	Purpose
LTC1	Clay reinforced by piles associated to 10cm high LTCs	Determining vertical bearing capacity
LTC5	Clay reinforced by piles associated to 8cm high LTCs	Determining vertical and horizontal bearing capacity - swipe test
LTC9	Clay reinforced by piles associated to 5cm high LTCs	Determining vertical and horizontal bearing capacity - swipe test
clay1	Clay	Determining vertical and horizontal bearing capacity - swipe test

5. **Experiments testing the loading device** The vertical and horizontal loading devices were not compatible. While the horizontal actuator applied dynamic loading, the vertical actuator, designed to work in static conditions, had to keep constant vertical load. As the foundation model settled under the horizontal dynamic loading, vertical actuator had to 'keep up' with this settlement and react by increasing the vertical load applied. This was a problem, since the vertical actuator was not fast enough to adjust the vertical load in order to keep it constant. Therefore the experimental program had

to be planned so the loading created such foundation settlements that would allow the vertical actuator to react in time. In order to find an experimental program suitable for the purpose of study and, at the same time, possible to realize with the loading devices, number of experiments had to be performed. Based on these experiments, a final experimental program was determined.

3.5.2 Dynamic experiments in the 'VisuCuve'

This section presents experimental program for experiments carried out in the 'VisuCuve'. The aim was to study by the reduced scale physical models the behaviour of the reinforced soil subjected to inertial loading. This kind of loading conditions, in reality, can be found during earthquakes or during wind and water impacts on structures. The experimental program was designed to simulate these loading conditions, taking into consideration limitations of the experimental set-up.

It is possible to divide the experimental program in two main phases.

1. Application of vertical static load; Force controlled

2. Application of horizontal dynamic load; Displacement controlled

The experimental set-up allowed application of static load that in reality represents weight of a superstructure. This static load was applied to the foundation model by a vertical actuator. The load was transmitted by the shallow foundation on the reinforced soil. The static vertical load was applied in 5 separate steps, reaching a maximum load of 5000 N, which is considered to be approximately 1/3 of the bearing capacity of the reinforced soil. This value of the ultimate bearing capacity was evaluated experimentally. After imposing each step of vertical load, the load was held constant in order to leave the clay massif to consolidate. The experimental device was designed to apply a horizontal dynamic load that in reality simulates a seismic event or a wind/water loading. The horizontal load was applied by a horizontal actuator connected to a trolley, which was carrying the foundation model. The horizontal dynamic loading was applied after the static consolidation, having an amplitude of +/-2mm and a frequency of 2.7Hz. During both loading stages, the performance of the physical model was monitored. Experiments performed under the described experimental program, or with minor modifications, are listed in Table 3.8. Modifications to the described experimental program were made mainly at the beginning, when the limitations of the experimental device were appearing.

Table 3.8: Summary of the experiments performed in the 'VisuCuve'

Experiment	LTC/LTP Height	Modifications to the experimental program
LTC1	10cm	Soil loaded by vertical static load to its bearing capacity; horizontal amplitude +/-5mm
LTC2	10cm	Vertical load applied in one stage
LTC3	8cm	Vertical load applied in one stage
LTC4	5cm	Vertical load applied in one stage
LTC5	8cm	Swipe test
LTC6	8cm	Vertical load applied in one stage
LTC7	8cm	Vertical load applied in one stage
LTC8	8cm	Vertical load applied in one stage
LTC9a	5cm	-
LTC9b	5cm	Swipe test
LTC10	10cm	-
LTC11	8cm	-
LTC12	8cm	Horizontal loading started in the opposite direction
LTC13	10cm	-
LTC14	5cm	-
LTP1	5cm	-
LTP2	8cm	-
LTP3	10cm	-
LTP4	5cm	-
LTP5	8cm	-
LTP6	10cm	-

3.6 Conclusion

The aim of this chapter was to present different aspects of the physical modelling performed in the reduced scale. Two different physical models of soil reinforcement are presented and their development and installation is described in detail. Soil surrounding this reinforcement is characterized by its mechanical properties, which were determined within the 3S-R Laboratory.

The experimental device 'VisuCuve' was created within the 3SR-Lab and was previously used for various studies. This device is described in detail and modifications made in order to adjust it to the current needs are mentioned.

The purpose of the experiments was to study the response of the reinforced soil to different types of loading - vertical static loading as well as loading simulating an inertial loading. The loading application as well as the monitoring system allowing to study the system response under various loading conditions are presented.

CHAPTER 4

Experimental Data Treatment

4.1 Introduction

A correct treatment of the obtained experimental data is essential and can eventually enable a proper understanding of the problem concerned. The following chapter describes the evaluation of the 'raw' data obtained from different sensors used in the experiments (section *Experimental Methodology/Monitoring*).

4.2 Physical Values Derived from Strain Gage Measurements

The pile was instrumented with twenty levels of strain gages. These strain gages were responding to bending of the pile, therefore the amount of strain measured was accounting only for flexural strain and no axial strain. The theoretical one dimensional elastic response of a material is according to Hooke's law:

$$\sigma = E * \epsilon \tag{4.1}$$

where E is the Young's modulus, ϵ is the strain and σ is the stress at the point of interest. Knowing the value of stress, the equation (4.2), which is based on Bernoulli's principle, is entered in order to obtain the value of bending moment M.

$$\sigma = M * \frac{r}{I} = r * E * \frac{d^2y}{dz^2} \tag{4.2}$$

Here, r is the distance from the neutral axis to a point of interest, y is the pile deflection

at position z and I is the area moment of inertia. The value of I was determined in the preliminary experiment described in section 3.5.1. Finally, knowing that

$$\frac{dM}{dz} + T = 0 \tag{4.3}$$

and

$$\frac{dT}{dz} + p = 0 \tag{4.4}$$

a set of equations having an important physical meaning is obtained:

$$p = -\frac{d^2M}{dz^2} \tag{4.5}$$

$$T = -\frac{dM}{dz} \tag{4.6}$$

$$\Theta = \int M * dz \tag{4.7}$$

$$y = \frac{1}{E * I} \int (\int M.dz).dz \tag{4.8}$$

where T is shear force, Θ is rotation and p is lateral pile resistance, all acting at one point of interest. The main difficulty in such an analysis is a correct interpolation of moment data along the pile length. This was done with a polynomial function of sixth degree, which was found to fit best the data concerned. An example of such a fit is shown in Figure 4.1. This approach, when the data are fitted with a polynomial function, allows a simple and time effective derivation and integration of the measured data.

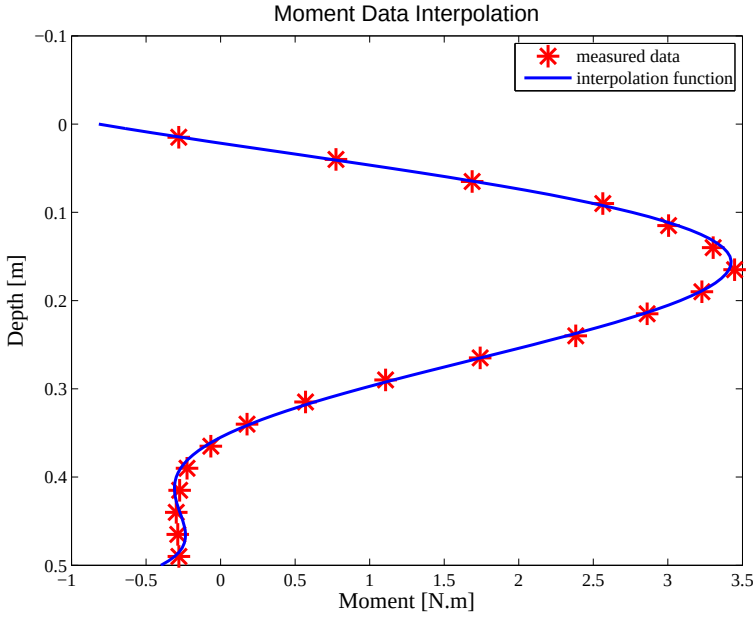

Figure 4.1: Interpolation function

Such a function was fitted to all time instants at which the data registration was done. This way, an evolution of moment along the pile was mathematically defined for all time instants. In order to perform a double integration of the polynomial functions, two integration constants were needed. These were obtained from setting the displacement and rotation at the pile toe to zero. This was considered as correct since the pile was firmly fixed at the 'VisuCuve' bottom. Having these two integration constants, each polynomial function was interpolated and derived in order to obtain the wanted physical values listed in equations (4.5) to (4.8).

4.3 Energy dissipation and stiffness evaluation

With industrial application of the studied soil reinforcement in seismically vulnerable sites comes a great deal of interest concerning the dynamic soil properties such as energy dissipation and damping ratio values. The following text summarizes the procedures which are used to analyse the energy dissipation and stiffness in different parts of the reinforced soil.
The physical model is horizontally divided into two parts, where each part is examined separately. The energy dissipation within the lower rigid part - represented by an aluminium pile and the surrounding clay, is obtained by the shear force T, lateral soil reaction P and deflection y data analysis. The second, upper flexible part of the physical models consists of LTP or LTCs surrounded by clay. Energy transfer within this part of the models is evaluated from the horizontal force and displacement measurements at the foundation level, comparing these to the shear force and deflection registered at the pile head. The hysteresis loops created serve to define the system stiffness. Knowing that global energy dissipated at the foundation level is in relation to the energy dissipated in the different parts of the physical model, a simplified rheological model is introduced to illustrate the energy balance in the reinforced soil.

4.3.1 Global energy dissipation

The experimental results showed that a relation between the cyclic horizontal displacement u of the shallow foundation and the horizontal force H acting on this foundation can be graphically shown as a hysteresis loop. If there would be no damping taking place, this force and the displacement would be in phase and proportional to each other and therefore the stress-strain relationship would have a completely reversible elastic evolution. When the viscous damping coefficient has a non-zero value, the hysteresis loop has an elliptical shape (Figure 4.2). This hysteresis loop is commonly used to describe the energy loss mechanism which is also called a damping mechanism. The shape, size and inclination of this loop depends on the energy dissipated in one cycle, energy stored in the system during one cycle and the stiffness of the system. Therefore, the desired dissipation, damping and stiffness values could be obtained from these hysteresis loops in the following way:

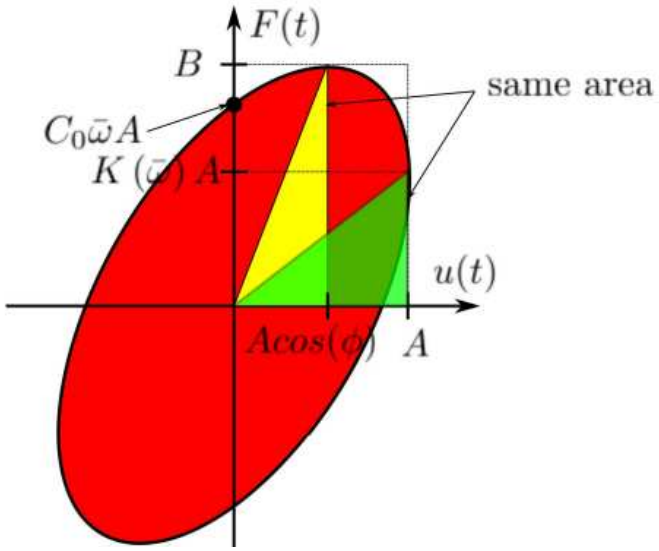

Figure 4.2: Hysteresis Loop, after (Grange, 2008)

$$Wd = \int_a^b F \frac{du}{dt} dt \tag{4.9}$$

$$a = t_0 \tag{4.10}$$

$$b = t_0 + \frac{2\pi}{\omega} \tag{4.11}$$

where Wd is the dissipated energy and ω is the angular frequency of the displacement signal. Because Wd corresponds to the area of the hysteresis loops, the integration is done over one cycle, setting the integration limits a and b. Referring to the Figure 4.2, the elastic strain energy Ws stored during one cycle and the system stiffness k $[N/m]$ is obtained by

$$Ws = A.B.\pi cos(\phi) \tag{4.12}$$

$$k = B/A.cos(\phi) \tag{4.13}$$

where Ws represents the area of the triangle shown in Figure 4.2. Having the values of Ws and Wd, the damping ratio ξ can be calculated:

$$\xi = \frac{Wd}{4\pi Ws} \tag{4.14}$$

Global energy loss is a result of energy loss in different mechanisms happening under the dynamic loading within the physical model. Since the physical model used is complex, simplifications cannot be prevented while analysing its behaviour in the context of energy conservation. In order to understand different relations between the dynamic soil characteristics

obtained for different parts of the physical model, a simplified rheological model based on the experimental result analysis is introduced in section 5.6.3.

4.3.2 Energy Dissipation within the flexible part of the model

Wanting to define the energy transfer within the flexible part of the physical models, two methods of energy loss evaluation are used in order to increase the reliability of obtained results.

4.3.2.1 Hysteresis loop based procedure

A relation between horizontal force H applied at the top of the stone column/mattress and the difference between the pile head and foundation horizontal displacement ΔU (i.e. u-y according to Figure 4.3) can be graphically shown as a hysteresis loop (see section 4.3.1). The desired dissipation, damping and stiffness values could be obtained from these hysteresis loops by applying equations (4.9)-(4.14).
In order to evaluate the stiffness of the flexible part of the model, it is noted that indeed, a relation between the force H and the displacement ΔU should be considered. The force H-T, T being the force applied at the pile head, is a force transferred from the foundation to the surrounding soil and to the soil around the rigid inclusion (see Figure 4.3).

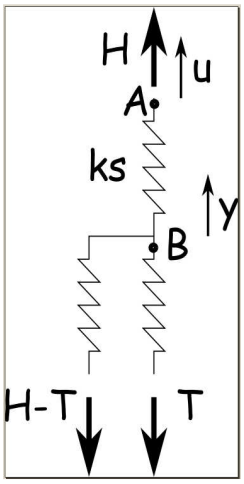

Figure 4.3: Evaluation of energy dissipation within the flexible part of the model, after S. Grange

4.3.2.2 Frequency response model

Introducing the horizontal force H applied at the foundation level as an input and the difference ΔU of displacements between the foundation level and the pile head as output, one can relate these two by the following relation:

$$\Delta U(\omega) = \chi(\omega) * H(\omega) \tag{4.15}$$

where U(ω) is the input and H(ω) is the output represented in a frequency domain. $\chi(\omega)$ is called a frequency response function or also a transfer function and once obtained, it can be represented as a complex number, having a real and an imaginary component:

$$Re(\chi(\omega)) = k(\omega) \tag{4.16}$$

$$Im(\chi(\omega)) = c(\omega) \tag{4.17}$$

where k is stiffness in [N.m] and c is a damping coefficient in [N. m/s]. Plotting the transfer function in a complex plane (i.e. Argand plane), an angle between the real axis and the complex number can be expressed as

$$\phi(\omega) = Arg(\chi(\omega)) = Arctan\frac{c(\omega)}{k(\omega)} \tag{4.18}$$

Having ϕ, the damping ratio can be obtained:

$$\xi = \frac{tan\phi}{2} \tag{4.19}$$

4.3.3 Energy Dissipation within the rigid part of the model

The energy dissipation in the rigid part of the model is said to be due to the interaction between the elastic pile model and the soil. The elastic energy produced under the pile solicitation is transferred to the soil, which can plastify. This plastification is assumed to be the cause of the energy dissipation. The lateral pile-soil interaction under dynamic conditions is described by a governing equation for the dynamics of an Euler-Bernoulli beam:

$$\frac{\delta^2}{\delta z^2}(E.I\frac{\delta^2 y}{\delta z^2}) = -\mu\frac{\delta^2 y}{\delta t^2} + p(z) \tag{4.20}$$

where z is the position along the pile [m], y is the deflection at a certain point [m], p is the external load [N/m], μ is the mass per unit length [kg/m], E is the pile Young's modulus [Pa] and I is the area moment of inertia [m^4]. Rewriting the previous equation,

$$\frac{\delta^2 M}{\delta z^2} = -\mu.\ddot{y} + p(z) \tag{4.21}$$

where the time derivations are denoted with a 'dot' superscript in order to distinguish them from the spatial derivations. Therefore $\ddot{y}$ stands for a second derivative of displacement with respect to time (i.e. the acceleration [m/s^2]). In the context of energy conservation, equation

(4.21) can be rewritten in terms of work, that is equal to the force acting on an object times its displacement. This power equation can be expressed as

$$\int_0^L p.\dot{y}.dz = \int_0^L \mu.\ddot{y}.\dot{y}.dz + \int_0^L E.I.\frac{d^4y}{dz^4}.\dot{y}.dz \tag{4.22}$$

where pile length is 0 to L. Rewriting p as a derivative of shear force T with respect to z and integrating this left term of equation (4.22) by parts, equation (4.23) is obtained. To do this, it is considered that the displacement, as well as its first and second derivative with respect to time, are equal to zero at the pile toe. This can be done since the pile model is firmly fixed at its base.

$$T(L).\dot{y}(L) - \int_0^L T.\frac{d\dot{y}}{dz}.dz = \mu \int_0^L \ddot{y}.\dot{y}.dz + \int_0^L p.\dot{y}.dz \tag{4.23}$$

Rewriting T as a derivative of moment M with respect to z and integrating this term by parts, eq (4.24) is obtained.

$$T(L).\dot{y}(L) - M(L).\frac{d\dot{y}(L)}{dz} - \int_0^L M.\frac{d^2\dot{y}}{dz^2}.dz = \int_0^L p.\dot{y}.dz + \frac{\mu}{2}.\frac{d}{dt}\int_0^L \dot{y}^2.dz \tag{4.24}$$

Integrating each term of equation (4.24) over one cycle, the power equation gains the following form

$$\int_{t=0}^{t=1cycle} [T(l).\dot{y}(L) - M(L)\frac{\dot{y}(L)}{dz}]dt = \int_{t=0}^{t=1cycle} [\int_0^L p.\dot{y}.dz]dt \tag{4.25}$$

It can be noticed that the two last terms on both sides of equation (4.24) disappeared, which is due to the fact that the pile model is assumed to behave elastically. Moreover, plotting a rotation against a moment at the pile head shows linear elastic behaviour and therefore no energy loss due to the pile rotation occurs. This finally yields the final power equation used in the energy dissipation analysis for the system pile-soil.

$$\int_{t=0}^{t=1cycle} T(l).\dot{y}(L).dt = \int_{t=0}^{t=1cycle} [\int_0^L p.\dot{y}.dz]dt \tag{4.26}$$

Equation (4.26) shows two possible ways of evaluating energy dissipation at the pile head:

1. Analysing T-y loops at the pile head, where T and y stand for shear force and displacement respectively. The T-y loops are treated as hysteresis loops (section 4.3.1) and therefore each cycle can be analysed for damping ratio, stiffness, dissipated and accumulated energy.

2. Analysing p-y loops and integrating along the pile. This procedure consists of pile discretization along its length and plotting p-y loops for each vertical position. P-y loops are then approximated by an ellipse and are treated as hysteresis loops (section 4.3.1), where each cycle can be analysed for damping ratio, stiffness, dissipated and accumulated energy. In order to obtain a global behaviour of the pile-soil system, global energy dissipation Wd_r and global energy accumulation Wa_r need to be obtained. For each cycle n, Wd_r and Wa_r are calculated as follows:

$$Wd_r = A_z.dz \tag{4.27}$$

$$Wa_r = \frac{1}{2}\int_0^H \frac{M^2}{E.I}.dz \tag{4.28}$$

where A is area of a loop at each vertical position z, dz is the distance between two vertical positions, E is the Young's modulus, I is the second moment of inertia, M is the maximal moment reached during the cycle considered and H is the pile length.

Once Wd_r and Wa_r are obtained, the damping ratio ξ_r can be calculated:

$$\xi_r = \frac{Wd_r}{4.\pi.Wa_r} \tag{4.29}$$

These two methods give similar results, although some uncertainty comes from discrete integration used in the second method.

4.4 Conclusion

Physical modelling of the reinforced soil response to different loading conditions provided monitoring data, which had to be subsequently treated and analysed in order to conclude on the system behaviour. The data analysis provided results on the foundation settlement and its horizontal response to the applied loading as well as on the lateral performance of the rigid inclusions in terms of bending moment, shear stress and deflection. Knowing the response of the rigid inclusions, behaviour of the flexible part of the models could be deduced. Energy dissipation within different parts of the model was analysed in order to evaluate the performance of the reinforced soil under seismic conditions.

CHAPTER 5

Analysis of Experimental Results

5.1 Introduction

Based on the procedures introduced in section 4, experimental data were treated in order to enable and facilitate subsequent data analysis, giving the results introduced in this chapter. The pile response served to analyse the role of the flexible part of the physical models. In order to avoid interpretation mistakes due to initial pile deflection caused by clay and gravel installation, this phenomenon was examined and results are presented at the beginning of the chapter.
The aim was to study the behaviour of the two configurations of soil reinforcement:

1. Piles associated to Load Transfer Column (LTC)
2. Piles associated to Load Transfer Platform (LTP)

Attention is given mainly to the pile lateral performance and the foundation settlement. The effect of combined static vertical and horizontal loading applied to the foundation model is then studied and a failure envelope is constructed. A comparison is made between the failure envelope obtained experimentally and its analytical description. Since the studied system of the soil reinforcement technologies is widely used in seismic zone areas, the main section of chapter 5 presents the effect of combined vertical static and horizontal dynamic loading on the reinforced soil. A parametric study is presented, where gravel column/mattress height/thickness is varied (Figure 5.2a) in order to see its influence on lateral pile performance and foundation settlement.

The experimental models (Figure 5.1) are composed of four rigid inclusions surrounded by clay, which are associated to a gravel column (LTC) or a gravel mattress (LTP). The reinforced soil

is subjected to vertical and horizontal loading applied by a foundation model. Behaviour of both physical models under different loading conditions is monitored. Lateral pile behaviour is studied in terms of bending moments M, deflection y, lateral soil reaction P and shear force T. These data were obtained from strain gage measurements along the pile (Figure 5.2b) which were expressed in terms of bending moment as a function of depth. The sign convention is based on relations introduced in 4, which are reminded:

$$EI.\frac{d^2y(z)}{dz^2} = M(z) \tag{5.1}$$

where M is the bending moment, EI is the pile bending stiffness, z is the depth and y is the displacement of the pile neutral axes. This displacement can be expressed in a form

$$y(z) = \frac{1}{E_pI_p}\int_0^z (\int_0^u M(t)dt)du + C_1z + C_2 \tag{5.2}$$

with C_1 and C_2 being the integration constants. Shear force T and lateral soil reaction p can be expressed as:

$$T(z) = -\frac{dM(z)}{dz} \tag{5.3}$$

$$p(z) = -\frac{d^2M(z)}{dz^2} \tag{5.4}$$

Such a data treatment provides P-y curves, which are presented in the following text. Observations are made on their dependence on depth, number of cycles and stone column/mattress height. Attention is given to analysing dissipation of energy coming from the foundation dynamic movement. Energy dissipation within the different parts of the physical model is analysed independently and conclusions are made on the coupled mechanism. Load Transfer Columns (LTCs) and Load Transfer Platform (LTP) are compared in terms of static and seismic response. Each experiment was repeated at least twice to verify the reliability of the obtained results. For the sake of readability, not all experimental results are presented in the following text and are placed in Annex B.

The reduced physical models presented in this work are submitted to a normal gravity '$g* = 1$' and the conditions for a rigorous similitude with respect to the stress level '$\sigma* = 1$' are not fulfilled. Even though the scaling laws are not strictly respected, the main objective of the physical modelling was to perform a qualitative study of the presented soil reinforcement, studying the behaviour of the two physical models under combined loading and comparing their performance in terms of seismic response. Using the results obtained, a 1/10 numerical model was calibrated in order to reproduce similar results as obtained experimentally. Such a model could further be extended into real scale, allowing a direct connection and use in the current practice.

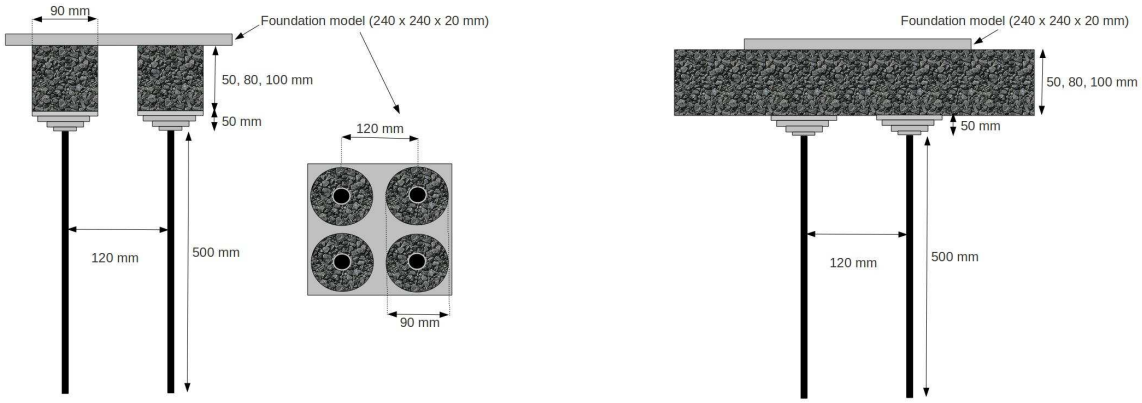

(a) (b)

Figure 5.1: Experimental models of soil reinforced by piles associated to a LTC and LTP

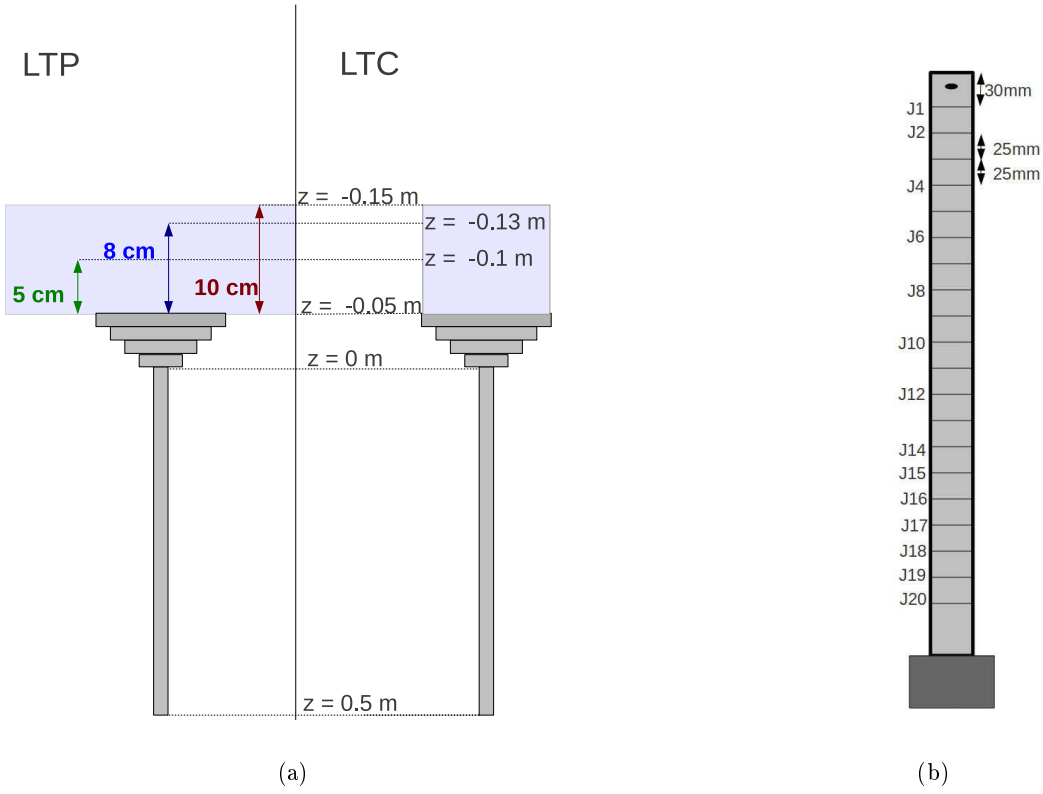

(a) (b)

Figure 5.2: a) Geometry of the reduced models, the LTC/LTP height was varied: 5cm, 8cm, 10cm
b) Position of strain gauges

5.2 Initial conditions

It was noted that due to the soil installation procedure, the instrumented pile undergoes an initial deflection. In order to understand at which stage of the installation procedure the

pile deflection is created, strain gauge measurements were registered at three stages of soil installation:

1. Stage 1: Clay reaches 10 cm below the pile head.
2. Stage 2: Clay reaches the level of the pile head.
3. Stage 3: Stone column installation.

The three stages are graphically shown in Figure 5.3

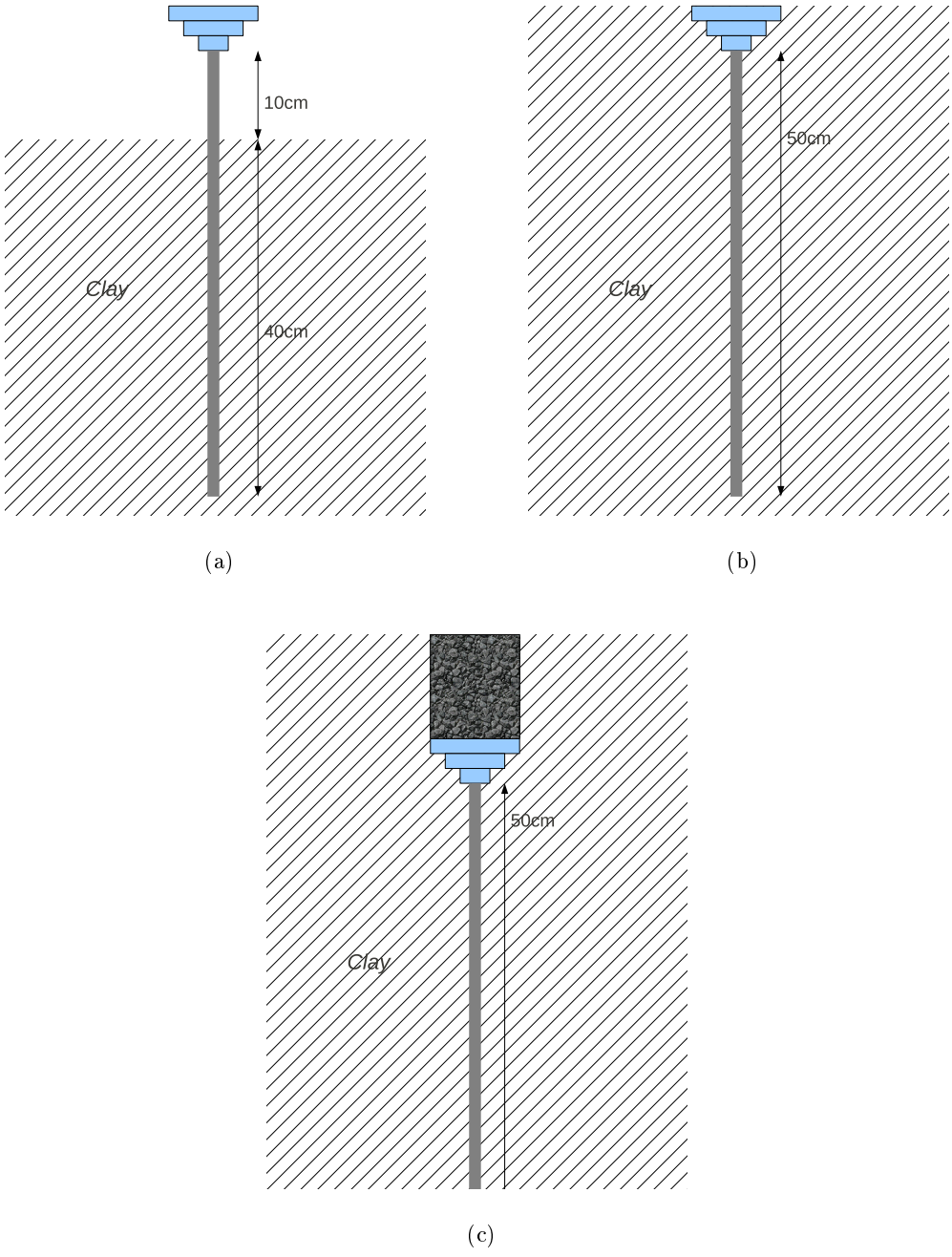

Figure 5.3: (a)Stage 1 (b)Stage 2 (c)Stage 3

It was found that the pile is deformed even before the stage 1, that means even before the top layer of clay is installed. Therefore the initial pile deformation was mainly caused during installation of the bottom layers of clay. These bottom layers of clay were not changed in between the experiments, because it was observed that at such a depth, the pile does not undergo any deflection caused by the applied loading. As a consequence, such an initial deflection was common for all the experiments (Figure 5.6). This did not present a problem, since the pile behaviour is considered to be elastic during the whole experimental study and therefore the initial pile deformation does not present a difficulty. Referring to Figures 5.4 and 5.5, it can be seen that a minor deformation was also mobilized between the stage 1 and the stage 3, although its value is negligible compared to the pile state of deformation at stage 1. Since the top layer of clay was installed around an 'already deformed' pile and its installation did not cause an important pile deformation, it is assumed that the values of moment M, shear force T and lateral soil reaction P measured at the pile top during the experiments are not highly influenced by the initial state of deformation. This is confirmed in Figures 5.4 and 5.5 where it can be seen that M and T values at the pile top tend to zero. The lateral soil reaction P shows a small increase created in between the stages 1 and 3, but this is acceptable since it is considered that the ultimate lateral soil reaction Pu is not mobilized. Indeed, referring to the work of Khemakhem (Khemakhem, 2012) who proposed the following relations for the ultimate lateral soil reaction P_u created at a pile deflection y_0:

$$y_0 = 0.05.B \tag{5.5}$$

and

$$P_0 = 11.27.B.cu \tag{5.6}$$

it is noted the pile deformation created between the stages 1 and 3 did not mobilize the values of y_0 equal to 0.9mm and the values of P_u equal to 3.5 kN/m. Therefore, it is a speculation that the soil was not pastified during the installation procedure.

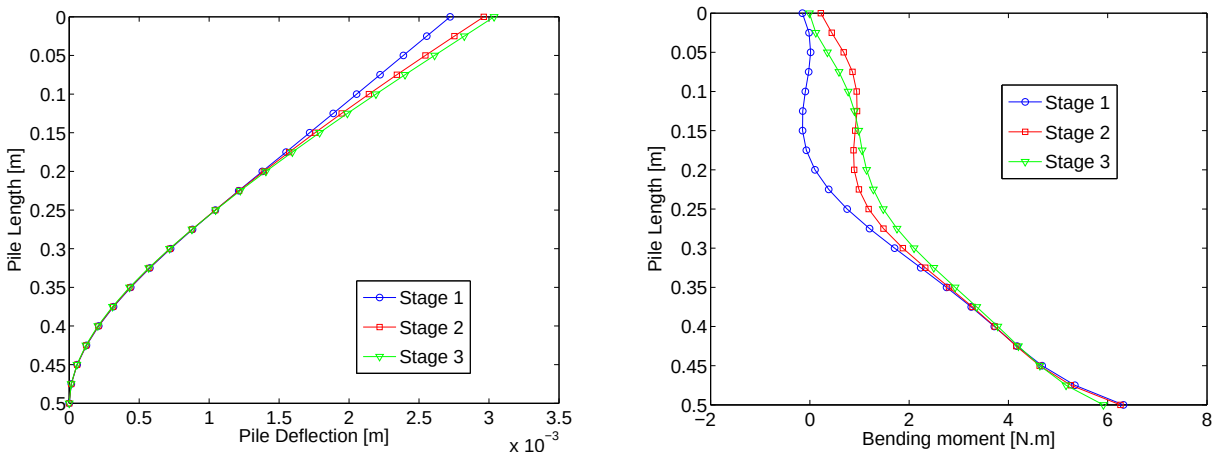

(a) (b)

Figure 5.4: (a) Deflection along the pile (b) Moment along the pile

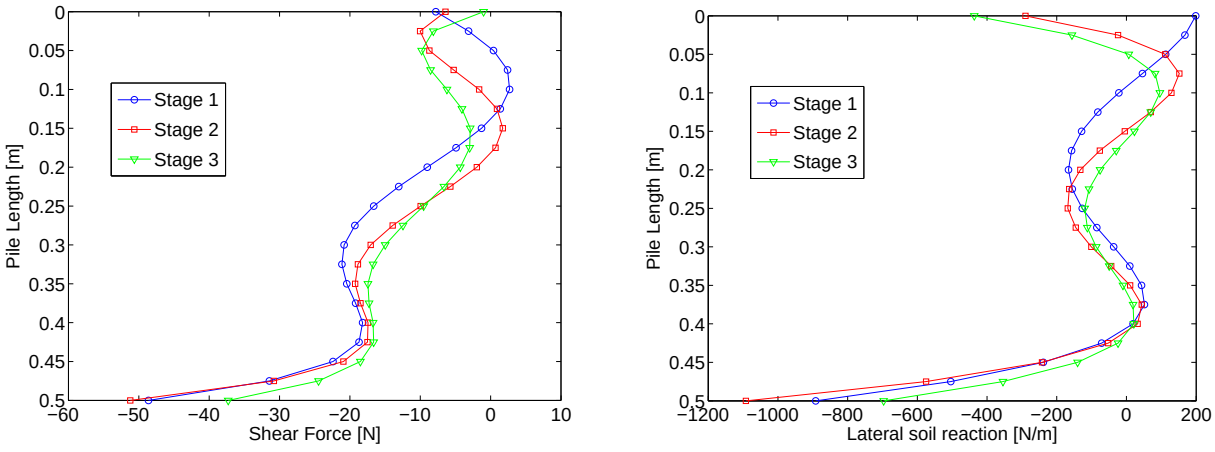

(a) (b)

Figure 5.5: (a) Shear force along the pile (b) Lateral soil reaction along the pile

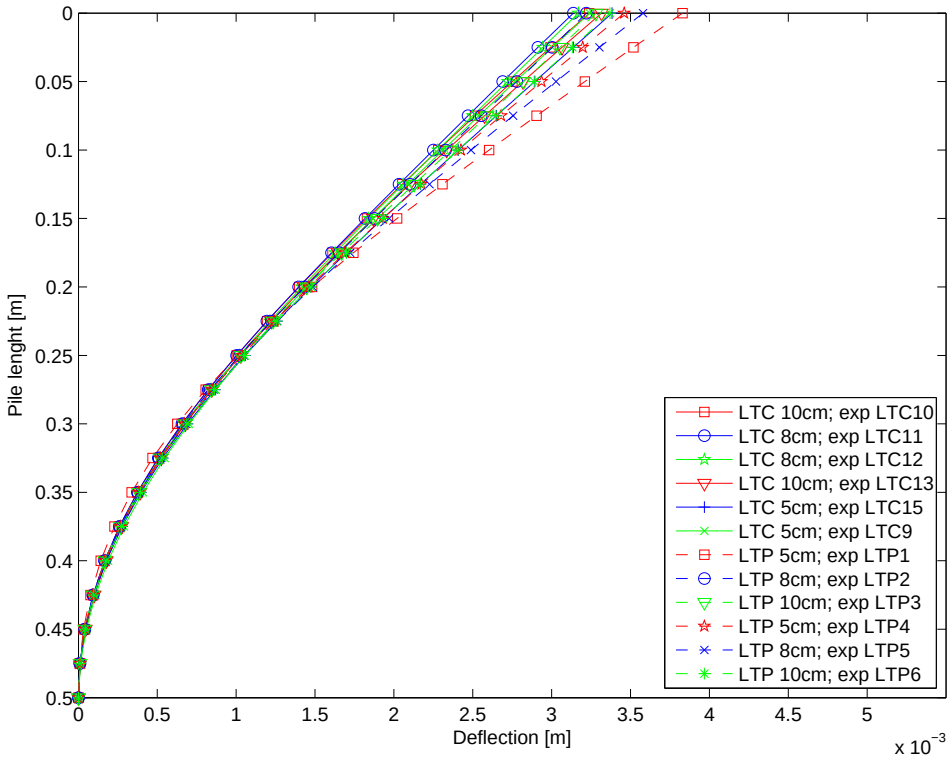

Figure 5.6: Initial deflection along the pile for different experiments. This deflection is caused by the soil installation procedure.

5.3 Pile data presentation with respect to the initial state of deformation

In this chapter results from experiments on soil reinforced by piles associated to a LTC and LTP are discussed. It is reminded that the experimental procedure consists of soil installation (time t0 to t1 in Figure 5.7), vertical loading V of the foundation up to one third of its bearing

capacity (t1 to t2 in Figure 5.7) and horizontal dynamic loading at a constant vertical load (from t2 further on in time - Figure 5.7). Figure 5.7 shows this graphically, defining *t0*, *t1* and *t2*. In order to have a proper understanding of the pile behaviour during each loading stage, three different ways of data presentation are defined:

1. Strain created during the soil installation as well as during the vertical and the horizontal loading is considered in the analysis. The strain level is zero at time *t0*. This data presentation will be referred to as *'Correction-0'*.
2. Strain created during the vertical loading and the horizontal loading is considered in the analysis. The strain level is put to zero at time *t1*. This data presentation will be referred to as *'Correction-ini'*.
3. Strain created during the horizontal cyclic loading is considered in the analysis. The strain level is put to zero at time *t2*. This data presentation will be referred to as *'Correction-Vload'*.

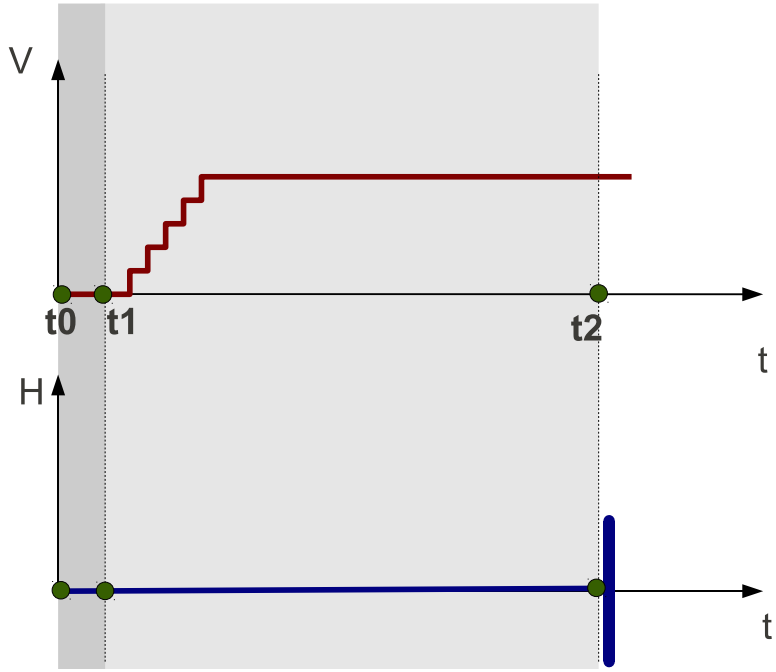

Figure 5.7: The applied vertical and horizontal loading during the experimental procedure

The following figures show the lateral pile performance under three different loading conditions referred to as *'Case1'*, *'Case2'* and *'Case3'*:

1. after the soil installation but before the application of the vertical load, i.e. at time *t1*; *'Case 1'*
2. after application of the vertical load, but before applying the horizontal loading, i.e. at time *t2*; *'Case 2'*
3. during the horizontal loading under a constant vertical load; *'Case 3'*

Figures 5.8 and 5.9 show the pile performance for the three cases listed, using the data presentation *'Correction-0'*. This means, that there were no adjustments made to the strain developed during the soil installation. Maximum envelopes for moment M, shear force T, deflection y and lateral soil reaction P are plotted for each one of the three loading cases[1]. This is done in order to show the global pile behaviour during the experiments. The following sections, analysing separately the effect of the vertical and the horizontal loading present the pile behaviour using mainly the *'Correction-ini'* and *'Correction-Vload'*, respectively. Otherwise it is mentioned when a different data presentation is used.

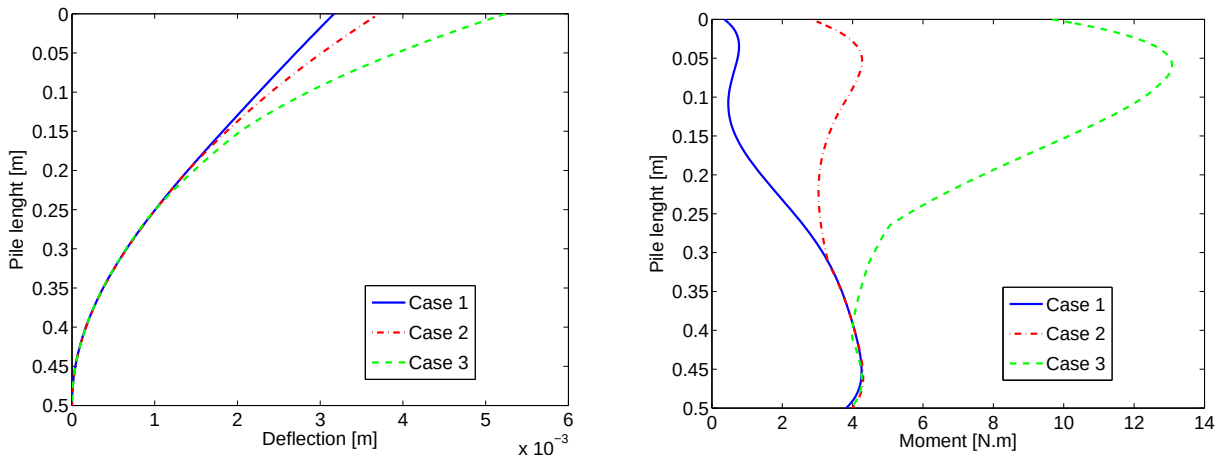

(a) (b)

Figure 5.8: (a) Deflection along the pile (b) Moment along the pile

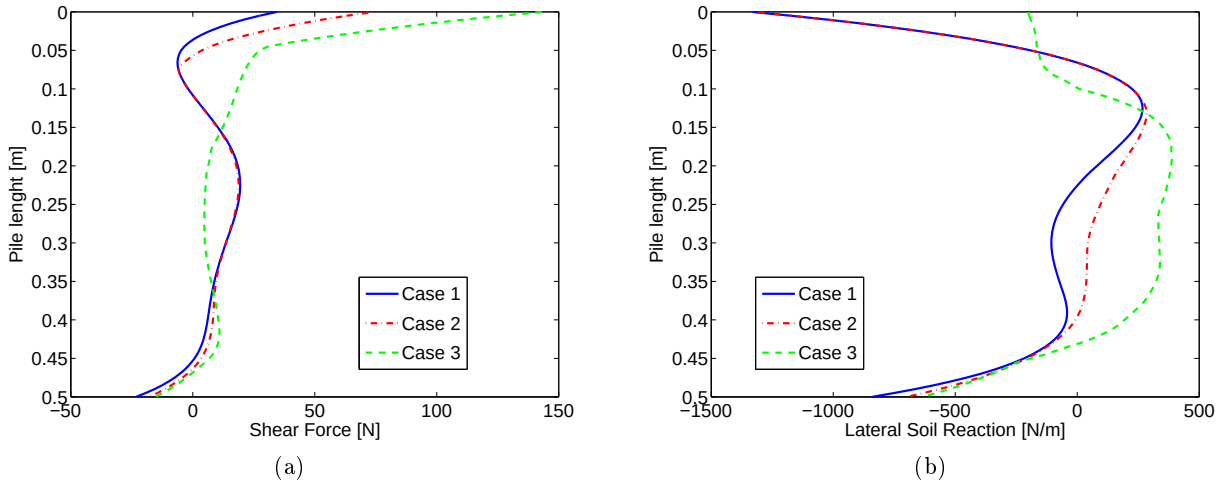

(a) (b)

Figure 5.9: (a) Shear force along the pile (b) Lateral soil reaction along the pile

[1] It is noted that throughout the following text, maximum and minimum envelopes are referred to as graphs showing the variation in respectively maximum or minimum values for a given function (such as M, T, y or P along the pile) due to the application of given loading conditions.

5.4 Static Vertical loading

A vertical load of 5000 N, representing approximately one third of the reinforced soil bearing capacity, is applied to the foundation model in five steps (1000N, 2000N, 3000N, 4000N and 5000N). During each step, a period of consolidation takes place, in order to stabilize the corresponding settlements. Three heights of LTC and LTP are tested, respectively. Each experiment is repeated at least twice to increase the reliability of the results, although for the sake of simplicity, not all the results are presented in the main text and are placed in Annex B. The foundation settlement under the increasing static load was studied for 3 different stone column/mattress heights - 5cm, 8cm and 10cm. Figures 5.10 to 5.12 present the results. The settlement considered in the graphics corresponds to the settlement taking place after the first loading stage of 1000N up to the last loading of 5000N. This is done to avoid interpretation mistakes due to initial settlements caused possibly by a bad contact between the foundation and the soil surface.

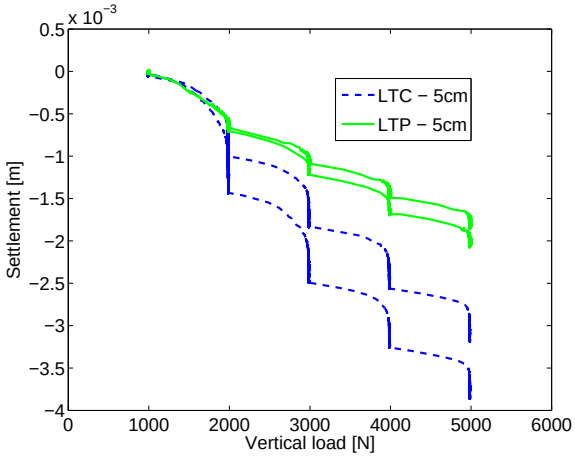

Figure 5.10: Foundation settlement under vertical static loading; column height/ mattress thickness 5 cm

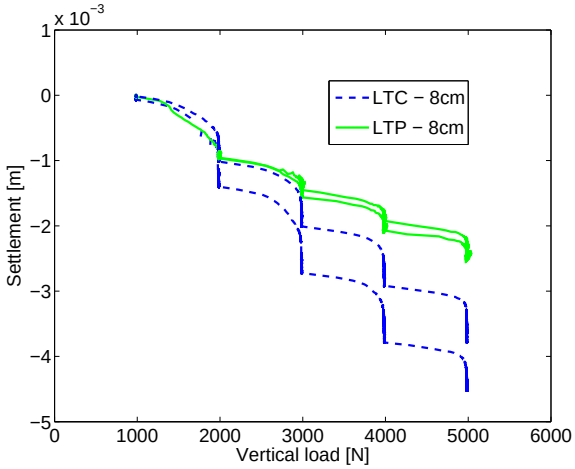

Figure 5.11: Foundation settlement under vertical static loading; column height/ mattress thickness 8 cm

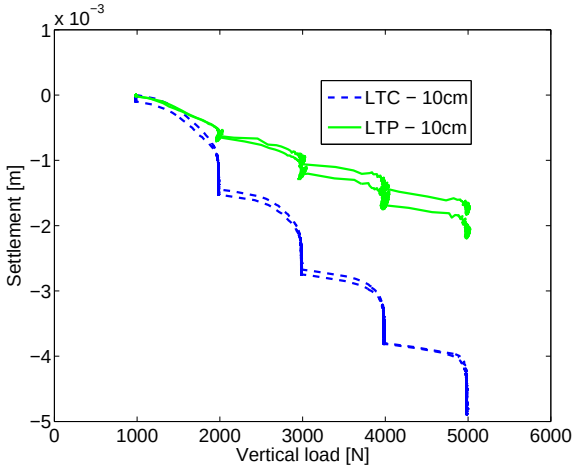

Figure 5.12: Foundation settlement under vertical static loading; column height/ mattress thickness 10 cm

Following comments on the results are made for the two soil reinforcements under static vertical loading:

•The settlement of soil improved by piles associated to LTC depends of the height of the stone column, where this settlement decreases with decreasing stone column height

•Soil improved by piles associated to LTP seems to be, in terms of settlement, less sensitive to the mattress thickness. This observation is valid within the range of the studied thickness.

•Foundation settlement on soil reinforced by piles associated to LTC varies between experiments performed with 5cm and 8cm stone column height. This is assumed to be an effect of the installation procedure. Experiments performed with 10cm high stone columns show a good repeatability

•For the case of LTC, there is a consolidation happening in between the load increments, which is visible in Figure 5.13. On the contrary, for the case of LTP, it seems as if all the settlement takes place during the application of the load increments and no consolidation occurs in between these increments. Therefore it is noted, that the foundation settlements are higher in the case of piles associated to LTC due to the lateral presence of clay, which allows lateral expansion of the stone column and therefore decrease in its height.

The response of the instrumented pile is monitored as vertical load is applied on the foundation model. Figures 5.14 and 5.15 show the bending moment, deflection and shear force along the instrumented pile under vertical load of 5000N. Figure 5.14 refers to the pile supporting a stone column (LTC) and figure 5.15 refers to a pile supporting a gravel mattress (LTP). More figures describing pile lateral behaviour are listed in Annex B.

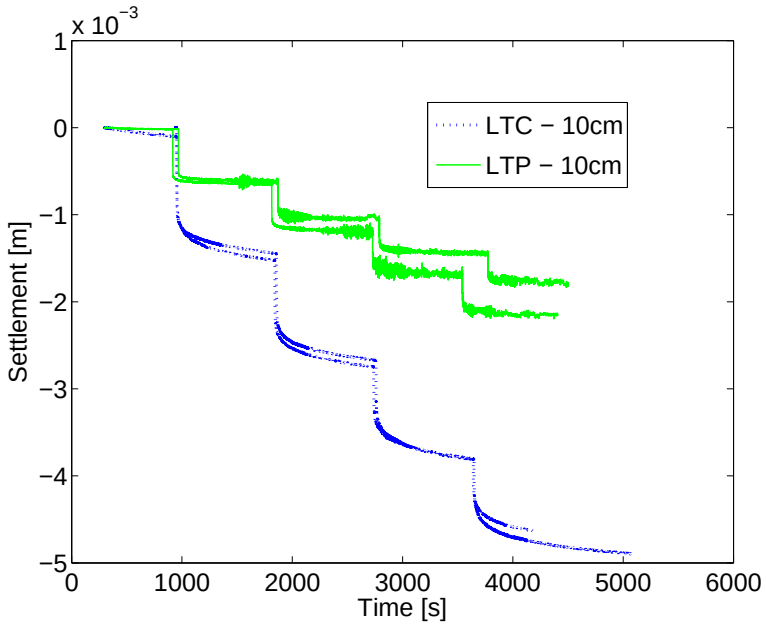

Figure 5.13: Foundation settlement under vertical static loading as a function of time; column height/ mattress thickness 10 cm

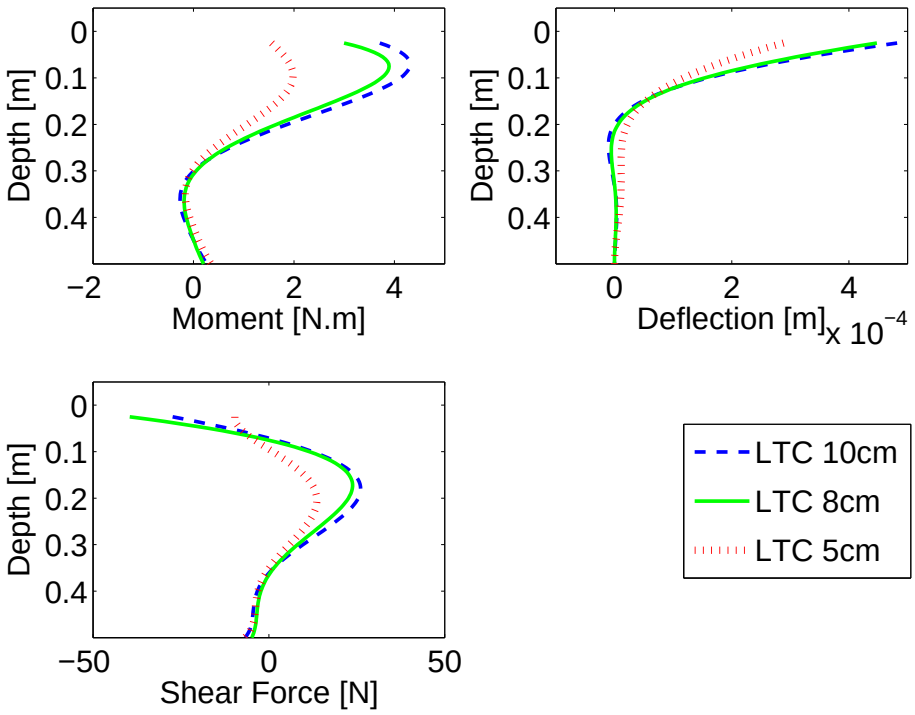

Figure 5.14: Lateral behaviour of the instrumented pile associated to a LTC, Vload = 5000 N

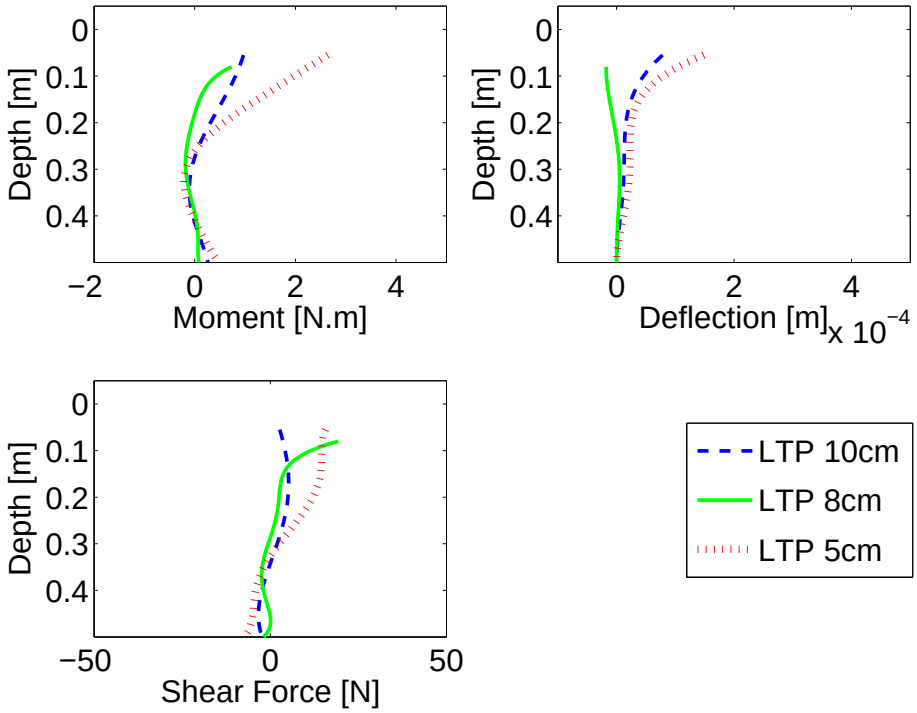

Figure 5.15: Lateral behaviour of the instrumented pile associated to a LTP, Vload = 5000 N

Following comments on the results are made for the two soil reinforcements under static vertical loading:

•The vertical loading has a little impact on the instrumented pile associated to a 8cm and 10 cm mattress (LTP).

•Lateral pile performance is comparable for the two soil reinforcement technologies when the stone column/mattress height is 5cm.

•For cases when the column (LTC) or the mattress (LTP) are 8cm and 10cm high, the pile head supporting the LTC undergoes higher moments, shear forces and deflection than in the case of LTP. This phenomenon could be explained by the geometry difference between the two physical models. In the case of pile supporting a LTC, a square foundation applies a vertical load on four gravel columns surrounded by clay. This load is transferred through the stone columns to the rigid transition zone and then to the pile. As V load increases, the foundation settles and the underlying soil has a tendency to migrate towards an area with lower pressure - non-reinforced clay surrounding the four columns. As a consequence, the stone columns undergo a rotation, which is then projected onto the rigid transition zone and the pile. In the case of LTP, the soil between the foundation and the transition zone is entirely composed of a gravel material. As a consequence, there is smaller tendency to lateral spreading of the soil (due to constant material stiffness and lower foundation settlement).

•The behaviour of pile associated to a LTC is sensitive to the stone column height. The higher the stone column, the bigger deflection of the pile. This can be due to the fact that the short stone columns act as a more rigid link between the foundation and the pile head and therefore less column rotation occurs. As a consequence, the pile head is subjected to lower bending moment and deflection for shorter columns.

•On the contrary, pile associated to a LTP seems to exhibit an opposite trend, that is increasing deflection with decreasing thickness of the gravel mattress. It is noted that the level of pile deflection in Figure 5.15 is small, with values less than 0.1mm and therefore no conclusions are be made due to a possible experimental error.

The pile response under the vertical loading suggests that there is an important role of the funnels which simulate the transition zone. The transition zone, for the real cases of CMMs, should serve as a ball-joint which transfers the vertical load to the rigid inclusions but which limits the transfer of the shear forces and moments. This transition zone is, for the real problems, composed of a mixture of gravel and concrete. In the performed experimental study, the transition zone consisted of a metal funnel filled with gravel, which was fixed to the pile. The joint between the pile and the funnel was created by screwing the funnel together with the pile, but the screws were not screwed entirely into the pile to allow some clearance. It is a speculation that this semi-rigid joint could have been transferring more moments and shear forces to the pile than is the case for the real scale CMMs.

5.4.1 Static P-y curves

Since applying vertical load on the foundation caused lateral pile deflection, P-y curves could be plotted. Figure 5.16 shows static P-y curves obtained at the pile head for three different stone column heights (LTCs). The P-y path is given for the 5 loading stages, where each loading stage is followed by a consolidation and relaxation (causing a 'hill-shape' of the P-y path). The results presented are valid for all experiments performed. It can be noticed that the mobilized lateral soil reaction P is greater when the pile supports a stone column of 8cm and 10cm. This is valid even when the pile undergoes the same level of deflection y. It is assumed that this is caused by different stress distribution in the reinforced soil for different stone column heights. While shorter columns, under vertical load, act as rigid elements and transfer the load vertically to the piles, longer columns tend to act in combination with the surrounding clay and transfer the load not only to the piles, but also to the clay (Figure 5.17). As the lateral soil reaction P increases with increasing stress in the soil, it can be assumed that P at the pile top is higher when soil is reinforced by piles supporting longer columns.
Considering such a load distribution as shown in Figure 5.17, it can be assumed that the longer stone columns have a tendency to rotate because their lower part is pushed towards the 'unreinforced' soil. This rotation is possibly transferred through the funnels to the pile heads and additional moments are created. This speculation is confirmed by Figure 5.14, where it can be seen that the moments and shear forces are higher for piles supporting longer stone columns.
The evolution of the P-y curves suggests that the ultimate soil lateral resistance was reached during the vertical loading. It is noted that the maximum values of P reached in Figure 5.16 do not represent the real values of P registered at the pile top. This is due to the fact, that the graphics in this section are plotted in the *'Correction-ini'* data presentation (see 5.3). The real P-y path obtained from data without applying the correction for the strain created during soil installation (i.e. *'Correction-0'* data presentation) shows values of P which are in general 1 kN/m higher than the values plotted in figure 5.16. The position of the P-y curves for both data presentations,i.e. for *Correction-0* and *correction-ini*, is plotted in Figure 5.18. It can be seen that the value of ultimate bearing capacity reached experimentally is around 2.2 kN/m.
Comparing the value of Pu which was determined analytically (see section 5.2) and the value

of Pu based on the presented experimental results, it can be noted that the experimentally obtained Pu represents 2/3 of the Pu determined analytically. Despite this, it is considered that the two values are in the same order.

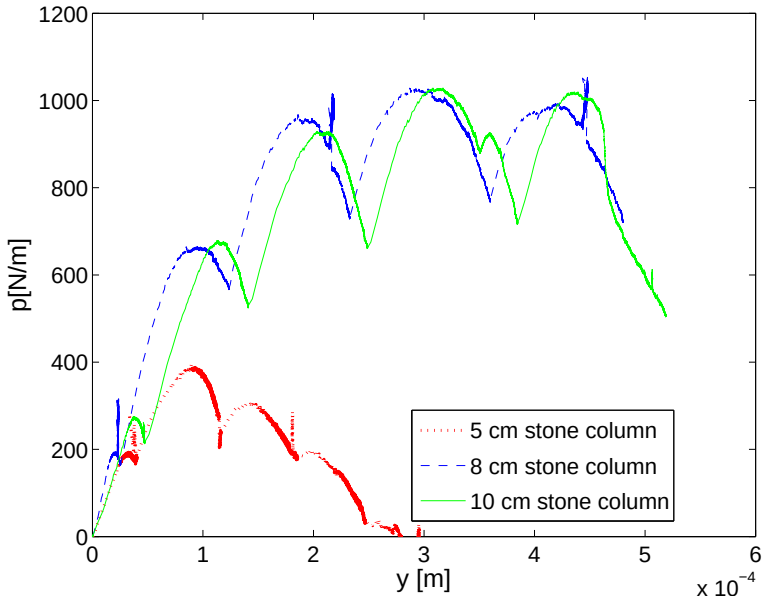

Figure 5.16: Static P-y curves plotted at the pile head, which is supporting a stone column (LTC) surrounded by clay

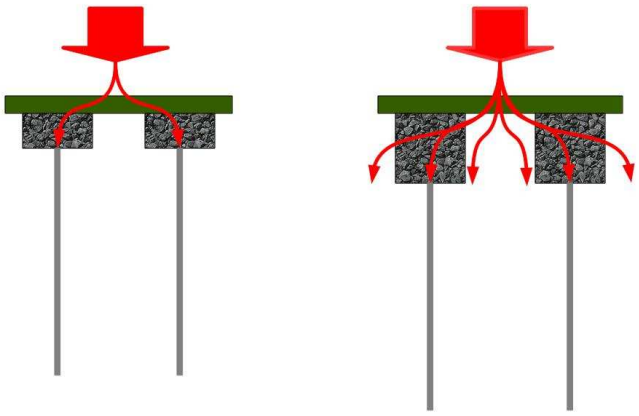

Figure 5.17: Proposed schedule of stress distribution in soil reinforced by piles associated to different column heights: shorter columns on the left, longer columns on the right

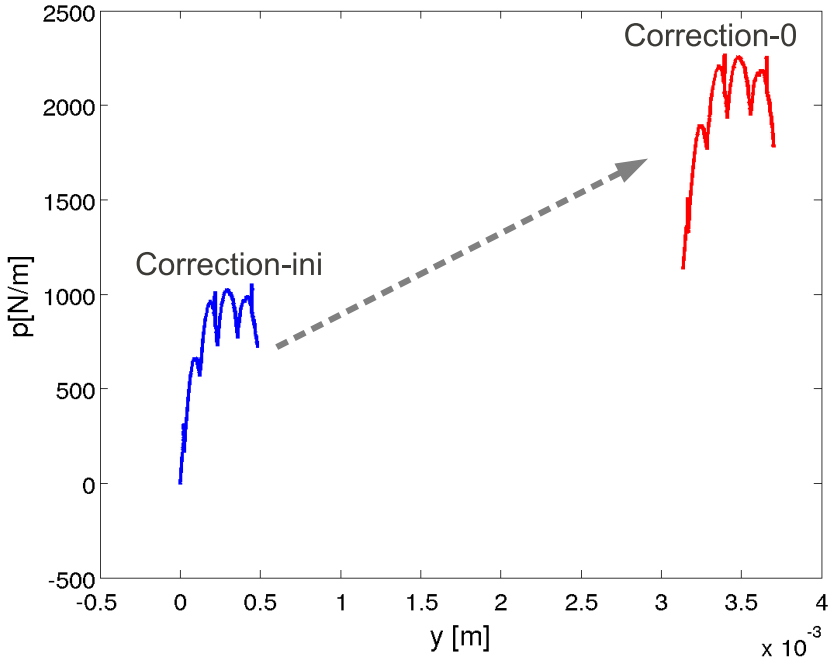

Figure 5.18: Static P-y curve plotted using two different data presentations: *Correction-0* and *correction-ini*; case when the pile is supporting an 8cm stone column

The initial part of the P-y curve is expressed by:

$$P = E_s.y \tag{5.7}$$

Being interested in the value of E_s, the P-y curves were plotted for the first loading stage, i.e. for the loading from 0N to 1000N (Figure 5.19). The E_s values found to be independent of the stone column height and to range form 6MPa to 11MPa. It is noted that the found range of E_s values might not be the correct initial value corresponding to virgin loading as the pile and the surrounding soil have been deformed during the soil installation. Despite this, the values of E_s found should be in the same order with the initial E_s values, since it is considered that the ultimate lateral resistance was not yet mobilized at the pile top during the soil installation as well as during the first loading stage (Figure 5.20). It is noted that Figure 5.20 presents the addressed problem in a simplified manner and is included only for clarity of the explanations.

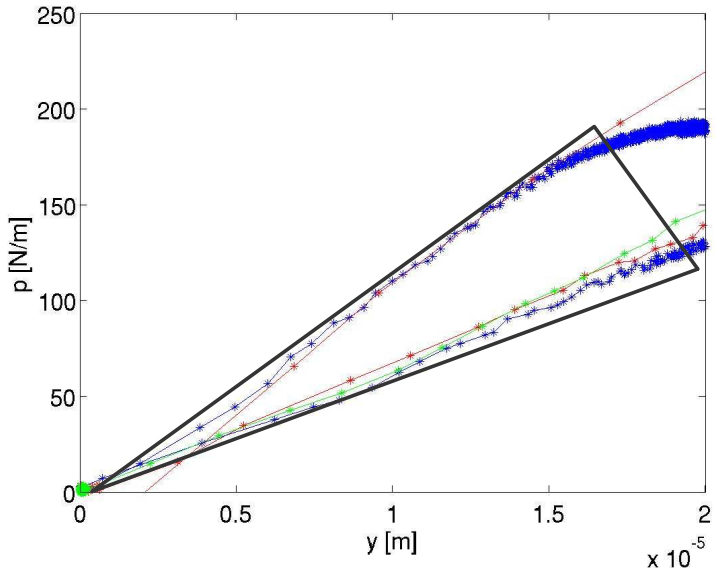

Figure 5.19: 'Initial' stiffness range

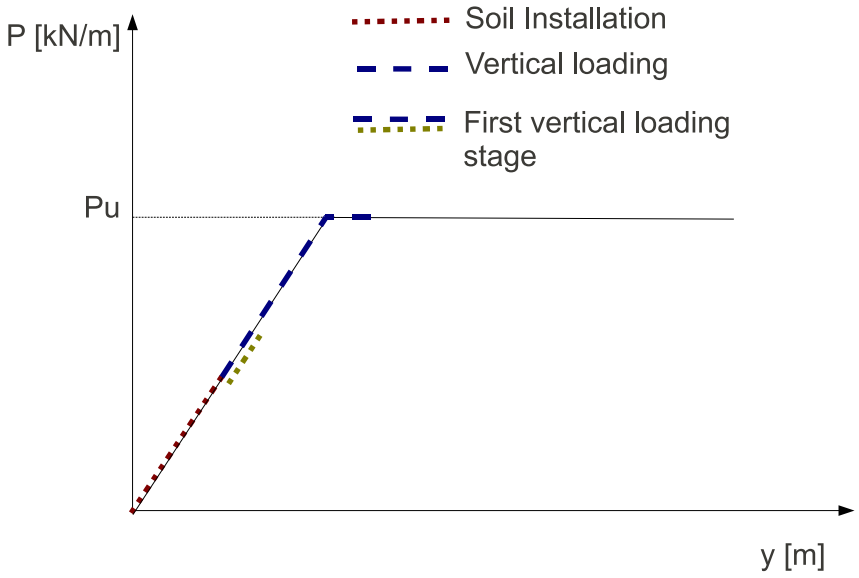

Figure 5.20: Simplified P-y path for the pile head

Comparing the experimentally found value of E_s with its analytical formulation, it was found that the experimental E_s is higher than what would be expected based on analytical formulations. Despite this, both E_s values are considered to be in the same order. The used analytical determination of E_s is described in the following:

Menard (Menard et al., 1969) proposes to calculate the sugrade-reaction modulus E_s as a function of the pressuremeter modulus E_m, rheologic coefficient α, the pile diameter d and a reference diameter d_0 which is equal to 0.6m.

For $d > d0$, the relation is

$$\frac{E_s}{E_m} = \frac{3}{\frac{2}{3}(\frac{d}{d_0})(2.65\frac{d}{d_0})^{\alpha} + \frac{\alpha}{2}} \tag{5.8}$$

Rheologic coefficient α depends on the soil type and is given in the following table (after (Baguelin et al., 1978)):

Soil Type	α
Peat	1
Clay	2/3
Silt	1/3
Sand	1/3

In order to calculate the equation 5.8, the pressuremeter modulus E_m has to be defined. The following equation was proposed by Menard (Menard et al., 1969) for a slightly overconsolidated clay:

$$12 < \frac{Em}{5.5cu} \leqslant 15 \tag{5.9}$$

Taking α equal to 2/3 and cu of 18 kPa, the sugrade-reaction modulus Es is defined to be around 2.4 MPa.

Using centrifuge to study lateral pile-soil interaction shows an increase of initial lateral clay reaction P and the initial stiffness E_s with increasing depth (Khemakhem, 2012). This phenomenon is not observed for cases, when the pile is surrounded by an overconsolidated clay with its properties constant with depth (Khemakhem, 2012). For such a case, the P-y curves are found to vary little with the depth.
The clay mass used in the experimental study was aimed to be homogeneous with a cu around 20 kPa. Plotting the stiffness evolution with depth (Figure 5.21), it was observed that the initial stiffness decreases up to a depth of around 10cm from the pile head and then stays constant. The pile behaviour at depth 10cm and deeper corresponds to what was shown by M. Khemakhem (Khemakhem, 2012) for a pile in slightly overconsolidated clay. The top 10cm of the pile show a decreasing stiffness with depth. This can be caused by two factors:

1. The vertical load applied to the soil by the foundation model decreases with depth and therefore cause the P to also decrease with depth. The area assumed to be influenced by the vertical load under the foundation model is shown in Figure 5.22 as the hatched area. It is a speculation that the vertical load applied by the foundation has no important influence at depth 10 cm from the pile head and further down.

2. As described in section 3.4.1, only the flexible part of the model (i.e. LTP or LTCs surrounded by clay) and the top 20cm thick layer of clay around the piles was replaced after each experiment which was carried out. After removing this part of soil, the clay and gravel installation procedure was once more repeated for the missing part of soil. Therefore the resulting clay mass around the pile was composed of two layers with different mechanical properties.

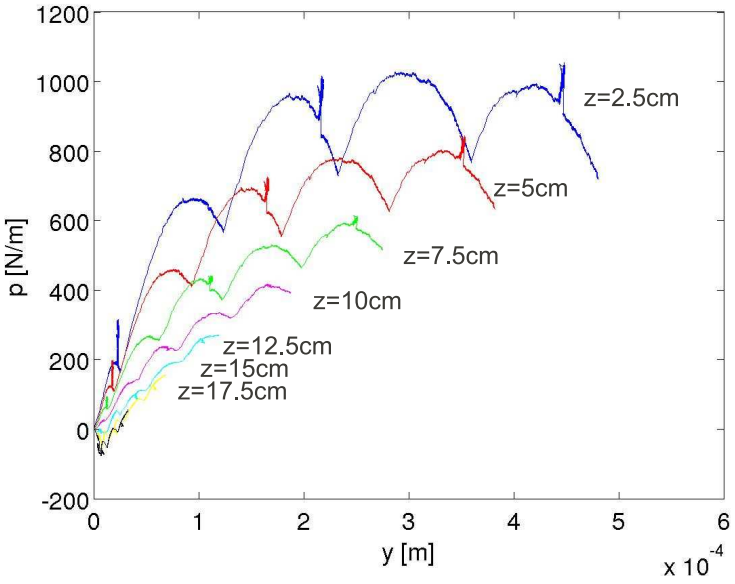

Figure 5.21: 'Initial' stiffness evolution with depth

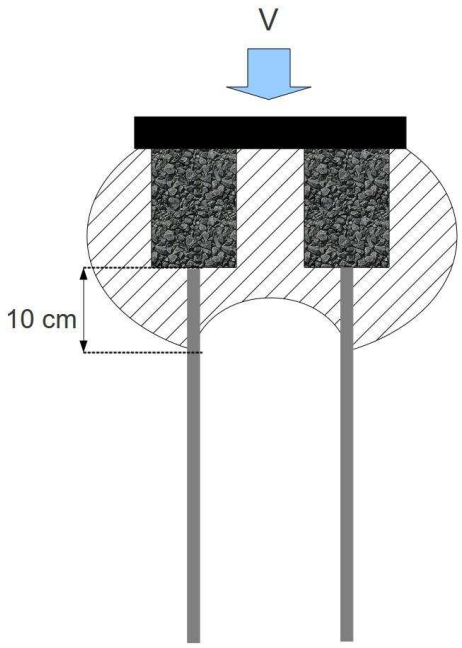

Figure 5.22: Area of influence of the vertical load caused by the shallow foundation

5.5 Combined static loading - Swipe Test

Experiments under combined static load are presented in the following section. The aim is to find the ultimate combination of vertical load V and horizontal load H that will cause a bearing capacity failure of a shallow foundation. One way how to analytically define a critical combination of H and V load is using the following equation (Butterfield and Gottardi, 1994):

$$\frac{H}{t_h} = \frac{V}{V_{max}}.(V_{max} - V) \tag{5.10}$$

where V_{max} is the vertical bearing capacity and t_h is a footing-soil friction coefficient with an experimentally defined value of about 0.5. This failure envelope can be found experimentally by vertical loading of a shallow foundation up to its ultimate bearing capacity, blocking the foundation at its vertical position and then applying horizontal displacement. This procedure is commonly referred as a 'swipe test' (Byrne and Houlsby, 2001). The measured vertical and horizontal force applied by the foundation on the soil provide the failure envelope.

5.5.1 Failure envelope - Foundation on clay

Undrained vertical bearing capacity qc of a simple shallow foundation is given by

$$q_c = c_u.N_c + p_0 \tag{5.11}$$

where N_c is a bearing capacity factor, cu is undrained shear strength and $p0$ is the total vertical stress at the foundation bottom. The N_c factor depends only on the shape of the foundation and its values were proposed by numerous authors. In order to calculate analytically the bearing capacity of the foundation model, a value of N_c proposed by (Day, 2006) was used, taking N_c equal to 5.53. For the case of the foundation model, the undrained vertical bearing capacity obtained with this equation is approximately 100kPa, 6kN. This value is used to plot a theoretical failure envelope (defined by equation (5.10)), which is graphically shown in Figure 5.23 by a full line. As shown by (Orozco, 2009), the failure envelope for an embedded foundation does not reach a value V=0 at H=0. Therefore it can be seen that the analytical formula does not take into account the foundation embedding. The dashed line shows a V-H path obtained from an experimental swipe test, where vertical bearing capacity was not reached since it was decided to stop the V load before. The foundation was embedded and therefore a lateral passive pressure has to be taken into account with respect to the analytical equation. It can be observed that the theoretical and experimental maximum horizontal load is in the same order, although its position in relation to the x axis is not in agreement.

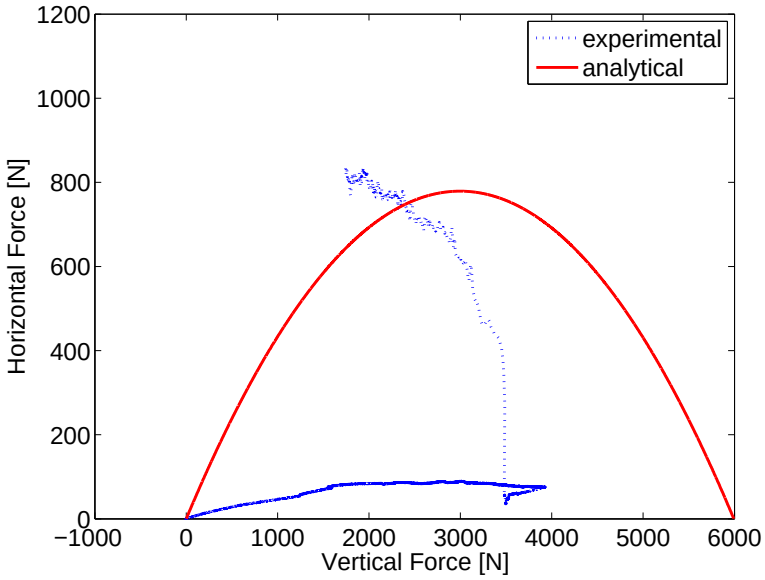

Figure 5.23: Comparison between experimental and analytical results

The maximum horizontal bearing capacity develops when: (Butterfield and Gottardi, 1994)

$$H_{max} \approx V_{max}/8 \tag{5.12}$$

This empirical observation is respected in the Figure 5.23.

5.5.2 Failure envelope - Foundation on soil reinforced by piles associated to the Load Transfer Columns (LTCs)

Introducing a soil reinforcement, the V-H load leading to bearing capacity failure increases. A swipe test was carried out for a case of a foundation embedded in pure clay and a foundation on soil improved by piles associated to the LTCs. A comparison of these two tests is shown in Figure 5.24. It can be seen that the failure envelope of a foundation on the reinforced soil is much larger than the failure envelope of a foundation in pure clay. The shape of the two envelopes is homothetic with a size ratio of approximately 4 between the swipe test envelope for the reinforced soil and the swipe test envelope for pure clay. The ultimate vertical bearing capacity for the reinforced soil is found to be around 280kPa (16000 N, Figure 5.24). The performed swipe test is also used to verify that the stress path corresponding to the imposed dynamic loading (presented in the next section) remains within the failure surface. Figure 5.25 shows that the cyclic loading path is situated inside the rupture surface.

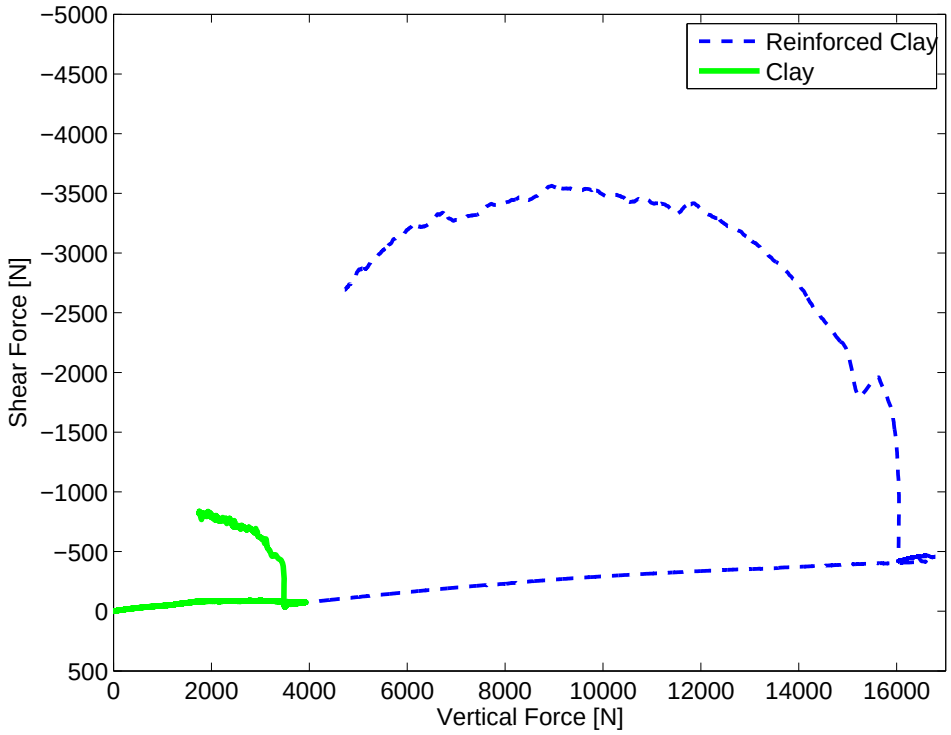

Figure 5.24: Swipe test performed on clay and on clay reinforced by piles supporting LTCs

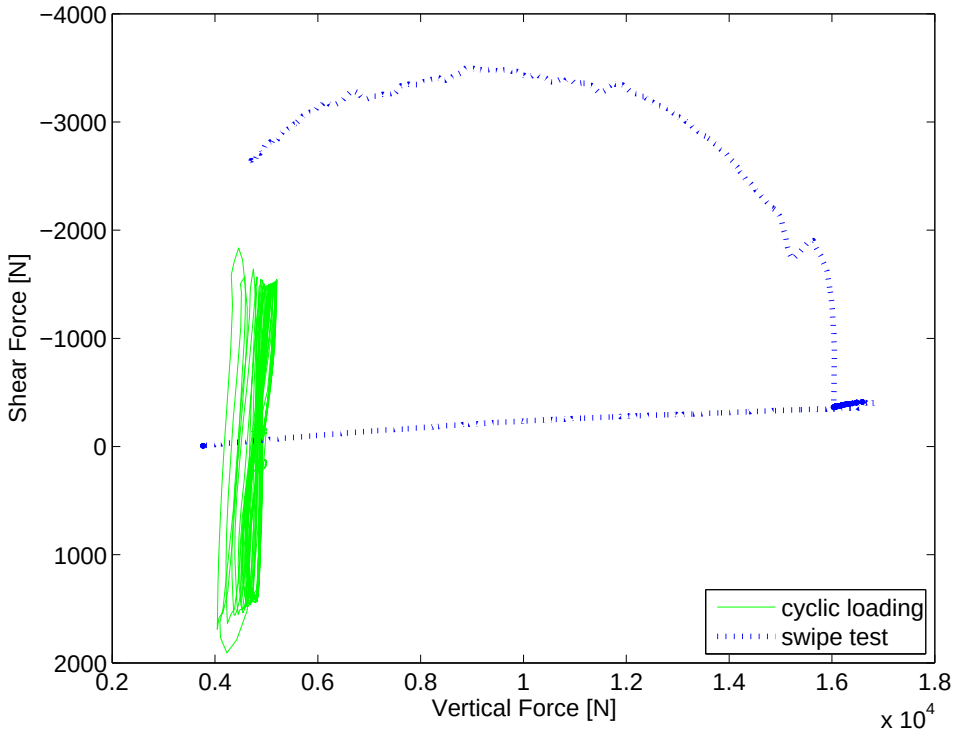

Figure 5.25: Position of a cyclic stress path with respect to the failure envelope

5.6 Combined Loading - Vertical Static load + Horizontal Dynamic load

After the stage of soil consolidation introduced in section 5.4, the vertical load of 5000N, which is applied to the reinforced soil, is set constant. This load represents one third of the foundation vertical bearing capacity. Thirty cycles of horizontal cyclic loading are then applied with a constant displacement amplitude of +/- 2mm and a frequency of 2.7Hz. The horizontal loading is controlled in displacement and is shown in Figure 5.26(b). The direction of the first horizontal loading is the direction 'A' (Figure 5.26), which makes the instrumented pile act as the 'front' pile in the group of the other piles during the loading in direction 'A'. It is noted that unless specified differently, the figures included in this section are plotted in the *'Correction-Vload'* data presentation (see 5.3).

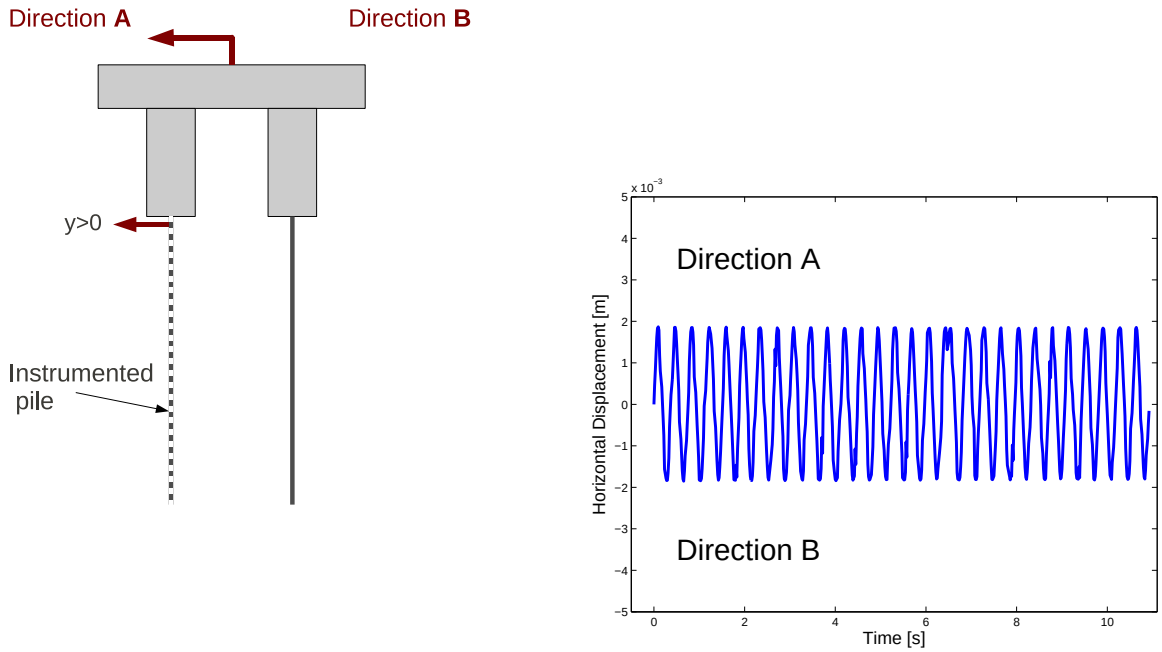

(a) (b)

Figure 5.26: Horizontal Cyclic Loading- Direction A, Direction B

5.6.1 Soil reinforced by piles associated to Load Transfer Columns (LTCs)

5.6.1.1 Foundation Settlement

The behaviour of a shallow foundation under a dynamic loading on soil reinforced by piles associated to LTCs is studied. Height of the stone columns was varied in order to study the effect of stone column height on the foundation settlement (Figure 5.27). It is observed, that the amount of settlement under the horizontal dynamic loading of the foundation increases with the increasing stone column height. This phenomenon can be explained by an assumption

that shorter stone columns tend to transfer a large amount of the imposed vertical load to the rigid inclusions and therefore the upper, flexible part of the system is less compacted under the combined loading. Total settlement accumulated during 30 cycles varies from 3 to 5.5 mm (i.e. approximately 0.01B to 0.02B) and doesn't reach a stabilization by the end of cyclic loading. It can be noticed that the value of the accumulated settlement is in the same order as the value of settlement caused by static vertical loading of the foundation model (Figure 5.10-5.12).

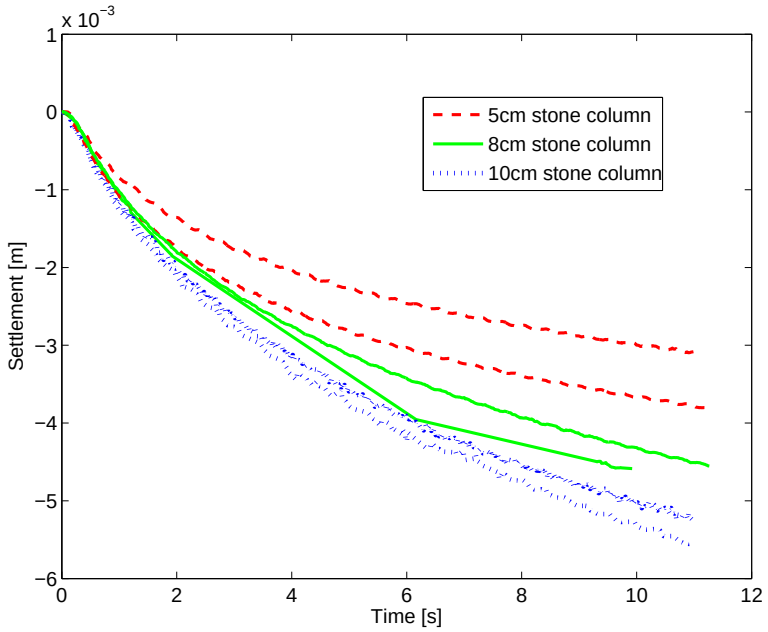

Figure 5.27: Foundation settlement under horizontal dynamic loading - soil reinforced by piles supporting the LTCs

5.6.1.2 Horizontal response of the foundation model

As the cyclic displacement with a constant amplitude was applied to the foundation model, the foundation response in terms of horizontal force was measured. The value of the horizontal force is dependent on the vertical pressure between the soil and the foundation as well as on the interface characteristics and lateral pressure acting on the sides of the foundation.
Figure 5.28(a) shows loops describing the relation between the horizontal displacement and the horizontal force measured at the foundation level. It was observed that the loops change their inclination throughout the cyclic loading and therefore it can be deduced that the system rigidity changes with the number of cycles. This rigidity increase is shown in Figure 5.28(b) and is explained by the fact that as the foundation settles throughout the cyclic loading, the LTCs become more dense and rigid and cause the global rigidity of the system to increase. There was observed no dependence of the system rigidity on the height of the LTCs.

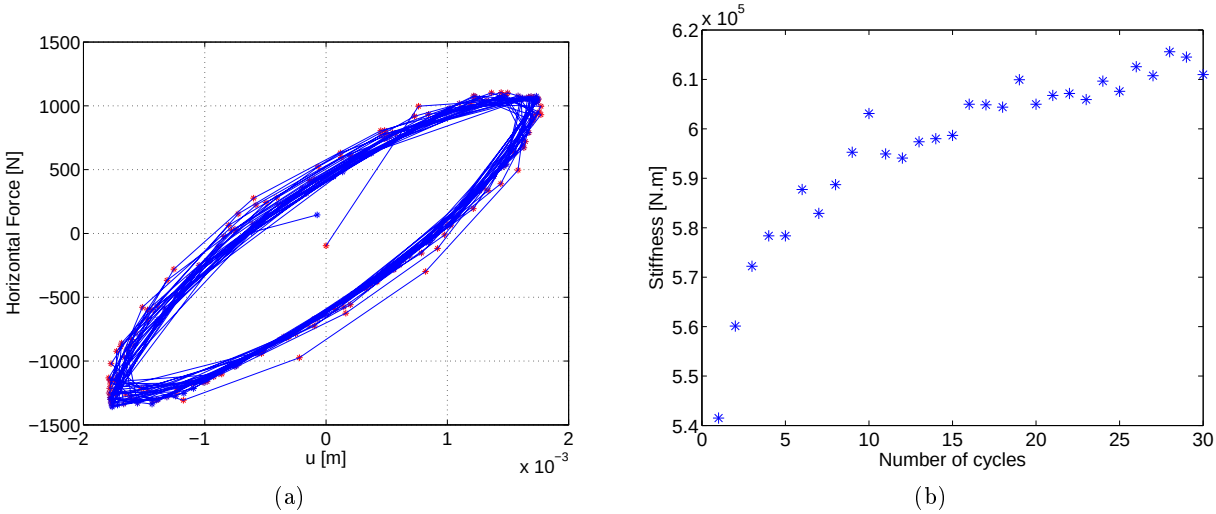

(a) (b)

Figure 5.28: (a) Horizontal force registered at the foundation level when it is subjected to cyclic displacement with a constant amplitude; (b)Increasing stiffness of the system soil-reinforcement throughout the cyclic loading; exp LTC11

5.6.1.3 Physical values derived from strain measurements in the pile associated to a LTC

Moment M, Deflection y and Shear Force T

The instrumented pile undergoes a deflection caused by cyclic loading of the foundation model. This deflection registered at the pile head was found to be in phase with the horizontal displacement of the foundation (Figure 5.29). Pile head deflection monitored by the top level of strain gages is used to define times when the pile deflection reaches its local maximum and minimum. These local maxima and minima are studied for the first, fifth, tenth, fifteenth and the thirtieth cycle and their location in the time domain are t1-t3-t5-t7-t9 for the maxima and t2-t4-t6-t8-t10 for the minima. The bending moment, deflection and shear force at time instants t1 to t9 are plotted in Figures 5.30 to 5.32 for 3 experiments with stone column height 5cm, 8cm and 10cm. More figures presenting such results from other experiments are listed in Annex B. The obtained results indicate that:

•It can be noticed that the pile performs a reversible behaviour only during the first five cycles. After the fifth cycle, the pile doesn't enter the zone of negative deflection and shows a very important deflection accumulation with the dynamic loading. This accumulated lateral displacement develops in direction 'A' towards unreinforced soil, i.e. out of the pile group.

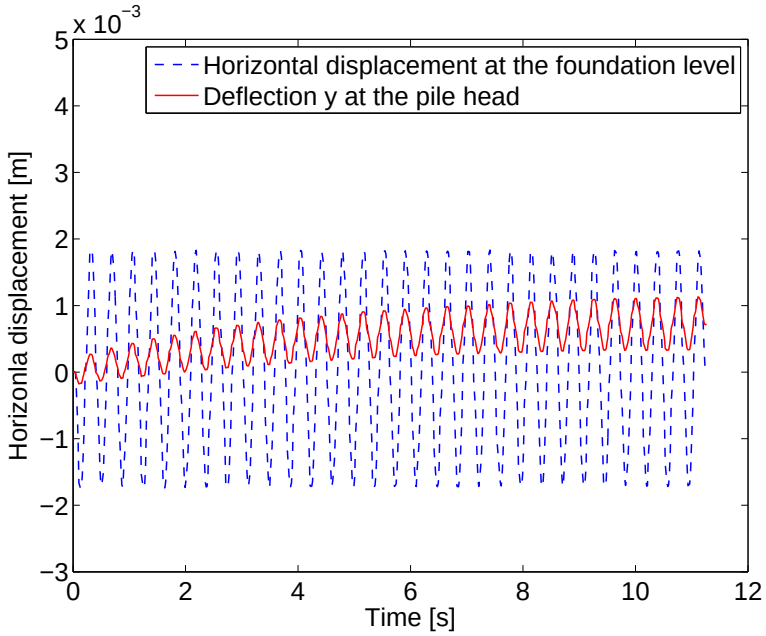

Figure 5.29: Deflection y registered at the pile head which is found to be in phase with the horizontal displacement of the foundation

•As the foundation moves in direction 'A', the pile undergoes positive lateral deflection. The deflection accumulation is the most important for the first five cycles and has a tendency to stabilize for the last ten cycles.

•The pile undergoes lateral movement up to a depth of approximately 20cm out of its 50cm length. Ratio between a depth of first pile deformation measured from the foundation surface d and foundation width B varies from 0.8 to 0.9:

$$\frac{d}{B} \in [0.8; 0.9] \tag{5.13}$$

•The position of local maximum shear force moves deeper along the rigid inclusion with the dynamic loading. Such a trend, although not as visible, can also be observed for the local maxima of the bending moment as their position moves deeper along the pile. This confirms observations made by (Khemakhem, 2012). This phenomenon is explained by the fact that as the pile undergoes lateral cyclic movement, the surrounding soil degradates and looses its strength. As a consequence, the load application moves to lower, more rigid soil layers.

•For the first cycle, M, T and y along the pile at times t1 and t2 reach the same absolute values. For the cycles 10 to 30 (t5 to t10), when the foundation moves in direction 'B' (subfigures with dashed lines in figures 5.30 to 5.32), the pile shows two shear force local maxima. This may be due to the contradiction that, on one hand, the pile moves in direction 'B' along with the foundation movement and on the other hand, the transition zone is constantly inclined towards the unreinforced soil in direction 'A'. Another possible explanation for the presence of the two local maxima of the shear force along the pile are the inertia effects.

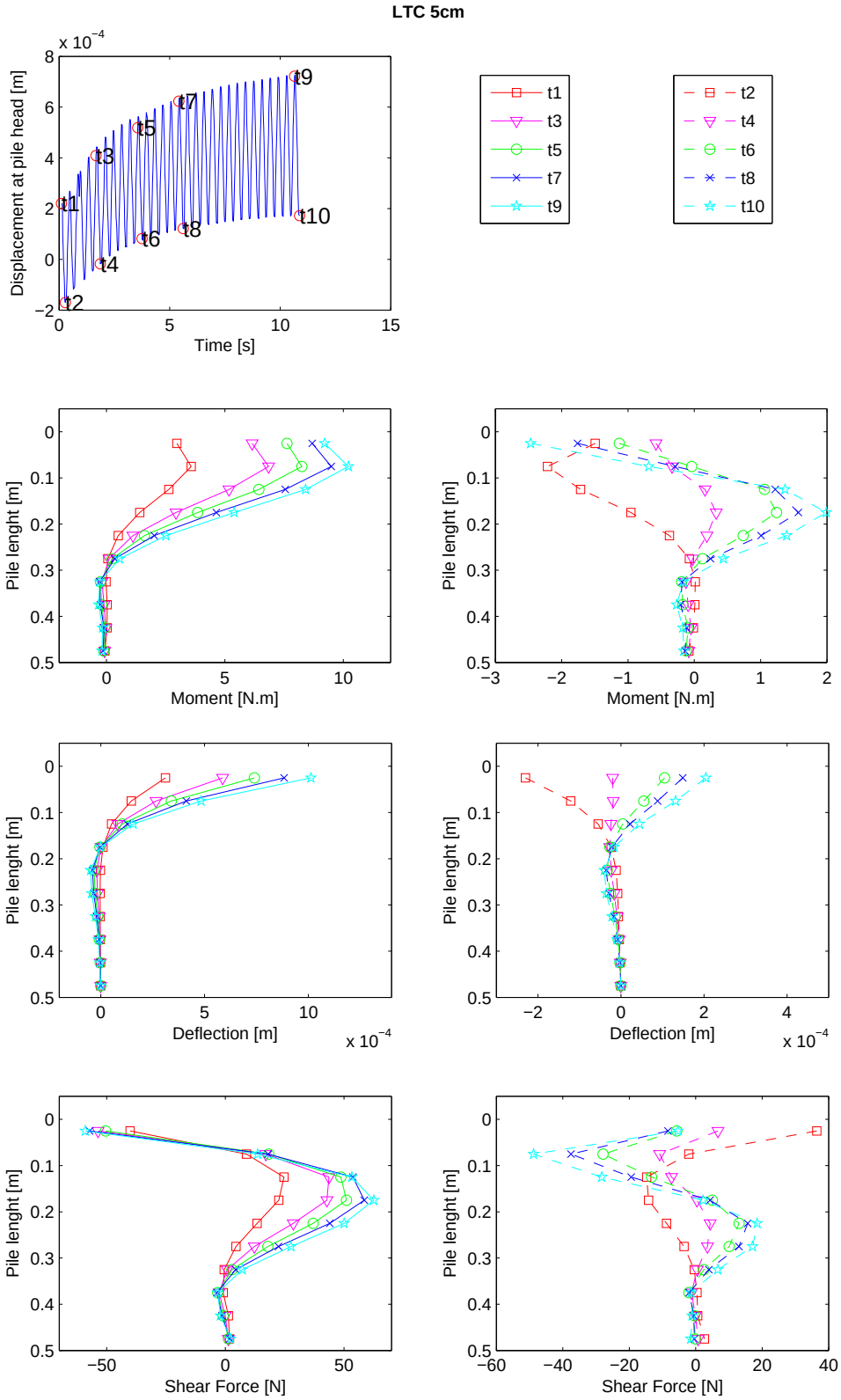

Figure 5.30: Bending moment, deflection and shear force along a pile associated to a LTC of 5 cm (exp LTC9); Direction 'A' = t1,t3, t5, t7, t9; Direction 'B' = t2, t4, t6, t8, t10

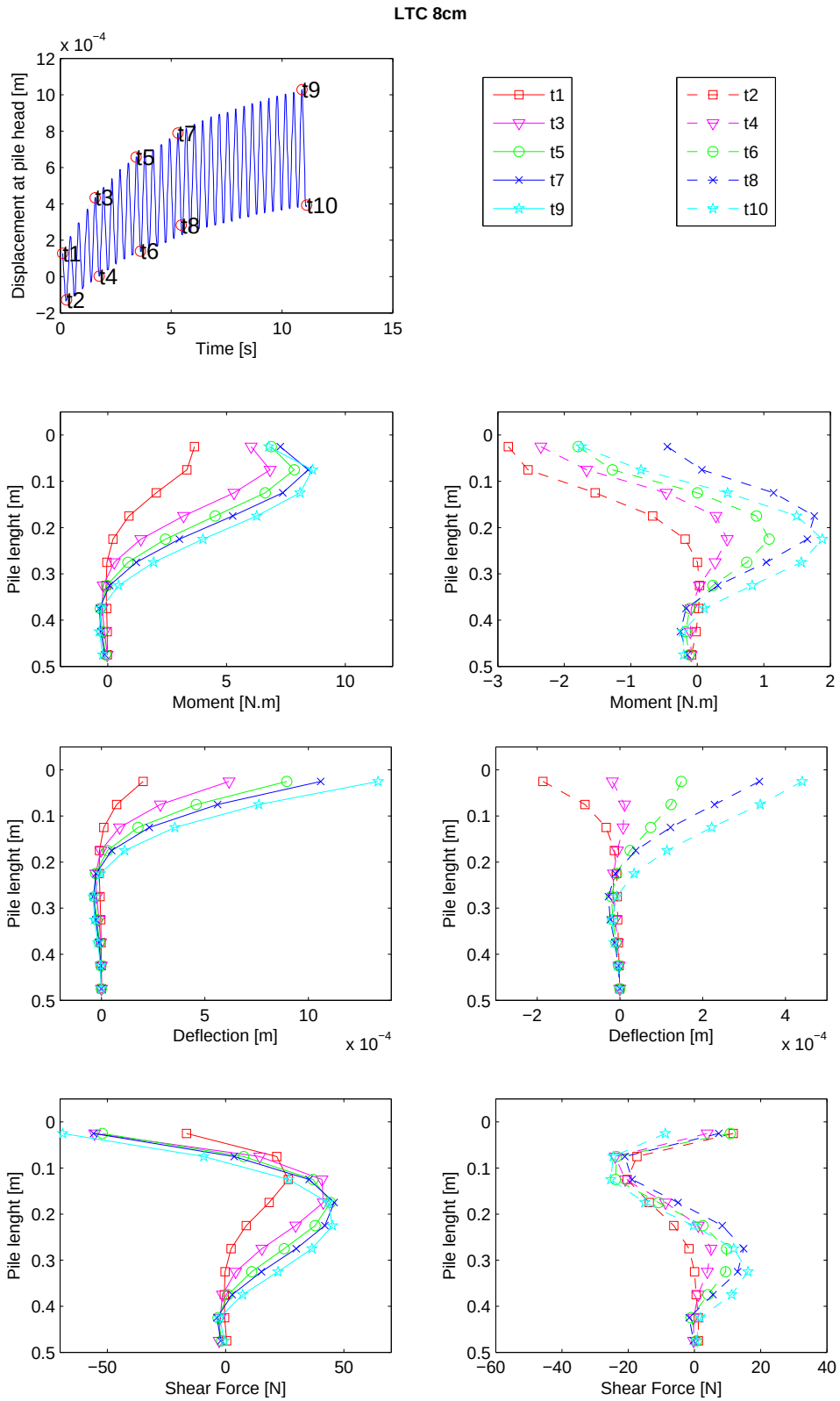

Figure 5.31: Bending moment, deflection and shear force along a pile associated to a LTC of 8 cm (exp LTC11); Direction 'A' = t1,t3, t5, t7, t9; Direction 'B' = t2, t4, t6, t8, t10

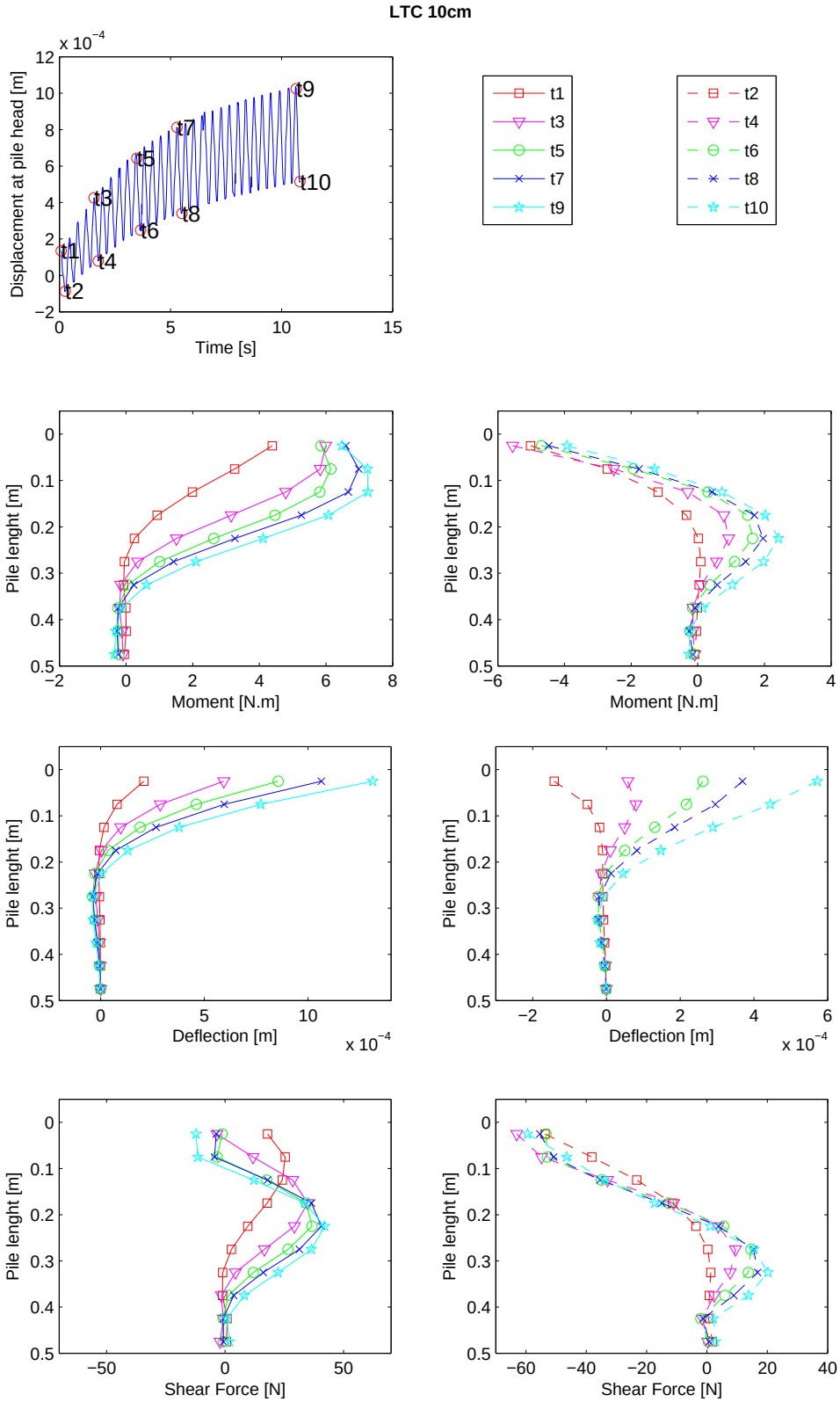

Figure 5.32: Bending moment, deflection and shear force along a pile associated to a LTC of 10 cm (exp LTC10); Direction 'A' = t1,t3, t5, t7, t9; Direction 'B' = t2, t4, t6, t8, t10

In order to analyze the influence of the stone column height on the lateral pile performance,

moment M, shear force T, deflection y and lateral soil resistance P envelopes were studied. The maximum M, T, y and P envelopes were plotted for the first cycle and then for the total horizontal loading sequence, i.e. 30 cycles:

- **The First loading cycle**

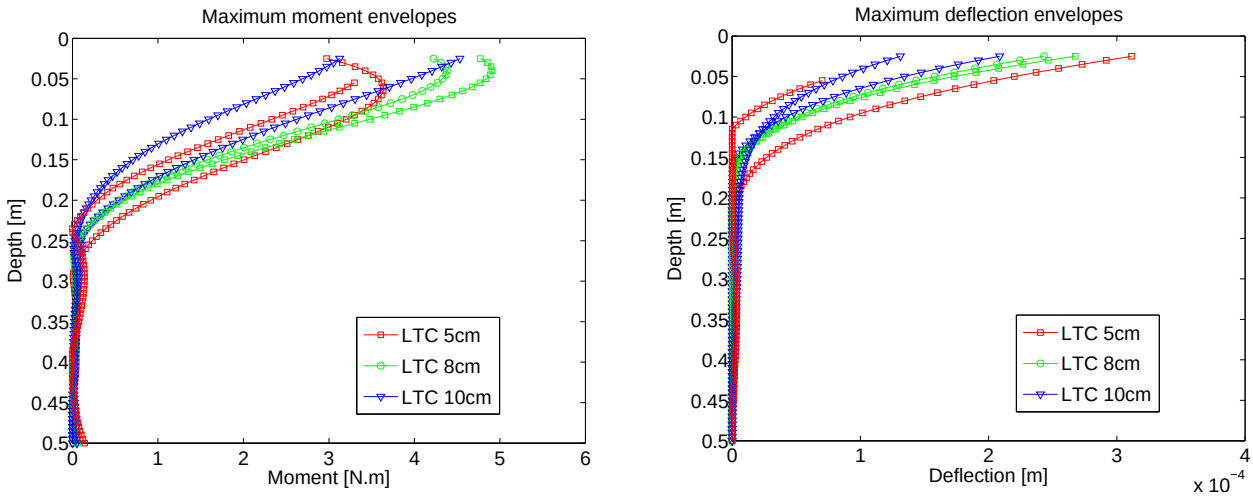

(a) (b)

Figure 5.33: Maximum moment M (a) and deflection y (b) envelopes for the first loading cycle

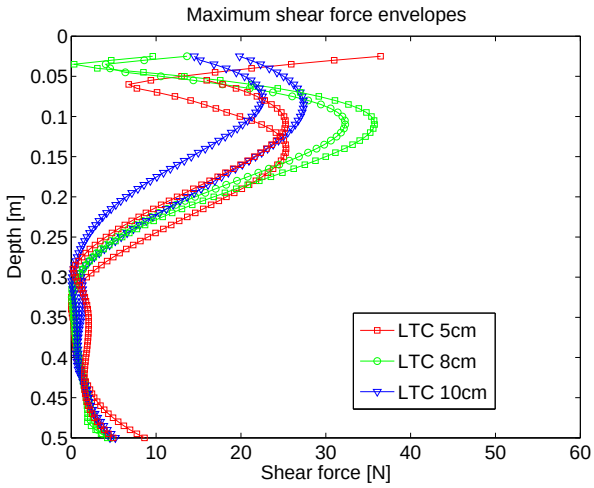

Figure 5.34: Maximum shear force F envelopes for the first loading cycle

Figures 5.33 to 5.34 show envelopes of maximum moment, shear force and deflection for the pile subjected to one loading cycle at the beginning of cyclic loading. In is noted

that during the first loading cycle, the pile response doesn't seem to be influenced by the stone column height (considering stone columns within the tested range of heights).

- **30 Loading Cycles**

Maximum bending moment, shear force and deflection envelopes are plotted in Figures 5.35 and 5.36. Each figure shows results of six experiments when each stone column height was tested twice. Following observations are made:

- Bending moment and shear force decrease with increasing column height.
- The position of the bending moment maximum and the shear force maximum moves deeper along the rigid inclusion with increasing column height.
- Pile deformation reaches larger depth for higher columns.

The pile response over the total 30 cycles suggests that shorter stone columns act as more rigid elements and therefore transfer higher bending moments caused by lateral foundation displacement. They allow less shearing than the higher columns and therefore may cause a higher pile head rotation. Deeper location of the bending moment maximum for piles followed by higher columns suggests that the soil around these piles degradates into larger depth than for piles supporting shorter stone columns. This is in agreement with the observation that the pile deformation reaches larger depths when the pile is associated to a higher column. It is noted, that an opposite trend was expected.

It is reminded that at the beginning of the cyclic loading stage, the pile is under a higher deflection and a higher bending moment for 8cm and 10cm stone column heights. Even though these initial 'deformation derived' values are put to zero at the beginning of the cyclic loading (this is done in order to see pure influence of cyclic loading on the pile performance), it is thought as necessary to keep their presence in mind during the results analysis.

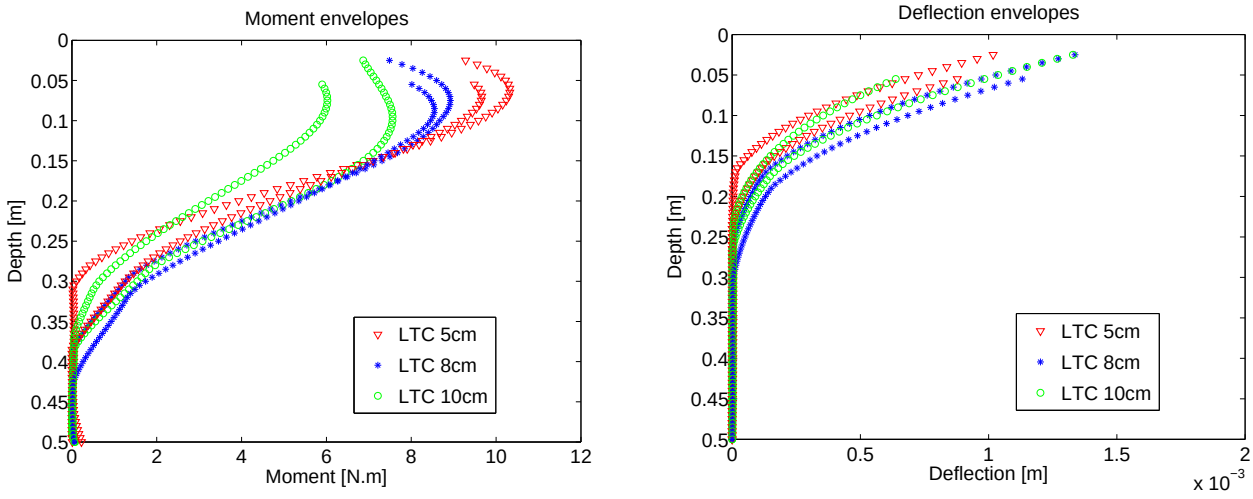

(a) (b)

Figure 5.35: Maximum moment M (a) and deflection y (b) envelopes for 30 loading cycles

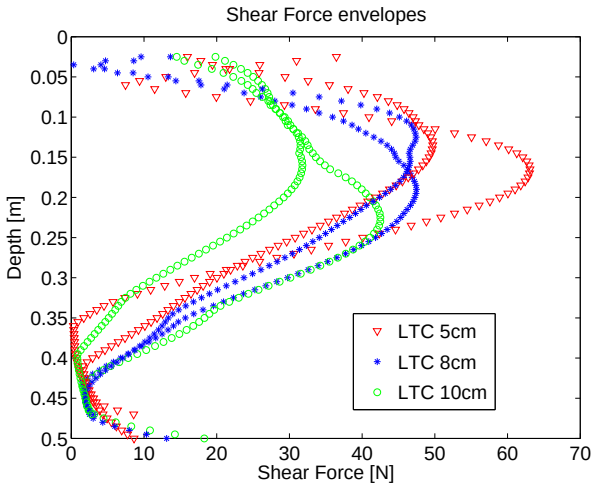

Figure 5.36: Maximum shear force T envelopes for 30 loading cycles

In order to have a proper understanding of the influence of the group effect on the instrumented pile, experiments were carried out where the horizontal cyclic displacement of the foundation model was started in an opposite direction than usual, i.e. in direction 'B'. The pile response to this loading was monitored and compared to the pile performance when the foundation motion starts in direction 'A'. A pile head lateral deflection for the two experiments is plotted in Figure 5.37. To compare lateral performance of the pile for these two experiments, values of bending moment M, shear force T and deflection y are compared for the first loading cycle. Pile responses registered at a moment when the pile deflection reaches its amplitude (P1 and P2 in Figure 5.37), are compared. It is observed, that when the foundation moves in direction 'B', i.e. in direction from the instrumented pile towards the other piles, the reached deflection, moment and shear force values are smaller, than when the foundation moves in direction 'A', i.e. in direction from the instrumented pile towards the unreinforced clay. These results can be seen in Figures 5.38 and 5.39 and confirm the classical 'shadow effect' in the interaction between front and rear piles in a group. Figure 5.38 also shows that the curves representing the pile response at times P1 and P2 are superimposed for the two experiments. This is also

observed for all the following cycles and therefore suggests that there is no influence of the initial loading direction on the global pile behaviour.

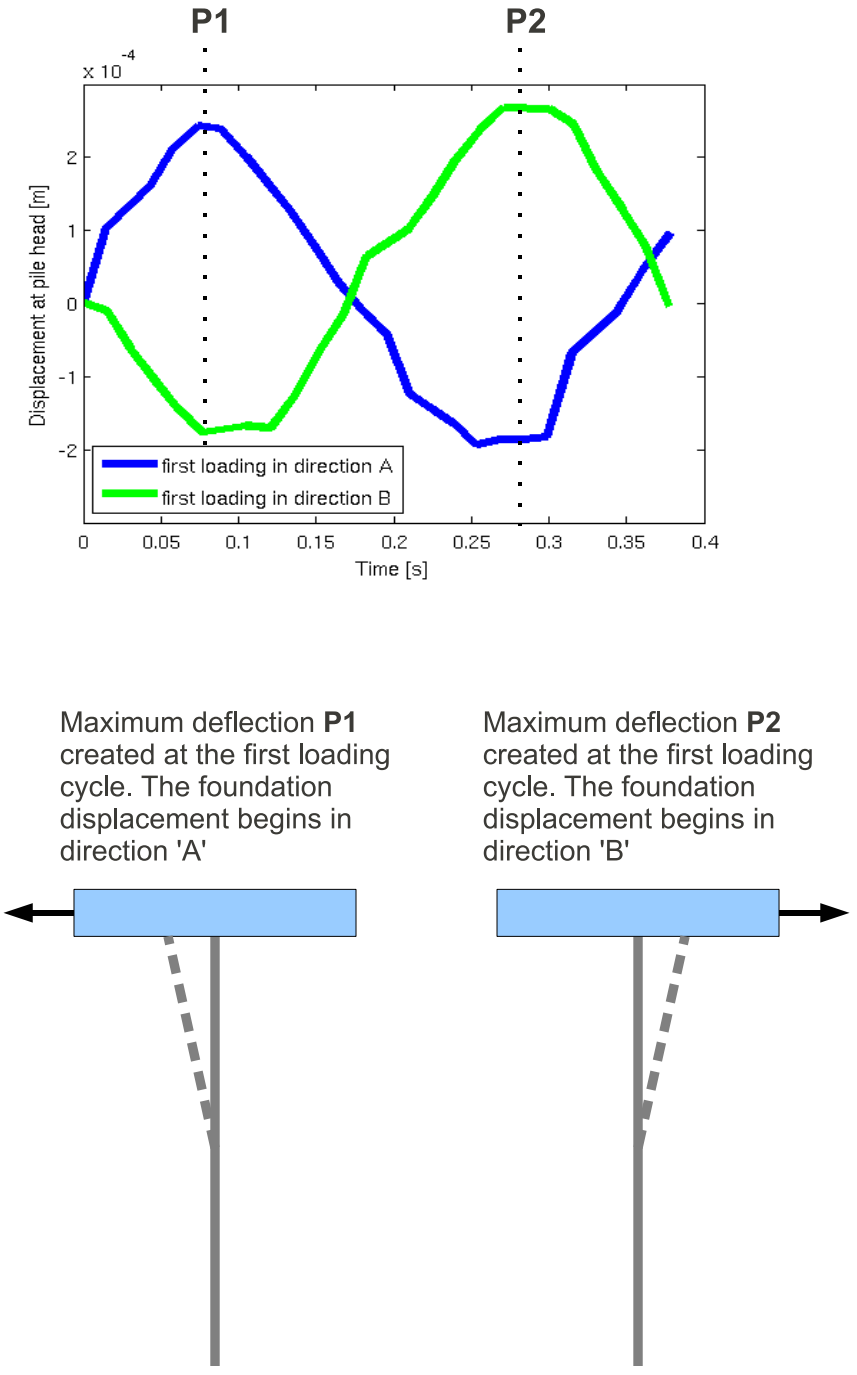

Figure 5.37: Effect of a pile group shown on an example when the foundation displacement is started in two oppsite directions - definition of P1 and P2

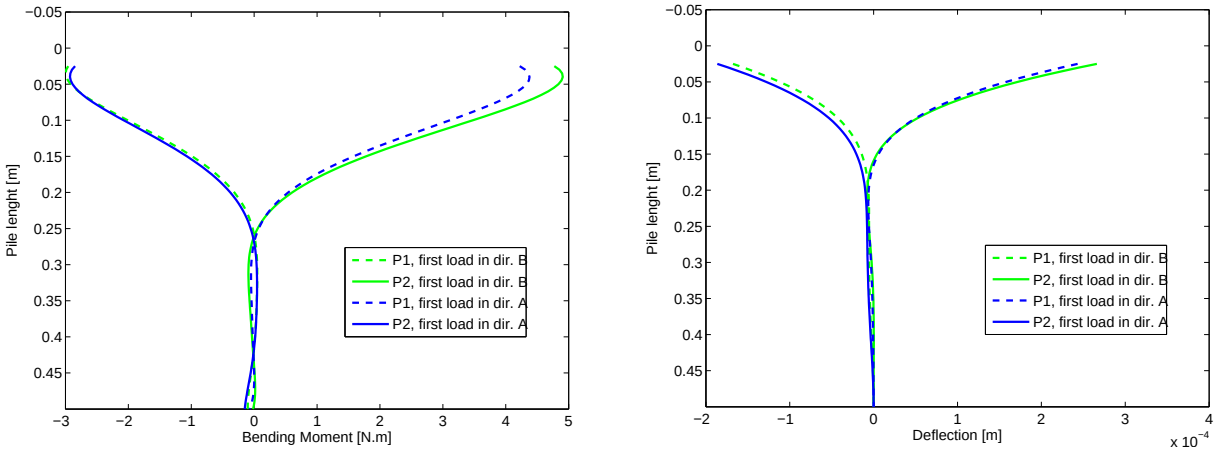

(a) (b)

Figure 5.38: M and y values at amplitudes of the pile head deflection (P1 and P2 in figure 5.37)

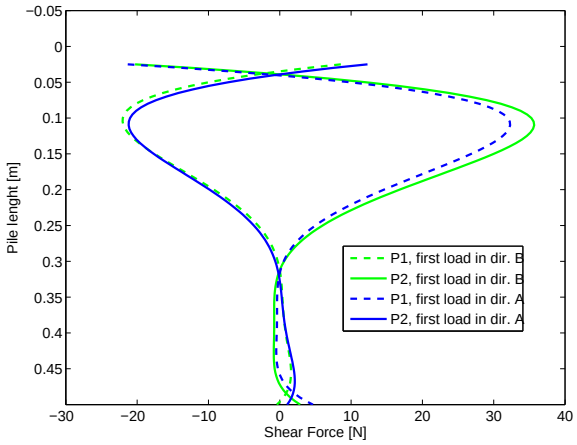

(a)

Figure 5.39: T values at amplitudes of the pile head deflection (P1 and P2 in figure 5.37)

P-y curves

As described in the chapter 4, the P-y loops could be derived from strain measurements. These P-y loops describe pile lateral performance not only in terms of lateral soil reaction and deflection, but also in terms of pile-soil stiffness and energy dissipation. Each P-y loop, obtained from one load cycle, is approximated by an ellipse. Area of this ellipse is used to calculate energy dissipation and its slope is used to calculate stiffness of the pile surrounded by clay.

Dependence of P-y curves on depth

The P-y loops are plotted in Figure 5.40 for four different vertical positions - 3cm, 5.4cm, 7.4cm and 10.4cm from the pile head. Each of the subfigures shows loops obtained at a certain depth during the 30 loading cycles. Logically the size and the area of the P-y loops is

decreasing with depth.
Position of the loops in the P-y space shows that the lateral soil resistance is mobilized more when foundation is loaded in direction 'A', i.e. in direction heading outside the pile group (Figure 5.26). This means, that the positive lateral soil reaction reaches higher values than the negative lateral soil reaction. Such an observation can be explained by the 'shadow effect' between front and rear pile in the group, which limits the instrumented pile deflection, and consequently the lateral soil reaction, when the foundation moves in direction 'B'. In the second half of the cyclic loading, values of negative lateral soil reaction start to decrease and move towards zero. This is assumed to mark a starting presence of a gap between the soil and the pile. This gap develops in direction 'B' from the instrumented pile and is shown in Figure 5.41.
Slope of the P-y loop expresses stiffness of the pile-soil system. It is shown by numerous authors (Rosquoët, 2004), (Khemakhem, 2012), etc. dealing with the lateral pile behaviour in the centrifuge that the pile-soil stiffness increases with depth. This phenomenon was not observed for the reduced physical model presented and is due to the fact that the soil has uniform properties with depth.

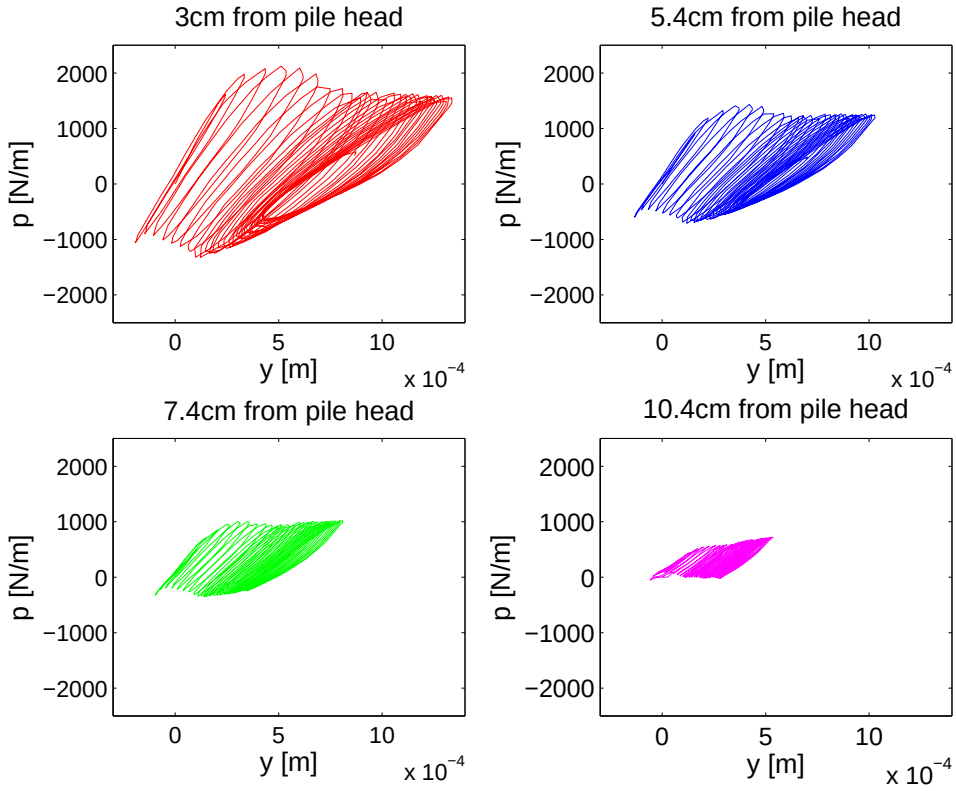

Figure 5.40: P-y curves plotted at different positions of a pile associated to a LTC with 8 cm height (exp LTC11)

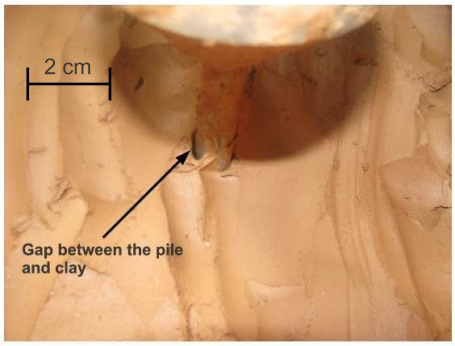

Figure 5.41: Gap created between the pile and the clay

Dependence of P-y curves on number of cycles

With the cyclic loading, the stiffness of the pile-clay system decreases. This phenomenon will be further referred as stiffness degradation. This is due to the fact, that as the pile penetrates horizontally into the surrounding clay, the soil gets disturbed. Due to the clay nature and cohesion, the generated gap doesn't close after the pile returns back to its initial position. Due to this gap opening and due to degradation of the clay mechanical properties, the stiffness of the pile-soil system decreases with the cyclic loading. The stiffness degradation has a tendency to stabilize in the second half of the cyclic loading.

Figure 5.42 shows a detail of a P-y loop at 2.5cm depth from the pile head. Beginning of the cyclic loading is marked by a red star. It can be seen, that the position of the loop in the P-y space stabilizes after approximately ten cycles. This is in agreement with the previously presented results that show M, y and T stabilization in the second half of cyclic loading.

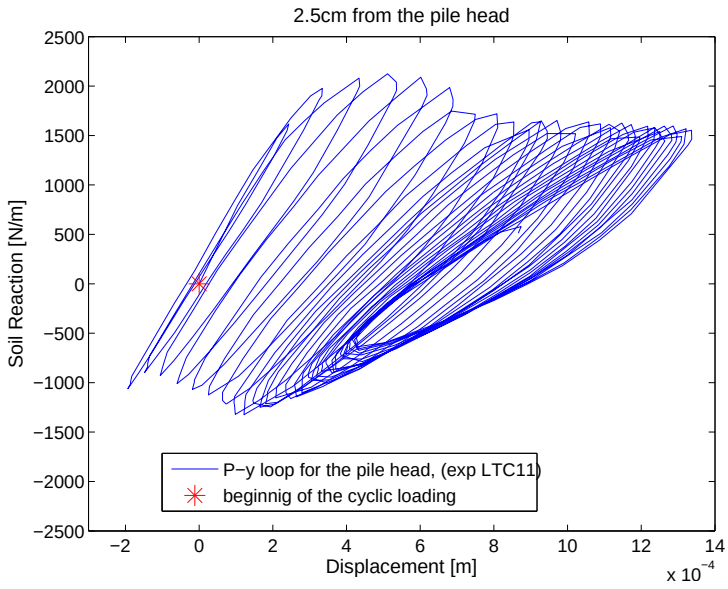

Figure 5.42: P-y curves for pile associated to a LTC with 8 cm height (exp LTC11)

Each P-y loading cycle can be approximated by an ellipse (Figure 5.43) representing a hysteresis loop. Each loop is then analysed and the P-y stiffness is calculated.
Figure 5.44 shows the stiffness evolution throughout the cyclic loading. Results of two experiments performed with the same column height are plotted and show a stiffness degradation with the increasing number of cycles. This tendency is common for all experiments performed. In general, no influence of the stone column height on the stiffness of the pile-soil system was found.
Evaluating the initial slope of the P-y loops in Figure 5.43, an initial value of E_s equal to 6MPa was obtained. This is in the same order as the initial value of E_s determined for the vertical loading (see Figure 5.19).

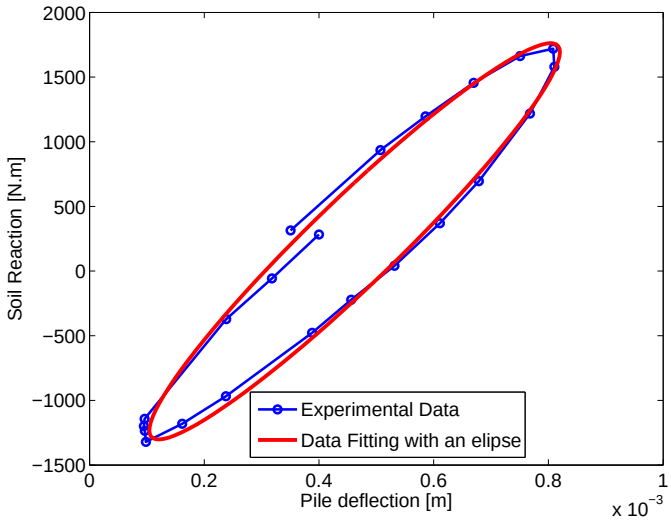

Figure 5.43: P-y curve approximated by an ellipse in order to evaluate the P-y stiffness (exp LTC11)

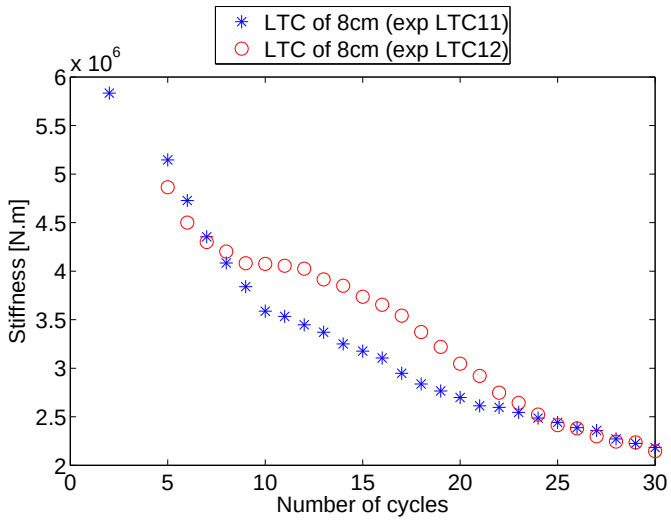

Figure 5.44: Stiffness evolution of the P-y curves during the cyclic loading. Results of experiments when piles were associated to LTCs of 8 cm (exp LTC11, LTC12)

5.6.2 Soil reinforced by piles associated to Load Transfer Platform (LTP)

5.6.2.1 Foundation Settlement

The behaviour of shallow foundation under a dynamic loading on soil reinforced by piles associated to a gravel mattress (LTP) was studied in the same way as for the soil reinforced by piles associated to a gravel column (LTC). Thickness of the mattress was varied in order to study its effect on the foundation settlement, which is shown in Figure 5.45. It was observed, that the amount of settlement under dynamically loaded foundation increases with increasing mattress thickness. This phenomenon can be explained by an assumption that thinner mattress tends to transfer more of the imposed vertical load to the rigid inclusions and therefore the upper, flexible part of the system is less compacted under the combined loading. Settlement accumulated during the 30 cycles varies from 2.8 to 7 mm, depending on the mattress thickness. For thinner mattress, a settlement stabilization is reached by the end of cyclic loading. It can be noticed that the value of the accumulated settlement is higher compared with the value of settlement caused by static vertical loading of the foundation model (Figure 5.10 - 5.12).

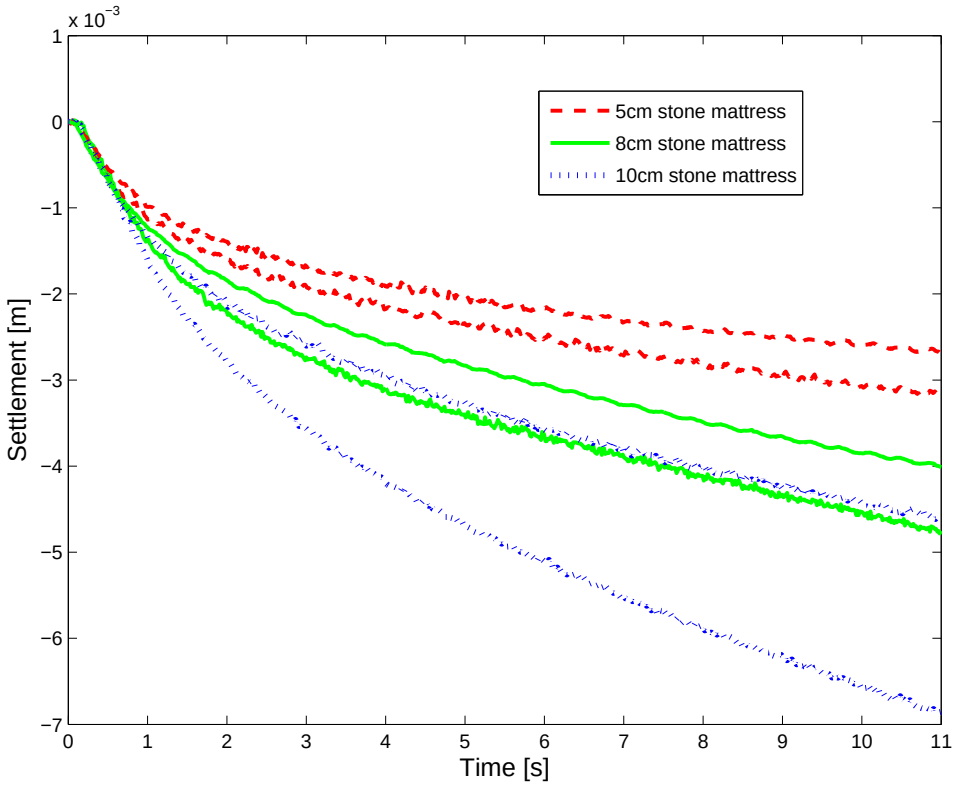

Figure 5.45: Foundation settlement under dynamic loading - soil reinforced by piles supporting a mattress (LTP)

5.6.2.2 Horizontal response of the foundation model

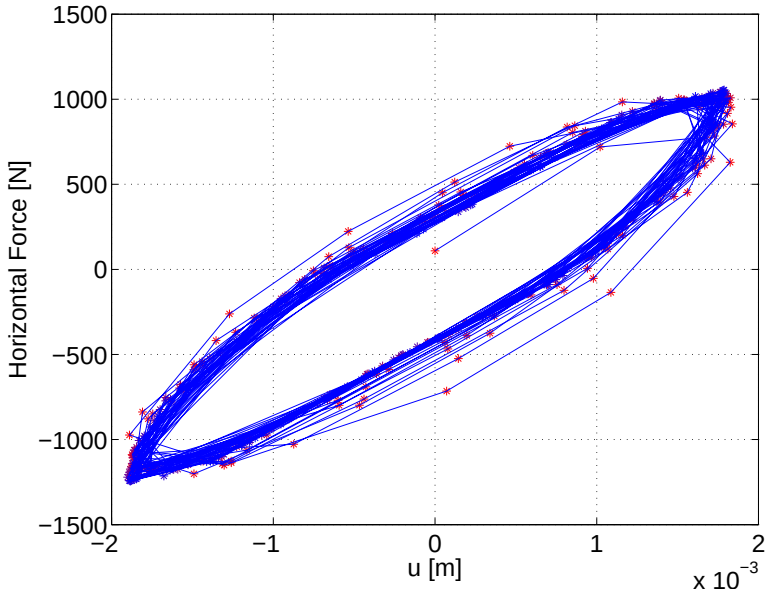

(a)

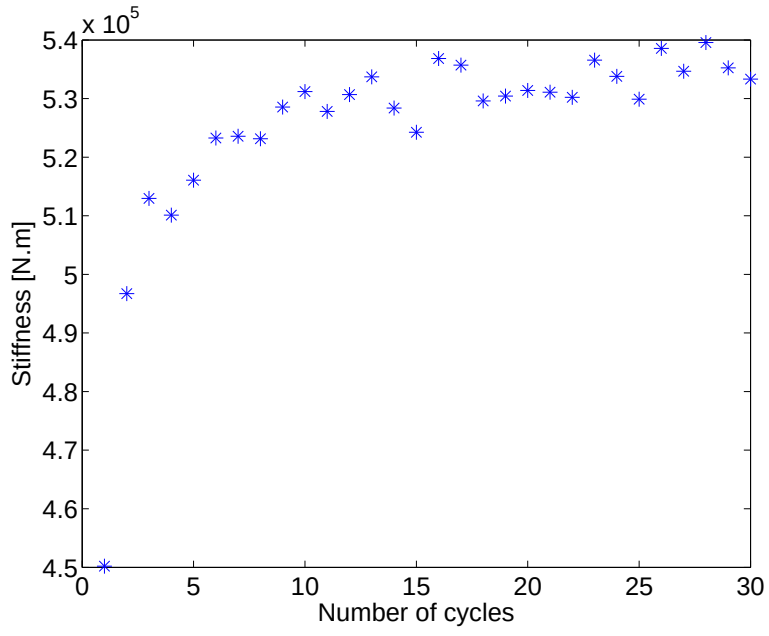

(b)

Figure 5.46: (a) Horizontal force registered at the foundation level when it is subjected to cyclic displacement with a constant amplitude; (b)Increasing stiffness of the system soil-reinforcement throughout the cyclic loading; exp LTP5

As the cyclic displacement with a constant amplitude was applied to the foundation model, the foundation response in terms of horizontal force was measured. The results are shown in

Figure 5.46(a) which shows loops describing the relation between the horizontal displacement and the horizontal force measured at the foundation level. It was observed that the loops change their inclination throughout the cyclic loading and therefore it can be deduced that the system rigidity changes with the number of cycles. This rigidity increase is shown in Figure 5.46(b) and is explained by the fact that at the foundation settles throughout the cyclic loading, the LTP becomes more dense and rigid and cause the global rigidity of the system to increase.

5.6.2.3 Physical values derived from strain measurements in the pile associated to a LTP

Moment M, Deflection y and Shear Force T

The bending moment, deflection and shear force created along the pile during the cyclic loading are plotted in Figures 5.47 to 5.49. Each of the three figures shows results from one experiment with a LTP height of 5cm, 8cm or 10cm. The results are presented in the way same as is the presentation used in section 5.6.1.3. More figures presenting results from other experiments are listed in Annex B. The obtained results indicate that:

•Varying the mattress thickness, it can be seen, based on the bending moment distribution, that the thinner 5cm gravel mattress tends to induce higher deformation of the pile. Such an observation is more visible from the P-y curves, presented in the following. This confirms that the thinner mattress transfers more loading to the rigid inclusion.

•Pile supporting 8cm and 10cm mattress exhibits similar behaviour.

•Eventhough the pile response under the first loading cycle is more or less symmetric, there is an important deflection accumulation (up to 1mm) with the dynamic loading. This accumulated lateral displacement develops in direction 'A' towards unreinforced soil, i.e. out of the pile group. The deflection accumulation is the most important for the first five cycles and has a tendency to stabilize for the last ten cycles. This phenomenon was observed for both reinforcement systems, i.e. for both cases when piles were associated either to LTCs or LTP.

•The pile undergoes lateral movement up to a depth of approximately 35cm out of its 50cm length. The lateral deformation is apparent at higher depths for the case when the pile is loaded in direction 'B'. Comparing the depth to which the pile is deformed when it is associated either to the LTP or the LTC, it can be seen that it undergoes deformation to larger depth when followed by the LTP.

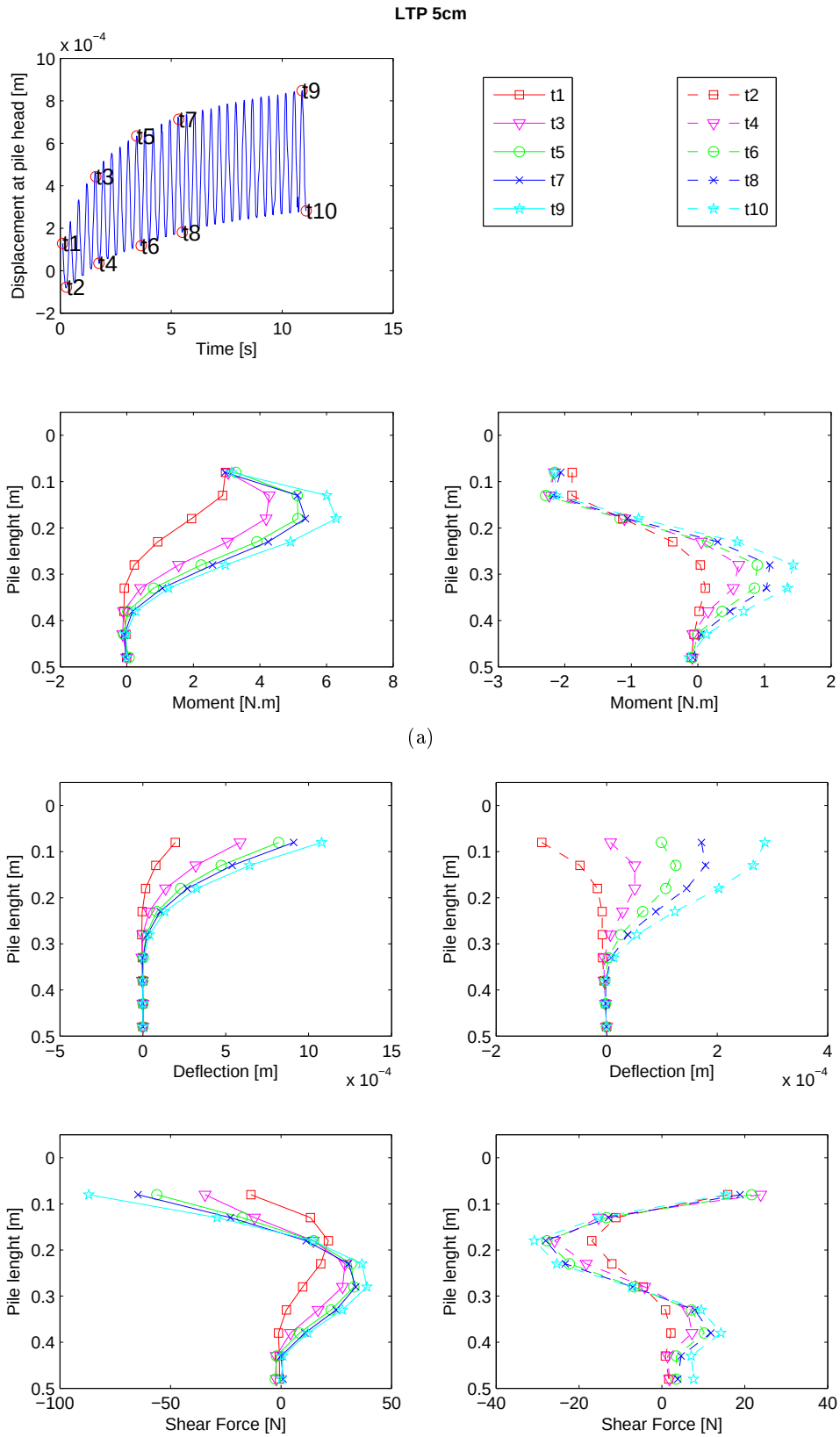

(a)

(b)

Figure 5.47: Bending moment, deflection and shear force along a pile associated to a LTP of 5 cm (exp LTP4); Direction 'A' = t1,t3, t5, t7, t9; Direction 'B' = t2, t4, t6, t8, t10

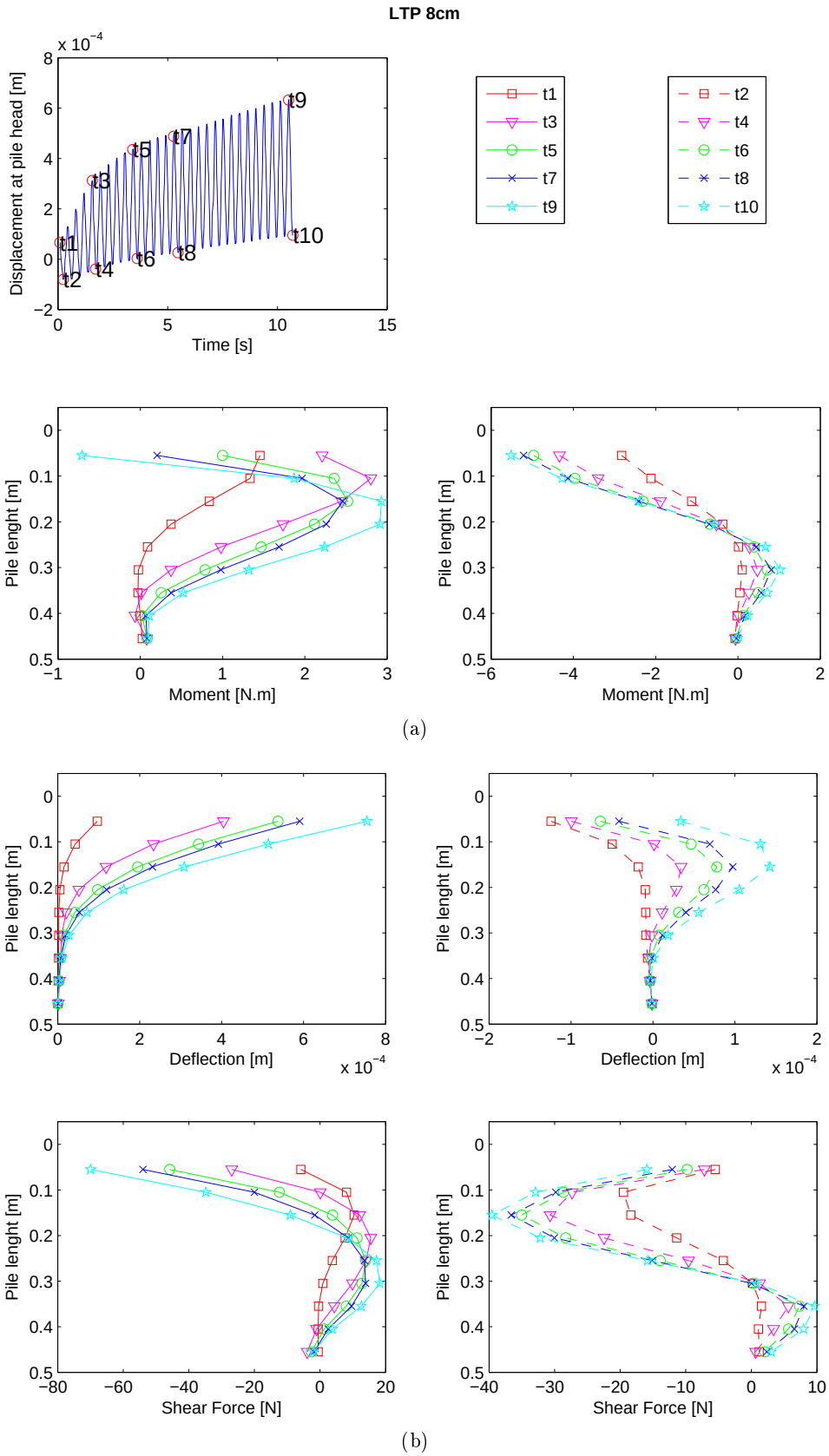

(a)

(b)

Figure 5.48: Bending moment, deflection and shear force along a pile associated to a LTP of 8 cm (exp LTP5); Direction 'A' = t1,t3, t5, t7, t9; Direction 'B' = t2, t4, t6, t8, t10

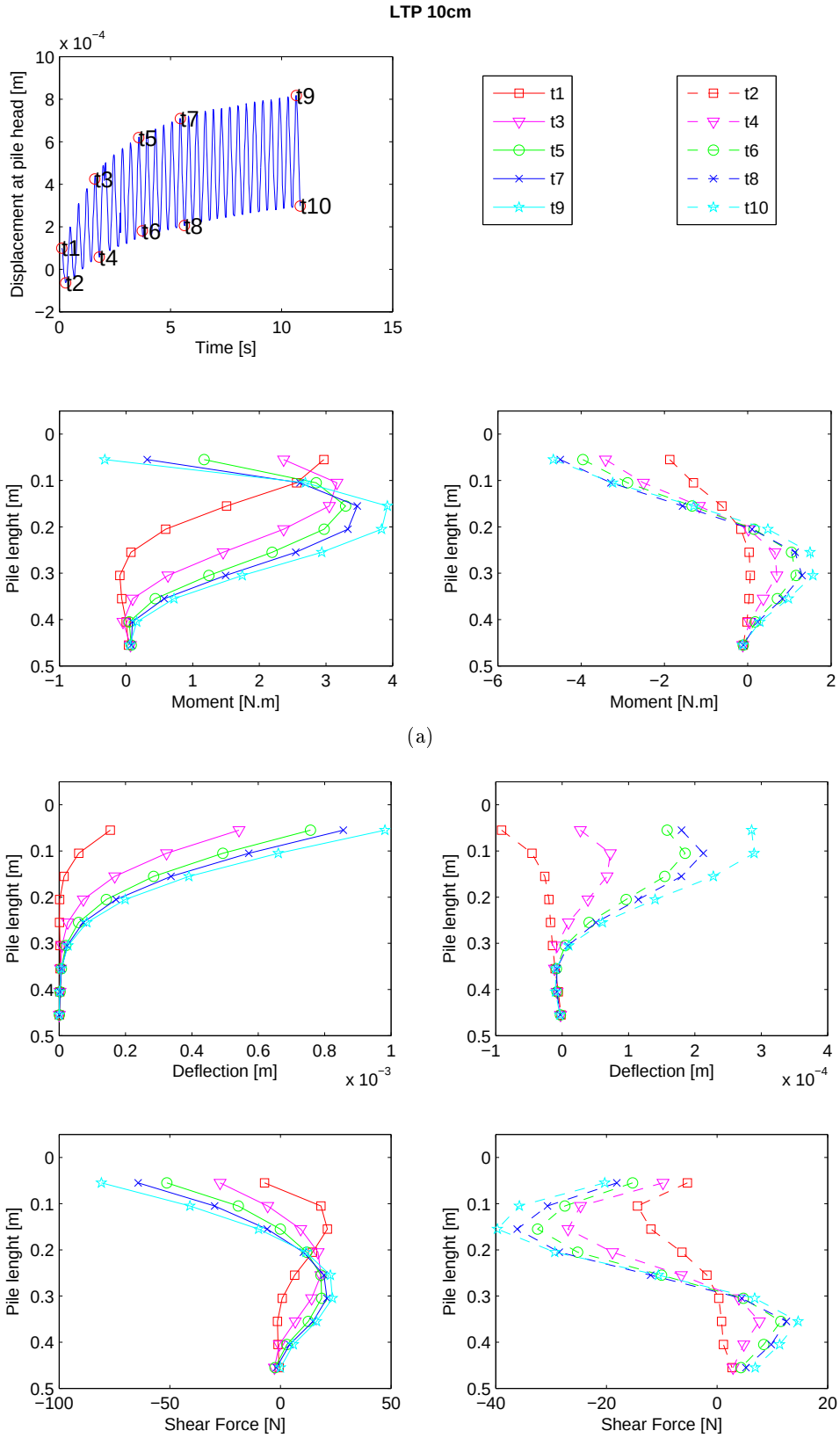

(a)

(b)

Figure 5.49: Bending moment, deflection and shear force along a pile associated to a LTP of 10 cm (exp LTP6); Direction 'A' = t1,t3, t5, t7, t9; Direction 'B' = t2, t4, t6, t8, t10

In order to analyze the influence of the mattress height on the lateral pile performance, moment M, shear force T, deflection y and lateral soil resistance P envelopes were studied. The maximum M, T, y and P envelopes were plotted for the first cycle and then for the total horizontal loading sequence, i.e. 30 cycles:

- **The First Loading Cycle**

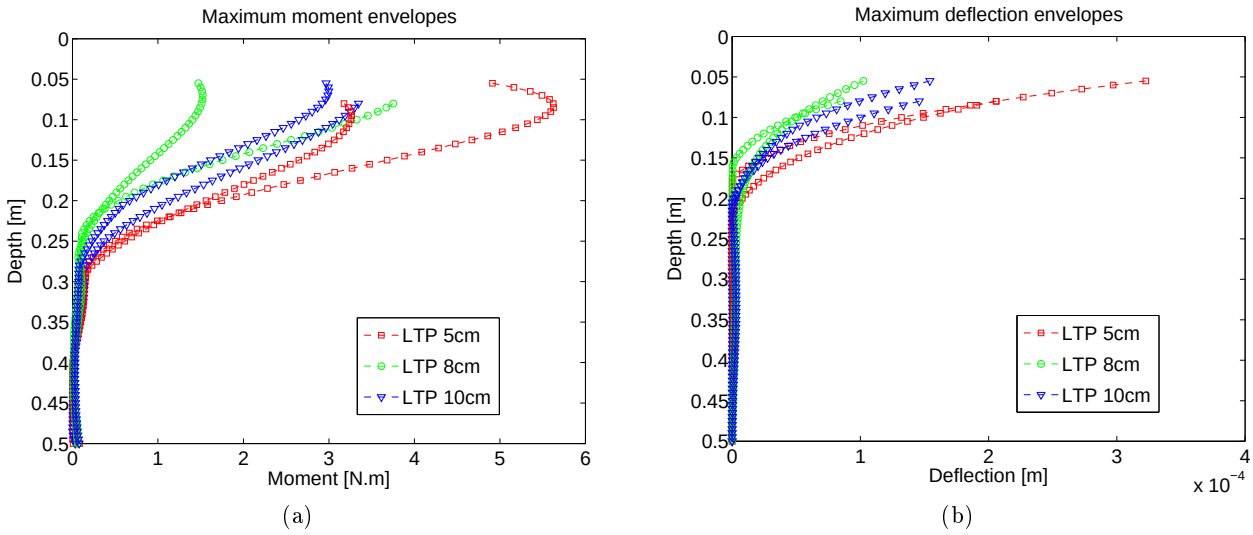

(a) (b)

Figure 5.50: Maximum moment (a) and deflection (b) envelopes for the first loading cycle

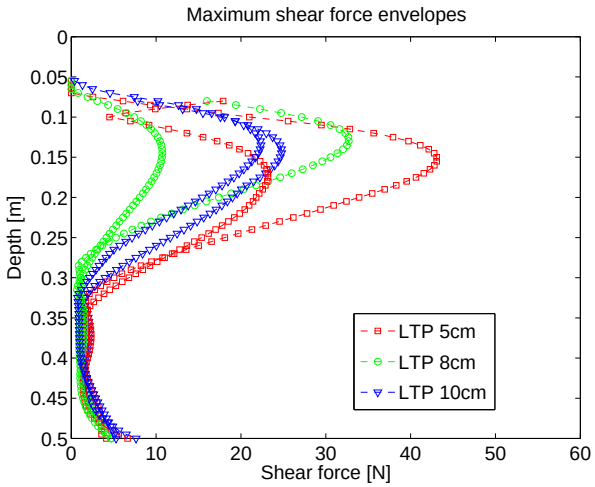

Figure 5.51: Maximum shear force envelopes for the first loading cycle

Figures 5.50 to 5.51 show envelopes of maximum moment, shear force and deflection for the pile subjected to one loading cycle at the beginning of cyclic loading. It is noted that during the first loading cycle, the pile response to the applied loading is higher when the pile is associated to a mattress of 5cm. Pile supporting a 8cm or 10cm mattress

seems to undergo an equivalent level of deformation. This pile behaviour presents a difference compared to cases when the pile is associated to the LTC - there the pile response during the first cycle doesn't show any influence of the column height.

- **30 Loading Cycles**
  Maximum bending moment, shear force and deflection envelopes are plotted in Figures 5.52 and 5.53. Each figure shows results of six experiments when the response of the pile associated to each mattress height was tested twice. Following observations are made:

  – The effect of the mattress height on the pile performance which was observed during the first loading cycle was confirmed for the pile performance during the total of 30 cycles: pile response to the applied loading is higher when the pile is associated to a mattress of 5cm, but is equivalent when the pile is associated to a 8cm or 10cm mattress.

  – The mattress height doesn't seem to have and influence on the position of the local maximum of the bending moment. As shown in the previous section, this was not the case when the pile was associated to a column (LTC). This suggests that there is a less degradation of soil stiffness when the pile is followed by a LTP than when the pile is followed by a LTC.

The pile response over the total 30 cycles suggests that the shorter mattress acts as a more rigid element and therefore transfers higher bending moments and shear forces caused by lateral foundation displacement. The higher mattresses seem to transfer an equivalent level of deformation to the pile head.

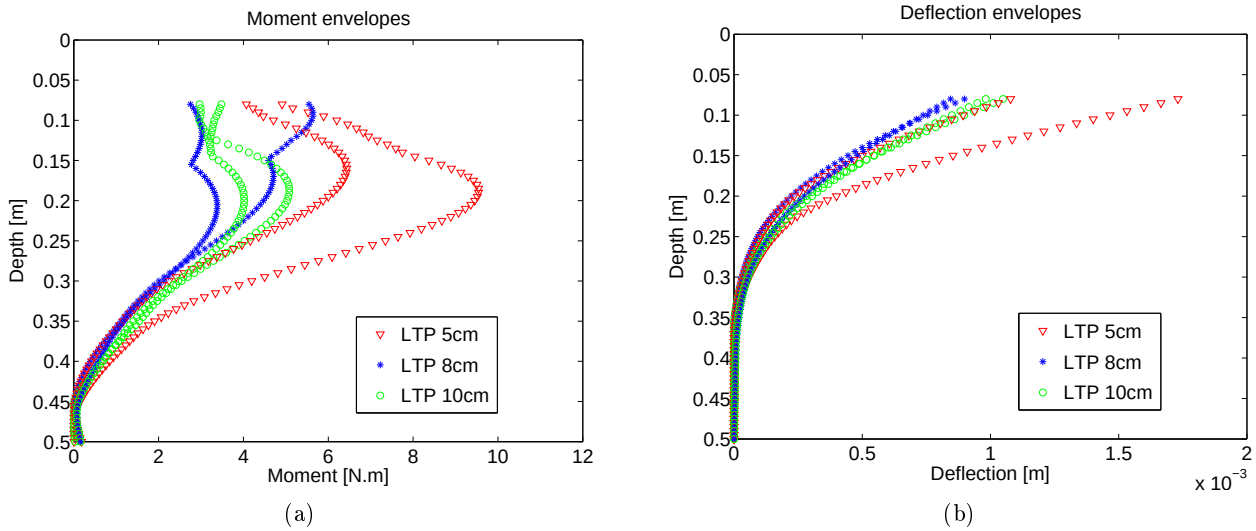

(a) (b)

Figure 5.52: Maximum moment (a) and deflection (b) envelopes for 30 loading cycles

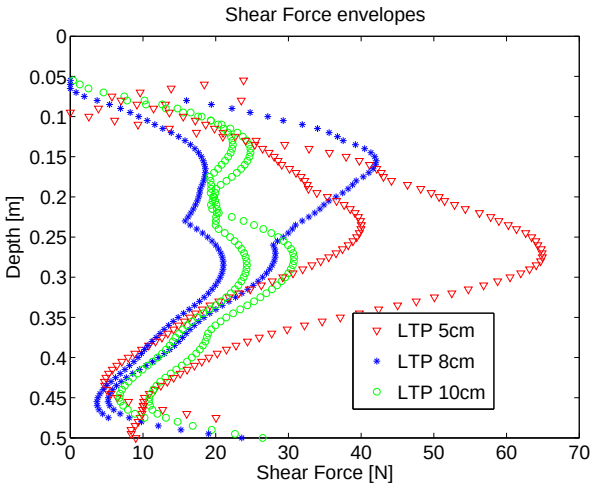

Figure 5.53: Maximum shear force envelopes for 30 loading cycles

P-y curves

This section analyses P-y curves obtained at the top of the instrumented pile associated to a gravel mattress (LTP). The figures are presented in the same manner as in section 5.6.1 which deals with soil reinforced by piles associated to the LTCs. Since there are strong similarities in the observed behaviour for a pile associated to a LTC or a LTP, it was decided not to repeat all the comments already made in the section 5.6.1.
It is noted that a direct comparison between the P-y curves obtained for the instrumented pile supporting the LTC or the LTP can not be made since the P-y curves were plotted for each case at a different vertical position. This was due to the fact that the strain gauges directly at the pile head did not work for experiments performed with the LTP.

Dependence of P-y curves on depth

P-y loops plotted (Figure 5.54) at four different vertical positions logically show that their size and their area is decreasing with depth. The accumulation of displacement in direction 'A' is the cause of mainly positive values of the pile deflection y and the lateral soil reaction P.

Dependence of P-y curves on number of cycles

Figure 5.55 shows a detail of a P-y loop at 5.4cm depth from the pile head. Beginning of the cyclic loading is marked by a red star. The figure well illustrates the pile-soil stiffness degradation.

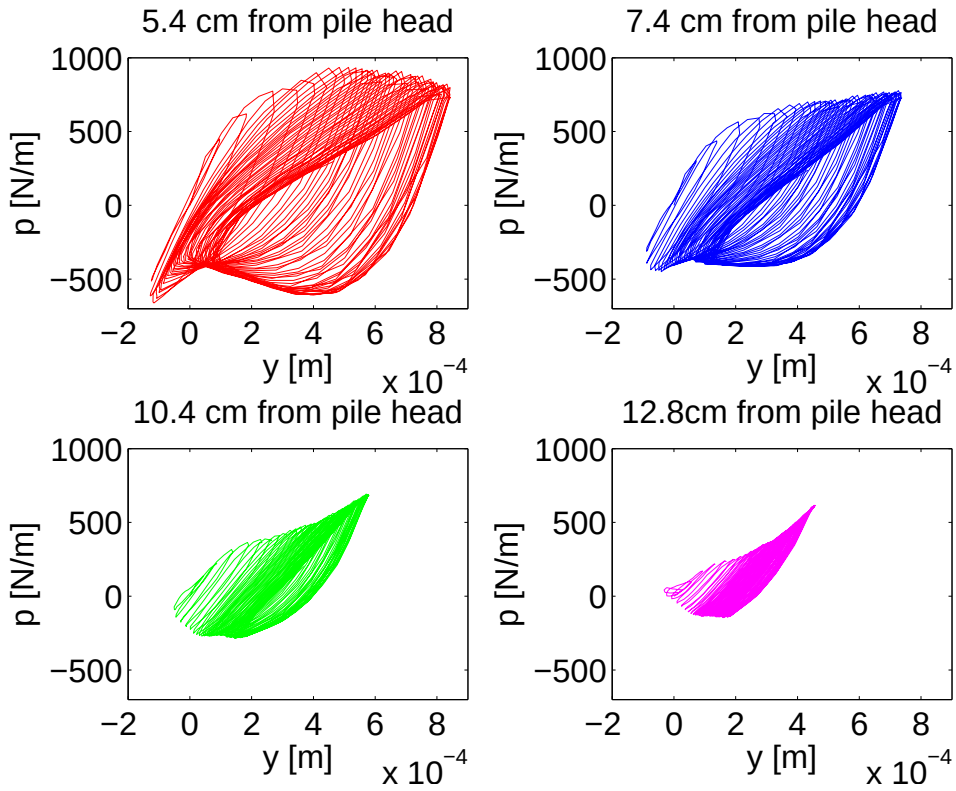

Figure 5.54: P-y curves plotted at different positions of a pile associated to a LTP with 8 cm height (exp LTP5)

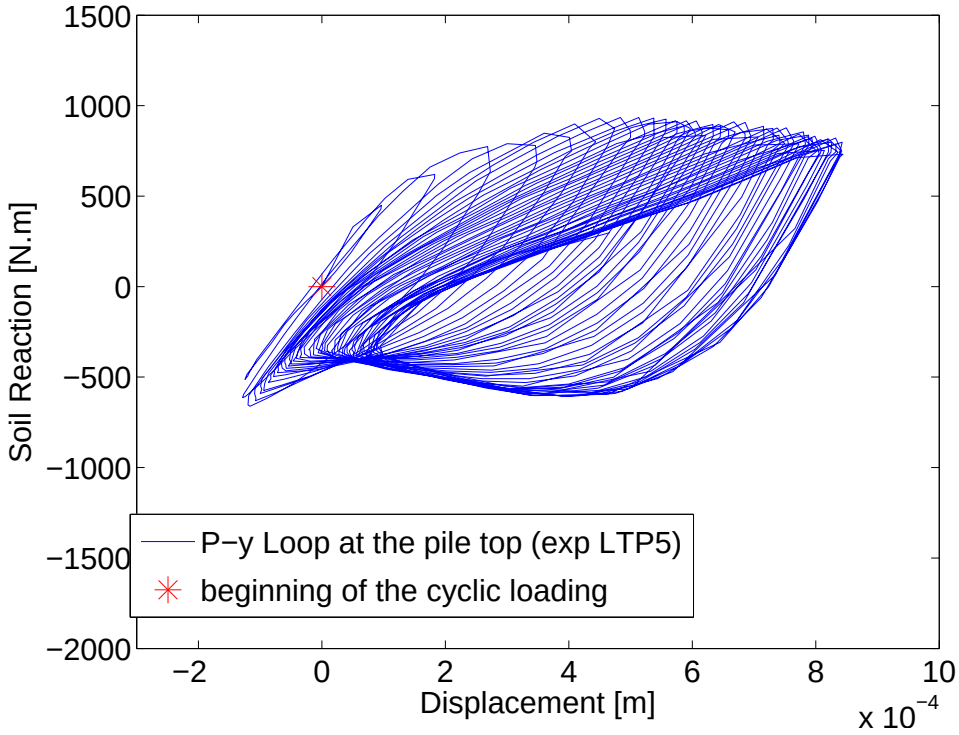

Figure 5.55: P-y curves for pile associated to a LTP with 8 cm height (exp LTP5)

Dependence of p-y curves on the stone mattress thickness
Figure 5.56 shows the pile behaviour in the P-y space for three different mattress thickness. The P-y curves are plotted at depth 8cm from the pile head. It can be seen that the soil reaction P [N/m] decreases with the increasing mattress thickness. This can be linked to the results showing that thinner mattress transfers higher forces to the pile than a thicker mattress and therefore it is logic that the lateral soil reaction P measured at the pile top is higher when pile is associated to a thinner mattress.

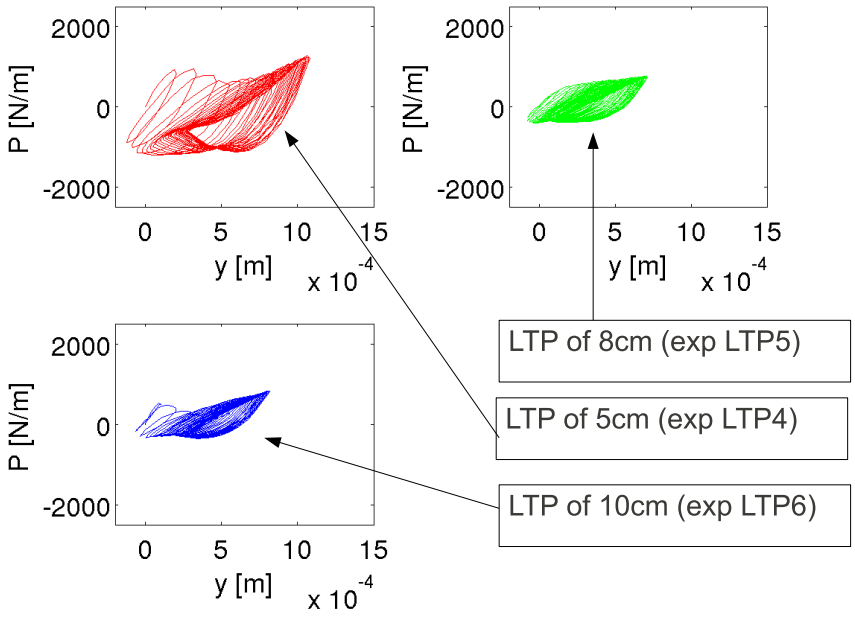

Figure 5.56: P-y loops obtained 8cm from the pile head for different gravel mattress thickness

5.6.3 Energy dissipation analysis

Since the studied soil reinforcement is widely used is seismic zone areas, lot of attention is given to analysing dissipation of energy induced by the foundation dynamic movement. To better understand the mechanism, the physical models are divided into three parts:

1. Foundation and the surrounding clay (1. in Figure 5.57)
2. Upper flexible part of the physical models - Load transfer column (LTC) and the surrounding clay or the Load Transfer Platform (LTP) (2. in Figure 5.57)
3. Pile and the surrounding clay (3. in Figure 5.57)

The energy dissipation in these parts is evaluated independently and conclusions on this coupled mechanism are made. Figures 5.57 illustrates the notations used in the following text.

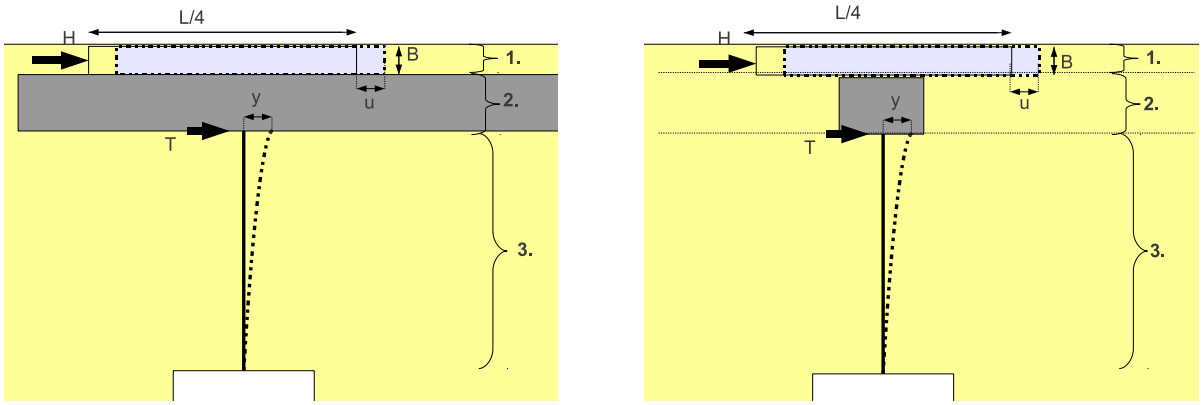

(a) (b)

Figure 5.57: Horizontal loading of a shallow foundation on soil reinforced by LTP (a) or LTC (b). Introduction of the notations used

Referring to Figure 5.57, H is said to be 1/4 of the total horizontal force applied to the foundation. This is done in order to evaluate the stiffness of soil associated to one out of the four piles which make part of the physical models. It is assumed that H is equal to the shear force applied at the top of the flexible parts (LTC or LTP) of the physical models. The foundation horizontal displacement is noted as u and is assumed to be equal to the horizontal displacement of the LTC or the LTP top. Lateral displacement of the pile head y is supposed to be equal to the horizontal displacement of the bottom of the LTC or LTP. Shear force measured at the pile head is denoted T and is considered to represent the shear force at the bottom of the flexible parts.

Global energy dissipation - energy dissipation at the foundation level

Evaluation of energy balance at foundation level can be obtained from measuring horizontal force needed to induce the lateral movement of the foundation. This shear force is dependent on vertical pressure between the soil and foundation, the interface characteristics and lateral pressure of soil acting on sides of the foundation. Because the aim is to evaluate energy balance within a soil section above one out of four piles, the total shear force measured is divided by four since there are four piles acting in the system. This is not entirely correct since it implies an assumption that each pile is subjected to the same amount of horizontal force. It is well known that the horizontal load distribution between a pile group shows that the front row of piles is subjected to higher lateral load than the back row (Brown et al., 1987). Despite this, the used approach is considered as acceptable since it is dealing with horizontal cyclic loading and therefore the used shear force H can be considered as an 'average' shear force acting on the top of the stone column throughout the cyclic loading.
Each H-u loop is approximated by an ellipse and a damping ratio, stiffness, accumulated energy and dissipated energy are evaluated according to procedures described in section 4.3.1. The results are summarized in the following paragraph.
Figure 5.58(a) shows H-u loops obtained for an experiment where the soil mass improved by piles associated to LTCs of 8cm height is subjected to a dynamic lateral loading of the shallow foundation model. Based on the methods described in section 4.3.1, damping ratio ξ_{eq}, stiffness k_{eq}, accumulated energy Ws_{eq} and dissipated energy Wd_{eq} are evaluated for each

cycle, as can be seen in Figure 5.58(b). The same presentation of the results but for a soil mass improved by piles associated to a LTP of 8cm height is shown in Figure 5.59.
Evaluating such results for each experiment performed, the following conclusions are made:

- The global stiffness and accumulated energy increase with cyclic loading.
- The global damping ratio and dissipated energy decrease with cyclic loading.
- The level of damping ratio degradation decreases with time. It is observed that during the first couple of cycles, damping ratio decreases to approximately two thirds of its initial value.
- In general, the system has a tendency to stabilize after 15 cycles for a case when the pile is associated to a LTP or after 20 cycles when the pile is associated to a LTC.
- As mentioned, the global stiffness increases with cyclic loading. This observation is in agreement with the decreasing energy dissipation during the cyclic loading, because as the system becomes more rigid, its capability to absorb energy decreases.

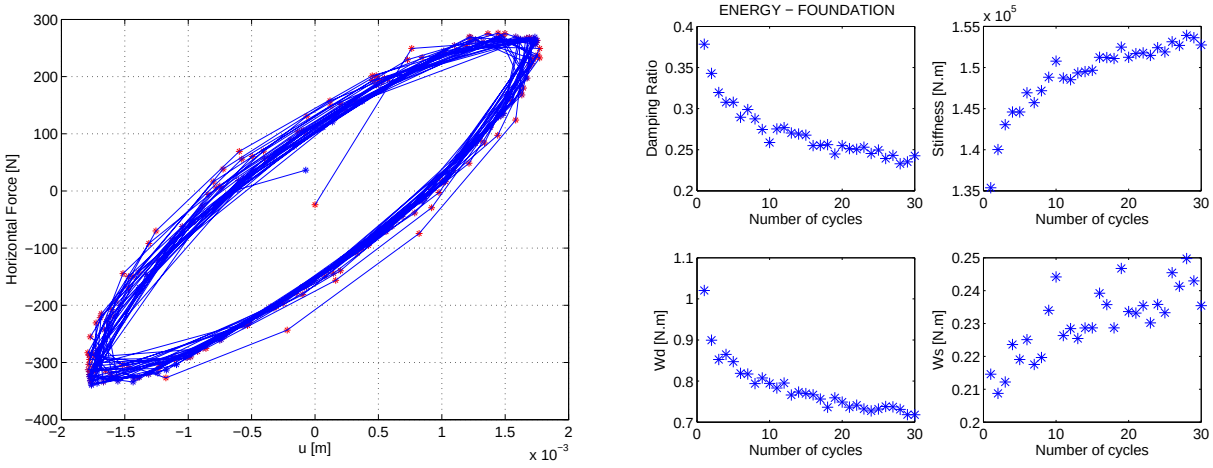

(a) (b)

Figure 5.58: Global energy dissipation; LTC 8cm (exp LTC11)

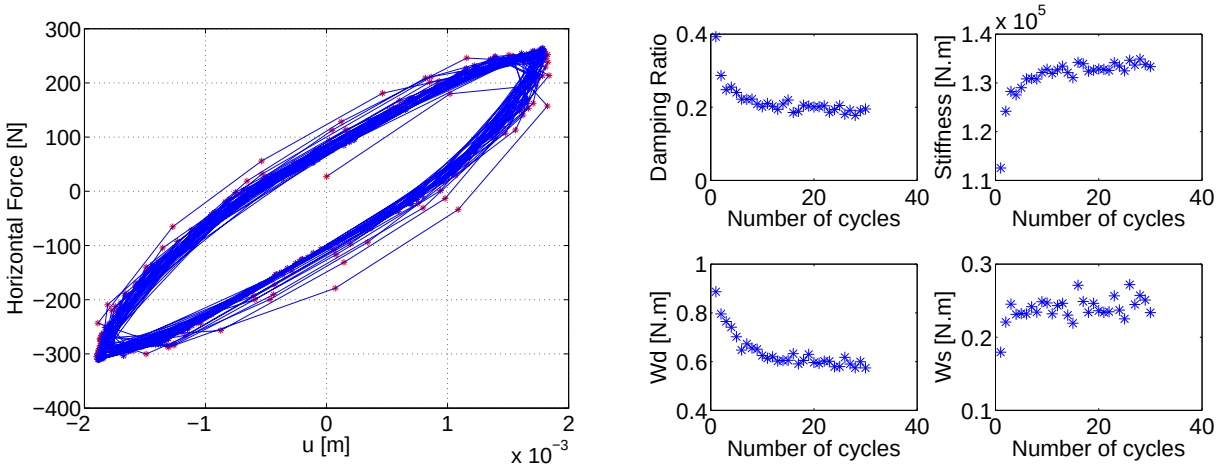

(a) (b)

Figure 5.59: Global energy dissipation, LTP 8cm (exp LTP5)

More figures showing results of other experiments are listed in Annex B.
Since the values of damping ratio ξ_{eq}, stiffness k_{eq}, accumulated energy Ws_{eq} and dissipated energy Wd_{eq} have a tendency to stabilize in the second half of cyclic loading, only values of ten last cycles are used in a Gaussian distribution performed. This gives, for the ten cycles, one value of ξ_{eq}, k_{eq}, Ws_{eq} and Wd_{eq} with a strongest probability. Such a process is repeated for each experiment with the aim of comparing the energy dissipation for experiments with different height of LTC or LTP. The results obtained for soil reinforced by piles associated to LTCs are plotted in Figures 5.60 and 5.61 and results obtained for soil reinforced by piles associated to LTP are plotted in Figures 5.62 and 5.63. These figures show height of the upper flexible layer on the x-axes and the values of ξ_{eq}, k_{eq}, Ws_{eq} and Wd_{eq} obtained with the Gaussian distribution are plotted on y-axis.

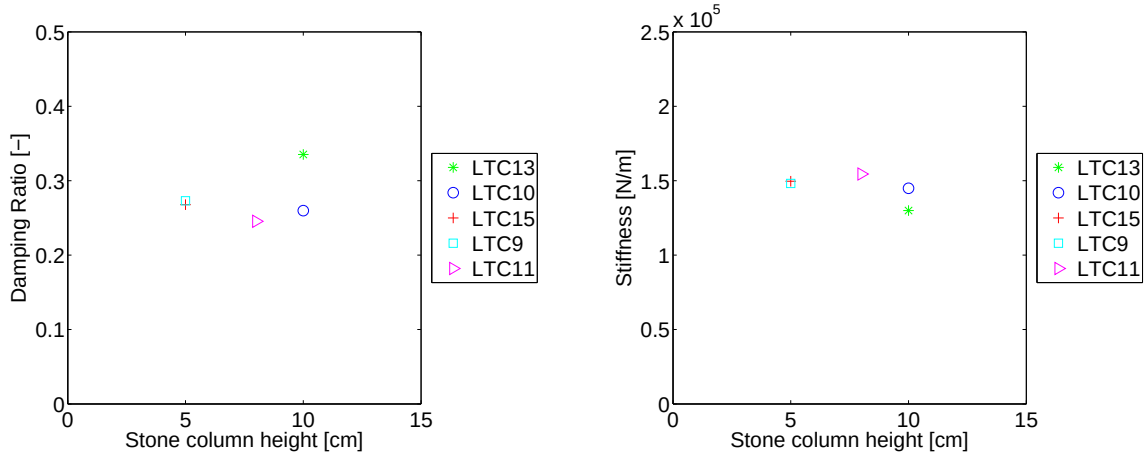

(a) (b)

Figure 5.60: Global damping ratio and dissipation for different heights of stone columns (LTC)

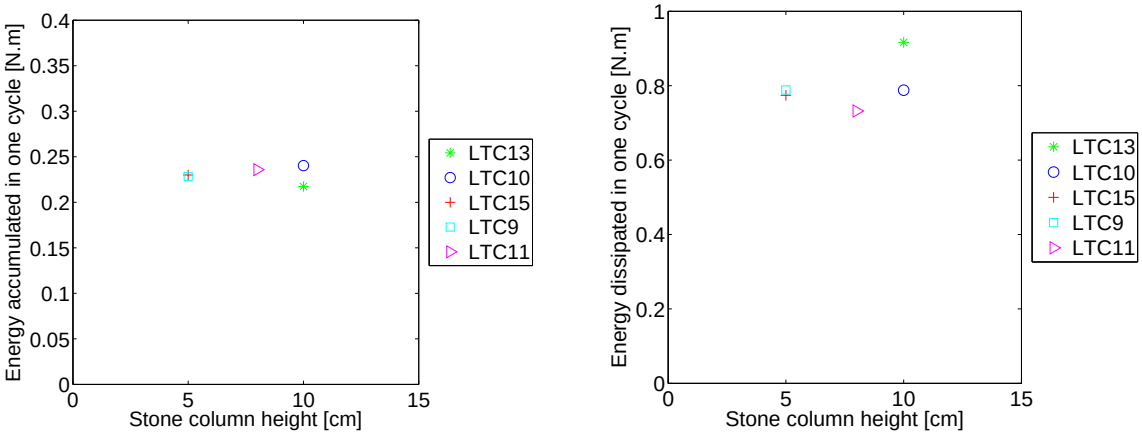

(a) (b)

Figure 5.61: Global energy balance for different heights of stone columns (LTC)

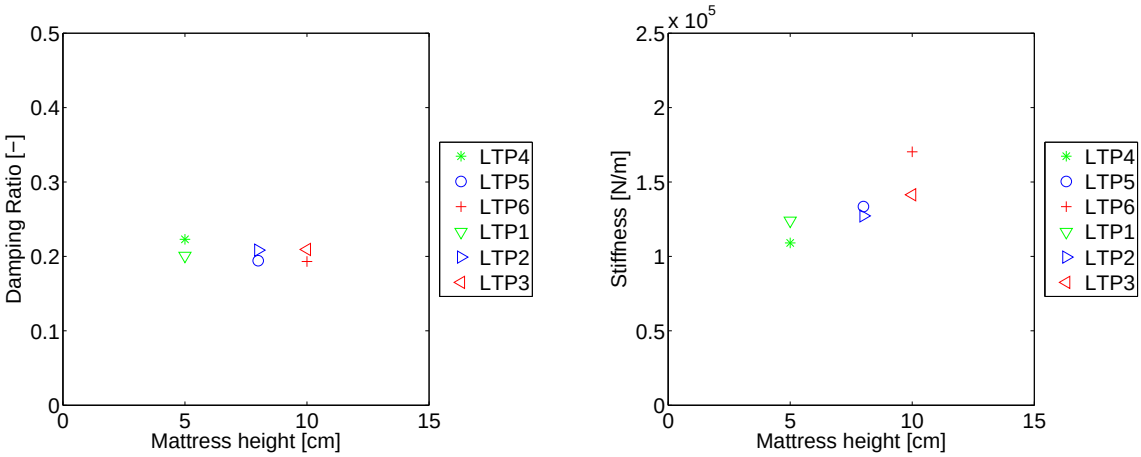

(a) (b)

Figure 5.62: Global damping ratio and dissipation for different mattress thickness (LTP)

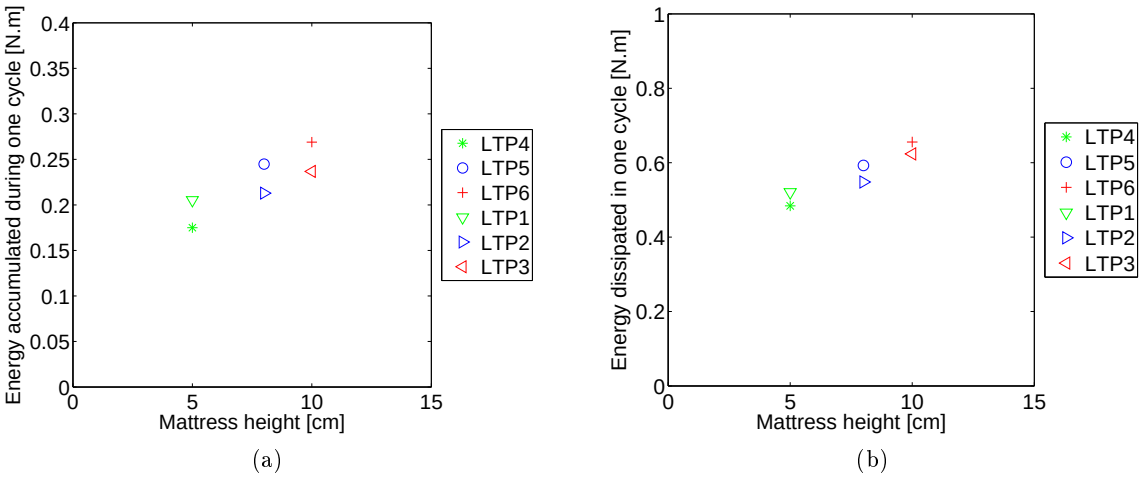

(a) (b)

Figure 5.63: Global energy balance for different mattress thickness (LTP)

The following table summarizes the results shown in Figures 5.60 to 5.63

Table 5.1: Global Dissipation

Soil reinforced with piles associated to LTCs		
	Stiffness	1.3e5 N/m to 1.55e5 N/m
	Damping ratio	0.24 to 0.28
	Energy dissipated	0.73 J to 0.92 J
	Energy accumulated	0.22 J to 0.24 J
Soil reinforced with piles associated to LTP		
	Stiffness	1e5 N/m to 1.7e5 N/m
	Damping ratio	0.18 to 0.23
	Energy dissipated	0.46 J to 0.7 J
	Energy accumulated	0.17 J to 0.27 J

In the case of soil reinforced by piles associated to LTCs, there can be seen no effect of the stone column height on the global stiffness, dissipated energy nor damping ratio. On the contrary, for soil reinforced by piles associated to a LTP, the global energy and stiffness seem to increase with the increasing LTP height.
Based on the results presented, piles associated to LTCs seem to be able to dissipate more energy than the piles associated to LTP.

Energy dissipation within the flexible part of the models

Evaluation of energy dissipated in the flexible part of the physical models composed of LTC surrounded by clay or LTP, can be obtained from relation between horizontal force applied at the foundation level H and the difference between the pile head and foundation displacement u-y (Figure 5.57). Each H-*(u-y)* loop is approximated by an ellipse and a damping ratio, stiffness, accumulated energy and dissipated energy are evaluated according to procedures described in section 4.3. The results are summarized in the following paragraph.
Figure 5.64(a) shows *H-(u-y)* loops obtained for an experiment when the soil mass improved by piles associated to 8cm high LTCs is subjected to a dynamic lateral loading of a shallow foundation model. Based on methods described in section 4.3, damping ratio ξ_s , stiffness k_s, accumulated energy Ws_s and dissipated energy Wd_s are evaluated for each cycle, as can be seen in Figure 5.64(b). The same presentation of the results but for a soil mass improved by piles associated to a LTP of 8cm height is shown in Figure 5.65.
Due to technical problems, deformation at the pile head y could not be measured for experiments performed with LTP. The first measurements that could be used for data interpretation were 8cm from the pile head. Because the pile response directly at the pile head was not known, deflection values at 8cm from the pile head were considered as y in the following evaluation. Evaluating results obtained for each experiment performed, the following conclusions are made:

- In general, the system has a tendency to stabilize after 15 and 20 cycles for experiments with LTP and LTC, respectively.

- The stiffness k_s and accumulated energy Ws_s within the flexible part of the models show the same trend as the stiffness k_{eq} and accumulated energy Ws_{eq} evaluated at the foundation level, i.e. their values increase with the increasing number of cycles. This phenomenon can be explained by the fact that the gravel densifies throughout the cyclic loading and therefore its stiffness rises, which implies a higher elastic energy accumulation.

- It is observed that reached k_s and ξ_s values are higher than the k_eq and ξ_eq.

$$k_{s(n)} > k_{eq(n)} \tag{5.14}$$

and

$$\xi_{s(n)} > \xi_{eq(n)} \tag{5.15}$$

where n is the cycle number varying from 1 to 30.

- Damping ratio ξ_s and energy dissipated Wd_s within the stone columns surrounded by clay show the same trend as the damping ratio ξ_{eq} and dissipated energy Wd_{eq} evaluated at the foundation level, i.e. their values decrease with the increasing number of cycles. This phenomenon can be explained by the fact that as the gravel densifies throughout the cyclic loading, less plastification is taking place. As a consequence, the dissipated energy, which is proportional to the degree of soil plastification, decreases with cyclic loading.

- It is observed that reached Ws_s and Wd_s values are logically smaller than the Ws_{eq} and Wd_{eq}.

$$Ws_{s(n)} < Ws_{eq(n)} \tag{5.16}$$

and

$$Wd_{s(n)} < Wd_{eq(n)} \tag{5.17}$$

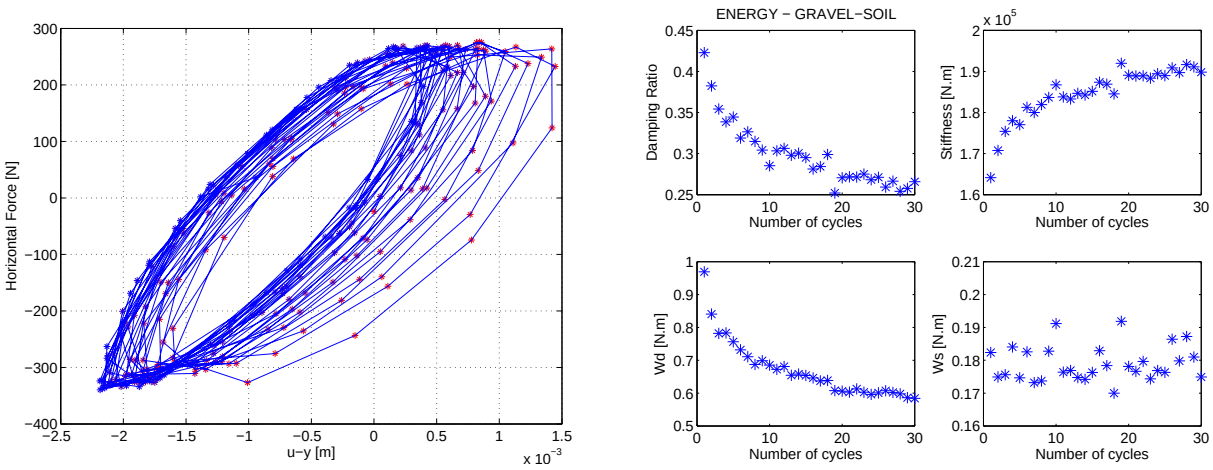

(a) (b)

Figure 5.64: Energy dissipation within an 8cm high column (LTC) surrounded by clay; (exp LTC11)

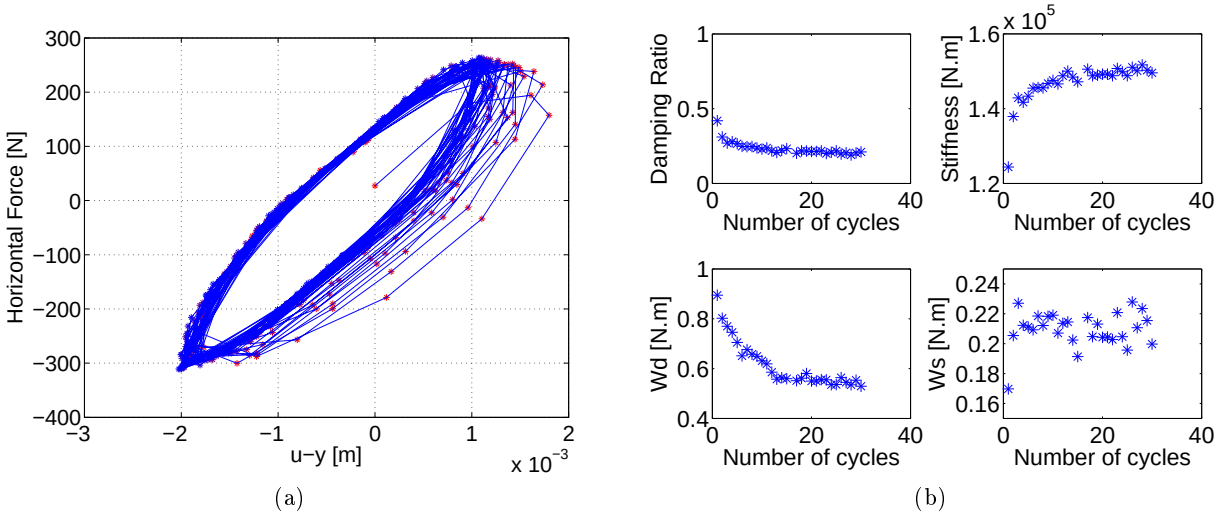

Figure 5.65: Energy dissipation within an 8cm high mattress (LTP); (exp LTP5)

More figures showing results of other experiments are listed in Annex B.
Performing a Gaussian distribution while taking into consideration only stabilized values of damping ratio ξ_s, stiffness k_s, accumulated energy Ws_s and dissipated energy Wd_s (i.e. their values for the ten last cycles) one value of ξ_s, k_s, Wd_s and Ws_s with a strongest probability was obtained. Such a process was carried out for each experiment with the aim of comparing the energy dissipation for experiments with different height of LTC or LTP. The results obtained for soil reinforced by piles associated to LTCs are plotted in Figures 5.66 and 5.67, and results obtained for soil reinforced by piles associated to LTP are plotted in Figures 5.68 and 5.69. Height of the upper flexible layer (LTC or LTP) is plotted on x-axes and the values of ξ_{eq}, k_{eq}, Ws_{eq} and Wd_{eq} obtained with the Gaussian distribution are plotted on y-axis.

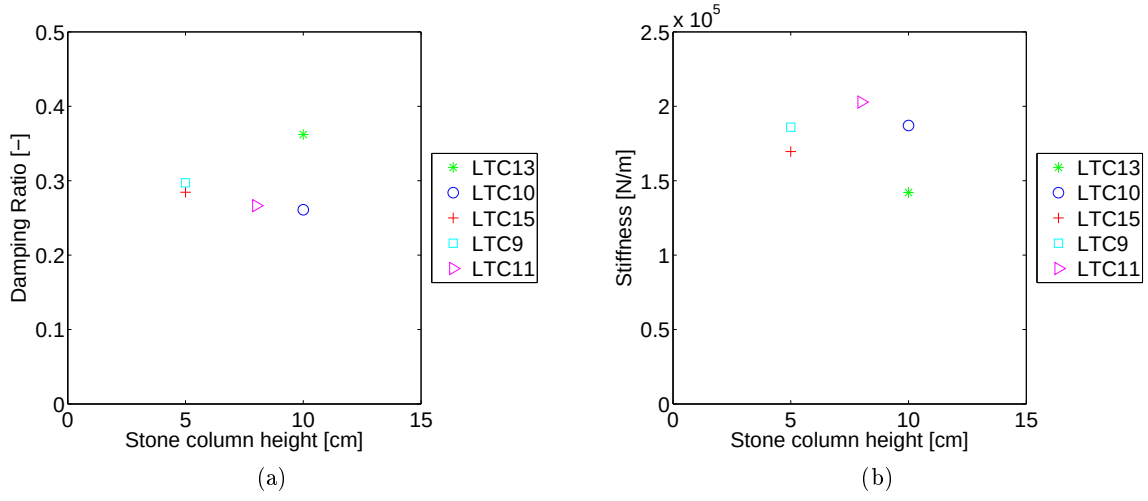

Figure 5.66: Damping ratio and dissipation for different heights of stone columns (LTC)

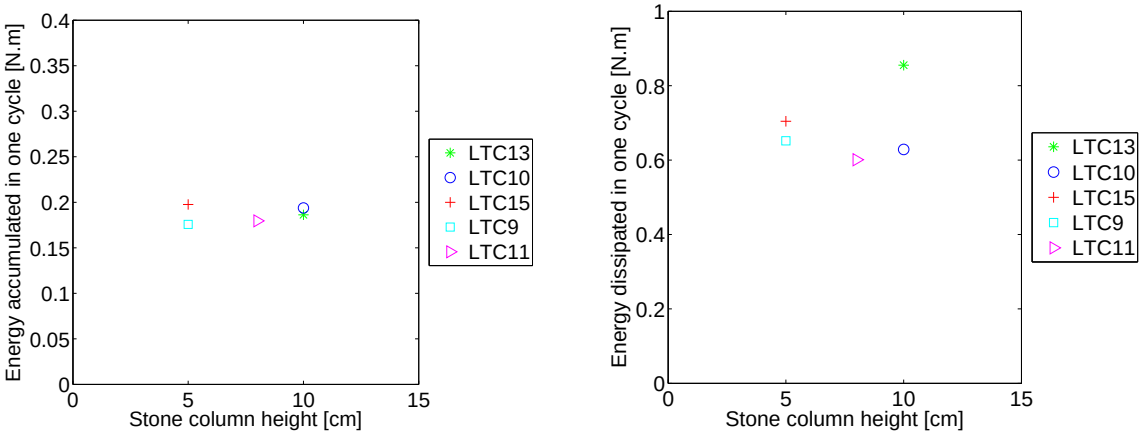

(a) (b)

Figure 5.67: Energy balance for different heights of stone columns (LTC)

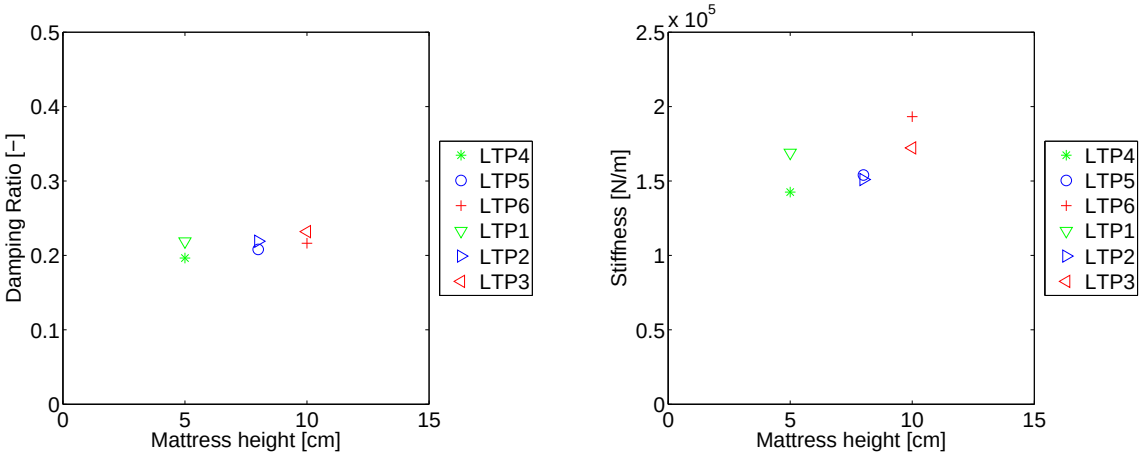

(a) (b)

Figure 5.68: Damping ratio and dissipation for different mattress thickness (LTP)

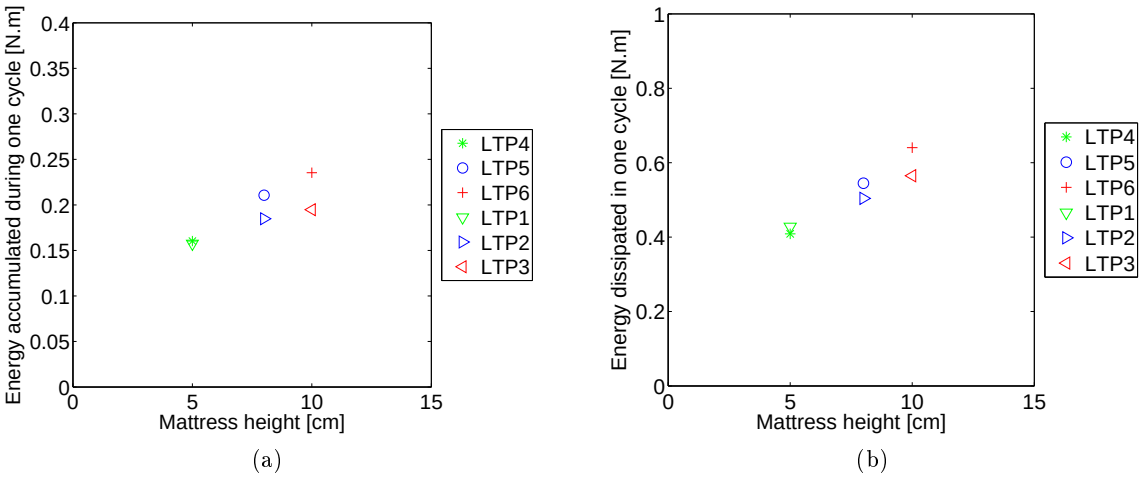

(a) (b)

Figure 5.69: Energy balance for different mattress thickness (LTP)

The following table summarizes the results shown in Figures 5.66 to 5.69

Table 5.2: Energy Dissipation within the flexible part of the models

Soil reinforced with piles associated to LTCs		
	Stiffness	1.4e5 N/m to 2.1e5 N/m
	Damping ratio	0.25 to 0.4
	Energy dissipated	0.6 J to 0.9 J
	Energy accumulated	0.15 J to 0.2 J J
Soil reinforced with piles associated to LTP		
	Stiffness	1.4e5 N/m to 1.9e5 N/m
	Damping ratio	0.18 to 0.24
	Energy dissipated	0.4 J to 0.65 J
	Energy accumulated	0.15 J to 0.25 J

Energy dissipation due to the pile-soil interaction

This paragraph evaluates energy dissipation within the rigid part of the physical model, meaning the bottom part, where the rigid inclusion interacts with the surrounding clay. Since the pile deformation is happening in the elastic region, the observed energy dissipation is assumed to be due to the plastification of the clay surrounding the pile and to nonlinear hysteresis response degradation.
As described in section 4.3.3, there are two methods used for the evaluation of energy dissipation within the rigid part of the model:

1. **T-y loop analysis**
   The shear force T obtained at head of the rigid inclusion and the deflection y measured at the same position as the shear force T give loops that will be further referred as *T-y* loops. Based on these T-y loops, damping ratio ξ_r , stiffness k_r, accumulated energy Ws_r and dissipated energy Wd_r are evaluated using the same procedure as for the *H-u* and *H-(u-y)* loops. Figure 5.70 (a) shows T-y loops obtained for an experiment when a soil mass improved by piles associated to a flexible layer (i.e. LTCs surrounded by clay or LTP) of 8cm in height is subjected to a dynamic lateral loading of the shallow foundation model. The corresponding damping ratio ξ_r , stiffness k_r, accumulated energy Ws_r and dissipated energy Wd_r are shown in figure 5.70(b).

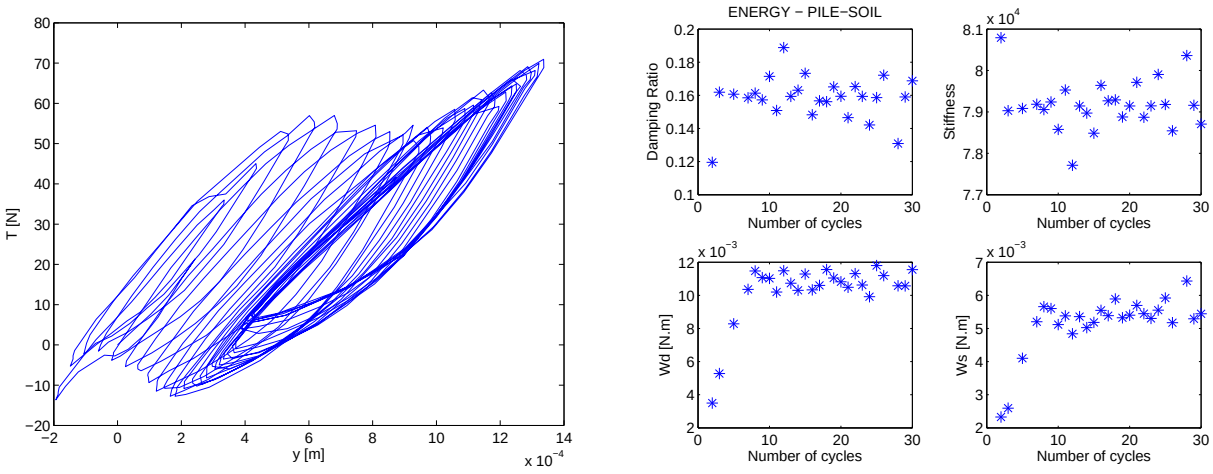

(a) (b)

Figure 5.70: Energy dissipation within the pile-soil system; LTC of 8cm height (exp LTC11)

More figures showing results of other experiments are listed in Annex B.
Due to accumulation of the pile lateral displacement with the cyclic loading, the *T-y* curves are not always possible to fit with an ellipse. The following conclusions are made based on a limited number of experiments:

- The values of dissipated energy Wd_r are in order of 0.015 J.
- The values of accumulated energy Ws_r are in order of 0.005 J.
- The values of stiffness k_r are in order of 7.5e4 N.m.
- The values of damping ratio ξ_r are in order of 0.15.

2. **P-y loop analysis**
The second method of evaluating energy dissipation within the rigid part of the physical models is to analyze the P-y loops. The pile is discretized in its length and P-y loops are plotted for each vertical position. P-y loops are then approximated by an ellipse, which is then treated as a hysteresis loop, providing energy dissipation parameters. Having these pile-soil characteristics for each vertical position, global pile-soil characteristics, such as dissipated energy Wd_r, accumulated energy Ws_r and damping ratio ξ_r, can be obtained using the equations (5.18), (5.19) and (5.20).

$$Wd_r = \sum_{n=1}^{n=30} Wd_n.dz \tag{5.18}$$

$$Ws_r = \int_0^l \frac{M_{max}^2}{EI}.dz \tag{5.19}$$

$$\xi_r = \frac{Wd_r}{Ws_r.4.\Pi} \tag{5.20}$$

where n is the cycle number, l is the pile length, dz is the distance between two vertical positions at which P-y loops are plotted and M_{max} is the maximum moment registered during one cycle n. It is found, that it is sufficient to consider P-y loops at the first 10cm

from the pile head. Below this depth, the P-y loop area becomes very small and could be therefore neglected. Figure 5.71(a) shows three vertical positions along the pile, for which P-y loops (5.71 (b), (c), (d)) were plotted and used to evaluate the local energy characteristics at the location concerned. These were subsequently used to evaluate global energy characteristics of the pile-soil system, such as damping ratio ξ_r, stiffness k_r, accumulated energy Ws_r and dissipated energy Wd_r. An example of the results obtained for an experiment when the soil mass is improved by piles associated to an eight cm high flexible layer composed of LTCs is shown in Figure 5.72.

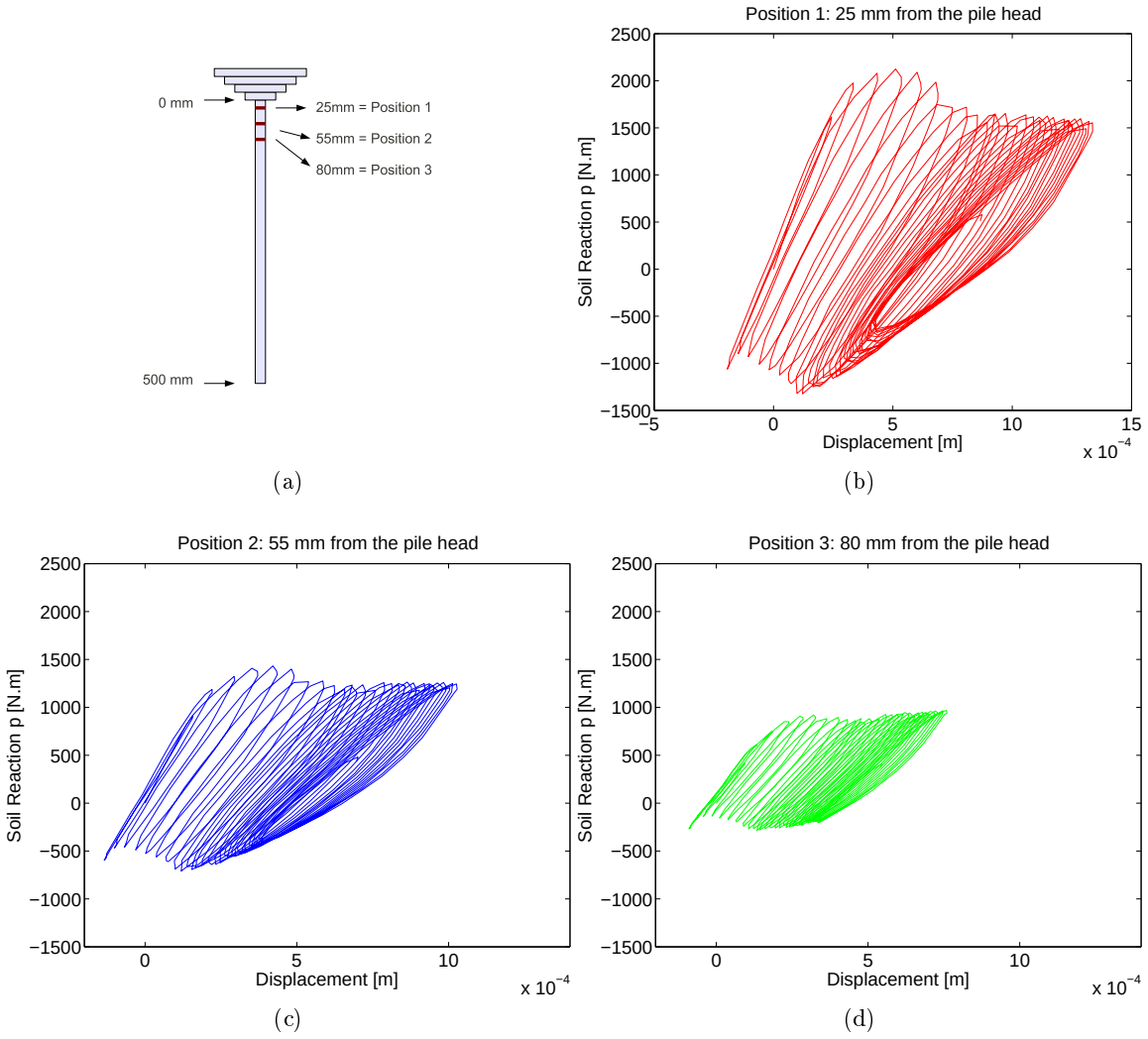

Figure 5.71: P-y curves corresponding to three vertical levels along the pile (position1-3); (exp LTC11)

More figures showing results of other experiments are listed in Annex B.
Due to the accumulation of pile lateral displacement with the cyclic loading, the P-y curves are not always possible to fit with an ellipse. Based on a limited number of experiments the value of energy dissipated Wd_r within the pile-soil system was evaluated to be in the order of 0.02 J (Figure 5.72).

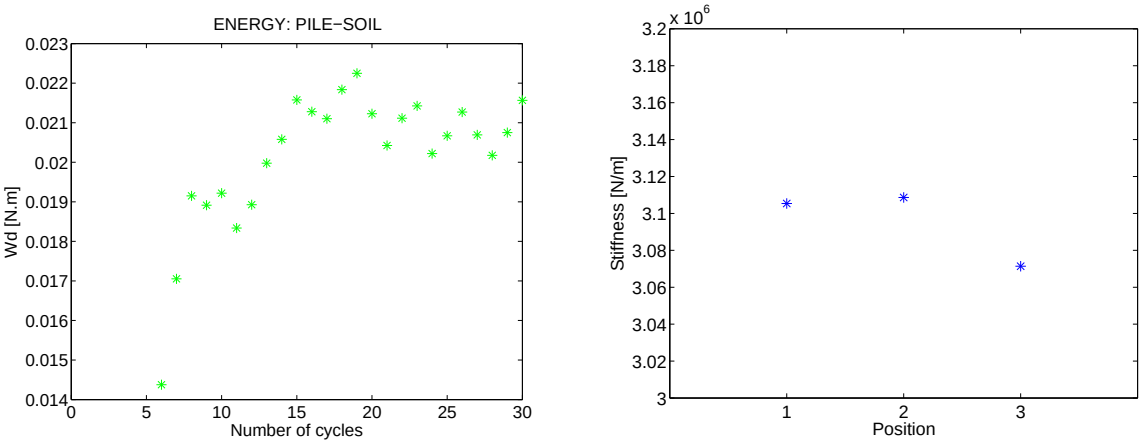

(a) (b)

Figure 5.72: Global characteristics of energy dissipation in the rigid part of the physical model (exp LTC11), results based on P-y loops

It is noted that the two methods agree on the value of energy dissipated within the system pile-soil.

It was shown that the flexible layer dissipates less energy when composed entirely of gravel mattress (LTP) than when composed of gravel columns (LTCs) surrounded by clay. This would logically imply that there is more energy transferred to a pile that is associated to the LTP. This is confirmed by comparing the P-y loops for the upper part of the pile and showing that the P-y loops for a pile supporting a LTP have a larger area than the P-y loops for a pile supporting a LTC. Figure 5.73 shows such P-y loops which are obtained at a depth of 8 cm from the pile head. It was not possible to plot the P-y loops directly at the pile head which was due to the technical problems when the deformation at the pile head could not be monitored for all the experiments performed.

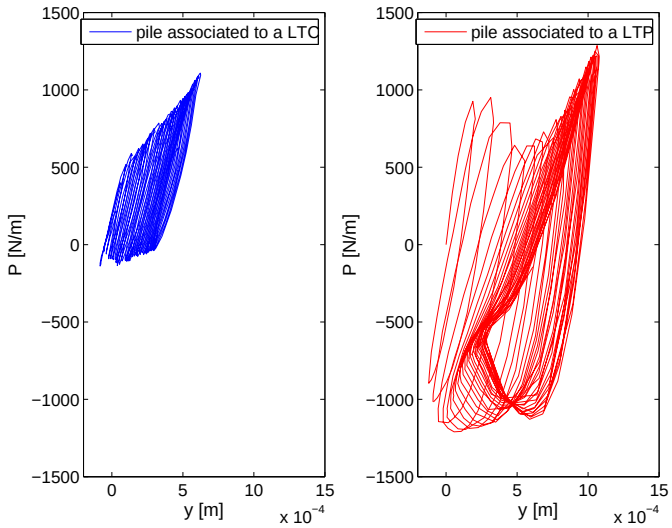

Figure 5.73: Comparison of the P-y loop area done for two cases - once when the pile is associated to a LTC and once when the pile is associated to a LTP. The P-y loops are plotted 8cm below the pile head

Discussion on results of energy dissipation

The previous text shows how energy dissipation is evaluated for three parts of the physical model, giving a stiffness of each of the parts:

1. Foundation and surrounding soil; stiffness = k_{eq}
2. LTC and the surrounding soil or LTP; stiffness = k_s
3. Pile and the surrounding soil; stiffness = k_r

In order to have a better understanding of the interaction between the three parts, an approximation of the physical model by a rheological model is made (Figure 5.74).

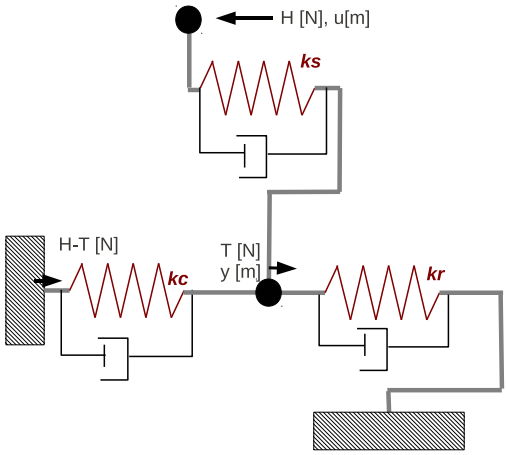

Figure 5.74: Rheological model

Taking k_{eq} as total stiffness of the reinforced soil, the following relation can be written, based on the rheological model presented:

$$k_{eq} = \frac{1}{\frac{1}{k_s} + \frac{1}{k_r + k_c}} \tag{5.21}$$

where k_r is the stiffness of the pile-soil system, k_s is the stiffness of the upper flexible part (LTC surrounded by clay or LTP) which is directly below the foundation and k_c is the stiffness added to the system due to lateral pressure of the soil surrounding the upper flexible part of the model. As a result of this stiffness k_c, only part of the force H which is applied at the top of the model is transferred to the pile head as force T. The stiffness of different parts of the model can be expressed as:

$$k_r = T/y \tag{5.22}$$

$$k_s = H/(u - y) \tag{5.23}$$

and

$$k_c = (H - T)/y \tag{5.24}$$

The force (H-T) is the force, that is passed to the clay surrounding the flexible layer which is underneath the foundation. This force can be also expressed as:

$$H - T = H - \alpha.H \tag{5.25}$$

where α is the ratio between the shear force obtained at the pile head and horizontal force applied at the foundation, i.e.

$$\alpha = T/H \tag{5.26}$$

H can be expressed as

$$H = \frac{k_r.y}{\alpha} \tag{5.27}$$

or

$$H = \frac{k_c.y}{1 - \alpha} \tag{5.28}$$

and hence following relation for k_c is obtained:

$$k_c = \frac{1 - \alpha}{\alpha}.kr \tag{5.29}$$

Based on the experimental results, it was found that one sixth to one eight of the force H applied at the foundation level is transferred to the pile head (see Figure 5.75). Being α the ratio between the force T transferred to the pile head and the force H applied at the foundation level, its value varies from $\frac{1}{6}$ to $\frac{1}{8}$. Using equations (5.21) and (5.29), the total stiffness k_{eq} can be obtained. This analytically calculated total stiffness is in the same order as the stiffness measured at the foundation level, which confirms the rheological model presented.

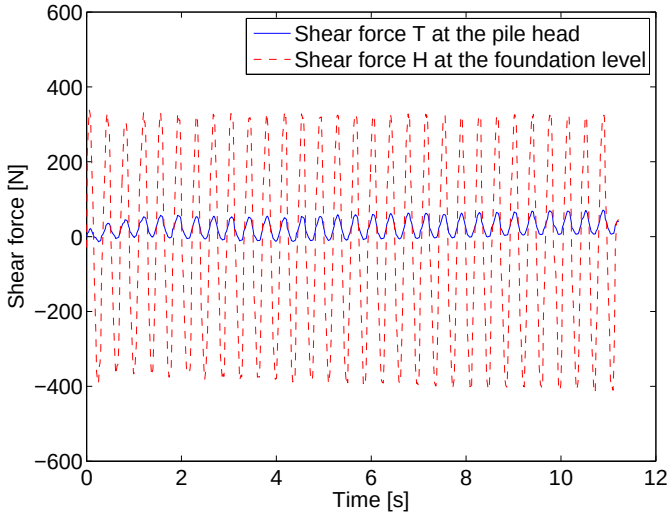

Figure 5.75: Amount of shear force H transferred to the pile head

It was observed that the values of energy dissipated Wd_s within the flexible layer were equal to around 90% of the global energy dissipation Wd_{eq} which was measured at the foundation level. The flexible layer dividing the foundation from the rigid inclusions showed that it is therefore able to dissipate most of the energy applied at its surface. The case of a LTC surrounded by clay was found to be able to dissipate more energy than a LTP and the amount of dissipated energy seems to be independent of the LTC height. On the contrary, for the case of LTP, the global energy dissipation seems to be increasing with the increasing height of the LTP, suggesting that a thicker mattress is able to dissipate more energy than a thinner mattress. The global energy balance for the LTCs and the LTPs is shown in Figures 5.76 and 5.77.

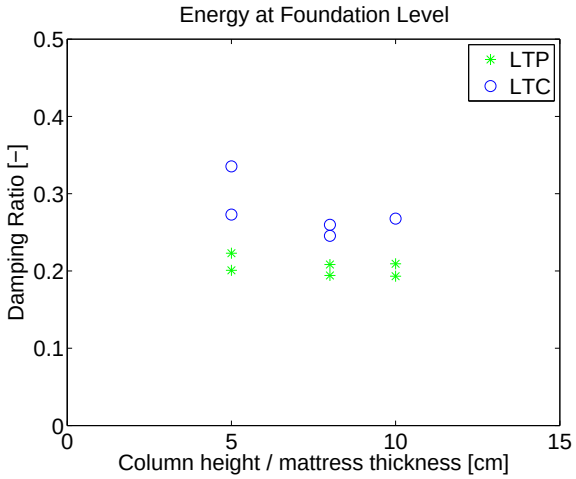

Figure 5.76: Comparison of global damping ratio of soil reinforced by piles associated to LTCs or LTP

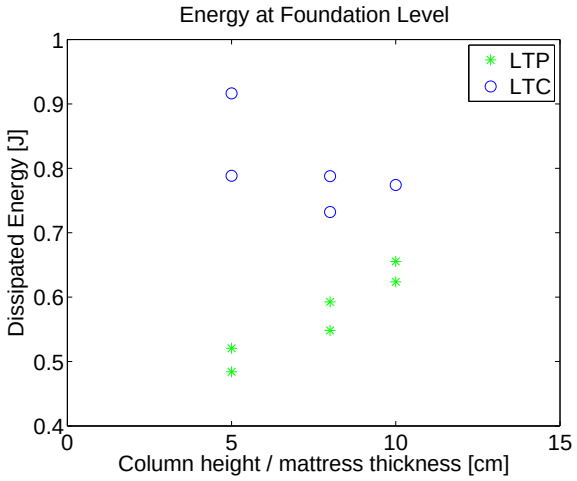

Figure 5.77: Comparison of global energy dissipation of soil reinforced by piles associated to LTCs or LTP

5.6.4 Discussion on the results presented - P-y loops and experiment repeatability

The validity of the results presented is linked to the repeatability of the experiments, which is discussed in the following, taking the P-y loops as an example. Cases for soil reinforced by piles associated to LTCs or LTP are discussed separately.

Experiments on soil reinforced by piles associated to Load Transfer Columns (LTCs)

Each of the figures 5.78, 5.79 and 5.80 shows two examples of experiments performed with one stone column height. It can be seen that for the 8 cm stone column height, the repeatability is satisfactory. On the contrary, the experiments with 10 cm and 5 cm high stone column show a larger scatter in the results. Aspects which are found to be a potential cause of such variation in the results obtained are listed in the following:

- Position of the force sensors and procedure used for their installation. This aspect is thought to have an important influence on the obtained results. Since it was desired to measure vertical force acting on the pile head, force sensors were installed on top of the transition zone. These sensors, having a non-negligible volume compared with the stone column dimensions may have influenced the mechanical behaviour of the whole system.
- Difference in the volumic weight of gravel within the stone column.
- Potential initial gap between the clay and the pile.

Based on careful examination of experimental protocols and on an experienced judgement, some experiments are considered as more reliable than others. Comparing the results of these experiments with those of the preliminary experiments and experiments performed

on non-consolidated soil mass (exp LTC1 - exp LTC8) finally lead to the presented results interpretation.

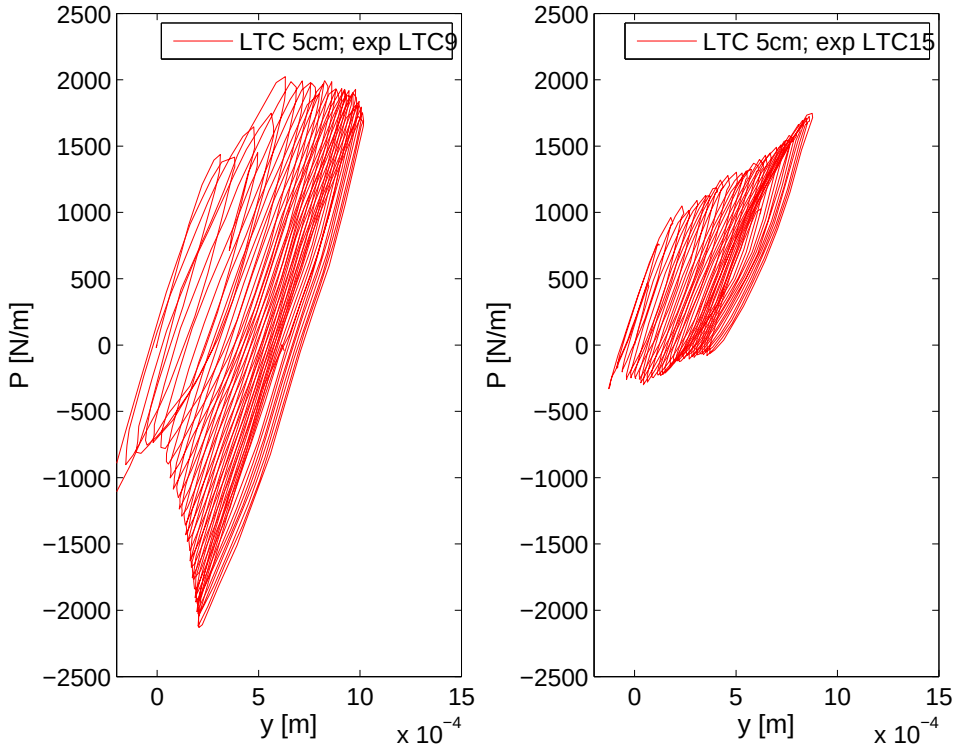

Figure 5.78: P-y loops obtained at pile head for stone column of 5 cm

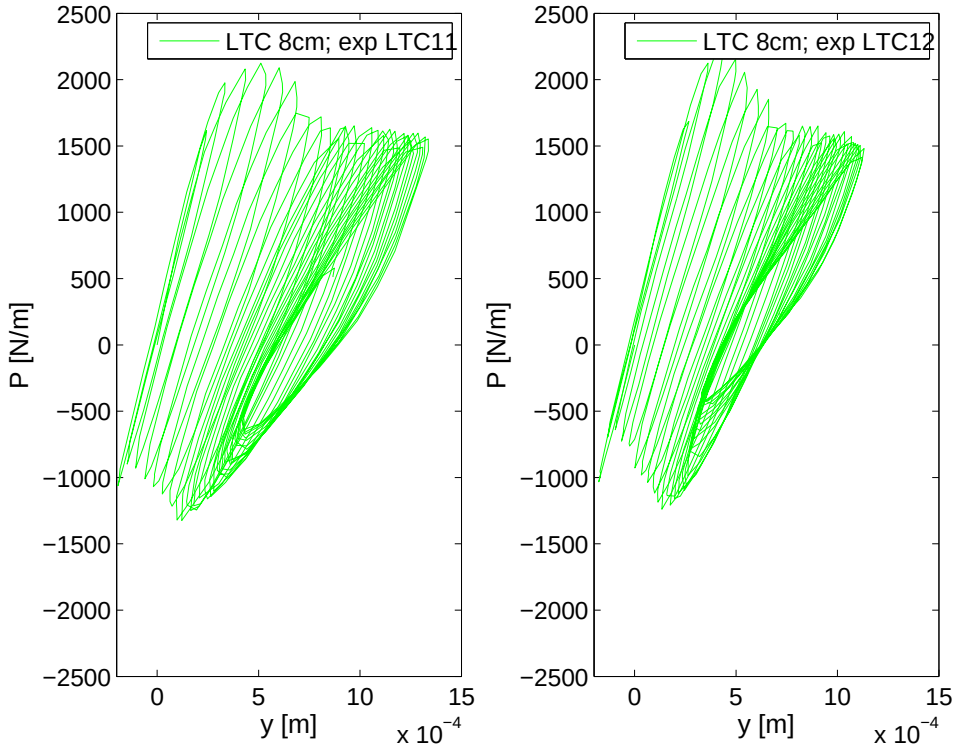

Figure 5.79: P-y loops obtained at pile head for stone column of 8 cm

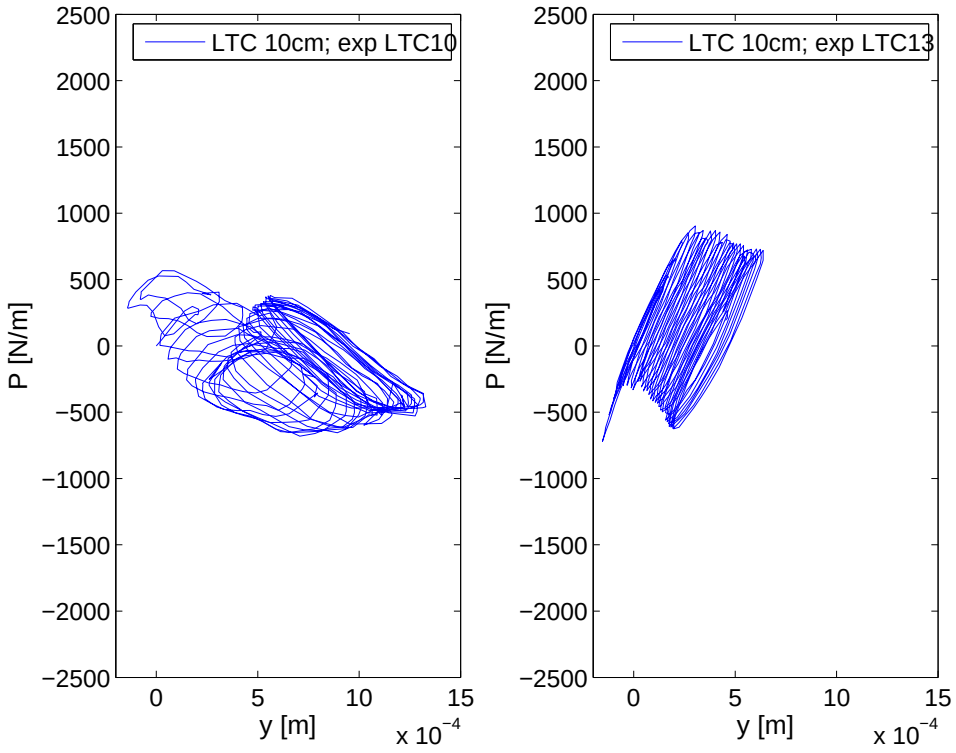

Figure 5.80: P-y loops obtained at pile head for stone column of 10 cm

Experiments on soil reinforced by piles associated to a Load Transfer Platform (LTP)

While carrying out experiments on soil improved by piles associated to a LTP, problems with strain gauge monitoring occurred. It is assumed that due to humid environment around the pile, gauges at the pile head were damaged. Therefore the previously shown results are influenced by the fact, that the strain was not known directly at the pile head. For experiments LTP1, LTP5 and LTP6, the top level of strain gauges was not working. For experiments LTP2, LTP3 and LTP4, the top two levels of strain gauges were not working. In cases of data evaluation, where a comparison between different experiments was made, a third level from the top (which is positioned 8cm from the pile head) was taken as a reference point.
In the previous result evaluation, an observation is made concerning the influence of the mattress thickness on the lateral pile performance. As presented, the thicker gravel platform seems to absorb more shear force that is applied by the shallow foundation, and therefore less bending moment is transferred to the pile head. The pile supporting a 5cm thick platform seems to be more affected by the cyclic loading of the foundation. The validity of this observation is linked to the repeatability of the experiments, which is discussed in the following, taking the P-y loops as an example.
Each of the figures 5.81, 5.82 and 5.83 show two examples of experiments performed with one mattress thickness. Looking at experiments with one mattress thickness, there can be noticed a difference between the two experiments. This difference is assumed to be mainly due to volumic weight difference between the two experiments. Experiments LTP1, LTP2 and LTP3 (plotted left on figures 5.81, 5.82 and 5.83) were carried out with less dense mattress than experiments LTP4, LTP5 and LTP6 (plotted right on figures 5.81, 5.82 and 5.83). The presented results evaluation was based on all experiments performed, although experiments with

higher mattress volumic weight are considered as more representative, since they correspond more to the current practice.

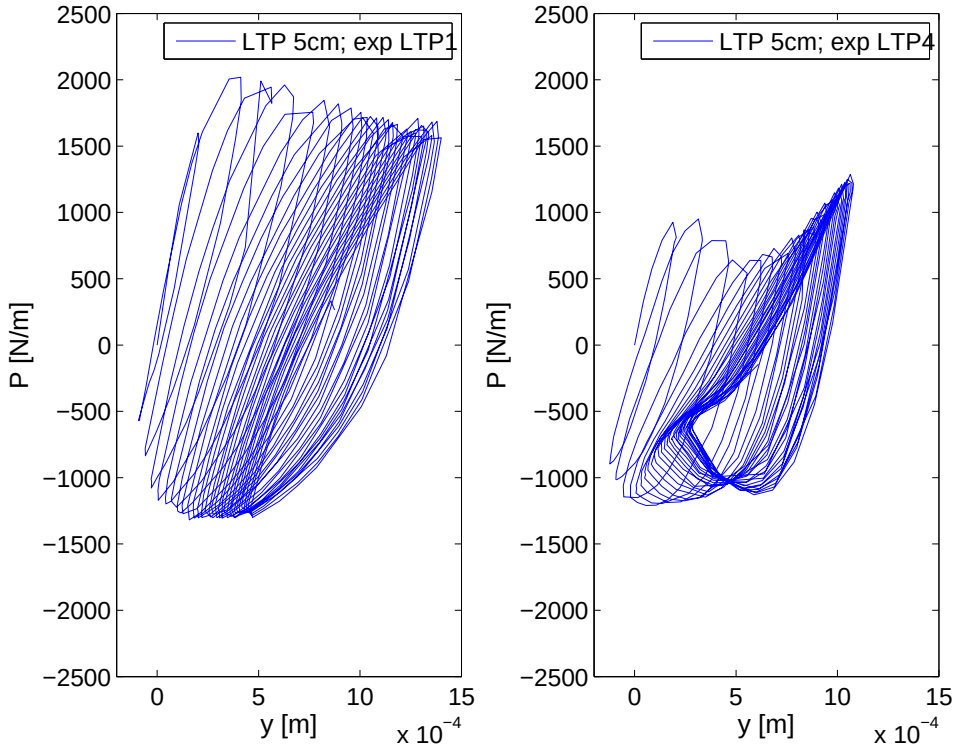

Figure 5.81: P-y loops obtained at pile head for gravel mattress of 5 cm

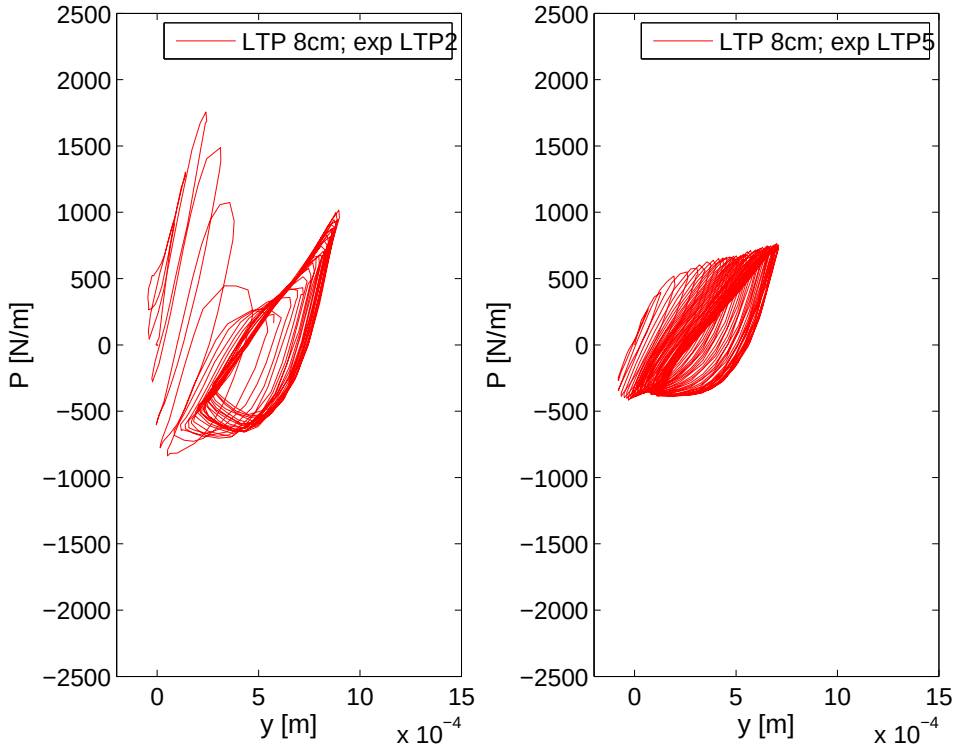

Figure 5.82: P-y loops obtained at pile head for gravel mattress of 8 cm

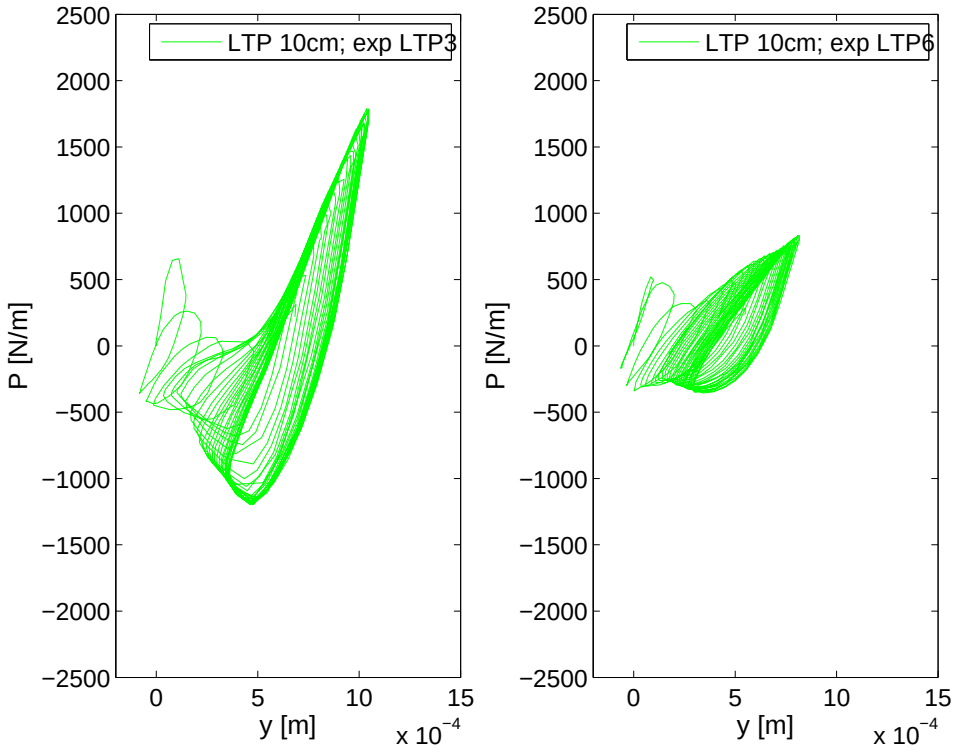

Figure 5.83: P-y loops obtained at pile head for gravel mattress of 10 cm

5.7 Problems encountered during the experimental work

1. An effort was made to obtain information on vertical load transfer within the reinforced soil. For this reason, force sensors were used in the experimental set-up. The results obtained were not interpretable due to the following reasons:

   - Small surface of the force sensors compared to the gravel grain size.
   - Drawer jamming effect occurring between the metal cover and the force sensor (see 3.3.5)
   - Hight sensitivity of the force measurements to any inclination of the 'load transition surface' (see 3.3.5).

2. Accelerometer fixed at the head of the instrumented pile did not give any valuable data. This was due to electromagnetic perturbations caused by the horizontal actuator, which entirely covered the accelerometer measurements with 'noise'. These electrical perturbations caused frequent dysfunction of different sensors and therefore measures had to be done in order to limit them:

   - The Visucuve and the physical model with all the sensors were electrically isolated from the horizontal loading device.
   - Sensor mass was connected to the amplifier mass.
   - Mass of the acquisition card was connected to the mass of the VisuCuve.
   - Modification of the control program in Labview

Despite the effort made, the perturbations never disappeared entirely and the accelerometer at the pile head provided a signal covered with noise.

3. While carrying out experiments on soil improved by piles associated to a LTP, problems with three top levels of strain gauges occurred. It is assumed that humidity from clay around the pile got through the protection membrane and affected strain measurements on the pile head.

4. The vertical and horizontal loading devices were not compatible. While the horizontal actuator applied dynamic loading, the vertical actuator, designed to work in static conditions, had to keep constant vertical load. As the foundation model settled under the horizontal dynamic loading, vertical actuator had to 'keep up' with this settlement and react by increasing the vertical load applied. This was a problem, since the vertical actuator was not fast enough to adjust the vertical load in order to keep it constant. Therefore the experimental programme had to be adjusted so the loading created less foundation settlement and therefore would allow the vertical actuator to react in time.

5.8 Conclusions

This chapter presents experimental study on the behaviour of reinforced soil under different kinds of loading conditions. Two types of soil reinforcement were studied - piles associated to Load Transfer Columns (LTCs) and piles associated to a Load Transfer Platform (LTP). The following conclusions were developed based on the experimental results:

1. Introducing soil reinforcement composed of piles associated to LTCs into the soil, a failure envelope, i.e. the combination of V-H load leading to a bearing capacity failure, increased by four times in its size with respect to the bearing capacity in the clay (Figure 5.24).

2. The foundation settlement is dependent on the LTC or LTP height - the higher the flexible part of the models, the larger the settlement observed.

3. Unlike for the combined dynamic loading when the foundation settlement was in the same order for both types (LTP or LTCs with clay) of the upper flexible part, it was observed that under vertical static loading the LTP allows less foundation settlement than a mixture of clay and LTCs. It is suggested that this is due to the fact that the clay, being present in between the LTCs, consolidates with time and therefore this type of the flexible part of the reinforcement system allows higher foundation settlement. This aspect is visible only if the loading period applied is long enough to allow the clay mass to consolidate. Since the vertical loading is applied in several loading stages where each stage is kept constant until the foundation settlement becomes small (i.e. the clay mass is partly left to consolidate), the foundation lying on soil with a presence of clay (i.e. LTCs surrounded by clay) settles more during the vertical static stage of loading. The dynamic horizontal loading is assumed to be in totally undrained conditions and therefore consolidation does not take place within the clay mass. As a consequence, the

dynamic settlement of the foundation is in the same order for both types of the flexible part of the model.
Figure 5.84 shows the results of the vertical loading steps during experiments performed on soil reinforced by piles associated to both types of the upper flexible part. It can be seen that the difference between the foundation settlement for the two technologies decreases with a decreasing height of the flexible parts of the models. This is in agreement with a phenomenon observed throughout the results evaluation, which shows increasing similarities in behaviour of the flexible parts as their height decreases.

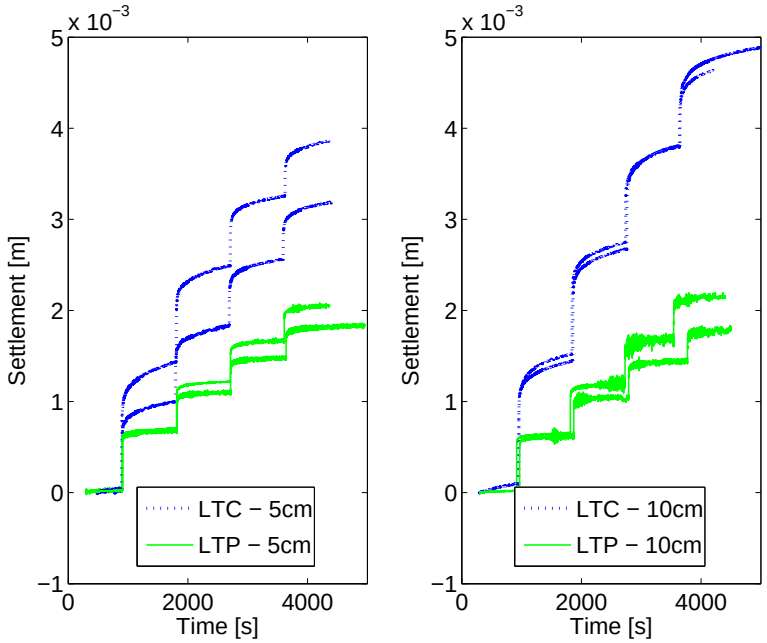

Figure 5.84: Foundation model settlement for soil reinforced by piles associated to LTCs or LTP of 5cm and 10cm height (each experiment was performed twice)

4. As shown in section 5.4 which describes the response of the rigid inclusion to vertical static loading applied by the foundation, both types (LTCs surrounded by clay or LTP) of the flexible part of the physical models transfer approximately the same amount of loading to the rigid inclusion when the height of the LTC or LTP is 5cm. As the height of the flexible part increases, the rigid inclusion underlying a LTC undergoes a higher deformation than rigid inclusion supporting a LTP. This phenomenon could be explained by the geometry difference between the two physical models. In the case of piles associated to LTCs, a square foundation applies a vertical load on four gravel columns surrounded by clay. This load is transferred through the stone columns to the rigid transition zone and then to the pile. As the V load increases, the foundation settles and the underlying soil has a tendency to migrate towards an area with lower pressure - non-reinforced clay surrounding the physical model. As a consequence, the stone columns undergo a rotation, which is then projected onto the rigid transition zone and the pile. In the case of LTP, the soil between the foundation and the transition zone is entirely composed of gravel material and therefore there is a smaller tendency to lateral spreading of the soil (due to constant material stiffness and lower foundation settlement).

It is a speculation that the rotation of the stone columns, which is most probably occurring while applying load to the physical model of soil reinforced by rigid inclusions associated to LTCs, would not take place in the real problems. This is due to the fact that the physical model was composed of only four rigid inclusions followed by a LTC, whereas in the real problems, the soil reinforcement is applied in the whole construction site. As a consequence, soil in the real scale problems offers a higher lateral stiffness which limits the effect of LTC rotation.

5. While carrying out experiments on soil improved by piles associated to LTP, problems with strain gauge monitoring occurred. It is assumed that due to a humid environment around the instrumented pile, gauges at the pile head were damaged. Therefore a third level of strain gauges (Figure 5.2b), being located 8.5cm from the pile head, served as a reference level. This allowed to plot and compare P-y loops at the pile top for piles supporting either a LTC (Figure 5.85) or a LTP (Figure 5.86) with varying heights. The main observation made based on Figures 5.85 and 5.86 is that the lateral soil reaction P at a depth of 8cm from the pile head reach more important values when the pile is acting in combination with the LTP. This phenomenon can be explained by a speculation that the LTCs surrounded by clay transfer more vertical load to the piles than transfers the LTP. As a consequence, the soil around the piles associated to LTCs is under a lower vertical stress and this implies that the lateral soil reaction P is lower.

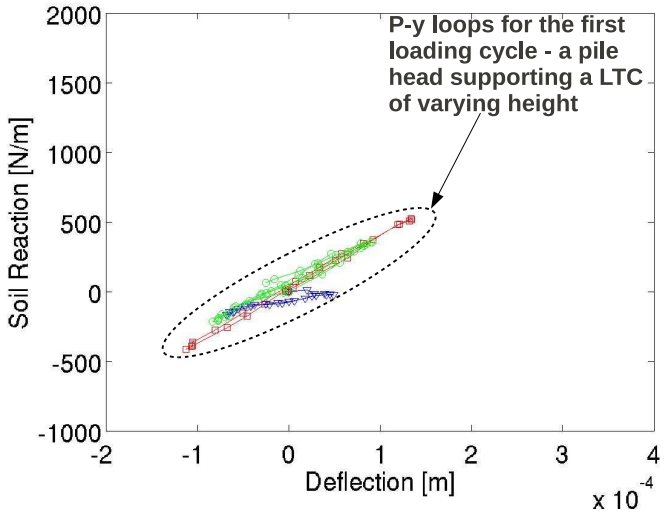

Figure 5.85: P-y loops for the first loading cycle plotted for experiments when the LTC height was varied. The aim of the figure is only to show the location of the loops in the P-y space.

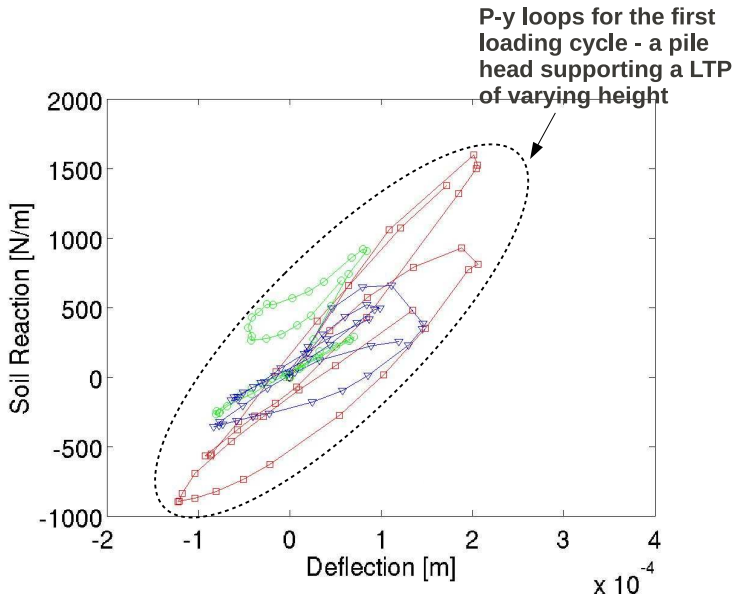

Figure 5.86: P-y loops for the first loading cycle plotted for experiments when the LTP height was varied. The aim of the figure is only to show the location of the loops in the P-y space.

6. Results presented show a presence of a gap opening on a side of the pile. This gap appears for cases when piles in clay are subjected to important lateral loading. Such important lateral pile loading happens very rarely in the real scale problems and therefore the gap presence is neglected in the current practice analysis. Wanting to compare lateral pile performance for the instrumented pile associated to a LTC or a LTP without having to consider the gap influence, pile response only during the first loading cycle (when an absence of a gap is speculated) was taken into account. It was observed that during the first loading cycle, the pile response was in the same order when associated to either of the type of the flexible part. Behaviour of the pile acting in combination with a LTC doesn't seem to be influenced by the stone column height. On the contrary, bending moment M, deflection y and shear force T measured along the pile supporting a LTP seem to suggest that there is a dependence of lateral pile behaviour on the mattress thickness. Lower 5cm mattress seems to transfer higher moments, shear forces and deflection onto the pile than a mattress of 8 and 10 cm. There is observed no apparent difference between pile behaviour for 8cm and 10cm mattresses height. It is noted that moment M and shear force T measured along the pile associated to a LTP reach their local maximum at a position deeper from the surface than for a pile associated to LTC. This suggests, that there is a higher soil degradation around a pile supporting a LTP.

7. Analysing the pile response to all 30 cycles of the cyclic loading, it can be observed that when the foundation moves in direction 'A', the pile top supporting a LTC is subjected to higher moments than a pile supporting a LTP (Figure 5.87). This is assumed to be due to higher rotation of the flexible LTC which is transferred to the rigid transition zone. This speculation, adding to the 'horizontal-loading' mechanism on the pile head

also a 'moment-loading' mechanism is in agreement with the fact, that the moment along a pile supporting a column occurs close to the pile head. Curves presented by Poulos (Poulos and Davis, 1980) show such a moment distribution, where the maximum moment for 'moment-loading' only occurs at the surface, whereas the maximum moment for 'horizontal-loading' only occurs at depths between 0.1L and 0.4L below the surface. It is noted, that such pile behaviour was already observed for the vertical static loading and the rotation was assigned to the geometry of the physical model. This presents one of the limitations of the presented physical model, which could be overcome by installing more CMMs into the soil or introducing a less rigid joint between the pile and the transition zone.

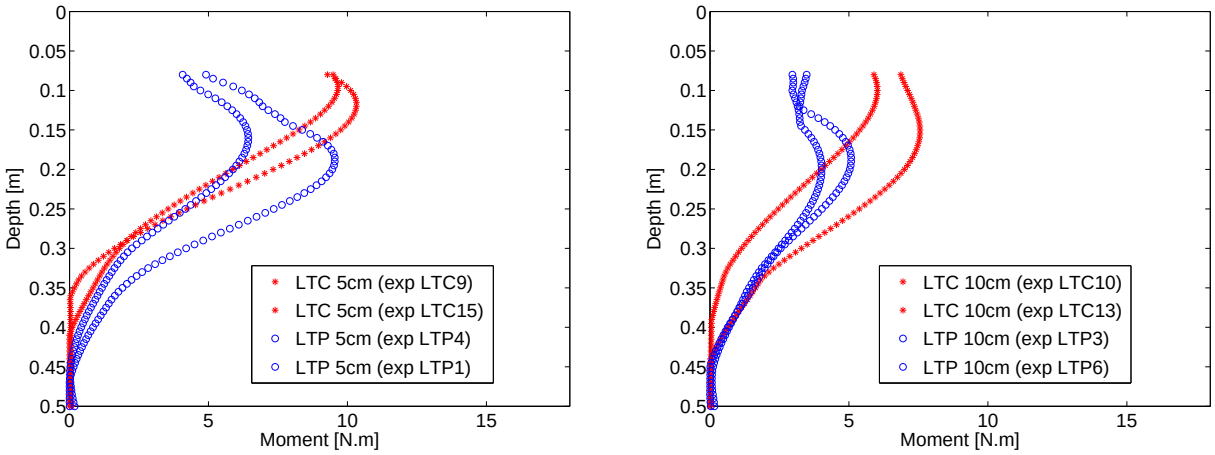

(a) (b)

Figure 5.87: Envelopes for maximum moment along the instrumented pile associated to either LTC or LTP; the height of the LTC or LTP is varied and each configuration is tested twice

8. The flexible part of the physical models is capable of dissipating 90% of the energy applied at the foundation level. The case when the flexible part consists of a LTC surrounded by clay was found to be able to dissipate more energy than a LTP. (Figures 5.76 to 5.77).

9. When analysing lateral pile behaviour within the soil reinforcement system, it is observed that the pile performs only a limited reversible deflection, meaning that the pile deflection stays almost entirely within a positive range of values. There is observed an accumulation of the lateral deflection when foundation is loaded in direction 'A'. This accumulation has a tendency to stabilize at the end of the cyclic loading. The position of a bending moment maximum moves deeper along the pile with the cycles evolution. This phenomenon was already observed in previous studies done on lateral behaviour of piles in clay (Khemakhem, 2012) and implies that as the pile undergoes the loading cycles, the soil strength is degradated to larger depths.
   In agreement with observations made in previous works (Khemakhem, 2012), (Matlock, 1970) lateral stiffness degradation of the pile-soil system was observed during the cyclic loading. This pile-soil stiffness degradation with increasing number of cycles is although compensated by the stiffness increase within the flexible part observed throughout the cyclic loading. As a consequence, the global stiffness of the reinforced soil increases with the cyclic loading.

10. In order to understand the mechanisms leading to the observed pile behaviour, all collected data was studied in detail. Comparing pile performance for the two types of the physical models and highlighting the differences helps to give a deeper understanding of the problem studied. Figures 5.30-5.32 and 5.47-5.49 show that the pile associated to LTP shows more reversible behaviour than a pile associated to a LTC. When the foundation applies displacement in direction 'B' (time t10 in Figure 5.88), the pile top supporting a LTP moves further in the loading direction. The pile top supporting a LTC, on the contrary, seems to be unable to perform such a reversible behaviour and stays almost entirely inclined in direction 'A' (Figure 5.88). As a consequence, the pile supporting a LTP undergoes larger deflection at its top and therefore the P-y loops plotted at the pile top show larger area for the pile associated to a LTP than for a pile associated to a LTC. Knowing that the P-y loop area is directly related to the amount of the dissipated energy, it is suggested that the energy transferred to the pile head is higher for the case when the pile is associated to LTP. This is in agreement with the results showing that the LTP is not capable to dissipate as much energy as the LTCs surrounded by clay (see Table 5.1).

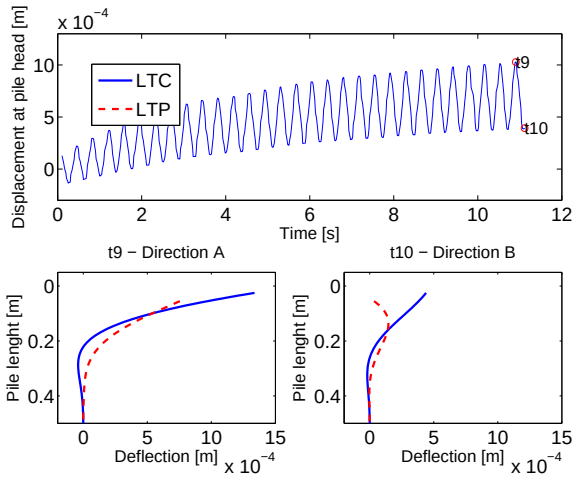

Figure 5.88: Pile deflection when foundation is loaded in loading direction 'A' (at time t9) and 'B' (et time t10). The pile response is shown for a case when the pile is associated to a LTP or a case when the pile is associated to a LTC

CHAPTER 6

Numerical Modelling

6.1 Introduction

Numerical simulations presented are carried out with FLAC3D, numerical modelling code that utilizes an explicit finite difference formulation. The problem studied numerically simulates physical experiments described in the previous chapters, addressing the trends observed for the response of the rigid inclusion to different loading conditions applied.

Numerical models of soil reinforced by rigid inclusions associated to different types of flexible parts are introduced. The system is subjected to inertial loading which causes, among other, a lateral response of the rigid inclusion. Analysing the moments and deflections created along the inclusion is considered as important since it provides not only information concerning the rigid part of the model itself but also provides information on the load transfer mechanisms happening in the flexible part of the models.

Aiming for a similar response of the numerical and physical simulations, calibration of the numerical model is done based on results obtained from the physical experiments.

The numerical results confirmed general trends observed for the pile behaviour in the experimental study. In order to compare these results with a numerical study presented by X. Zhang (Zhang, 2011), another type of a flexible part was introduced. The numerical simulations were therefore carried out not only with the two types of flexible parts that were studied experimentally (LTC, LTP), but also with a third type, which is a modification of the LTP. This type of the flexible zone, which is new in the presented study, is described further in the text and will be referred as 'reduced LTP - block'.
Unlike the previous numerical study (Zhang, 2011), the current model simulates the clay behaviour using a modified Cam-clay constitutive model instead of a Mohr-Coulomb model. The modified Cam-clay model offers a more realistic simulation of the non-linearities in the

stress-strain relationship but it is, same as in the case of Mohr-Coulomb model, not capable of a proper simulation of the non-linear cyclic soil behaviour. Constitutive models which are able to realistically reproduce under dynamic conditions the hysteresis behaviour of soil, the energy balance and the stiffness degradation during the unloading and reloading are not used in the presented numerical study due to their complexity. The modified Cam-clay is although considered as sufficient model for the purpose of this numerical study, *i.e.* to study the lateral performance of a rigid inclusion in clay, addressed in terms of bending moments and deflection created along the pile. The system response to the inertial loading related to its hysteresis behaviour is not studied numerically and stays as one of the perspectives for the future works.

6.2 The numerical code used - FLAC3D

FLAC3D is a three dimensional explicit finite-difference program. It numerically studies the mechanical behaviour of a continuous three-dimensional medium as it reaches equilibrium or steady plastic flow. The code comprises of mathematical model and its numerical implementation. General principles of continuum mechanics, such as Cauchy stress definition, equilibrium equation, motion equation, boundary conditions and initial conditions, form the base of a mathematical model. Adding an appropriate constitutive equation describing the nature of particular material, mechanics of a medium is defined. Resulting set of partial differential equations defining stress-stain rate relationship is being numerically solved for particular case modelled. Numerical solution applies an explicit finite difference approach in time. For every time step, the calculation sequence can be summarized as follows:

1. New strain rates are derived from nodal velocities.
2. Constitutive equations are used in their incremental form to calculate stress increments from strain rates and stresses at the previous time.
3. Nodal mass and out-of-balance force is computed at a global node. The out-of balance force is monitored to detect whether the system has reached an equilibrium state or a steady flow state. Taking damping into account, new nodal velocities and displacements are derived from known out-of-balance forces.

This sequence is repeated every time step. If the out-of-balance force approaches to zero, the system modelled has reached an equilibrium state. Out-of-balance force approaching a constant indicates that the system, or its portion, has reached a steady state flow of material.

The described numerical scheme is an alternative to implicit methods used to solve non-linear problems by incremental methods. This dynamic explicit method reformulates a problem as a dynamic, inducing nodal velocities, accelerations and inertia. The problem at time $t + \delta t$ is solved incrementally using a state at time t, which is the difference compared to the implicit methods, which solve a problem for time $t + \delta t$ using a state at t and $t + \delta t$. Explicit methods do not use iterations to enforce equilibrium at each step like do the implicit methods. As a consequence, the increments need to be small to ensure good accuracy. If the number of increments is not sufficient, the solution tends to drift from the correct solution.
Comparing FLAC3D to more common finite element methods (FEM), the following differences in the two approaches can be listed (FLAC3D, 2006):

- By using an explicit solution scheme, a nonlinear problem can be solved almost in the same computer time as a linear problem. Implicit solutions take longer to solve nonlinear problems but on the contrary demand shorter computation time for linear simulations. FLAC3D is most effective when applied to nonliear or large strain problems.
- Plastic collapse loads and plastic flow are modelled more accurately in FLAC3D that in FEM thanks to using a mixed discretization scheme.
- FLAC3D uses the dynamic explicit method described in the previous text to solve nonlinear problems. Full dynamic equations of motion are used even when the system modelled is essentially static. The most commonly used FEM methods use an implicit numerical scheme with Newton-Raphson iteration procedure.
- Thanks to using an explicit scheme, FLAC3D does not store any matrices, which allows a time efficient modelling of large number of elements with a modest memory requirement.

Dynamic analysis option within FLAC3D permits to analyse soil-structure response to dynamic motion thanks to a fully nonlinear method embodied in FLAC3D. Based on explicit finite difference scheme, equations of motion are solved using lumped grid point masses derived from the density of the surrounding zones.

6.3 Numerical models

Numerical models were constructed in Flac3D with the aim to simulate the physical experiments done in the VisuCuve. The observed trends were compared to the previous numerical modelling carried out on the same problematic (Zhang, 2011).

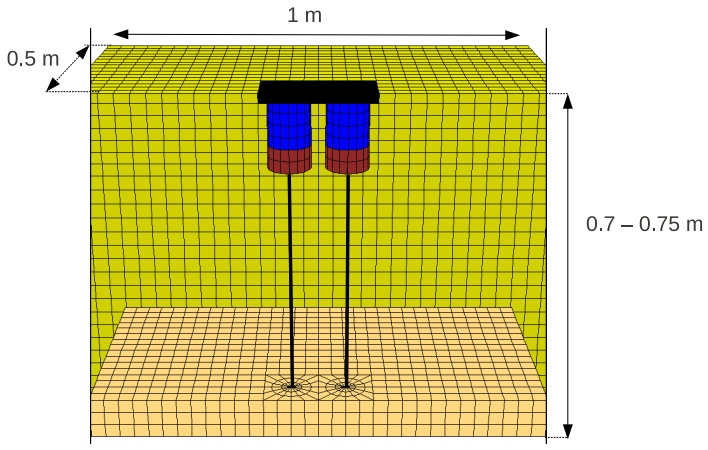

Figure 6.1: Numerical model of soil reinforced by piles associated to Load Transfer Columns (LTCs) surrounded by clay

The grid was generated according to the geometry and dimensions of the physical models. Soil reinforced by pile elements associated to either Load Transfer Columns (LTCs) surrounded by clay or to a Load Transfer Platform (LTP) was subjected to an inertial loading applied by a shallow foundation. The grid generated to model such conditions, corresponding to the two series of experiments, is shown in Figures 6.1 and 6.2. In order to compare the obtained numerical results with the results obtained within the scope of a thesis done by X. Zhang (Zhang, 2011), additional modifications to the model geometry were done - the LTP was reduced in its size to have the same length and width as the foundation and the created gravel 'block' was surrounded by clay (Figure 6.3). Such a modification of the flexible part of the model allowed a better understanding of the role of different elements within the flexible 'load transfer layer'.
Constitutive laws applied in the numerical modelling were chosen with respect to mechanical properties of different components of the physical models. A symmetrical behaviour of both physical models is assumed, with a plane of symmetry cutting the model in half. This vertical plane of symmetry is parallel to the loading direction.
The models represent a soil reinforced by rigid inclusions associated to one of the three types of the flexible part (Figures 6.1, 6.2 and 6.3). The connection between the flexible and the rigid part of the models is simulated by a transition zone. This transition zone is linked to the pile through a joint which is modelled, unless specified differently, as a joint allowing free rotations but fixing the translational movement of pile head to be the same as the translational movement of the surrounding grid, *i.e.* the pile head and the transition zone undergo the same translational movement. Section 6.5.2 compares the pile performance when a different kind of joint disabling the rotations is used.
Bottom of the piles is fixed in both displacement and rotation. Even though Flac3D provides different types of seismic boundaries, the presented numerical models didn't deliberately use any of these in order to realistically model the physical experiments. The reason for this is that the physical model was bordered by the sides of VisuCuve tank. Therefore considering any refraction and reflection amortization would be in conflict with the reality. A *local* damping was used as an approximate way to include hysteretic damping. It operates by adding or subtracting mass from a grid point during a cycle oscillation. Calibration of constitutive laws for geomaterials considered in the numerical study was based on laboratory experiments and the results obtained from the physical modelling.

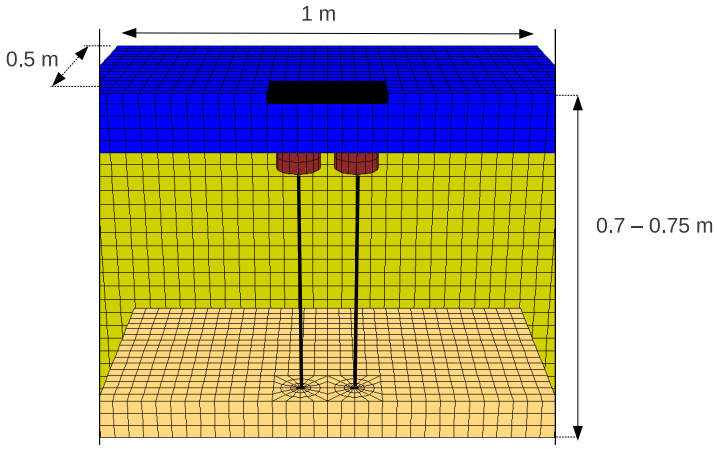

Figure 6.2: Numerical model of soil reinforced by piles associated to a Load Transfer Platform (LTP)

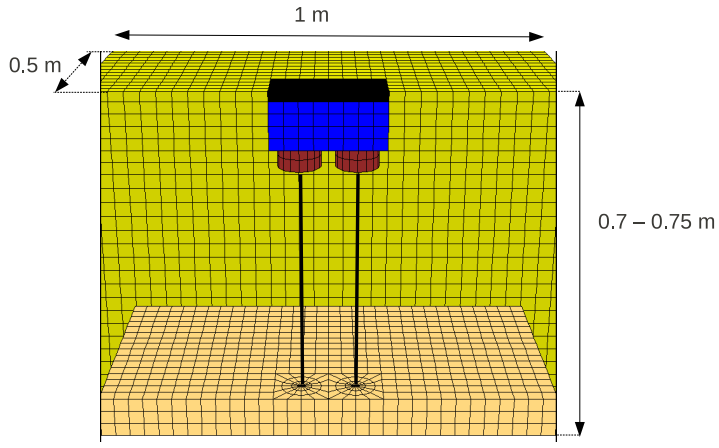

Figure 6.3: Numerical model of soil reinforced by piles associated to a Load Transfer Platform which is reduced in its size

Following table shows the corresponding parameters used between the physical and the numerical model:

Table 6.1: Physical model VERSUS Numerical Model - part 1

Physical Model	Numerical Model
Clay cu=17kPa, w=0.3	Material defined by modified Cam-Clay constitutive model with parameters: • Bulk modulus (small strain, undrained) = $60MPa$ • Shear modulus (small strain, undrained) = $17MPa$ • Wet unit weight = $17kN/m^3$ • $\lambda = 0.115$ • $\kappa = 0.029$ • Preconsolidation pressure = $50kPa$ • Reference pressure = $1kPa$ • Specific volume at reference pressure = 1.82
Tubes representing rigid inclusions: aluminium external diameter = 0,016m; diameter = 0,008m	Pile structural elements properties: • Density = $2.7g.cm^{-3}$ • Youngs modulus = $69GPa$ • Poisson's ratio = 0.35 • Cross-sectional area = $1.51e-4m^2$ • Polar moment of inertia = $6.032e-9m^4$ • Second moment with respect to pile y-axis = $3.016e-9m^4$ • Second moment with respect to pile z-axis = $3.016e-9m^4$ • Perimeter = $0.05m$ PileSEL properties: • Shear coupling spring stiffness per unit length = $1e10N/m$ • Shear coupling spring cohesion(force / unit length) = $4.25e3N/m$ • Shear coupling spring friction angle = 7.97^o • Normal coupling spring stiffness per unit length = $1e10N/m$ • Normal coupling spring cohesion (force / unit length) = $4.25e3N/m$ • Normal coupling spring friction angle (degrees) = 7.97^o • Normal coupling spring gap-use flag = on
Compacted gravel with grain size 2mm-4mm	Material defined by Mohr Coulomb constitutive model with parameters: • Bulk Modulus = $66MPa$ • Shear Modulus = $100MPa$ • Unit weight = $25kN/m^3$ • Friction Angle = 48^o • Cohesion = $0kPa$

Table 6.2: Physical model VERSUS Numerical Model - part 2

Physical Model	Numerical Model
Transition zone - aluminium cone filled with gravel	Structural element representing a metal cylinder having 90 mm in diameter and 50 mm in height. Interface metal-clay is characterized in a same way as for the aluminium-clay interface.
Foundation -aluminium	Material defined by elastic constitutive model with parameters: • Bulk Modulus = $69GPa$ • Shear modulus = $27GPa$

6.3.1 Grid generation and interfaces

Polyhedral elements are fitted together to represent the geometry of the problem. Geometry of the numerical models was done in order to respect geometry and dimensions of the physical models. A grid defining model geometry in physical domain was created. A care was taken to make it in one hand sufficiently fine in order to accurately represent the wave transmission through the material body, but on the other hand to have a calculation with a bearable calculation time[1]. Grid of the LTCs as well as of the transition zones was defined using radial cylinders with a height varying from 5cm to 10cm (Figure 6.4). These columns were surrounded by a fine grid to which a clay constitutive law was assigned. Foundation applying loading to the the reinforced soil was embedded. It was desired to represent the foundation surface as a plane on which sliding or separation can occur. This was done by creating an interface between the foundation and the surrounding soil. The fundamental contact relation between the soil and the footing was defined by linear Coulomb shear-strength criterion (ϕ, c) and normal (k_n) and shear stiffness (k_s). The values used to characterize the interfaces are listed in Table 6.3. In order to allow only either intact or broken bond between the foundation and the soil, it is necessary to define high rigidity ks and kn, although the values should not be higher than ten times the stiffness of the most rigid surface (FLAC3D, 2006).

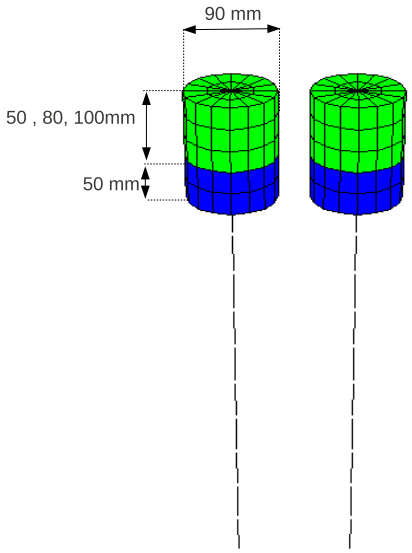

Figure 6.4: CMM grid

[1]One calculation of 30 loading cycles performed in dynamic conditions took around three weeks

Table 6.3: Interface characteristics

Gravel-Foundation Interface	
Friction angle ϕ	45^o
Cohesion c	$0kPa$
Shear stiffness ks	$1e12N/m$
Normal stiffness kn	$1e12N/m$
Clay-Foundation Interface	
Friction angle ϕ	0^o
Cohesion c	$17kPa$
Shear stiffness ks	$1e12N/m$
Normal stiffness kn	$1e12N/m$

6.3.2 Structural elements

Structural elements in FLAC3D describe structural support used for stabilization of rock or soil mass, such as beams, cables, piles, shells, geogrids and liners. For the presented analysis, pile elements were used to model aluminium tubes used in the physical experiments as a representation of the rigid part of the soil reinforcement. Each pile element, defined by its geometry, interacts with the grid via shear and normal coupling springs. These springs are defined in terms of stiffness k, cohesive strength c and friction angle ϕ. Mechanical behaviour of the pile in the shear and normal direction is defined by these parameters, as well as the effective confining stress. Spring properties used in the numerical analysis to define the soil-inclusion interface are the same as the characteristics used for the aluminium-clay interface described in Table 6.3. For lateral pile loading, a gap development may be observed between the pile and the surrounding material. This gap can be numerically modelled in FLAC3D and the option was used in the presented analysis.

6.3.3 Constitutive models

Modified Cam-clay model [2] was used to represent clay, which was surrounding the stone columns and rigid inclusions. Behaviour of gravel within the gravel columns or mattress was described by a Mohr-Coulomb model. Even though none of these models is able to properly reproduce cyclic behaviour of soils, their performance is considered as sufficient to study the lateral performance of a rigid inclusion in clay, addressed in terms of bending moments and deflection created along the pile.
Input parameters for both constitutive models were, in the first step, obtained from laboratory experiments (3.3.4). Calibration of the models was then based on experimental results obtained from physical experiments in the VisuCuve. An example of such calibration is graphically shown in Figures 6.5 and 6.6. Input parameters used in the final model are listed in table 6.4 and 6.5.

[2]Modified Cam clay model was introduced by Roscoe and Burland (1968) as a modification of an original Cam-clay model described by Schofield and Wroth (1968). These Cam clay models take the classical state boundary surface as a yield surface and as a plastic potential surface. Hardening is related to the plastic volumetric strains. The modified Cam clay model differs from the original Cam clay model by a form of an equation used to describe the yield curves - modified Cam clay describes the yield curves as ellipses, where as the original Cam clay describes them as logarithmic spirals (Atkinson, 1993).

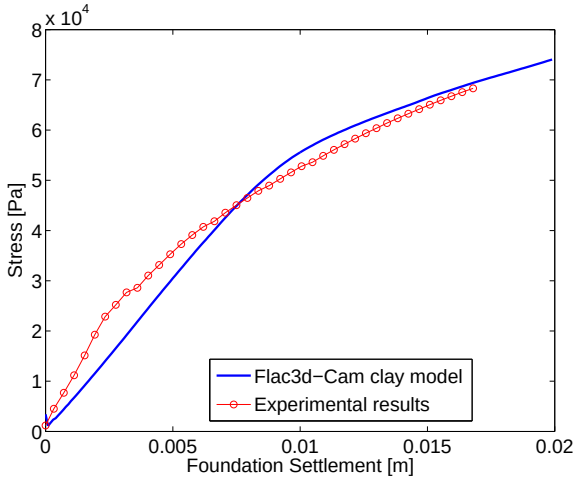

Figure 6.5: Bearing capacity of a footing on pure clay, experimental versus numerical results

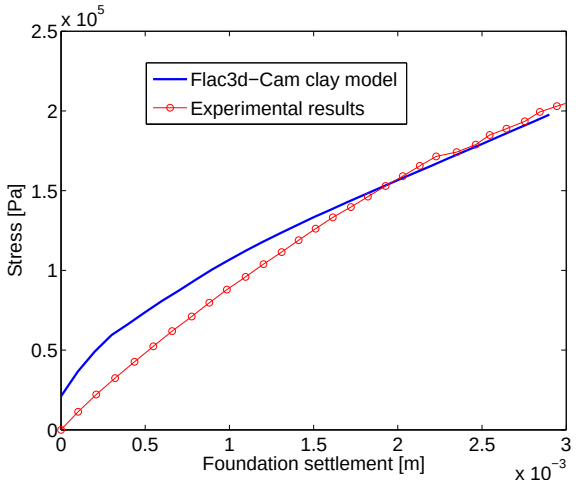

Figure 6.6: Bearing capacity of a footing on clay reinforced by LTC, experimental versus numerical results

Table 6.4: Input parameters -Cam-clay model

Bulk modulus (small strain, undrained)	$60MPa$
Shear modulus (small strain, undrained)	$17MPa$
λ	0.115
κ	0.029
Preconsolidation pressure	$50kPa$
Reference pessure	$1kPa$
Specific volume at reference pressure	1.82

Table 6.5: Input parameters -Mohr-coulomb model

Bulk Modulus	$66MPa$
Shear Modulus	$100MPa$
Unit weight	$25kN/m^3$
Friction Angle	48^o
Cohesion	$0kPa$

6.3.4 Damping

None of the constitutive laws that were used in the numerical modelling contains an adequate representation of the hysteresis that occurs in a real material and therefore an additional damping was applied. Dealing with a simple dynamic case, when a sinusoidal velocity is applied to a footing, *local* damping, which is implemented in FLAC3D was chosen to be used. This option of damping, when treated with caution, provides good results because it is frequency independent and needs no estimate of the natural frequency of the system being modelled. Local damping operates by adding or subtracting mass from a gridpoint or structural node at certain times during an oscillation (FLAC3D, 2006). Increments of kinetic energy, induced by adding mass to a gridpoint or node, are activated twice per oscillation cycle at velocity extremes. Local damping value is in FLAC3D defined by a local damping coefficient α_l, which is directly related to fraction of critical damping D:

$$\alpha_l = \pi D \tag{6.1}$$

In the presented dynamic analysis, 5% damping was used for clay and gravel material and 2% damping was used for the structural elements.

6.3.5 Joint acting between the flexible and the rigid part of the models

A joint between the transition zone and pile had to be defined. Referring to the physical model, metal funnel was fixed by a set of screws to the pile. The screws allowed a slight funnel displacement and therefore the joint between pile and funnel could be defined as semi-rigid. The pile element was numerically simulated by a 'beam structure element' composed of 11 nodes. These nodes are connected with the surrounding grid by '*links*', which implement interactions that occur between the beam element and the grid. By default, these nodes are attached to the grid such that translational degrees-of-freedom are rigidly connected to the grid and the rotational degrees-of-freedom are free (FLAC3D, 2006). Wanting to modify the attachment conditions between the pile head and the transition zone, links between the node at the pile head and the surrounding grid have to be redefined. The numerical study of the soil reinforced by rigid inclusions each attached to a transition zone and a LTC was performed considering two different types of attachment conditions:

1. Translational movement of node being at pile head is the same as the translational movement of the grid. Rotations of the node are free, without any connection to the surrounding grid. As a consequence, the pile head is subjected to same displacement as the transition zone but is not influenced by any rotation of the transition zone.

2. Translational movement and rotation of node being at pile head is the same as the translational movement and rotation of the grid. As a consequence, the pile head is subjected to same rotation and displacement as the transition zone.

Results of numerical calculations performed under these two configurations are presented in the following.

6.4 Numerical procedure - loading

The aim was to numerically reproduce the same loading procedure as was applied in the experimental study. This was done by dividing the numerical calculation in stages. After reaching an initial consolidation of the clay mass, the soil reinforcement and the footing were added into the soil. Vertical stress of 87 kPa (equivalent to load of 4 kN) was then applied to the footing and an equilibrium was reached. Keeping the vertical stress constant, a dynamic input was applied. Wanting to simulate the same horizontal dynamic loading as applied in the experimental study, a velocity history described by a FISH [3] function was applied. Figure 6.7 shows the horizontal cyclic displacement of the footing.

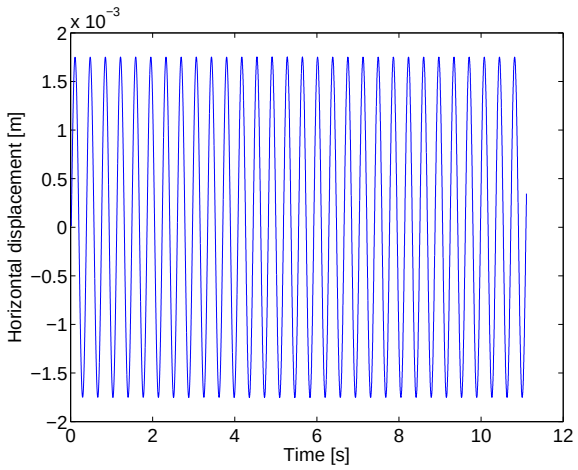

Figure 6.7: Displacement applied to the footing

6.5 Numerical results

Results of numerical calculations simulating response of the reinforced soil to inertial loading are presented in the following. Three different modifications of soil reinforcement were modelled:

1. Piles associated to Load Transfer Columns (LTCs) surrounded by clay (Figure 6.1)

2. Piles associated to a Load Transfer Platform (LTP) (Figure 6.2)

[3] language used in FLAC3D

3. Piles associated to a LTP which is reduced in its size to have the same length and width as the foundation and the created gravel 'block' is surrounded by clay (Figure 6.3). This type of a transition zone is referred in the figures as 'LTP - block' .

The foundation behaviour as well as the pile response were studied under vertical static loading and combined dynamic loading.

6.5.1 Vertical loading

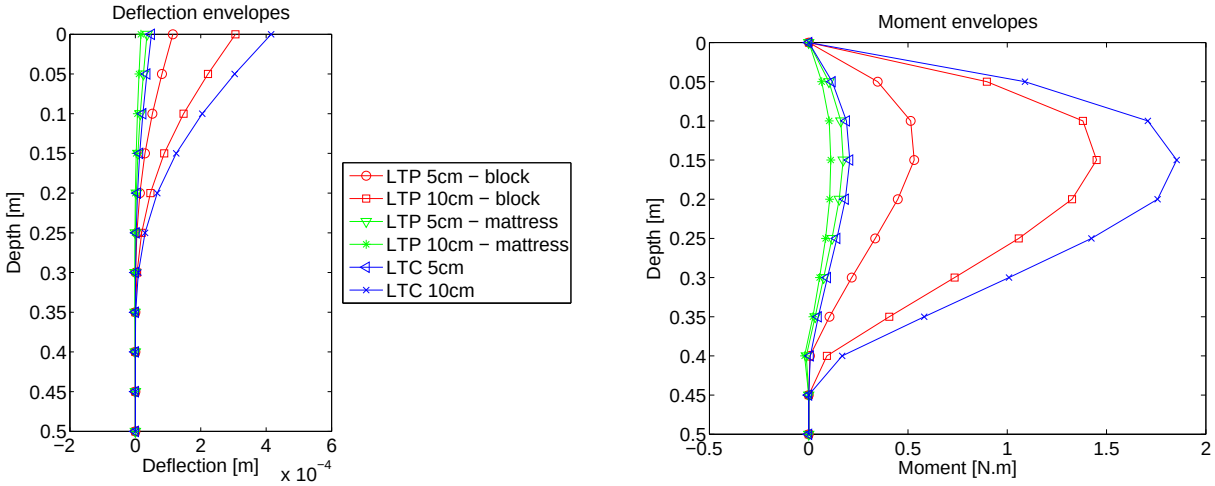

(a) (b)

Figure 6.8: Numerically obtained lateral pile response to vertical loading of the reinforced soil. Soil reinforcement composed of piles associated to different types of upper flexible parts: LTCs surrounded by clay, LTP or a reduced LTP - block. Deflection along the pile (a); Bending moment along the pile (b)

Figures 6.8(a) and (b) show a maximum bending moment (b) and a maximum deflection (a) experienced by the pile when the vertical loading is applied to the reinforced soil. The rigid pile was associated to the three different types of the upper flexible part. It can be observed that a 5cm high LTC surrounded by clay transfers approximately the same amount of forces to the pile as a 5cm high LTP. As the height of the LTCs and LTP increases, the difference in the load transfer between the two flexible parts becomes visible - LTCs with 10cm high columns transfer larger amount of forces to the pile than LTP with the same height. The previous suggests that there is a dependence between the pile behaviour and the LTC height when the higher column seems to transfer larger moments to the pile than a shorter column. This, even though contradictory on the first site, is considered to be due to better ability of the 5 cm stone columns to transfer the vertical forces applied by the foundation directly to the pile head without inducing a moment and shear forces which are created by the 10cm column due to the column rotation. Short columns are therefore considered to act as more rigid elements which do not undergo as much rotation under the vertical loading as the higher columns.
Opposite to the case when the pile is associated to the LTC, the pile lateral performance don't seem to be dependent on the height of the upper flexible part when it is composed entirely of gravel (LTP), although this is valid only in the range of the heights tested.

Comparing the load transfer within the LTCs surrounded by clay or within the reduced LTP in a form of a block lying below the foundation, it can be seen that the pile response to the applied loading is in the same order for both types of the flexible part.

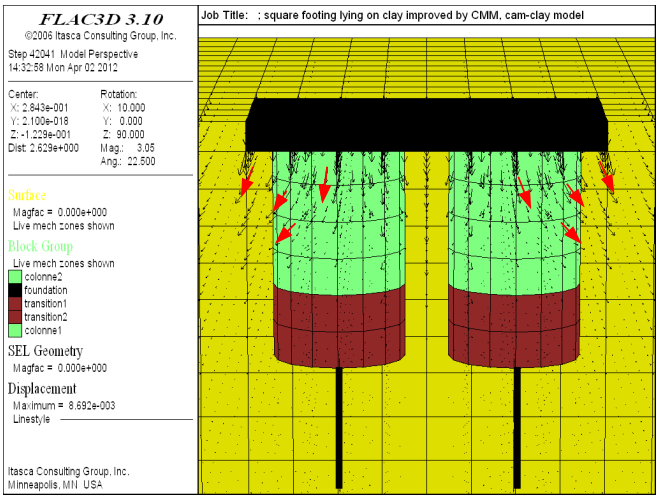

(a)

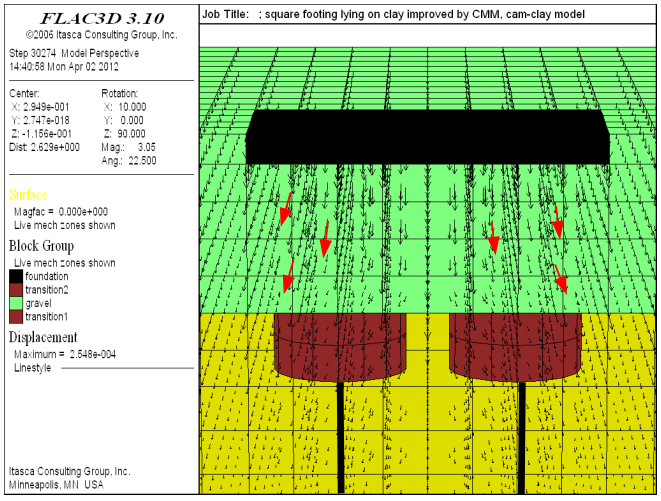

(b)

Figure 6.9: Soil migration towards the non-reinforced soil

The general trends observed numerically are in agreement with the experimental observations. It is concluded that when the pile is associated to a thinner, 5cm flexible layer and the

foundation is loaded with a vertical load, the pile response is in the same order when associated to either LTCs or LTP. Therefore the type of the flexible layer does not have an important influence on the lateral pile performance. On the contrary, as the height of the flexible part increases, the LTC with its transition zone seem to undergo a rotation, which induces a deformation of the pile below. This deformation is higher than a deformation on the pile associated to the LTP. It is suggested that the rotation of the LTC is caused by the migration of the soil underneath the foundation towards the unreinforced soil. This phenomenon is confirmed by the numerical modelling which shows that the migration of soil towards the unreinforced soil is more important when the flexible layer is composed of gravel columns (LTCs) surrounded by clay than when it is composed entirely of gravel mattress (LTP). Figure 6.9 shows two graphical outputs of FLAC3D, where displacement vectors were plotted. Figure 6.9(a) shows a case when the foundation is lying on LTCs surrounded by clay and Figure 6.9(b) shows a case when the foundation lies on LTP. The bigger red arrows were added to the graphics in order to highlight the direction of the displacement vectors which is not as clear from the original FLAC3D outputs. The size of the vectors should not be taken into account since the scale is not the same for (a) and (b) plots. The Figure 6.9 shows that the mixture of columns and clay (plot(a)) has a bigger tendency to migrate into the sides, out of the area beneath the foundation than the gravel (plot(b)). Knowing this and the fact that the foundation settlement is the highest for the foundation on the soil reinforced by piles associated to LTCs (Figure 6.10), it is logic that the pile underneath the LTC undergoes higher moments and deflections.

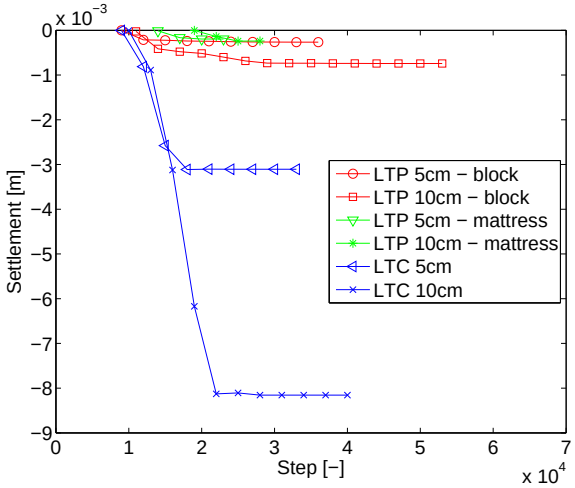

Figure 6.10: Settlement of the foundation lying on soil reinforced by piles associated to different types of flexible part

6.5.2 Combined dynamic loading

After imposing the vertical static load to the foundation, a horizontal dynamic loading was applied. In order to facilitate the comparison between the numerical results and the experimental results, the pile deformation at the beginning of the cyclic loading stage was considered to be zero and therefore the same presentation (i.e. the data presentation *'Correction-Vload'* - see section 5.3) was used for the numerical and the experimental results. The pile response to the horizontal dynamic loading which was composed of 30 cycles, was studied for the first cycle and then for the total 30 cycles.

The results are presented in form of envelopes of maximum deflection y and maximum bending moment M. These envelopes are graphs which show the variation in the maximum values for the M or y along the pile due to the application of the loading conditions. The envelopes are obtained by superimposing the individual diagrams for the M or y function. The resulting envelope of maximum bending moment or maximum deflection shows the upper bound for the M or y function, respectively.

Pile response during the first loading cycle

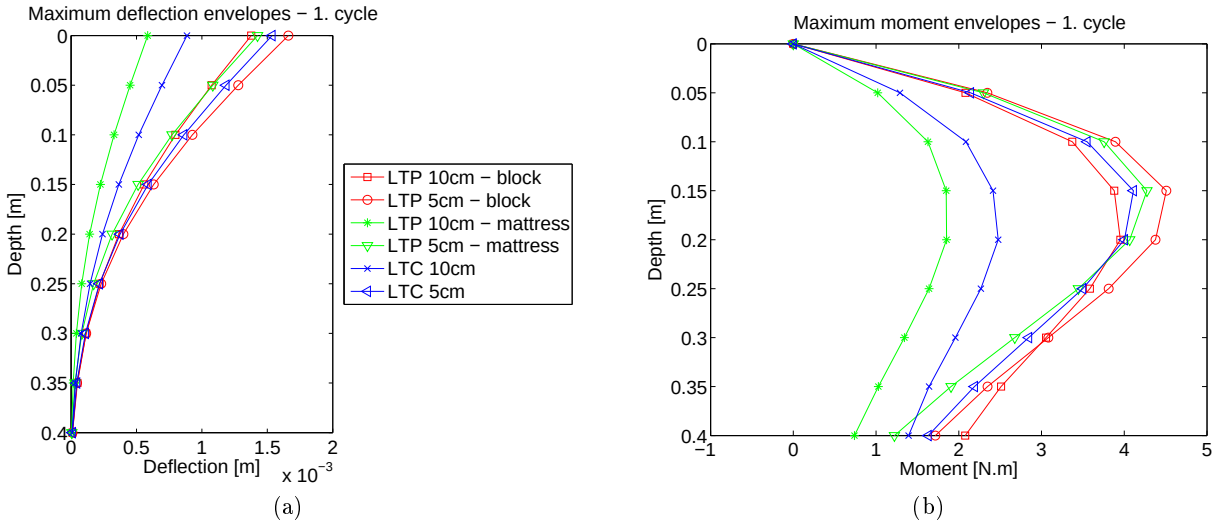

(a) (b)

Figure 6.11: Numerically obtained lateral pile response to 1 cycle of horizontal dynamic loading of the reinforced soil. Soil reinforcement composed of piles associated to different types of upper flexible parts: LTCs surrounded by clay, LTP or a reduced LTP - block. Maximum deflection experienced along the pile (a); Maximum bending moment experienced along the pile (b)

On the contrary to the vertical loading, the pile response to the applied combined loading is higher for a smaller height of the flexible part. That means, that more of the forces created by the inertial loading of the foundation are transferred to the pile when the flexible layer is 5 cm high than when it is 10 cm high. It is suggested that this is due to the behaviour of the flexible parts of smaller heights which act as more rigid elements transferring most of the loading to the piles below. Since the loading is not only in the vertical but also in the horizontal direction, moments and shear forces are created within the pile. These are higher than in the case when the pile is associated to higher flexible parts because it is assumed that the higher flexible parts have an ability of absorbing more of the inertial forces.
Figure 6.11 also shows that the type of the flexible part does not play an important role in the transfer mechanism of the inertial loading to the pile when the flexible part is sufficiently small. This conclusion is based on the fact that the pile response for a pile supporting a 5 cm high LTC, a 5 cm high LTP or a 5cm high reduced LTP ('block') is in the same order. The same phenomenon was observed for the pile response to the vertical loading of the reinforced soil.
On the contrary, when the height of the LTC is 10 cm, the pile is subjected to higher moment

and deflection than when associated to a 10 cm high LTP. It is assumed that this is caused by the rotation of the LTC created due to the soil migration towards the area where the soil was not reinforced. This soil migration is shown to be more important in the zone composed of stone columns surrounded by gravel than in the zone which is composed entirely of gravel (see Figure 6.9).
The reduced LTP, creating a block of gravel below the foundation, seems to transfer high level of solicitation to the pile and there seems to be no important influence of its height on the lateral pile performance.

Pile response during the 30 loading cycles

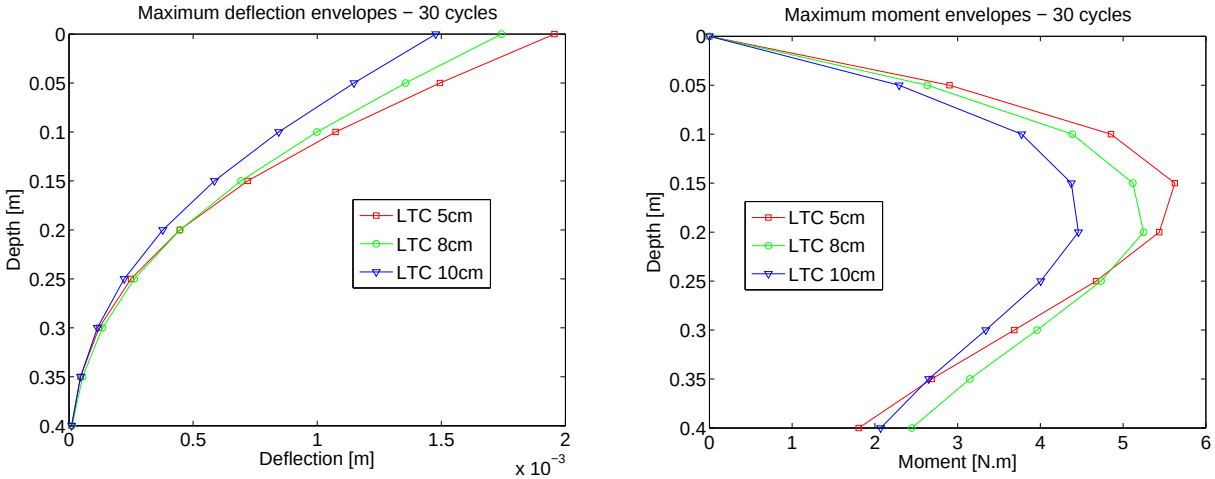

(a) (b)

Figure 6.12: Numerically obtained lateral pile response to 30 cycles of horizontal dynamic loading of the reinforced soil. Soil reinforcement composed of piles associated to LTCs surrounded by clay. Maximum deflection experienced along the pile (a); Maximum bending moment experienced along the pile (b)

Carrying out 30 cycles of the horizontal cyclic loading did not change the general trends observed for the pile response to one loading cycle. Therefore the same conclusions can be made concerning the pile behaviour in relation to different types of the flexible part (LTC, LTP and a reduced LTP-'a block') for the first loading cycle and all the 30 loading cycles. To illustrate this, Figure 6.12 shows the response of a pile associated to a Load Transfer Column (LTC) of varying height (5cm, 8cm, 10cm) to the applied cyclic loading. The results are presented in form of envelopes of maximum bending moment M and maximum deflection y for the total loading sequence of 30 cycles. It can be seen that indeed, the trend that a flexible part of a smaller height transfers larger inertial loading applied at the foundation level to the pile is confirmed.

In order to present the evolution of the pile deformation during the cyclic loading, an example when the pile is associated to a LTC is presented. It was observed that when the foundation moves in a direction 'out of the pile group' (i.e. in direction A - see Figure 5.26), the pile deflection increases with every loading cycle. This deflection accumulation with the cyclic loading is visible from Figure 6.13. Figure 6.13(a) shows a pile head deflection which was used to define the times of its local maximum and minimum for the first and the last

loading cycle. These were denoted $y_{max1.cycle}$, $y_{min1.cycle}$, $y_{max30.cycle}$ and $y_{min30.cycle}$. The pile deflection was then plotted in Figure 6.13(b) for $y_{max1.cycle}$, $y_{min1.cycle}$, $y_{max30.cycle}$ and $y_{min30.cycle}$. It can be seen that when the foundation moves in direction 'towards the pile group' (i.e. in direction B), the pile deflection decreases in value with the cyclic loading. This shows that the pile is gradually more and more inclined towards the unreinforced soil. This phenomenon was also observed experimentally.

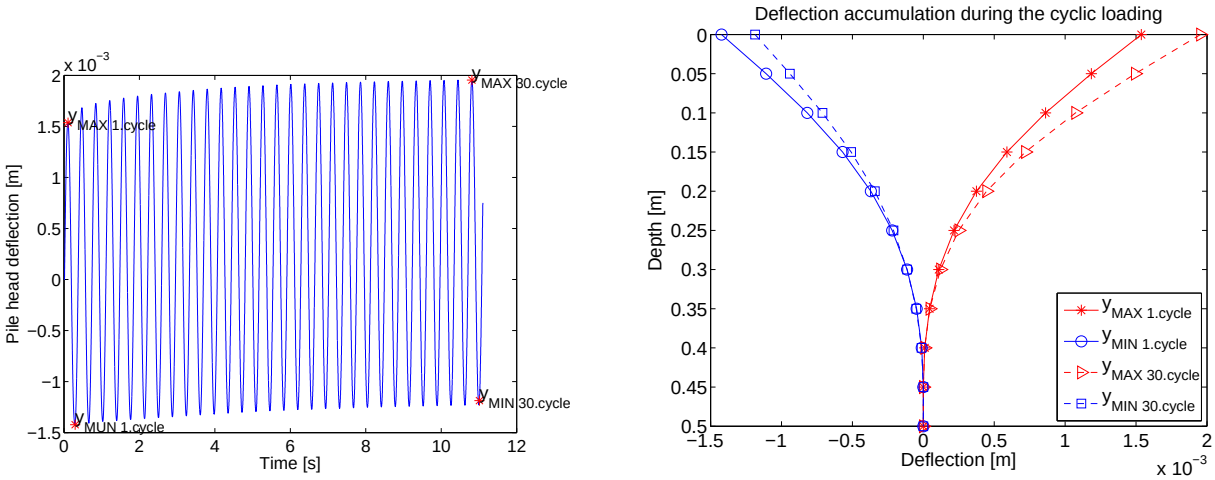

(a) (b)

Figure 6.13: (a) Deflection at the pile head which was used to define the times of its local maximum and minimum for the first and the last loading cycle. These were denoted $y_{max1.cycle}$, $y_{min1.cycle}$, $y_{max30.cycle}$ and $y_{min30.cycle}$. (b) The pile deflection plotted for $y_{max1.cycle}$, $y_{min1.cycle}$

Comments on the stiffness of the joint between the transition zone and the pile head

In order to understand the role of the joint rigidity between the transition zone and the pile, numerical simulations of piles associated to LTCs where the transition zones were connected to the piles in two different manners were carried out. The joints were defined either permitting a free rotation of the pile head (Case 1) or disabling this rotation, setting it rigid with respect to the transition zone (Case 2). For both cases, the translational movement of the pile head was set to be the same as as the translational movement of grid forming the transition zone (see section 6.3.5).

While imposing cyclic loading to the foundation, piles undergo elastic deformation. Referring to the experimental study, one pile was equipped with strain gauges and therefore its behaviour could be monitored. Numerical study of lateral pile behaviour was performed, respecting the pile position within the pile group and respecting the loading direction.

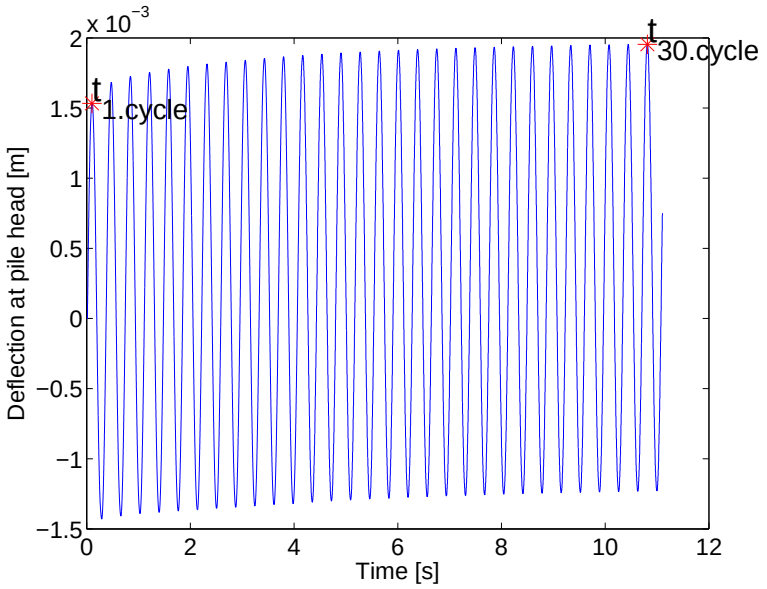

Figure 6.14: Pile head deflection maximum is reached for the first loading cycle at time $t_{1.cycle}$ and for the last loading cycle at time $t_{30.cycle}$

Pile head deflection was used to define times when the pile deflection reaches its local maximum. During the first loading cycle, the local deflection at the pile head was reached at time $t_{1.cycle}$ (see Figure 6.14) and during the last (i.e. thirtieth) loading cycle, the local deflection at the pile head was reached at time $t_{30.cycle}$ (see Figure 6.14). Figures 6.15 and 6.16 show the response of a pile associated to LTCs of varying height to the inertial loading applied by the foundation. The moment and deflection along the pile is plotted for times $t_{1.cycle}$ and $t_{30.cycle}$. Figure 6.15 shows results obtained for the *Case 1* and Figure 6.16 refers to the *Case 2*.

It can be seen from the presented numerical results that the attachment conditions between the pile head and the transition zone are very important in terms of lateral pile behaviour. For the *Case 2*, when the translational movement and rotation of node at pile head is the same as the translational movement and rotation of the transition zone, the pile undergoes negative moments at its upper part. This seems to suggest that as the foundation imposes inertial loading to the reinforced soil, the LTC and the transition zone undergo a rotation, which is then projected on the pile due to the rigid connection between the pile head and the transition zone.
Comparing numerically and experimentally obtained pile behaviour, it is assumed that better results would be obtained with a possible application of a semi-rigid joint between the pile and the transition zone. This aspect, i.e. parametric study of the joint rigidity, stays to be resolved by future calculations.

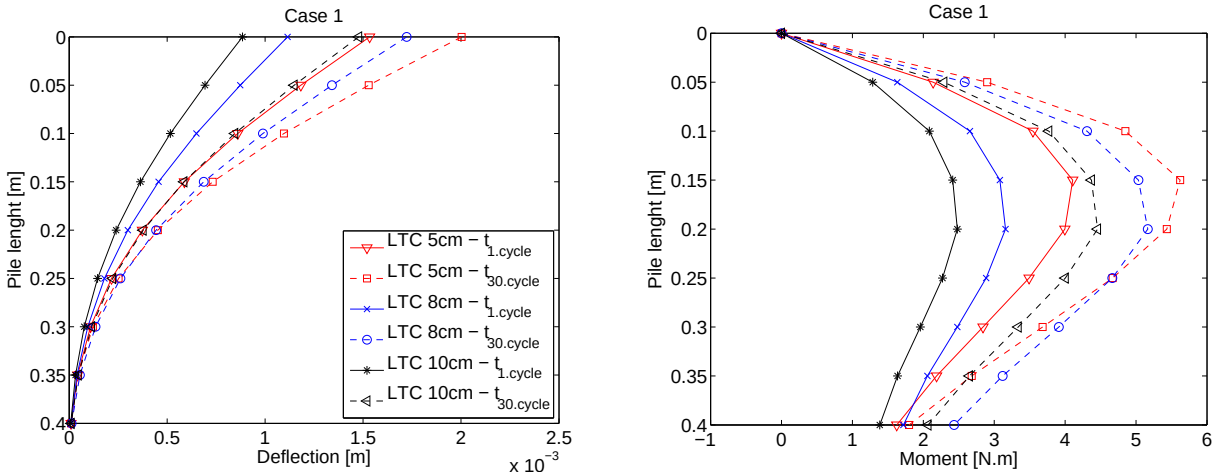

(a) (b)

Figure 6.15: Response of a pile associated to LTC of varying height to the inertial loading applied by the foundation. The joint between the transition zone and the pile is defined according to the ***Case 1***. The moment and deflection along the pile is plotted for times $t_{1.cycle}$ and $t_{30.cycle}$ which are defined in Figure 6.14

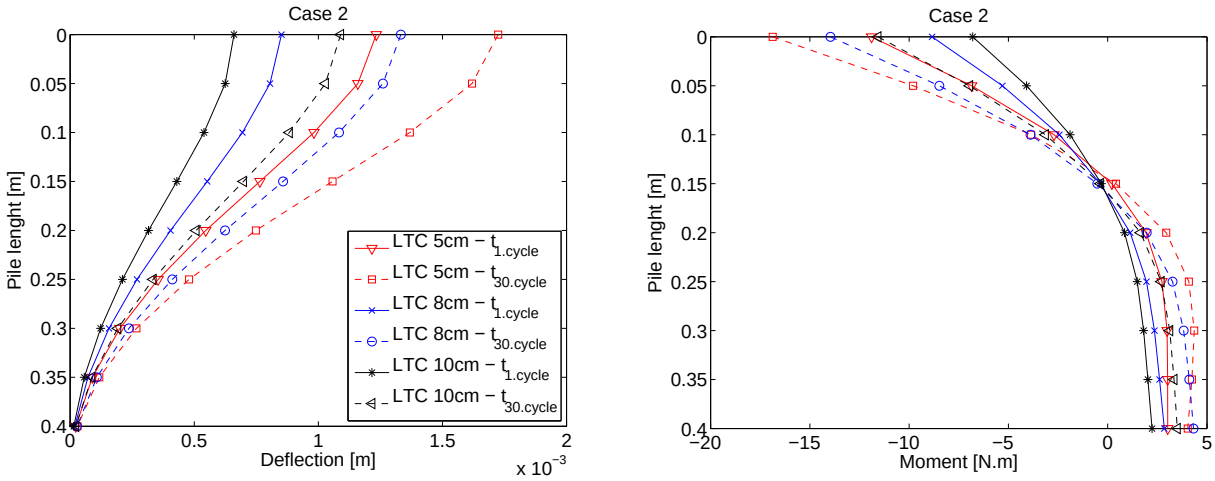

(a) (b)

Figure 6.16: Response of a pile associated to LTC of varying height to the inertial loading applied by the foundation. The joint between the transition zone and the pile is defined according to the ***Case 2***. The moment and deflection along the pile is plotted for times $t_{1.cycle}$ and $t_{30.cycle}$ which are defined in Figure 6.14

6.5.3 Experimental versus numerical results

It is noted that the numerical results are in general agreement with the experimental results. The numerically obtained deformation of the pile is in the same order as the experimental pile deformation. Figure 6.17 shows a comparison between the numerically and experimentally obtained deflection of a rigid inclusion, which is associated to either a 10 high LTC or a 10cm high LTP. Figures 6.17a and 6.17b refer to the response of the rigid inclusion under vertical loading of the foundation and inertial loading of the foundation, respectively.

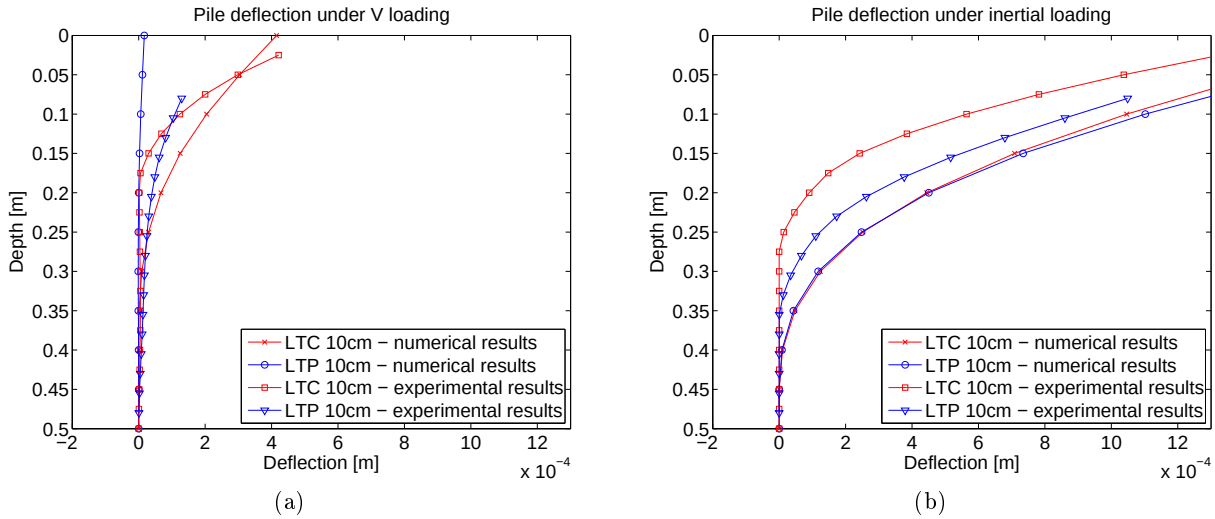

Figure 6.17: An example showing that the numerically and experimentally obtained deflection of a rigid inclusion, which is associated to either a 10 high LTC or a 10cm high LTP, is in the same order

In agreement with the experimental results, it seems that the pile response is independent of the type of the flexible part when its height is sufficiently small. On the contrary, as the height of the flexible part increases, the differences between the load transfer mechanisms for different types of the flexible parts become more apparent. The Load Transfer Columns (LTCs) seem to undergo a rotation, which induces bending moments on the pile below. This column rotation is caused by migration of the soil below the foundation to areas with lower pressure and where there is no reinforcement present. It is considered as important to point out that this could explain higher moments along the pile associated to LTC than along a pile associated to a LTP.

Numerical model of soil reinforced by piles associated to a reduced LTP in a form of a block was not completed with a physical model. It is suggested, based on the numerical results, that this type of a flexible upper part of the soil reinforcement transfers the highest level of solicitation to the pile.

The presented numerical results show that the attachment conditions between the pile head and the transition zone are very important in terms of lateral pile behaviour. Comparing numerically and experimentally obtained pile behaviour, it is assumed that better results would be obtained with a possible application of a semi-rigid joint between the pile and the transition zone. This stays to be confirmed by the future numerical modelling.

Foundation settlement obtained by numerical and experimental methods is compared in Table 6.6 for vertical static loading and in Figure 6.18 for the combined (vertical static and horizontal dynamic) loading. It is noted, that the numerical and experimental results are in the same order and show an increase of level of settlement with the increasing stone column height. The cyclic settlement stabilization is not reached by the end of the cyclic loading. Settlement based on numerical results seems to exhibit larger dependence on the stone column height.

Table 6.6: Vertical loading of the foundation - experimental versus numerical settlement

Height of the LTC	Numerical results	Experimental results
5cm	3mm	3.5mm
8cm	-	4mm
10cm	8.2mm	5mm

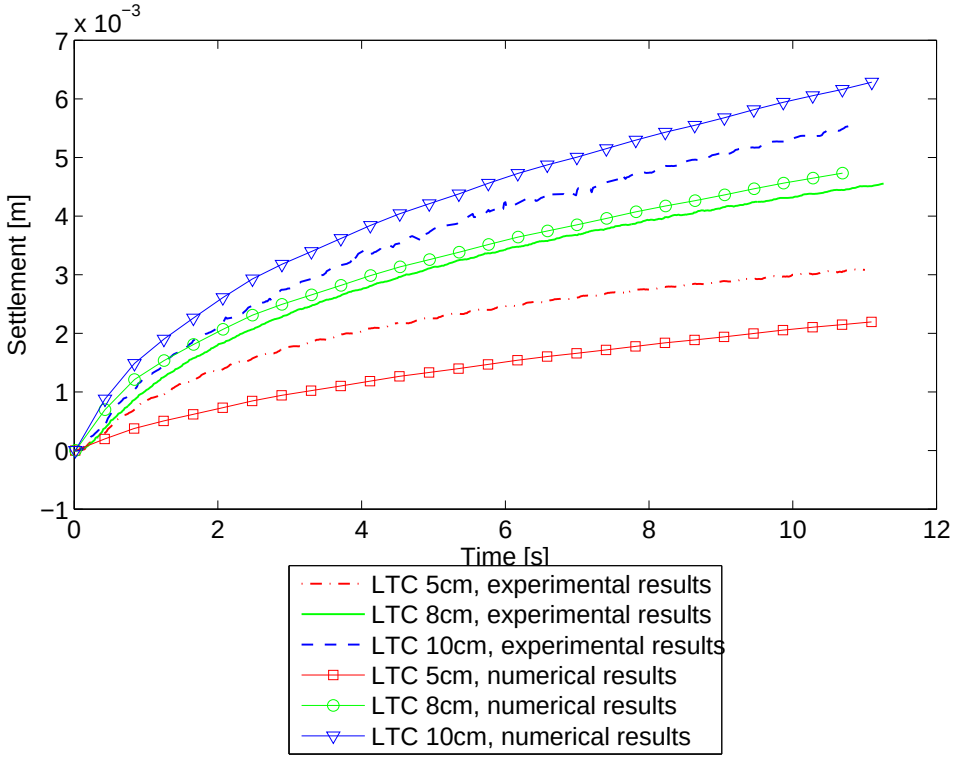

Figure 6.18: Comparison between experimental and numerical foundation settlement

6.6 Conclusion

The presented numerical modelling was carried out in order to verify and complete the experimental results, addressing mainly the lateral performance of the rigid inclusion and its comparison between different reinforcement types studied.

The numerical results confirmed that under vertical static loading, the lateral performance of the rigid inclusion is in the same order for all three types of the flexible part (i.e. LTC, LTP or a reduced LTP-'block'). Such an observation was explained by a better ability of the flexible parts with smaller heights to transfer the vertical forces applied by the foundation directly to the head of the rigid inclusion without inducing a moment or shear forces, as happens in the case of higher flexible parts. On the contrary, as the height of the upper flexible part of the physical models increases, the differences in the load transfer mechanism become more visible. It was observed, that in the case of rigid inclusions associated to the LTCs, an important mechanism taking place is the column rotation. This rotation is caused by the migration of the soil underneath the foundation towards the unreinforced soil. It was proved that the soil

migration is more present in the case of LTCs than in case of LTP. As a consequence, the rigid inclusion supporting the LTP is found to undergo less deformation under the applied vertical loading than when supporting the LTC.

Analysing the response of the rigid inclusion to the applied inertial loading, it was found that when the height of the flexible part is sufficiently small, the type of the flexible part does not play an important role in the mechanism of load transfer from the foundation towards the rigid inclusion. The same phenomenon was observed for the pile response to the vertical loading of the reinforced soil. As the height of the flexible part increases, once again, the soil migration towards the unreinforced soil plays its important role and causes the rigid inclusion supporting the LTC to undergo higher deformation than the rigid inclusion supporting a LTP. On the contrary to the vertical loading, the rigid inclusion undergoes higher deformation under the applied inertial loading for smaller height of the flexible part. It is suggested that this is due to the behaviour of the flexible parts of smaller heights which act as more rigid elements transferring most of the inertial loading to the rigid inclusion below.

It is noted, that the rigidity of the joint between the rigid inclusion and the transition zone plays an important role in the transfer of moments and shear forces from the foundation to the head of the rigid inclusion. It is therefore necessary to define the nature of this joint for the *in-situ* conditions, presenting details on its stiffness in rotation and shear.
A parametric study on the joint rigidity stays one of the perspectives of the presented numerical study.

Comparing the performed experimental study with the study of X. Zhang (Zhang, 2011), the same dependence of the deformation of the rigid inclusion on the LTC height was observed - the deformation of the rigid inclusions under the dynamic loading increases with the decreasing stone column height. This trend was observed in the presented experimental and numerical study where the LTC height was varied form 5cm to 10cm and for the work of X. Zhang (Zhang, 2011) where the stone column height was varied from 3cm to 15cm.
In both numerical studies, the reduced LTP - 'block' seems to induce more sollicitation of the rigid inclusion than the LTC.

The energy dissipation was not addressed in the presented numerical study due to the constitutive laws applied. The numerical response of the pile-soil system to the applied loading stayed entirely elastic and therefore with no energy dissipation taking place. The zones which plastified during the numerical analysis were within the flexible part of the model, where a Mohr-Coulomb model was used in order to approximate the behaviour of the gravel. This model is not capable to realistically simulate the hysteresis behaviour and therefore neither the energy dissipation taking place within the flexible part of the model.

The experimental and numerical results were found to be in the same order, although only response of the rigid inclusion to the applied loading and foundation settlement were studied in detail. The numerical study served mostly as a tool to verify the experimentally obtained lateral performance of the rigid inclusion with respect to the type of loading applied as well as to the type and height of the flexible part used. Speculations made while analysing the experimental data were examined also numerically.

CHAPTER 7

Conclusions and Perspectives

The presented work addresses the subject of soil reinforcement and its response to the inertial loading. The project was carried out under a BDI[1] contract with a financing divided between *CNRS*[2] and *Keller, Fondations spéciales*. The aim of this primarily experimental study was to deepen the knowledge on seismic behaviour of soil reinforcement, which is composed of rigid inclusions associated to different types of flexible parts. Rigid inclusions associated to Load Transfer Columns (LTCs) were designed to simulate a soil reinforcement technology known as Mixed Module Columns (CMM). Associating the rigid inclusions to a Load Transfer Platform (LTP) overtook the main principles of a technology known as Rigid Inclusions (RI).

The literature review of the thesis shows that even though numerous research projects concerning the soil reinforcement by rigid inclusions connected to a flexible part are carried out, there seems to be a lack of studies addressing this problematic in seismic conditions. Moreover, a little number of the experimental studies of CMM and RI soil reinforcement under seismic loading are carried out in 3D, which is assumed to be due to the complexity of the 3D physical models and due to a difficult monitoring of the system response to the dynamic loading.
The presented study therefore attempts to approach the subject of CMM and RI soil reinforcement in seismic conditions, although limiting to the reduced physical modelling without respecting the similarity conditions. Therefore only information on a qualitative basis are provided by the experiments performed. A numerical model is consequently calibrated based on these results, making a future possible extension of the model into the real scale. The results obtained numerically served, for the time being, as a tool to verify the behaviour of the rigid inclusions which was observed experimentally. The role of the joint stiffness between the transition zone and the pile was also addressed numerically, which proved its importance in the load transfer from the flexible part to the rigid one. Therefore it is proposed that the

[1] Bourses de docteur ingénieur
[2] Le Centre national de la recherche scientifique

nature of this joint should be defined for the *in-situ* conditions in order to have a proper knowledge of its rotational and translational stiffness.

The response of the reinforced soil to the inertial loading is monitored at the foundation level and at the level of the rigid inclusions. The flexible parts of the models stay without being instrumented with sensors and therefore their behaviour has to be deduced from measurements obtained at the foundation level and at the rigid inclusions.
A method of energy evaluation is proposed, which separately analyses the energy balance at the foundation level, within the flexible part of the models as well as within the rigid inclusions surrounded by soil. This analysis is done entirely with measurements obtained by monitoring the response of the foundation and of the rigid inclusion during the inertial loading. Results seem to suggest that 90% of the global energy is dissipated within the flexible parts of the models. The flexible layer dividing the foundation from the rigid inclusions showed that it is therefore able to dissipate most of the energy applied at its surface. The case of the Load Transfer Column (LTCs) surrounded by clay was found to be able to dissipate more energy than the Load Transfer Platform (LTP) and the amount of dissipated energy seems to be independent of the LTC height. On the contrary, for the case of LTP, the global energy dissipation seems to be increasing with the increasing height of the LTP, suggesting that a thicker mattress is able to dissipate more energy than a thinner mattress.
The area of the P-y loops, plotted for the upper part of the rigid inclusions, is larger for the LTP when compared to the LTC system. Since the area of a P-y loop is proportional to the amount of energy dissipated at the point where it is plotted, and the area is larger for the LTP system (keeping in mind that the energy input is the same) we must conclude that more energy is transferred into the rigid inclusion in the LTP system when compared to the LTC system.

From energy balance, if more energy is transferred into the rigid inclusion, then less energy is absorbed by the flexible part of the model, above. Therefore, we can conclude that the LTP dissipates less energy than the LTC surrounded by clay. This confirms the results presented above.

Along with the cyclic loading, the stiffness of the flexible layer increases. As the system becomes more rigid, its ability to absorb energy decreases and therefore the observed energy dissipation becomes less important with the number of cycles.

In order to provide information for the current design practice, a parametric study was performed, relating the height of the flexible part to the lateral behaviour of the rigid inclusion. Analysing the response of the reinforced soil to the applied loading, it was found that when the height of the flexible part is sufficiently small, its type (i.e. LTC surrounded by clay or LTP) does not play an important role in the mechanism of load transfer from the foundation towards the rigid inclusion. This phenomenon was found to be common for the vertical static as well as the inertial loading. As the height of the flexible part increases, a mechanism of soil migration towards the unreinforced soil begins to play an important role and causes the rigid inclusion supporting the LTC to undergo higher deformation than the rigid inclusion supporting a LTP. This speculation, which was based on the experimental observations, was subsequently proved by the numerical simulations.
On the contrary to the vertical loading, the rigid inclusions undergo higher deformation under

the applied inertial loading for smaller heights of the flexible part. It is suggested that this is due to the fact that the flexible parts of smaller heights act as more rigid elements and hence transfer most of the inertial loading to the rigid inclusion bellow.
In the current practice, feasibility and economic aspects are a cause to the fact that rigid inclusions are often associated to either 0.5m high LTP (for the RI technology) or 1m to 1.5m high LTCs (for the CMM technology). The results presented show that under the horizontal cyclic loading, the decreasing height of the flexible part induces higher solicitation of the rigid inclusions. As a consequence, it can be said that for the inertial type of loading, the CMMs present an improvement of the RI technology used in the current practice.

Interpreting the lateral behaviour of the rigid inclusions in clay was found to be a difficult task. This was due to the fact that the rigid inclusions were nor free-head, nor fixed head and the load transferred from the foundation to the rigid inclusions was decomposed into horizontal force application and bending moments. As a consequence, we were dealing with a pile having a semi-rigid link to the load application device and by coupled mechanism, both bending moment and shear forces were applied to the head of the rigid inclusions. Even more, these shear forces and bending moments were created not only by the inertial loading of the foundation, but also by the non-homogeneous stress distribution within the reinforced soil, which caused a migration of soil towards areas with lower pressure (i.e. areas which were not directly below the foundation and where the soil was not reinforced). This soil migration possibly gave rise to rotation of the stone columns (LTCs), which applied additional bending moments to the heads of the rigid inclusions.

The lateral performance of the rigid inclusions within the soil reinforcement system showed that the inclusion preforms only a limited reversible behaviour, meaning that its deflection stays almost entirely within a positive range of values. There was observed an accumulation of this lateral deflection when the foundation was loaded in direction 'out of the pile group'. The deflection accumulation seems to have a tendency to stabilize at the end of the cyclic loading. The phenomenon of the non-reversible behaviour and the deflection accumulation is explained by the 'shadow effect' of the pile group.

It is considered as important to point out that the presented study is primarily an experimental study. Numerical modelling was originally carried out only to verify the experimental results on the lateral behaviour of the rigid parts of the models. The numerical simulations subsequently also served as a tool to verify the speculations made on the mechanisms occurring within the soil reinforcement.

The presented study provided not only results that helped to clarify the current state of knowledge on the problematic addressed, but also revealed number of unsolved questions and tasks to be done. These, which are listed below, stay as one of the perspectives for the future works.

- The aim of the presented experimental study was to analyse the behaviour of the reinforced soil under different types of loading conditions. The flexible part of the physical models was varied in its type and height. Result on lateral response of the rigid inclusions were presented, showing bending moments M, shear forces T and deflections y

created along these inclusions.
The current experimental set-up was not instrumented to obtain values of normal force transferred to the rigid part of the models. Even though attempts were made to obtain such information (see section 5.7), the data obtained were considered as hardly interpretable, with low representativity. Knowing the normal force distribution within the reinforced soil, it would allow to estimate the amount of normal force transferred from the foundation to the rigid part of the models. For the current practice, the ratio between the normal force and the shear force applied to the head of the rigid inclusion is important since it helps to determine the need of a steel reinforcement of the concrete piles.
Making a speculation that the LTCs acting as rigid elements in clay would transfer more normal forces to the rigid inclusions than the LTP, this would be a very important aspect for the current design practice. It would mean that in the case of LTCs, the moments created at the heads of the rigid inclusions would be 'compensated' by the high normal forces acting on the inclusions and the soil reinforcement could be designed in such a way, that the compressive stresses (created by the structure weight) would exceed the shear stresses (created by horizontal foundation loading) applied to the rigid inclusions.
It is therefore considered as important to perform further studies on the normal force distribution within the reinforced soil.

- As visible from results presented, the geometry of the reduced model of rigid inclusions associated to the LTCs could have caused physical mechanisms, which are not occurring in the *in-situ* conditions. It is thought that further studies should be made on the dynamic behaviour of shallow footing on a group of CMMs, where the number of CMMs exceeds the number used in the presented study. This could help avoiding such phenomena as stone column rotation under the applied loading as well as the soil migration towards the unreinforced soil.

- Instrumenting more rigid inclusions within the physical models would not only increase the reliability of the results but would also enable the study of a 'shadow effect'.

- Further experiments should be done, testing stone column heights which differ more than they differed for the experiments performed. This should be done to see, more clearly, the differences in lateral pile behaviour when supporting the LTCs or LTP with different heights. Although the presented study suggests such observations, this knowledge should be extended.

- The reduced physical models presented in this work are submitted to a normal gravity '$g* = 1$' and the conditions for a rigorous similitude with respect to the stress level '$\sigma* = 1$' are not fulfilled. Even though the scaling laws are not strictly respected, the main objective of the physical modelling was to perform a qualitative study of the soil reinforcement, studying its behaviour under inertial loading and pointing out important mechanisms, which should be taken into account by the current practice. The experimental results subsequently served to calibrate numerical models which helped to verify the experimentally observed behaviour of the rigid part of the models. These numerical models could serve as a basis to further numerical simulations, which could be extended into the real scale. It is noted that in order to realistically reproduce the system response to the inertial loading with all the aspects of the cyclic soil behaviour and the energy dissipation, an appropriate constitutive laws should be implemented into the proposed numerical models.

- Following the presented work, a quantitative study should be performed, respecting the similarity conditions. This could be done either by carrying out reduced-scale experiments in the centrifuge or by performing experiments in the real scale. The presented experimental study could then serve as a preliminary study, pointing out not only important aspects of the mechanisms taking place within the system, but also highlighting the crucial points of the physical modelling of such a problematic. An experimental study respecting the similarity conditions would help to specify and valorise the trends observed in the presented study.

Annex A

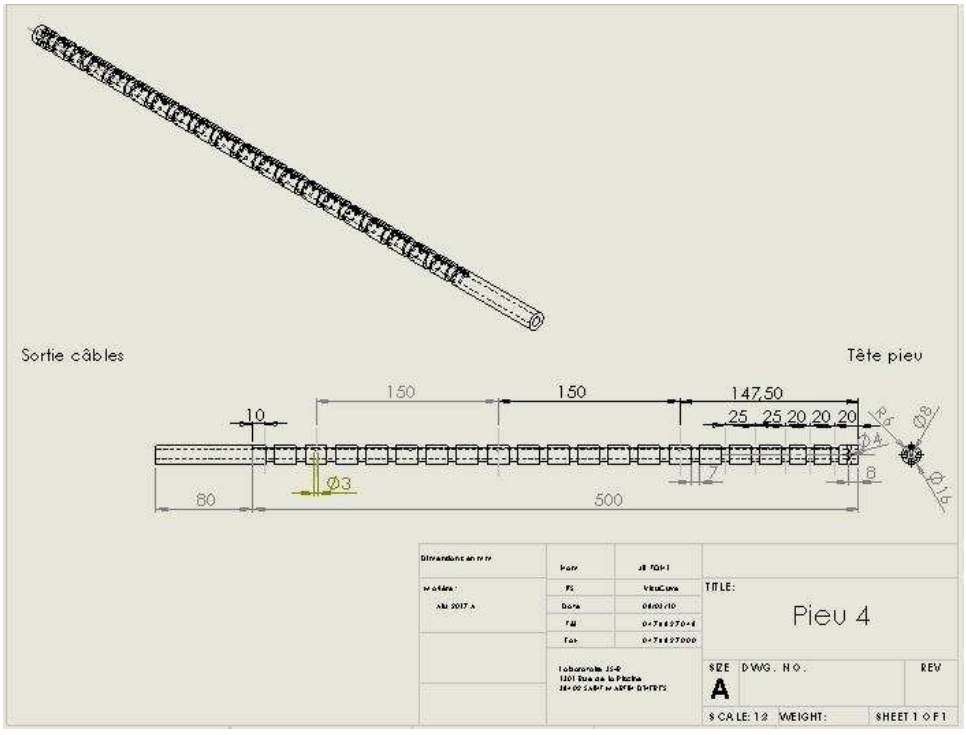

Figure 7.1: Plan of the instrumented pile

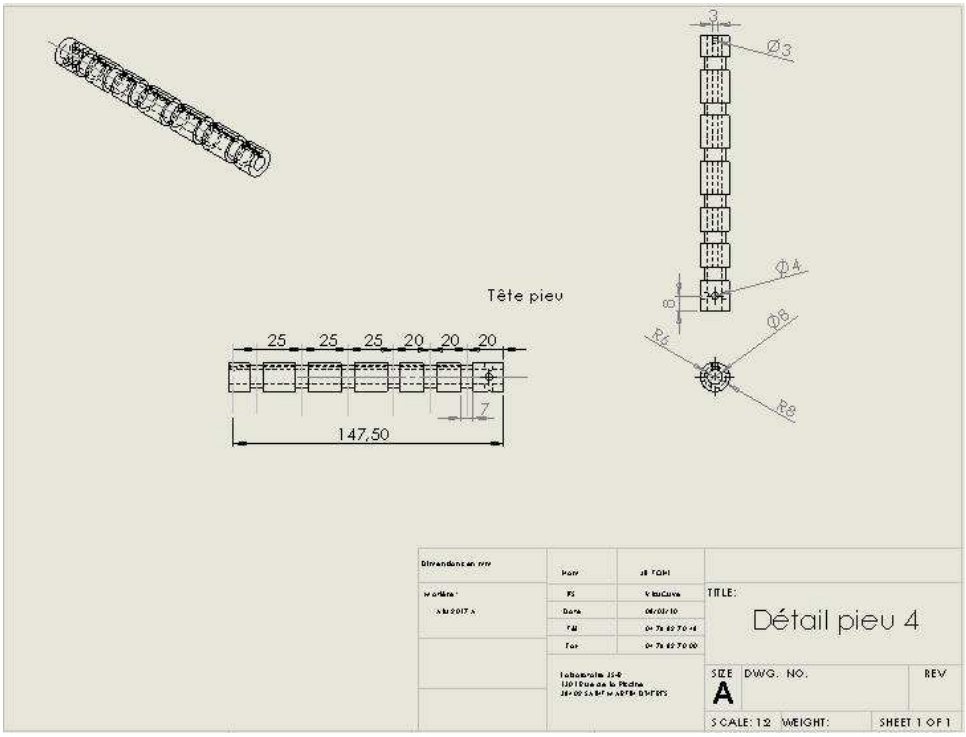

Figure 7.2: Plan of the instrumented pile

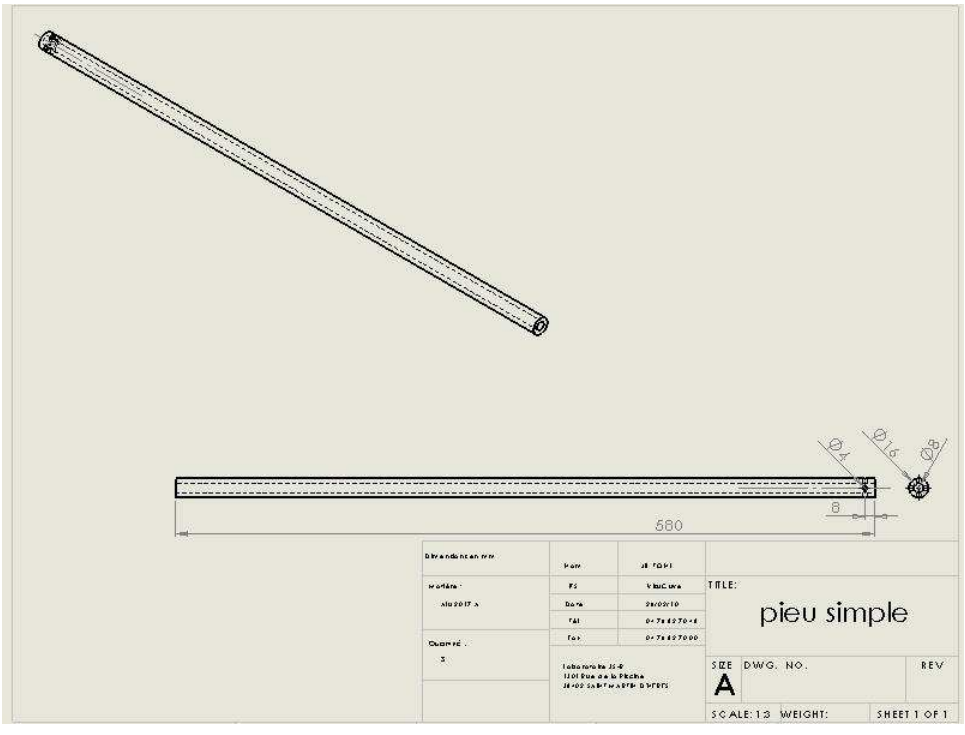

Figure 7.3: Plan of piles not instrumented with strain gauges

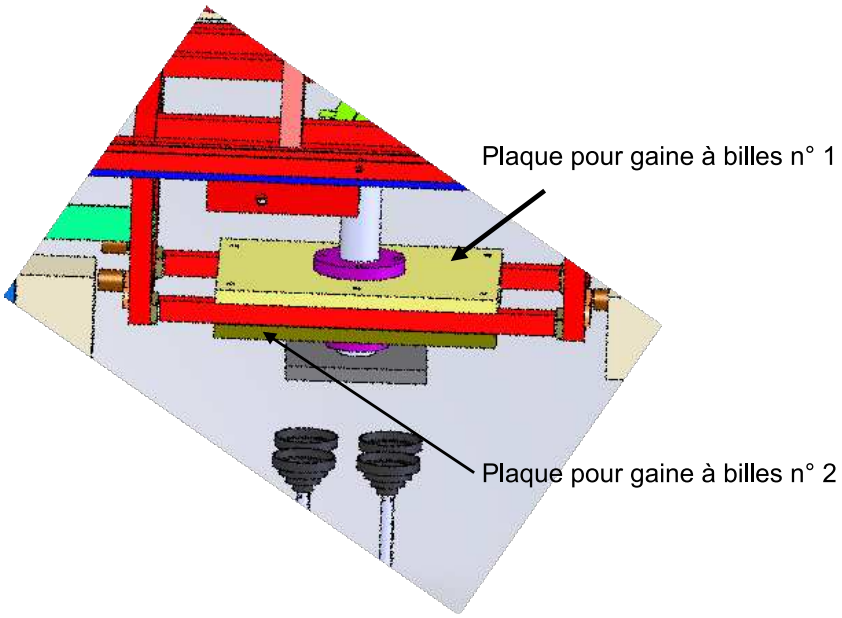

Figure 7.4: Plates supporting the ball bearing

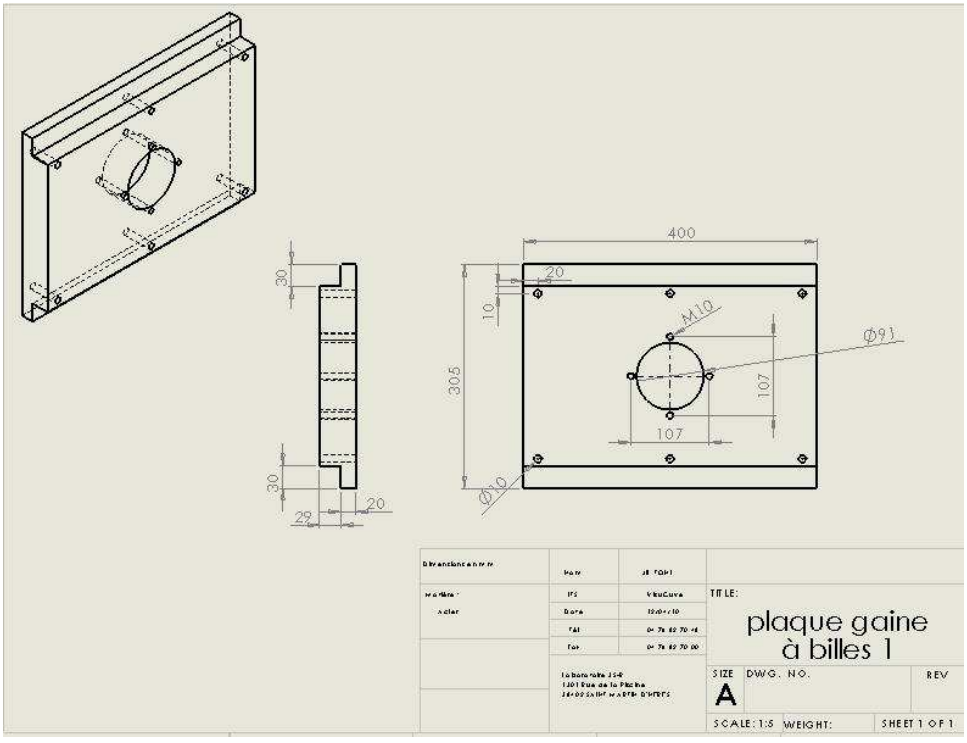

Figure 7.5: Plan of plate 1 supporting the ball bearing

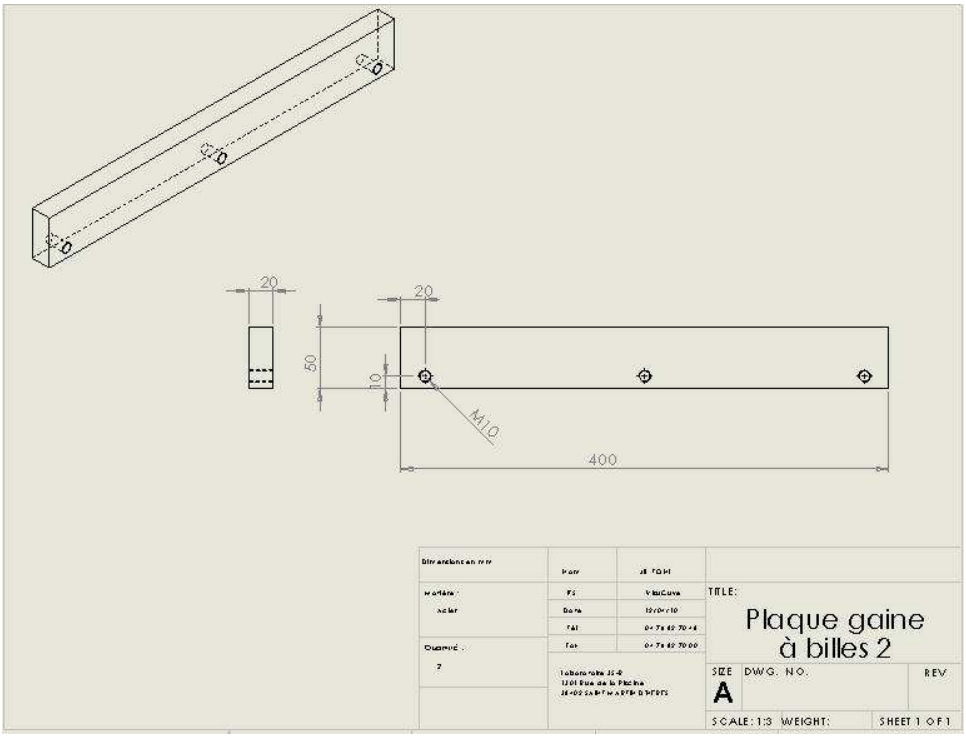

Figure 7.6: Plan of plate 2 supporting the ball bearing

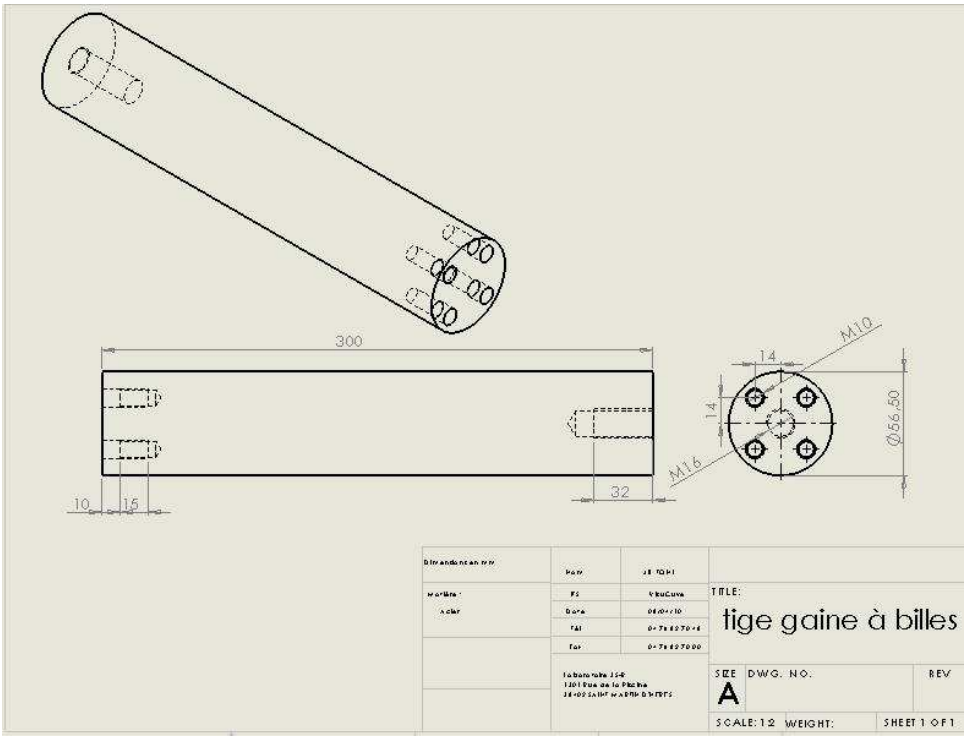

Figure 7.7: Metal rod passing through the ball bearing

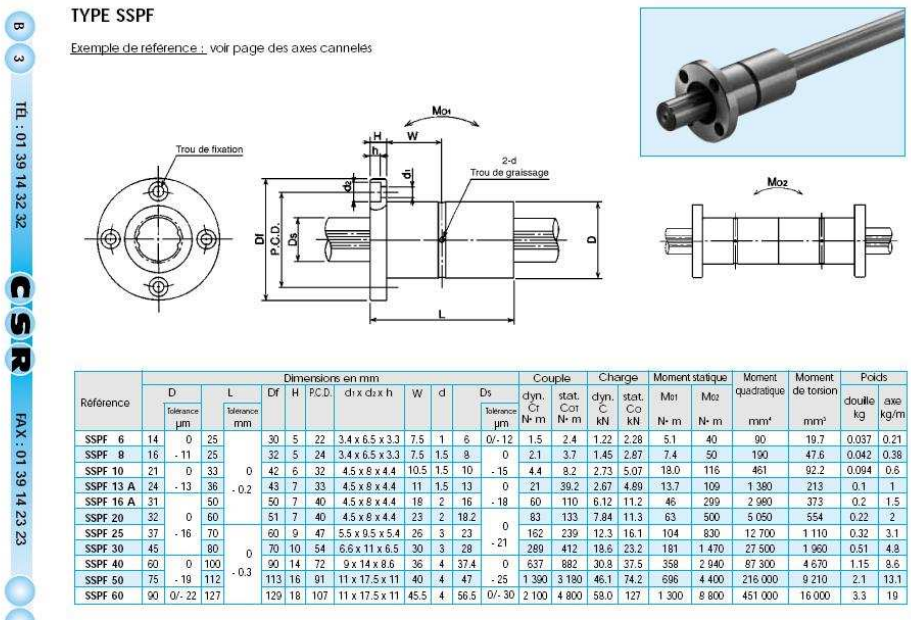

Référence	Dimensions en mm												Couple		Charge		Moment statique		Moment quadratique	Moment de torsion	Poids	
	D		L		Df	H	P.C.D.	d1 x d2 x h	W	d	Ds		dyn. Ct N·m	stat. Cot N·m	dyn. C kN	stat. Co kN	Mo1 N·m	Mo2 N·m			douille kg	axe kg/m
		Tolérance µm		Tolérance mm								Tolérance µm							mm⁴	mm²		
SSPF 6	14	0	25		30	5	22	3.4 x 6.5 x 3.3	7.5	1	6	0/- 12	1.5	2.4	1.22	2.28	5.1	40	90	19.7	0.037	0.21
SSPF 8	16	- 11	25		32	5	24	3.4 x 6.5 x 3.3	7.5	1.5	8	0	2.1	3.7	1.45	2.87	7.4	50	190	47.6	0.042	0.38
SSPF 10	21	0	33	0	42	6	32	4.5 x 8 x 4.4	10.5	1.5	10	- 15	4.4	8.2	2.73	5.07	18.0	116	461	92.2	0.094	0.6
SSPF 13 A	24	- 13	36	- 0.2	43	7	33	4.5 x 8 x 4.4	11	1.5	13	0	21	39.2	2.67	4.89	13.7	109	1 380	213	0.1	1
SSPF 16 A	31		50		50	7	40	4.5 x 8 x 4.4	18	2	16	- 18	60	110	6.12	11.2	46	299	2 980	373	0.2	1.5
SSPF 20	32	0	60		51	7	40	4.5 x 8 x 4.4	23	2	18.2	0	83	133	7.84	11.3	63	500	5 050	554	0.22	2
SSPF 25	37	- 16	70		60	9	47	5.5 x 9.5 x 5.4	26	3	23	- 21	162	239	12.3	16.1	104	830	12 700	1 110	0.32	3.1
SSPF 30	45		80	0	70	10	54	6.6 x 11 x 6.5	30	3	28		289	412	18.6	23.2	181	1 470	27 500	1 960	0.51	4.8
SSPF 40	60	0	100	- 0.3	90	14	72	9 x 14 x 8.6	36	4	37.4	0	637	882	30.8	37.5	358	2 940	87 300	4 670	1.15	8.6
SSPF 50	75	- 19	112		113	16	91	11 x 17.5 x 11	40	4	47	- 25	1 390	3 180	46.1	74.2	696	4 400	216 000	9 210	2.1	13.1
SSPF 60	90	0/- 22	127		129	18	107	11 x 17.5 x 11	45.5	4	56.5	0/- 30	2 100	4 800	58.0	127	1 300	8 800	451 000	16 000	3.3	19

Figure 7.8: Anti-rotational ball bearing

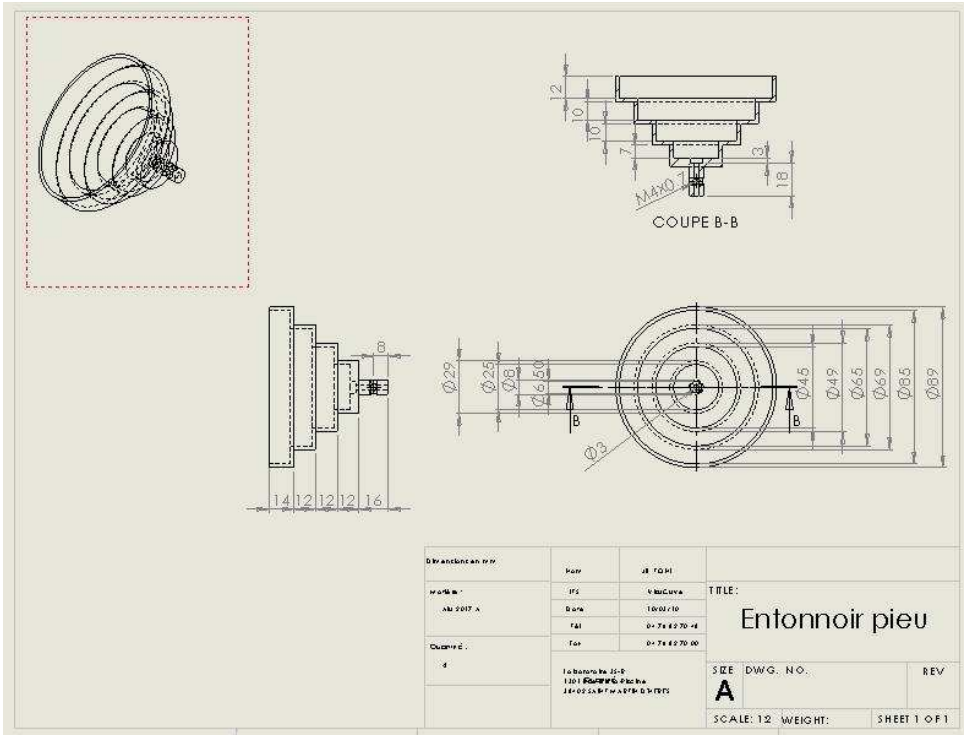

Figure 7.9: Funnel representing a transition zone

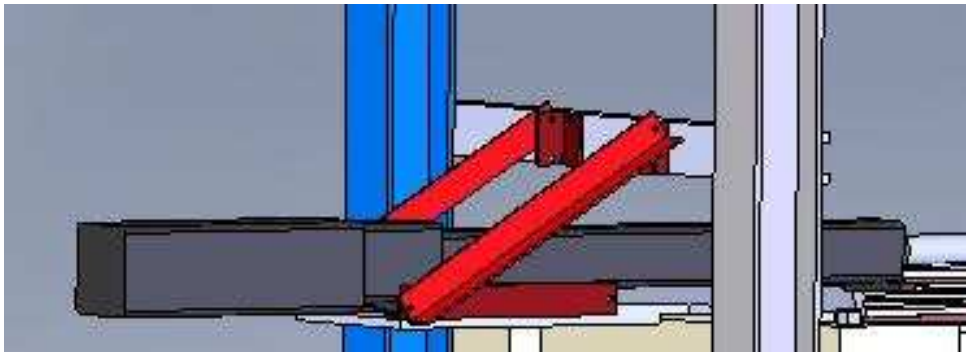

Figure 7.10: Vibration measures - angle irons (in red) reinforcing the system supporting horizontal actuator

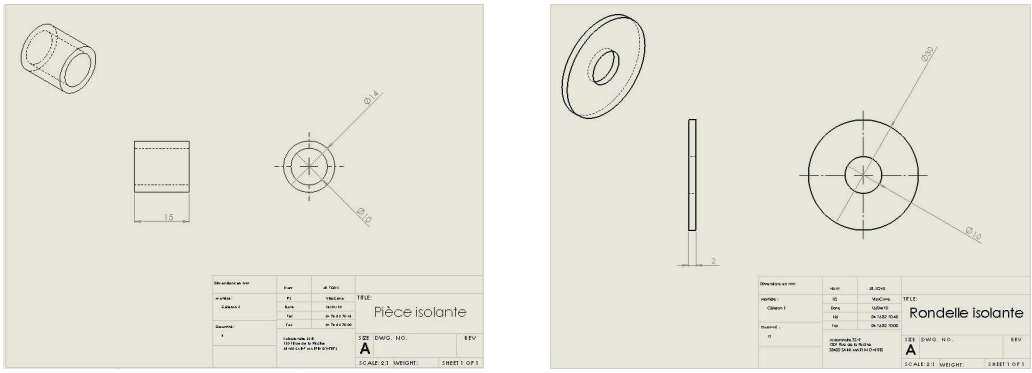

(a) (b)

Figure 7.11: Electical izolation used

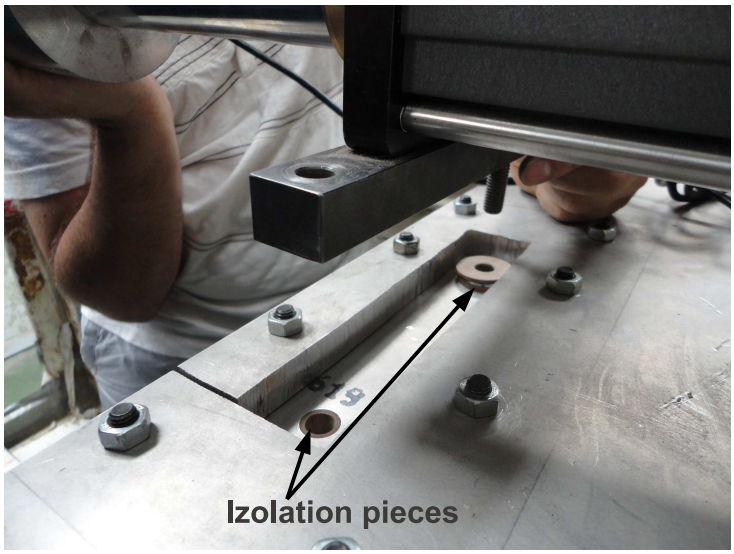

Figure 7.12: Electical izolation used

Type SFWR - Modèle applique

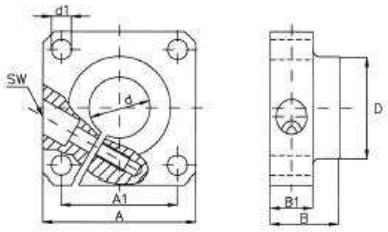

Référence *Type*	d	A	B	D	A1	d1	B1	SW	Poids - *Weight* g
SFWR 12	12	40	20	23.5	30 +0.12	5.5	12	3	60
SFWR 16	16	50	20	27.5	35 +0.12	5.5	12	3	80
SFWR 20	20	50	23	33.5	38 +0.15	6.6	14	4	100
SFWR 25	25	60	25	42.0	42 +0.15	6.6	16	5	150
SFWR 30	30	70	30	49.5	54 +0.25	9	19	6	245
SFWR 40	40	100	40	65.0	68 +0.25	11	26	8	700
SFWR 50	50	100	50	75.0	75 +0.25	11	36	8	1.200

Trous de fixation suivant DIN912-8.8 - *Mounting bolts according to DIN912-8.8.*

Figure 7.13: Mechanical support component

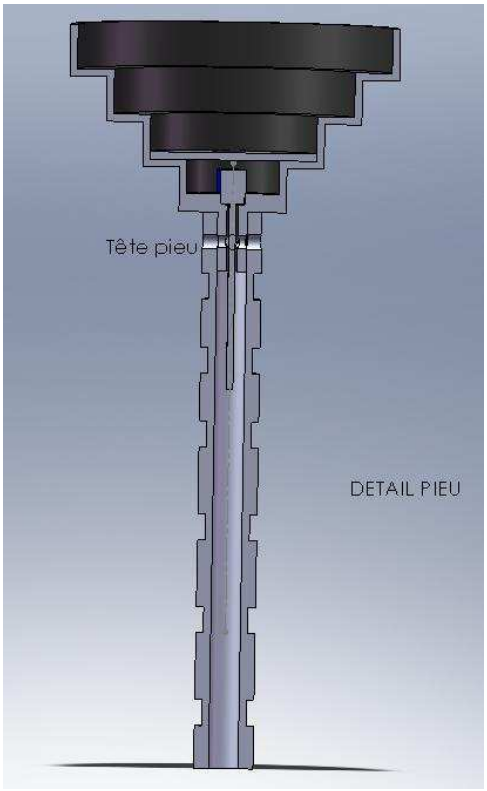

Figure 7.14: Accelerometer fixed to the pile head and protected by an aluminium plate

FICHE TECHNIQUE

N° de série	Désignation	DATE et VISA
26131 – 6303	Equipement d'un pieu	01/07/2010

Type de montage

Pont complet de flexion
type 6

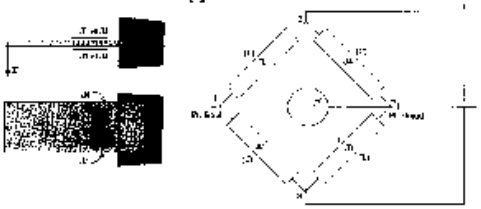

Connexions

Longueur de câble : 4 m

Tension d'excitation : 7V.

Pont complet	N° Câble	P+	P-	S+	S-
P1	1	Rouge	Noir	Vert	Blanc
P2		Bleu	Violet	Orange	Jaune
P3		Naturel	Rose	Marron	Gris
P4	2	Rouge	Noir	Vert	Blanc
P5		Bleu	Violet	Orange	Jaune
P6		Naturel	Rose	Marron	Gris
P7	3	Rouge	Noir	Vert	Blanc
P8		Bleu	Violet	Orange	Jaune
P9		Naturel	Rose	Marron	Gris
P10	4	Rouge	Noir	Vert	Blanc
P11		Bleu	Violet	Orange	Jaune
P12		Natural	Rose	Marron	Gris
P13	5	Rouge	Noir	Vert	Blanc
P14		Bleu	Violet	Orange	Jaune
P15		Naturel	Rose	Marron	Gris
P16	6	Rouge	Noir	Vert	Blanc
P17		Bleu	Violet	Orange	Jaune
P18		Naturel	Rose	Marron	Gris
P19	7	Rouge	Noir	Vert	Blanc
P20		Bleu	Violet	Orange	Jaune

DOERLER MESURES 57 bis, rue Raymond Poincaré 54500 Vandoeuvre
Tél : 03 83 56 46 64 - Fax : 03 83 56 43 43

Figure 7.15: Strain gauges set-up; part 1

FICHE TECHNIQUE

N° de série	Désignation	DATE et VISA
26131 – 6303	Equipement d'un pieu	01/07/2010

Type de jauge	Coefficient de jauge	Résistance d'une jauge	Câble	Désignation Pont complet de flexion X	Déséquilibre initiale en mV/V
TK-MC-S085N-350/DPM3	2.20	350Ω	1	P1	-0.121
TK-MC-S085N-350/DPM3	2.20	350Ω		P2	-0.343
TK-MC-S085N-350/DPM3	2.20	350Ω		P3	-0.423
TK-MC-S085N-350/DPM3	2.20	350Ω	2	P4	-0.167
TK-MC-S085N-350/DPM3	2.20	350Ω		P5	-0.074
TK-MC-S085N-350/DPM3	2.20	350Ω		P6	-0.007
TK-MC-S085N-350/DPM3	2.20	350Ω	3	P7	0.367
TK-MC-S085N-350/DPM3	2.20	350Ω		P8	0.166
TK-MC-S085N-350/DPM3	2.20	350Ω		P9	-0.338
TK-MC-S085N-350/DPM3	2.20	350Ω	4	P10	-0.379
TK-MC-S085N-350/DPM3	2.20	350Ω		P11	0.271
TK-MC-S085N-350/DPM3	2.20	350Ω		P12	0.226
TK-MC-S085N-350/DPM3	2.20	350Ω	5	P13	-0.663
TK-MC-S085N-350/DPM3	2.20	350Ω		P14	-0.087
TK-MC-S085N-350/DPM3	2.20	350Ω		P15	0.273
TK-MC-S085N-350/DPM3	2.20	350Ω	6	P16	-0.111
TK-MC-S085N-350/DPM3	2.20	350Ω		P17	-0.111
TK-MC-S085N-350/DPM3	2.20	350Ω		P18	0.003
TK-MC-S085N-350/DPM3	2.20	350Ω	7	P19	0.082
TK-MC-S085N-350/DPM3	2.20	350Ω		P20	-0.183

DOERLER MESURES 57 bis, rue Raymond Poincaré 54500 Vandoeuvre
Tél : 03 83 56 46 64 - Fax : 03 83 56 43 43

Figure 7.16: Strain gauges set-up; part 2

FICHE TECHNIQUE

N° de série	Désignation	DATE et VISA
26131 – 6303	Equipement d'un pieu	01/07/2010

Type de Jauge

HOERLER MESURES 57 bis, rue Raymond Poincaré 54500 Vandoeuvre
Tél : 03 83 56 46 64 - Fax : 03 83 56 43 43

Figure 7.17: Strain gauges set-up; part 3

Annex B

7.1 Vertical Load

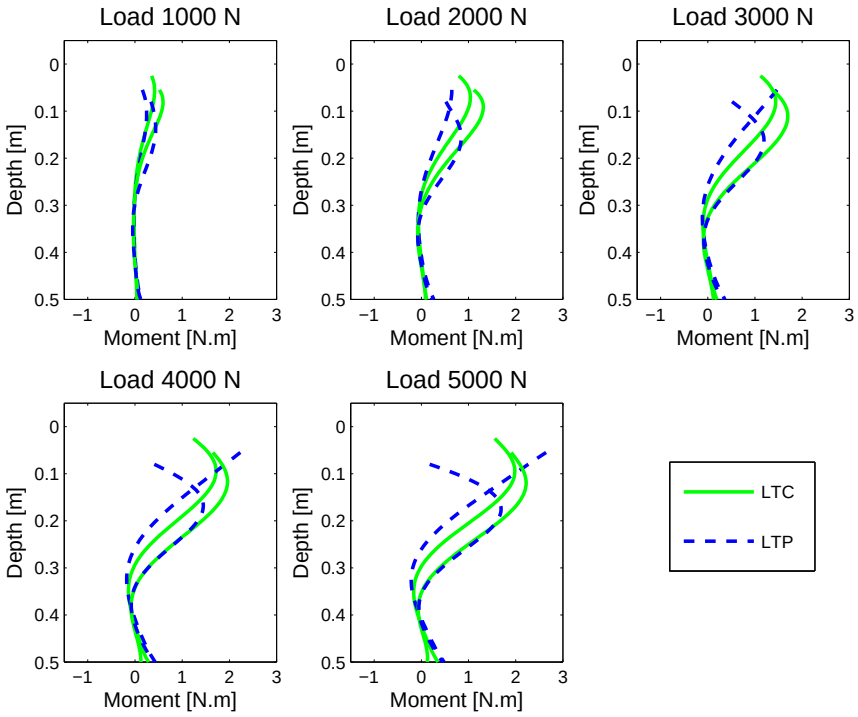

Figure 7.18: **5cm gravel column/mattress** - Moment along the pile under 5 Vertical loading stages

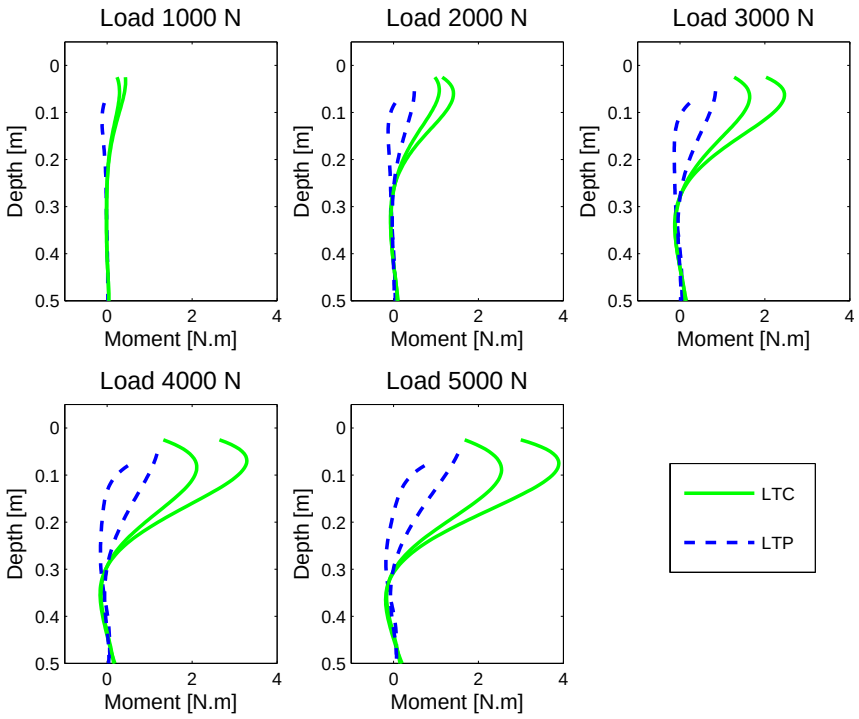

Figure 7.19: **8cm gravel column/mattress** - Moment along the pile under 5 Vertical loading stages

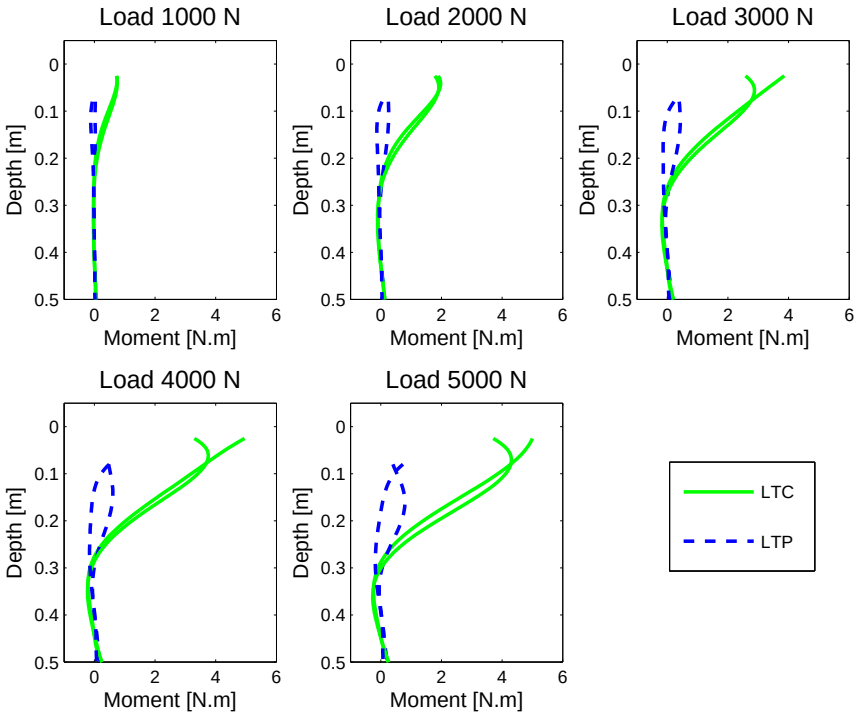

Figure 7.20: **10cm gravel column/mattress** - Moment along the pile under 5 Vertical loading stages

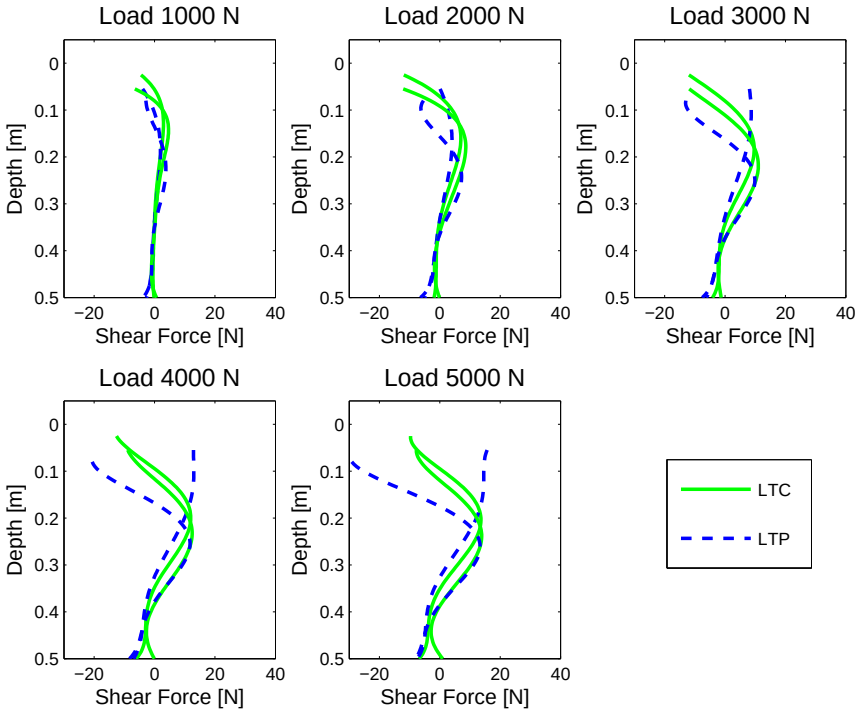

Figure 7.21: **5cm gravel column/mattress** - Shear Force along the pile under 5 Vertical loading stages

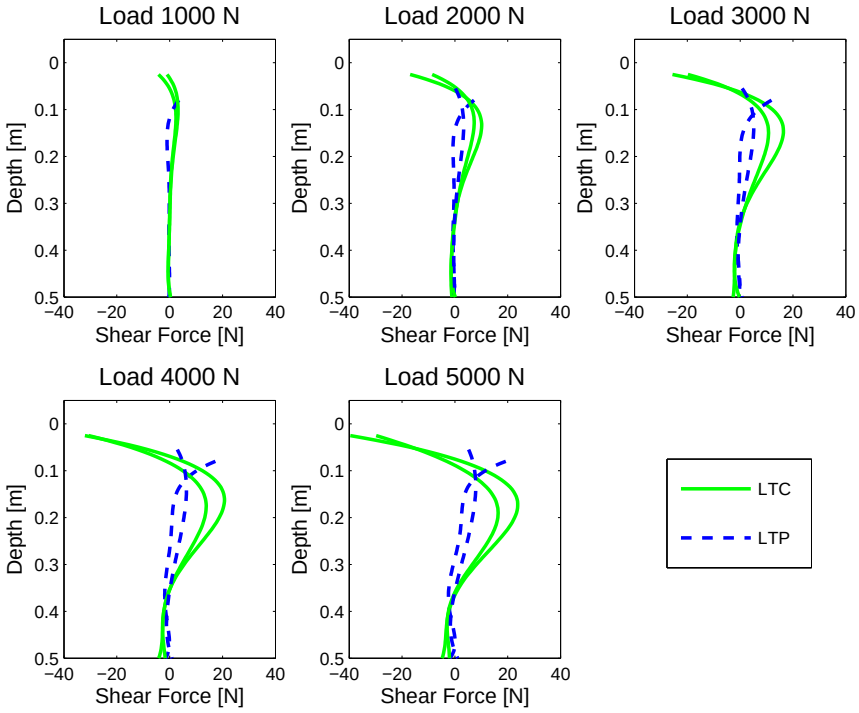

Figure 7.22: **8cm gravel column/mattress** - Shear Force along the pile under 5 Vertical loading stages

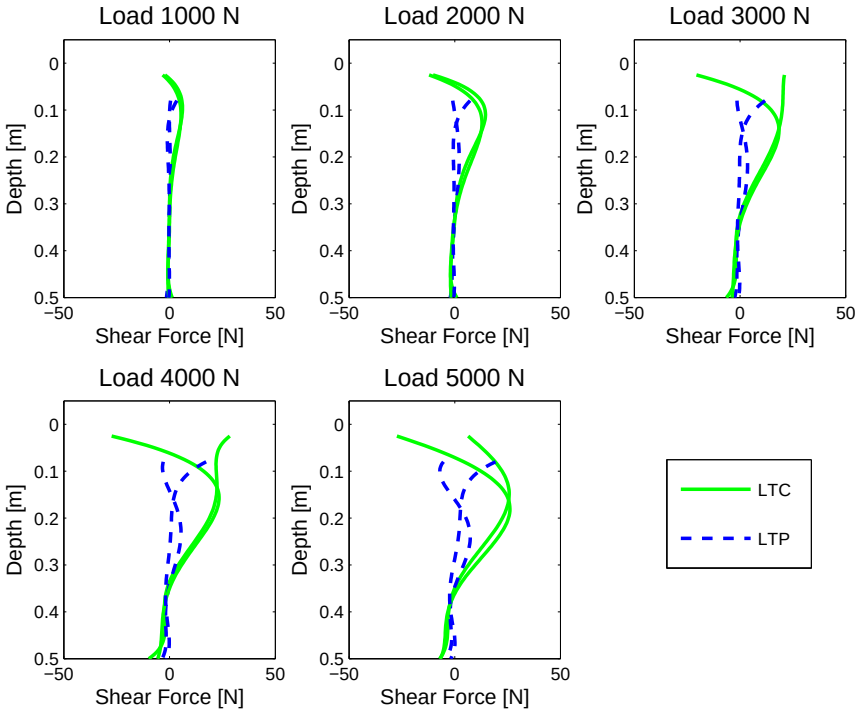

Figure 7.23: **10cm gravel column/mattress** - Shear Force along the pile under 5 Vertical loading stages

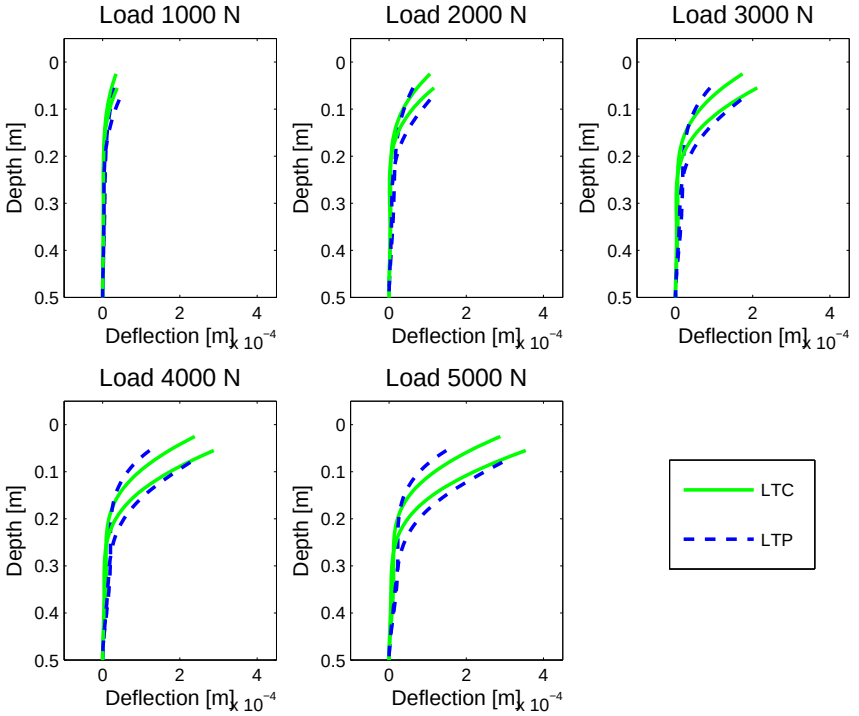

Figure 7.24: **5cm gravel column/mattress** - Deflection along the pile under 5 Vertical loading stages

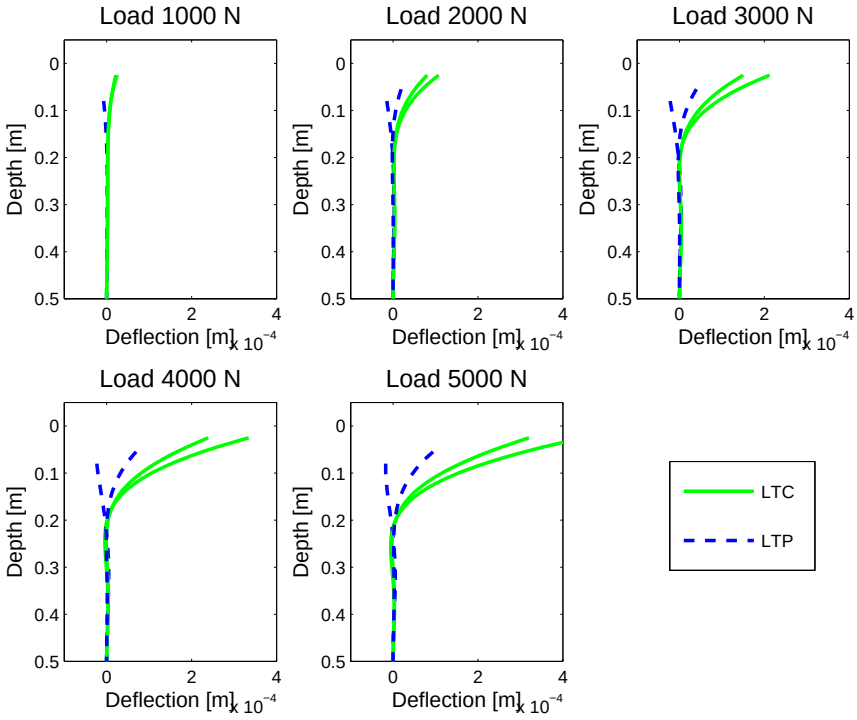

Figure 7.25: **8cm gravel column/mattress** - Deflection along the pile under 5 Vertical loading stages

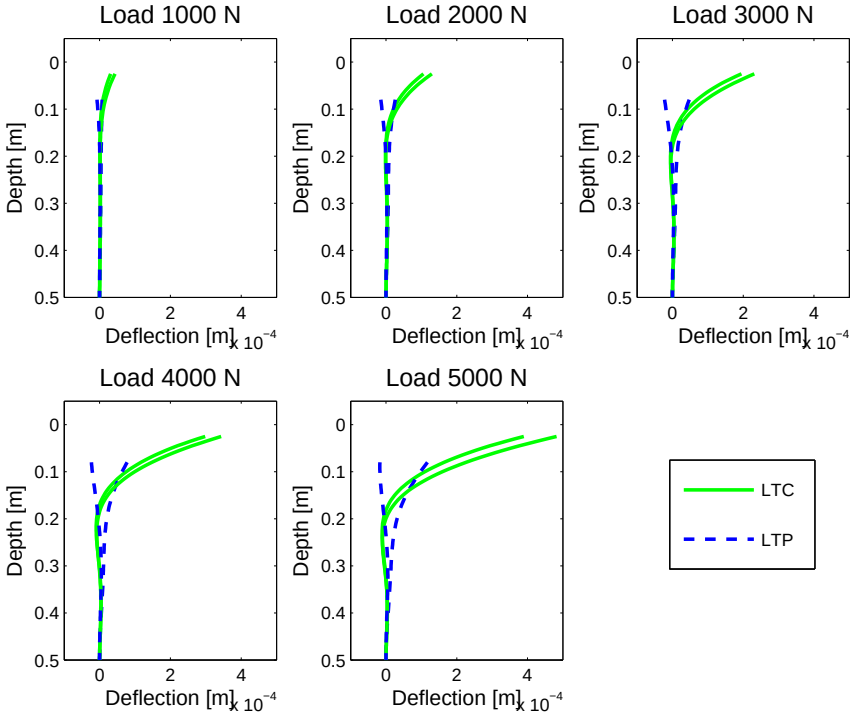

Figure 7.26: **10cm gravel column/mattress** - Deflection along the pile under 5 Vertical loading stages

7.2 Combined Loading - LTC

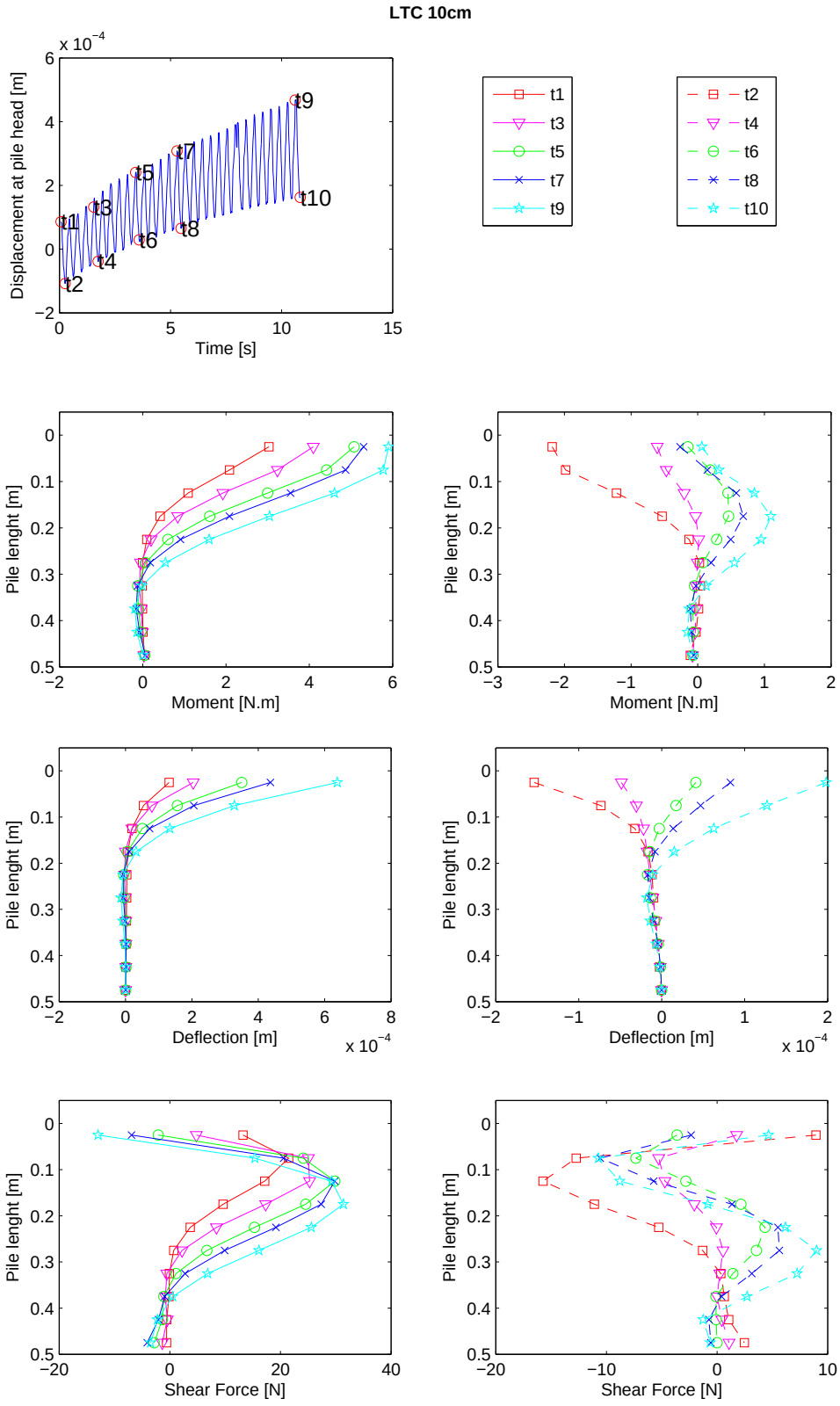

Figure 7.27: Bending moment, deflection and shear force along a pile associated to a LTC of 10 cm (exp LTC13)

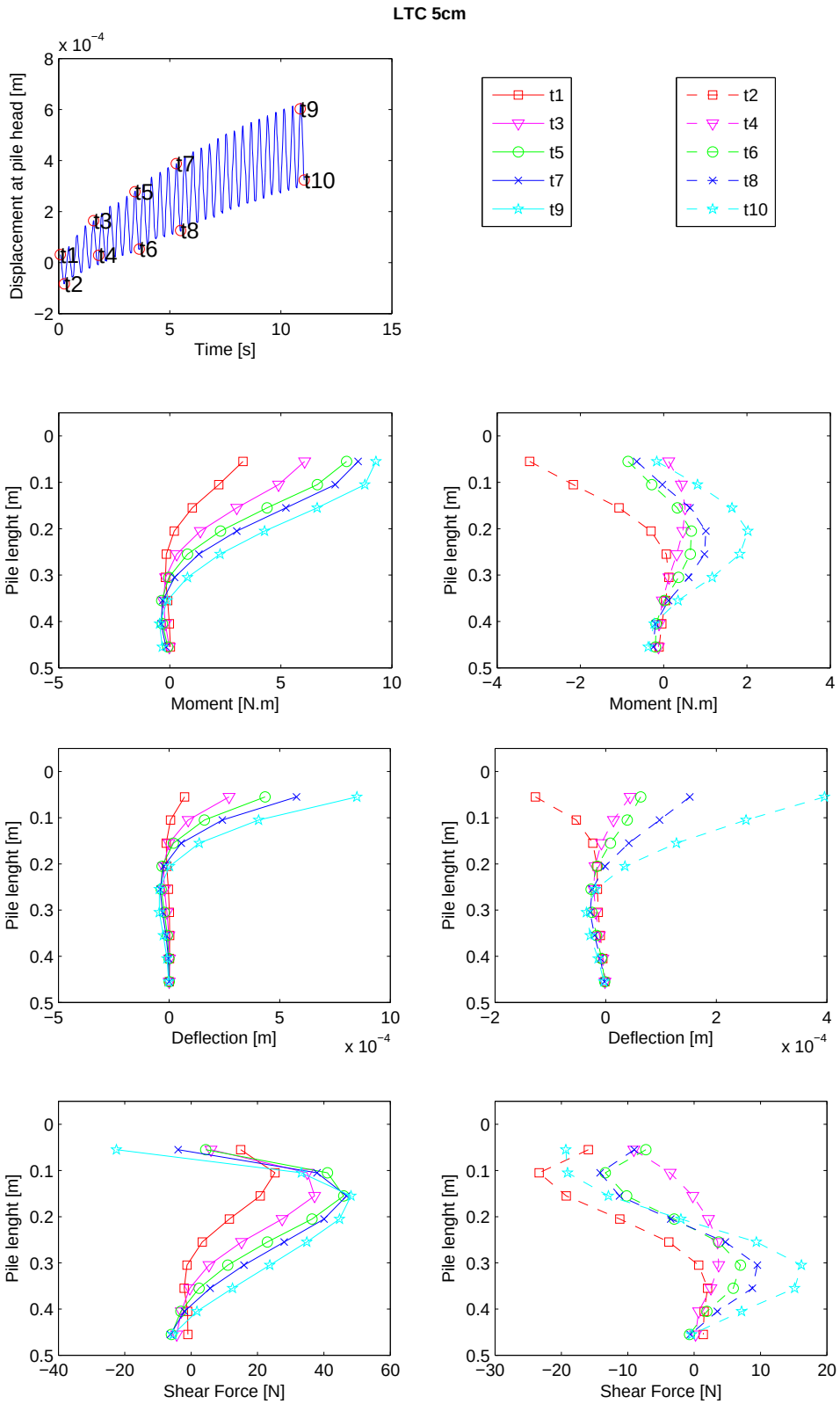

Figure 7.28: Bending moment, deflection and shear force along a pile associated to a LTC of 5 cm (exp LTC15)

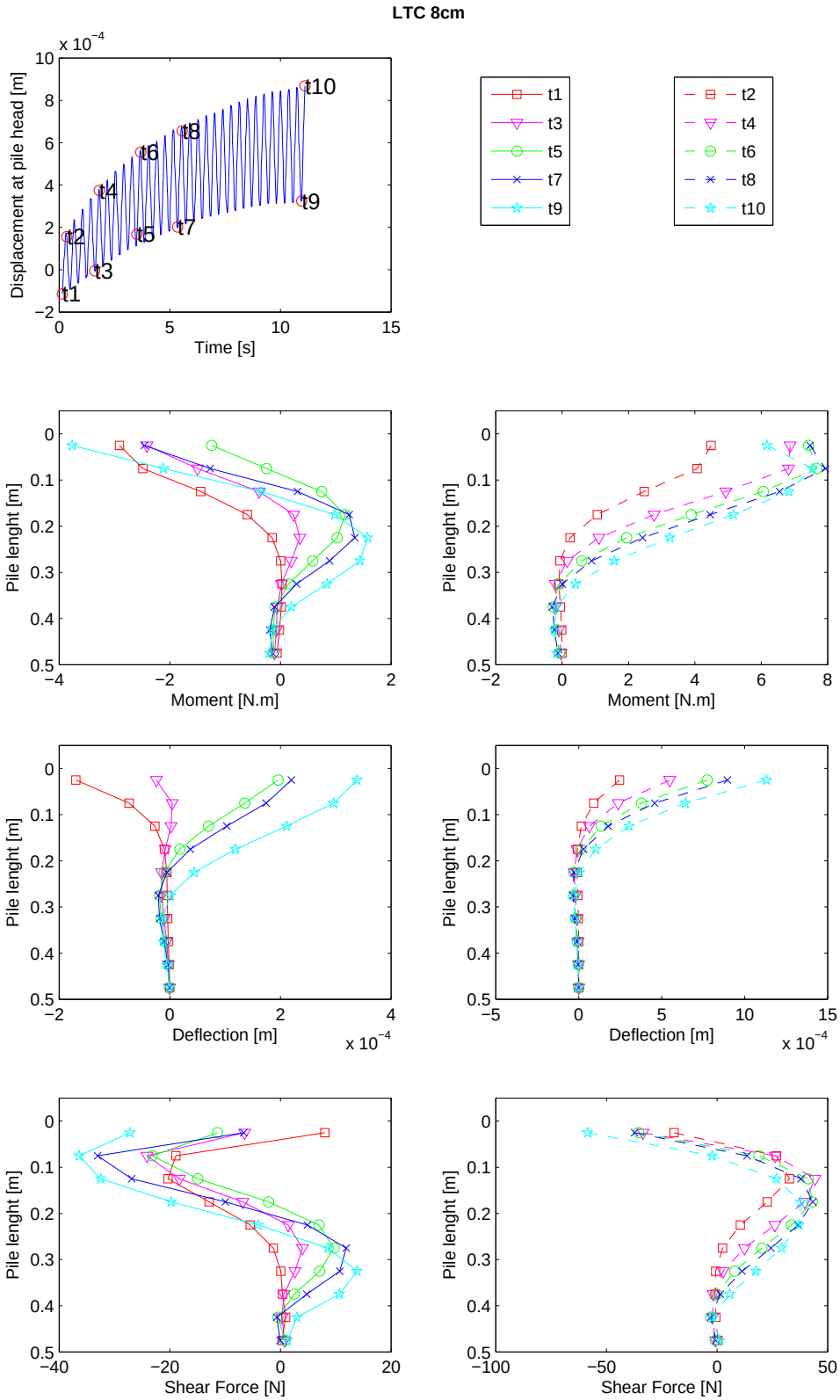

Figure 7.29: Bending moment, deflection and shear force along a pile associated to a LTC of 8 cm (exp LTC12) - cyclic loading started in an opposite direction (in direction 'B') than usual

7.3 Combined Loading - LTP

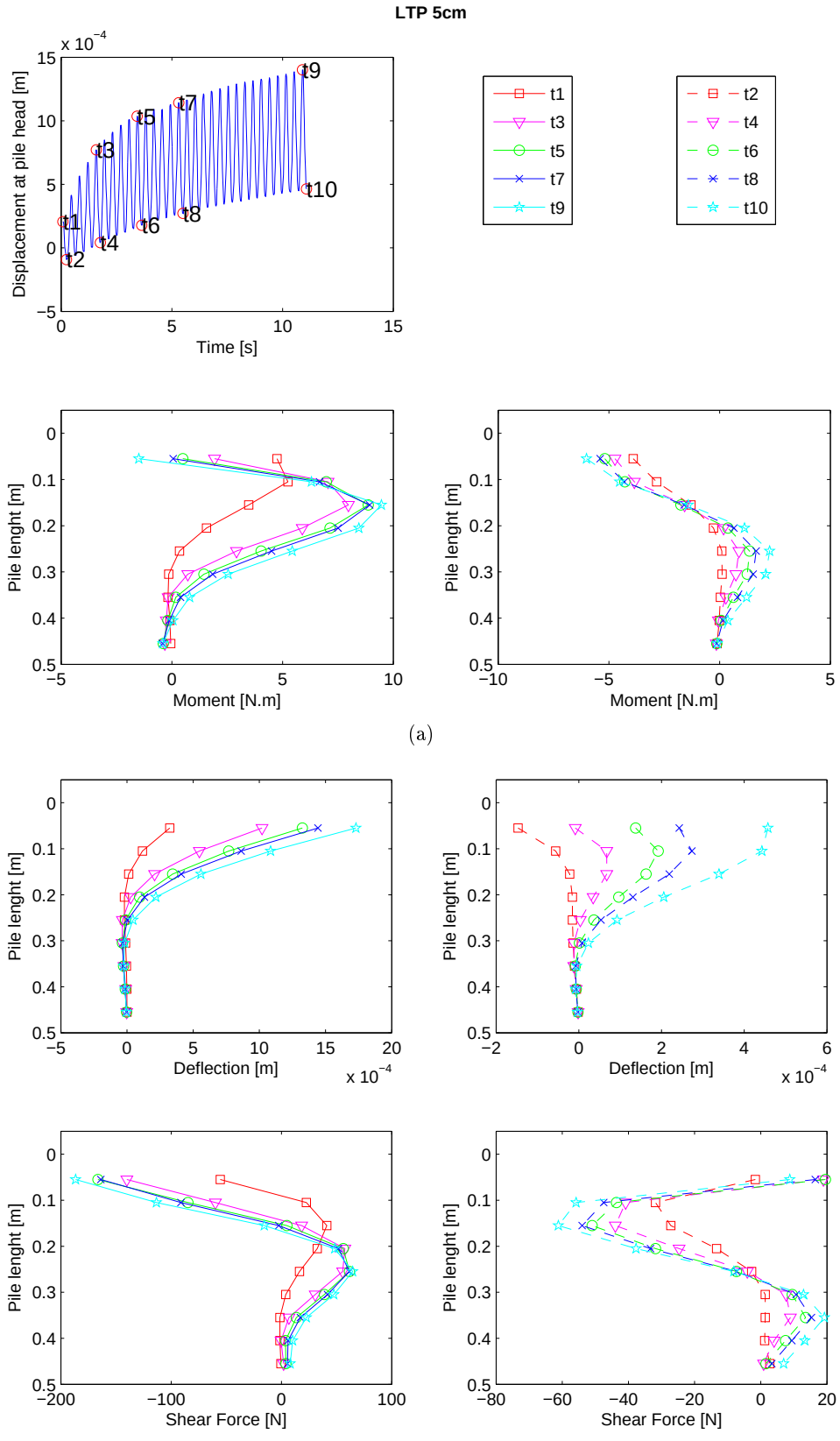

(a)

(b)

Figure 7.30: Bending moment, deflection and shear force along a pile associated to a LTP of 5 cm (exp LTP1)

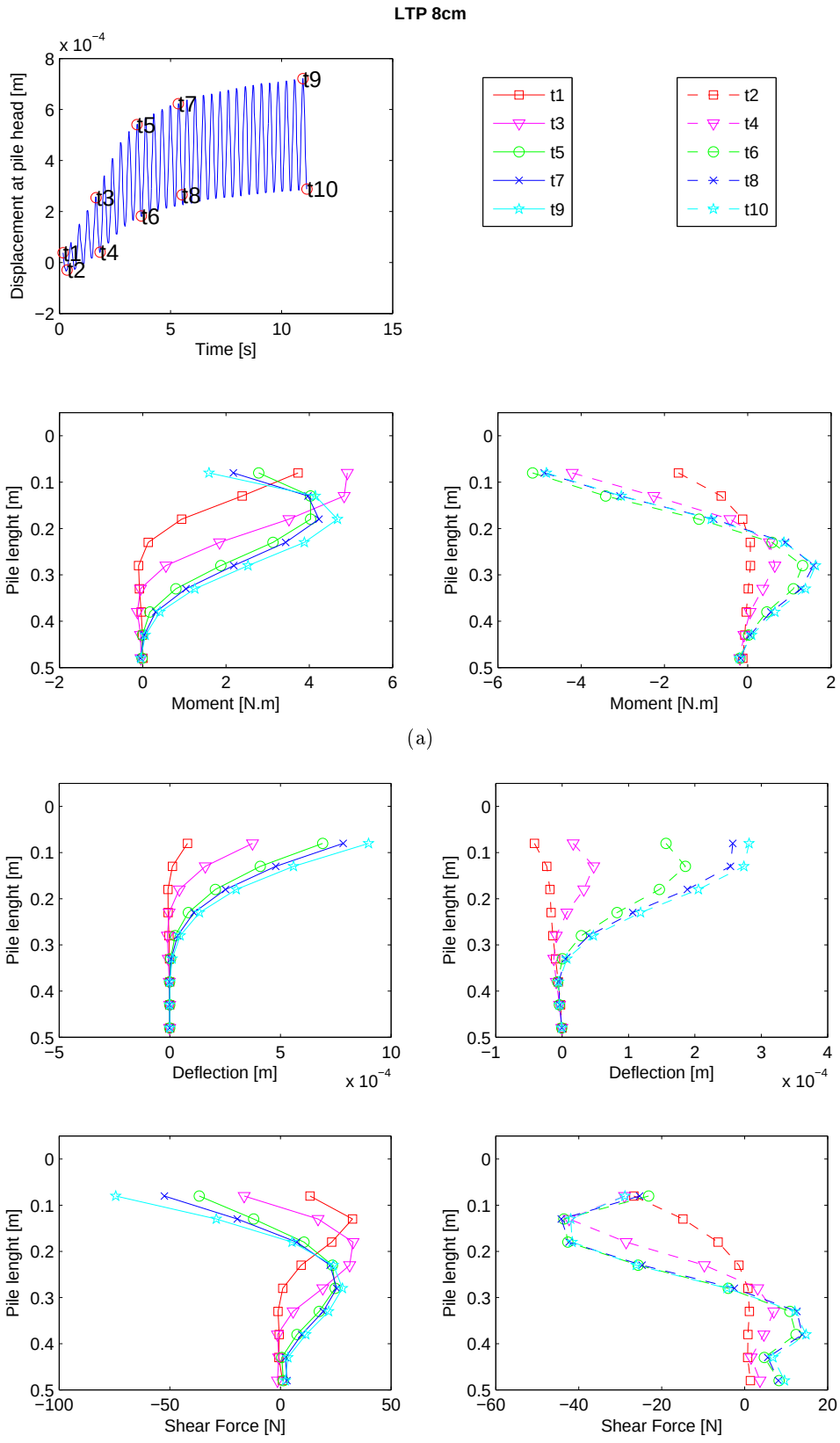

(a)

(b)

Figure 7.31: Bending moment, deflection and shear force along a pile associated to a LTP of 8 cm (exp LTP2)

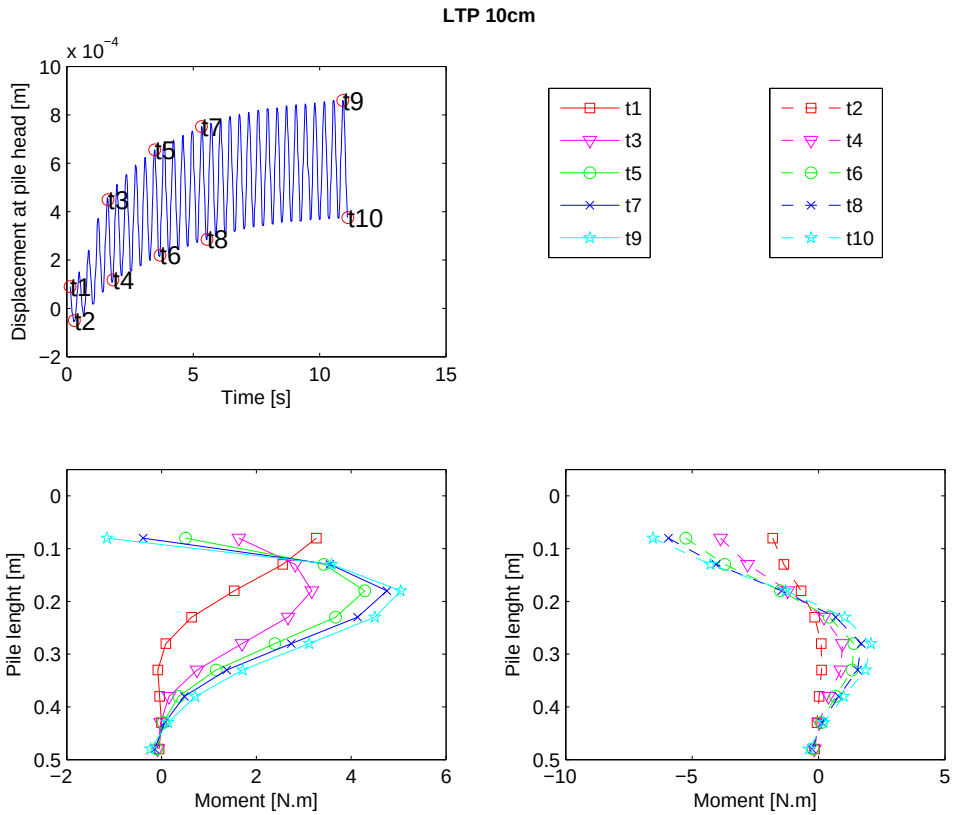

(a)

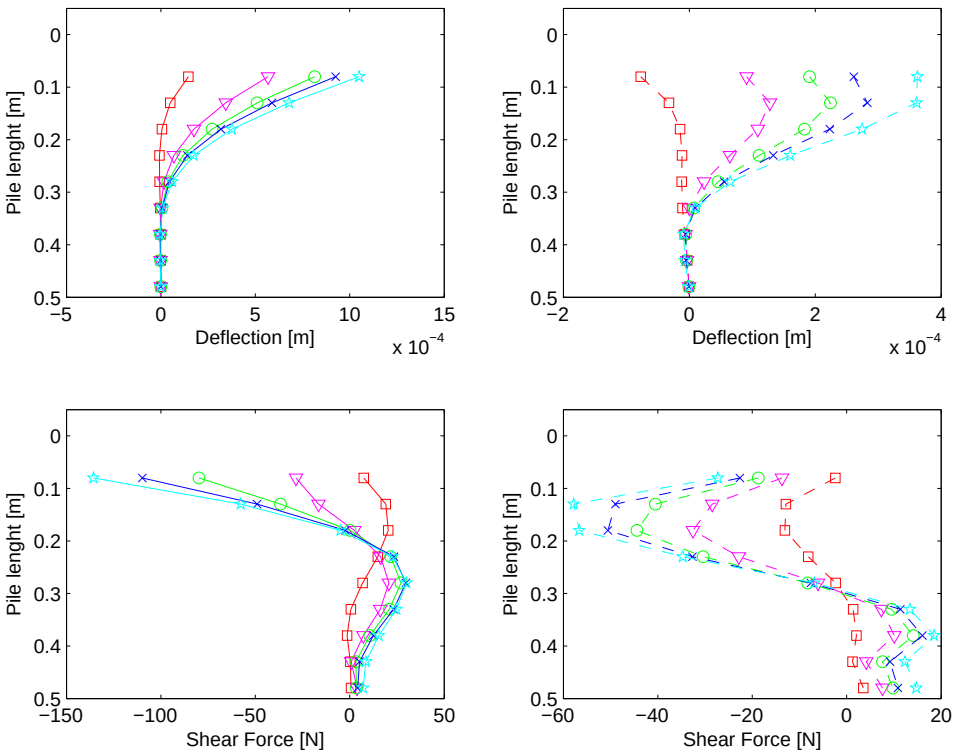

(b)

Figure 7.32: Bending moment, deflection and shear force along a pile associated to a LTP of 10 cm (exp LTP3)

7.4 Energy Dissipation

7.4.1 Experiments on consolidated soil mass

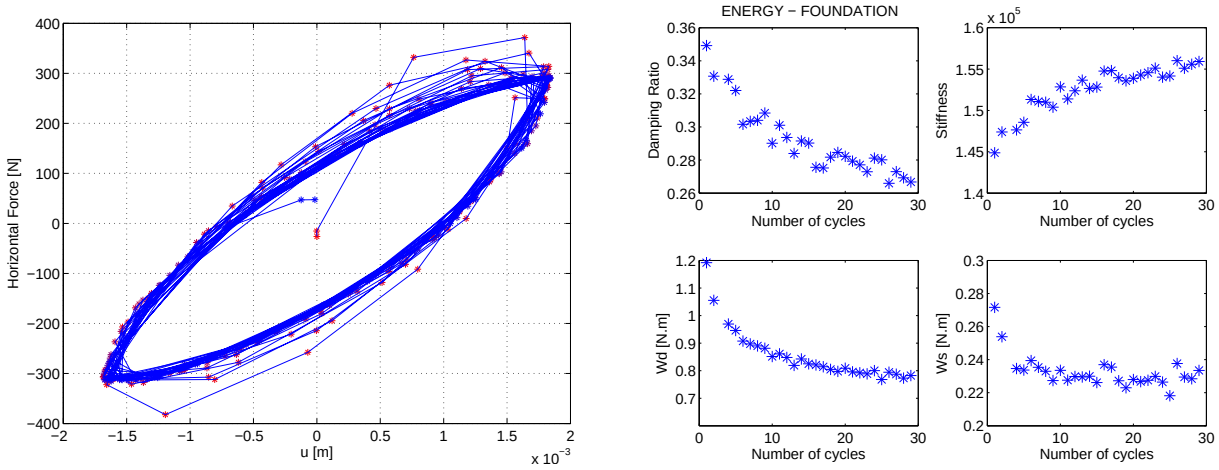

(a) (b)

Figure 7.33: LTC 5cm H-u Loop (exp LTC9)

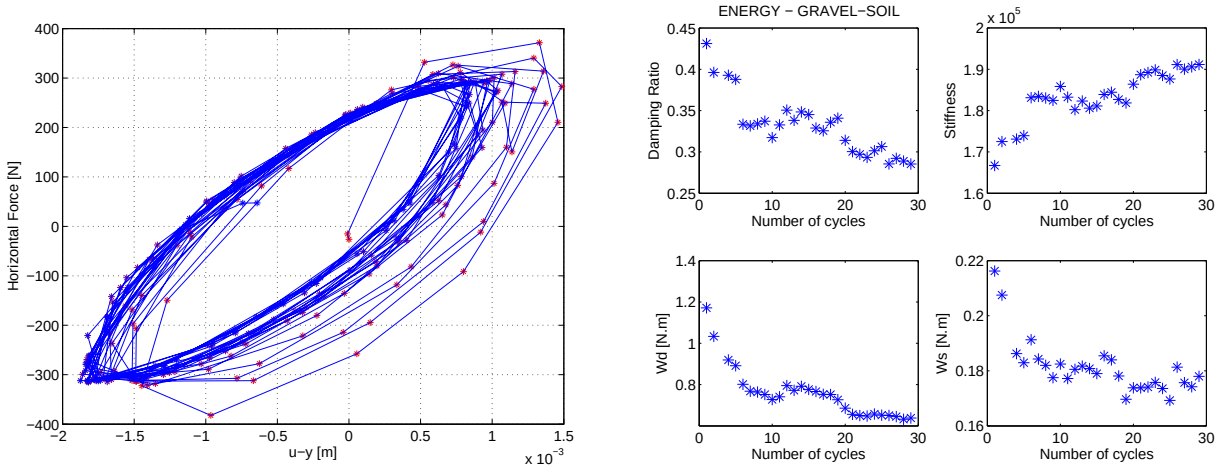

(a) (b)

Figure 7.34: LTC 5cm H-(u-y) Loop (exp LTC9)

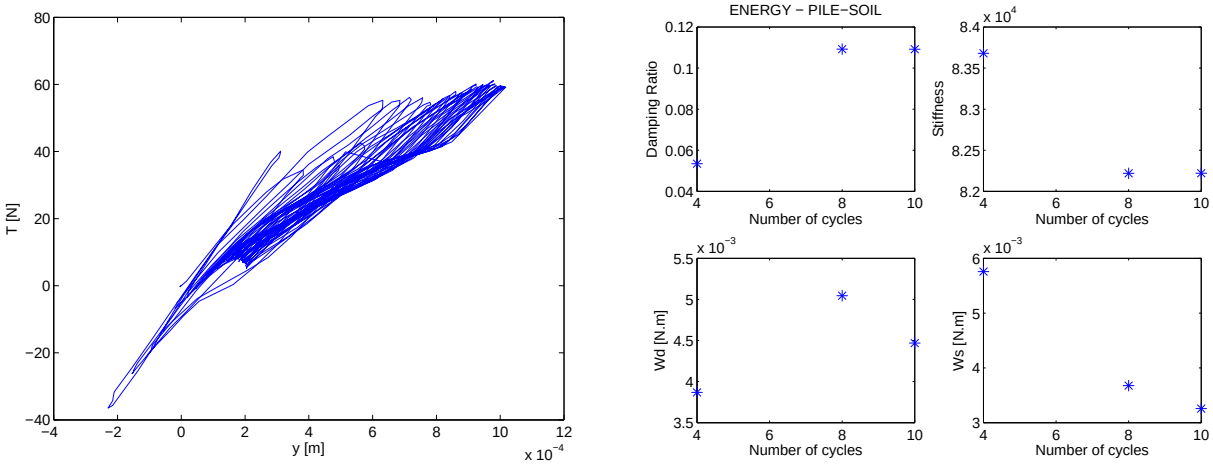

(a) (b)

Figure 7.35: LTC 5cm T-y Loop (exp LTC9)

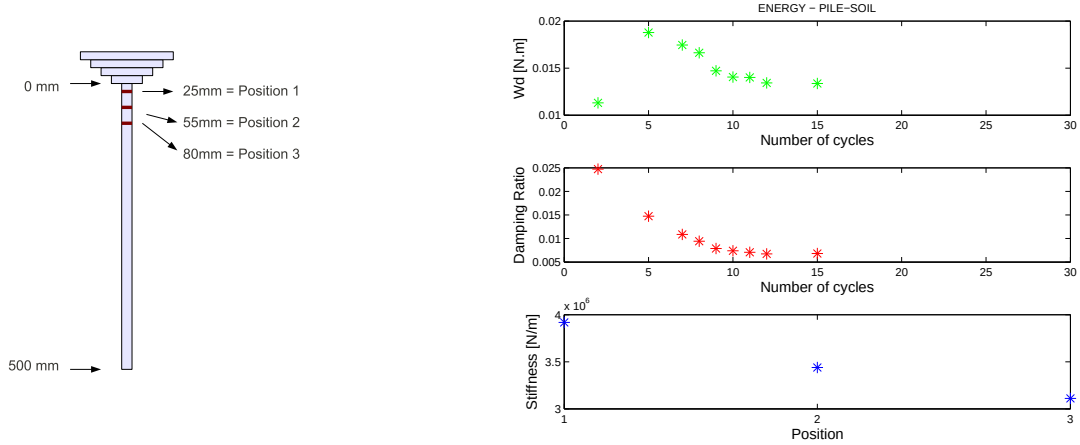

(a) (b)

Figure 7.36: LTC 5cm P-y Loop (exp LTC9)

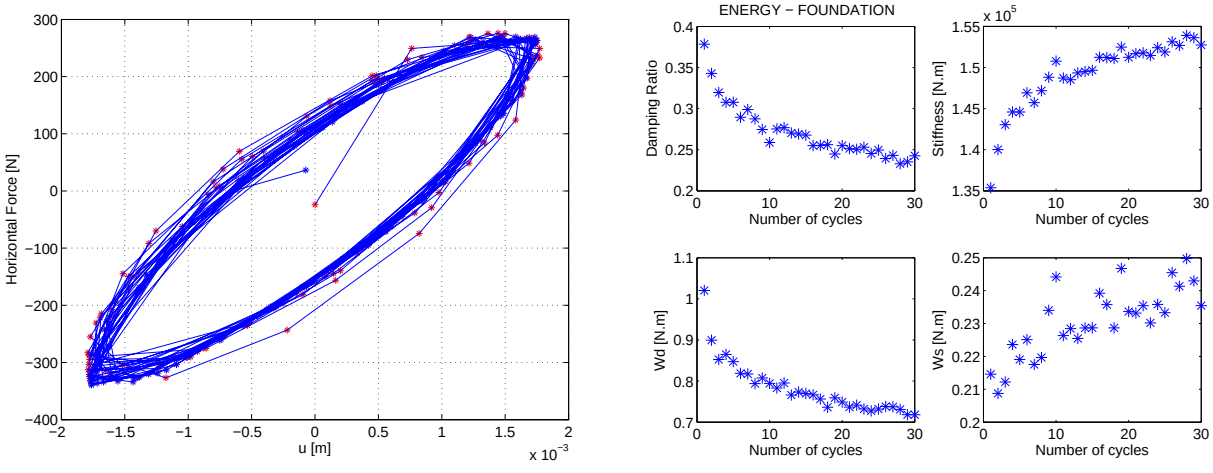

(a) (b)

Figure 7.37: LTC 8cm H-u Loop (exp LTC11)

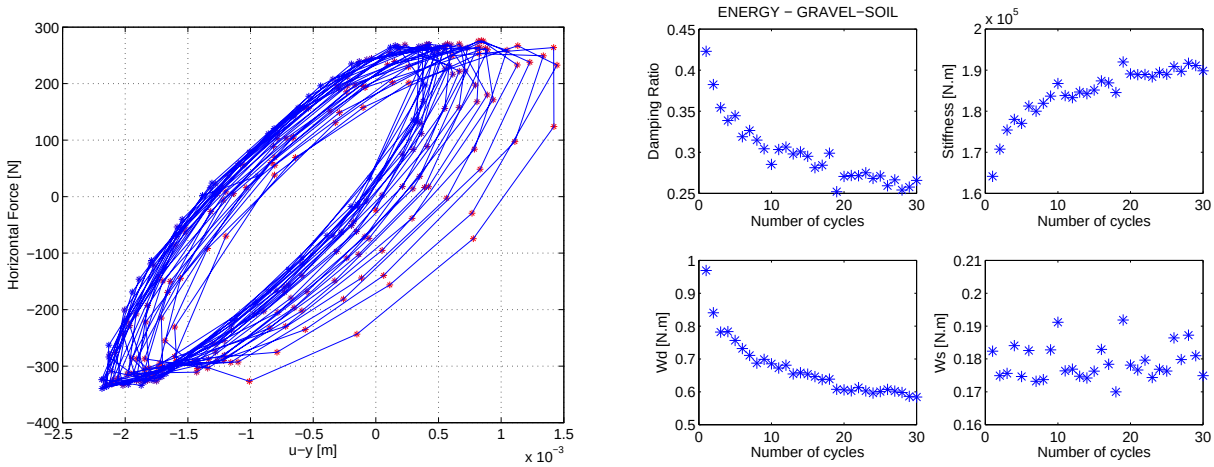

(a) (b)

Figure 7.38: LTC 8cm H-(u-y) Loop (exp LTC11)

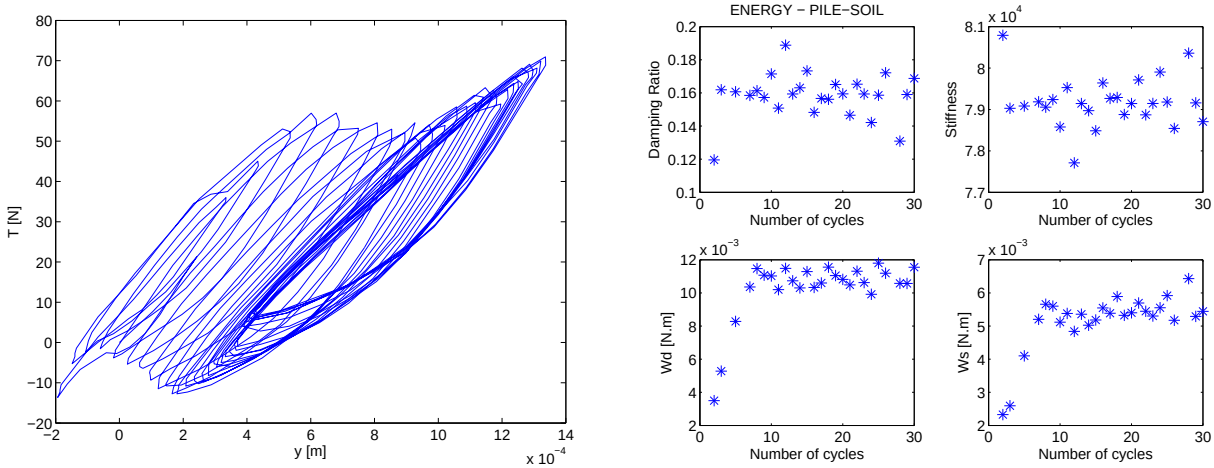

(a) (b)

Figure 7.39: LTC 8cm T-y Loop (exp LTC11)

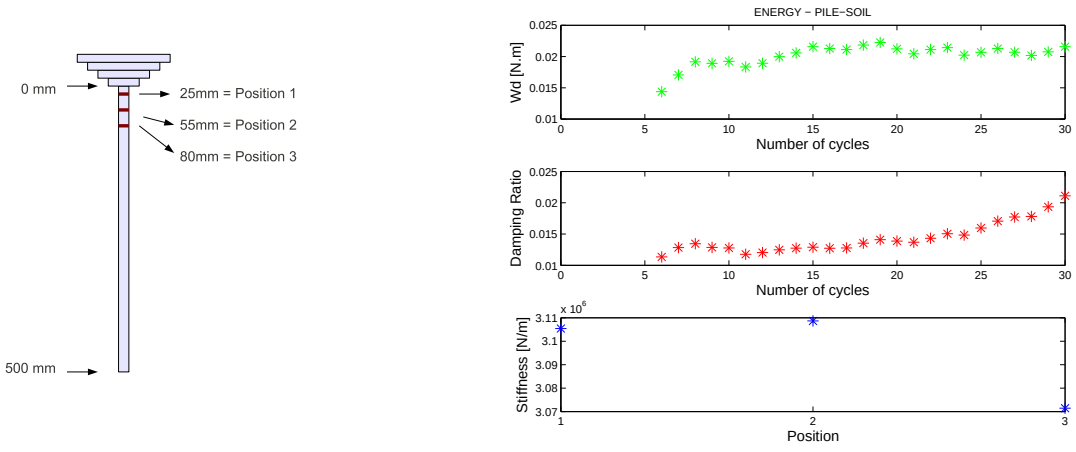

(a) (b)

Figure 7.40: LTC 8cm P-y Loop (exp LTC11)

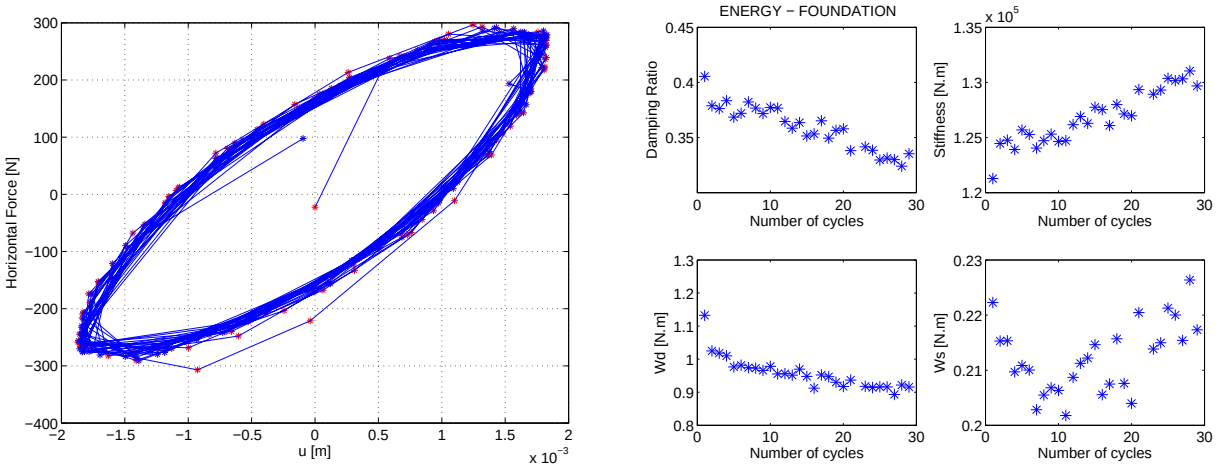

(a) (b)

Figure 7.41: LTC 10cm H-u Loop (exp LTC13)

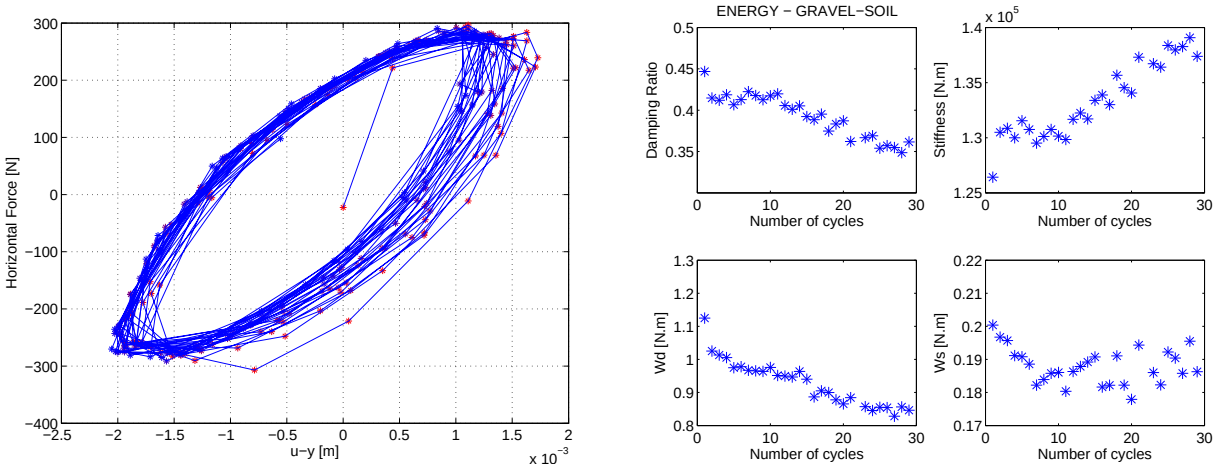

(a) (b)

Figure 7.42: LTC 10cm H-(u-y) Loop (exp LTC13)

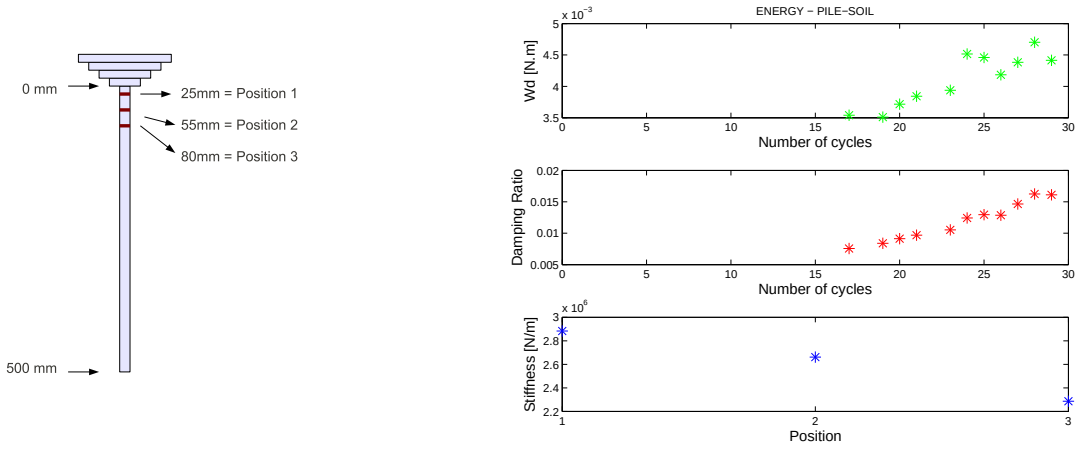

(a) (b)

Figure 7.43: LTC 10cm P-y Loop (exp LTC13)

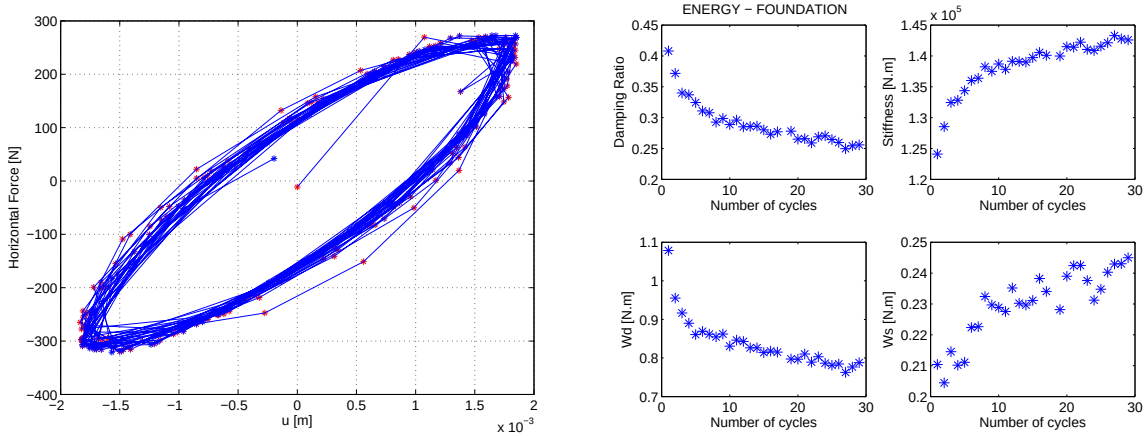

(a) (b)

Figure 7.44: LTC 10cm H-u Loop (exp LTC10)

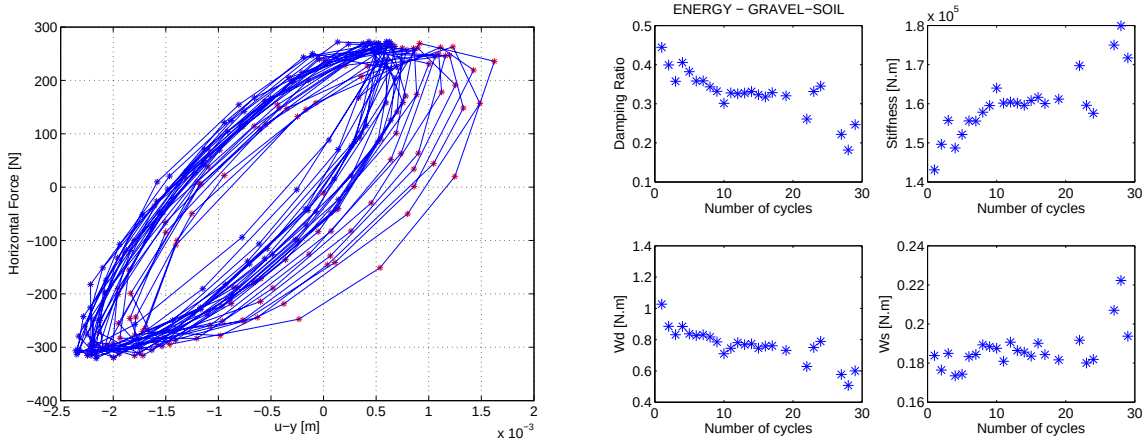

(a) (b)

Figure 7.45: LTC 10cm H-(u-y) Loop (exp LTC10)

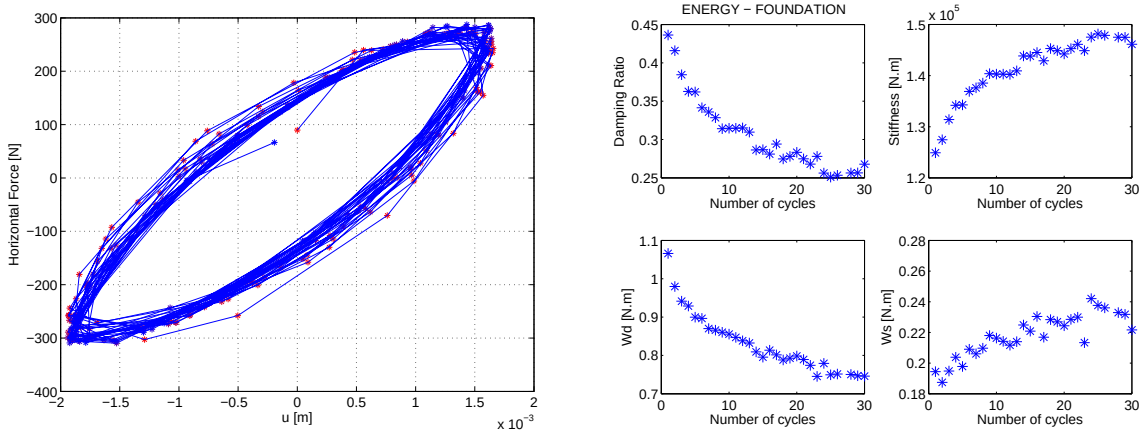

(a) (b)

Figure 7.46: LTC 5cm H-u Loop (exp LTC15)

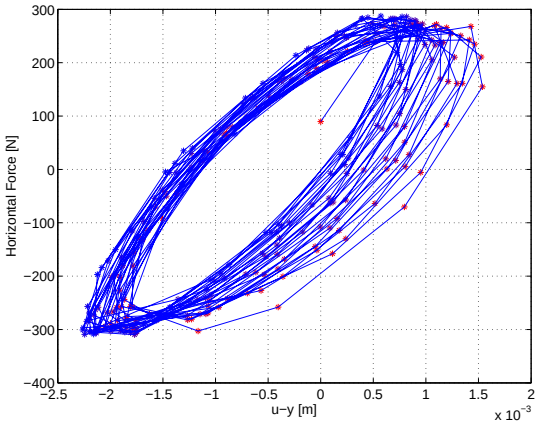

(a)

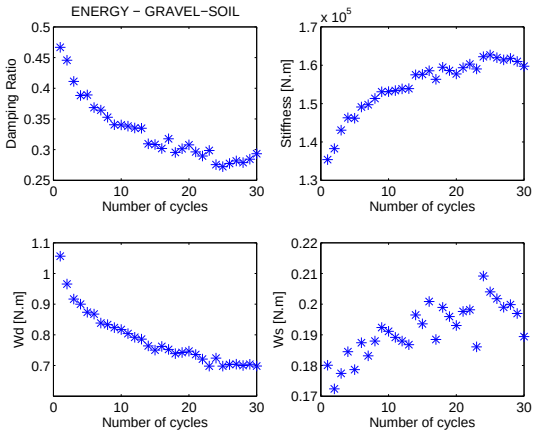

(b)

Figure 7.47: LTC 5cm H-(u-y) Loop (exp LTC15)

7.4.2 Experiments on unconsolidated soil mass

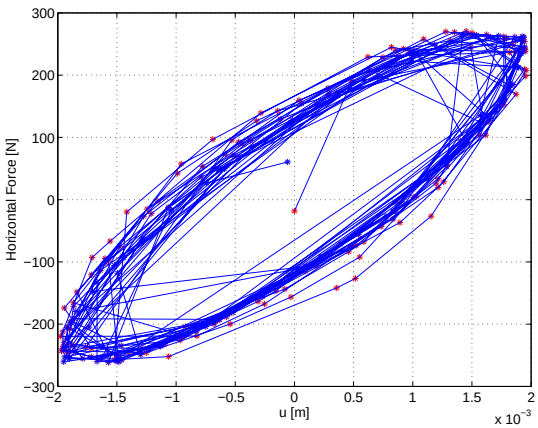

(a)

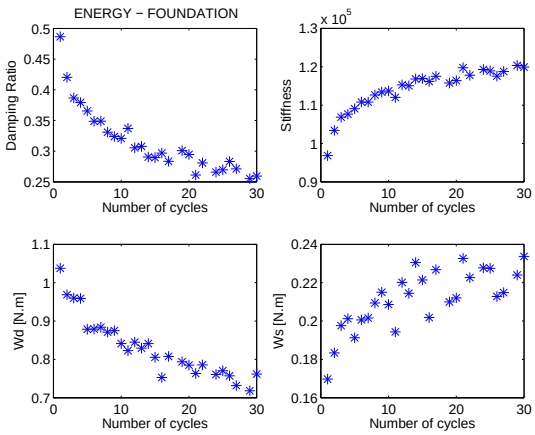

(b)

Figure 7.48: LTC 5cm H-u Loop (exp LTC4)

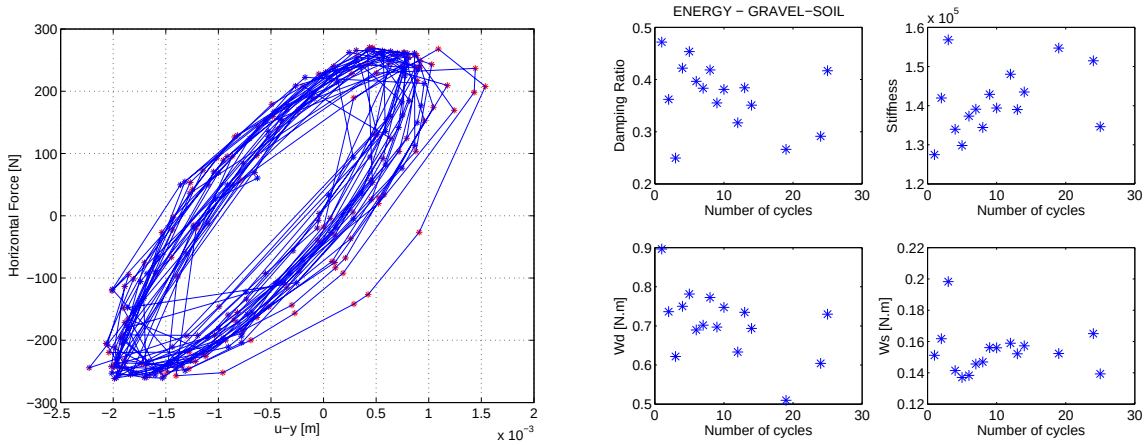

(a) (b)

Figure 7.49: LTC 5cm H-(u-y) Loop (exp LTC4)

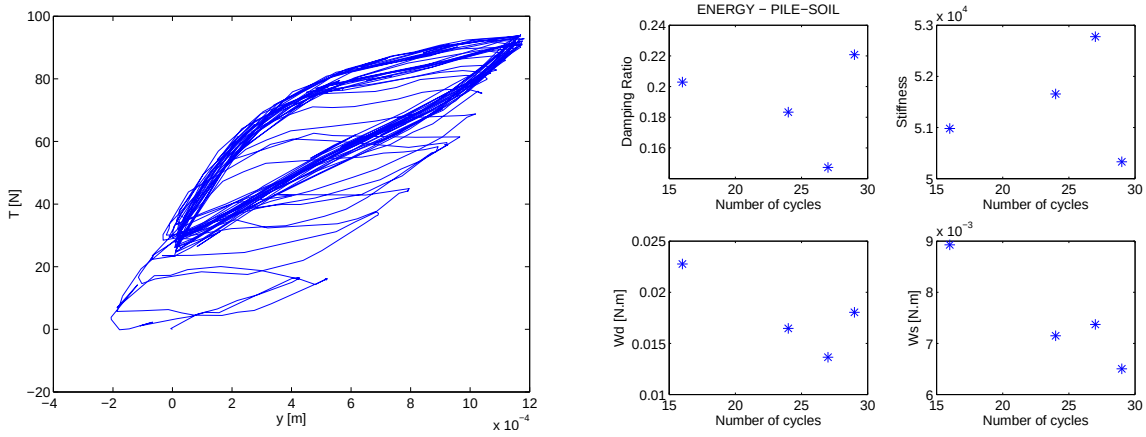

(a) (b)

Figure 7.50: LTC 5cm T-y Loop (exp LTC4)

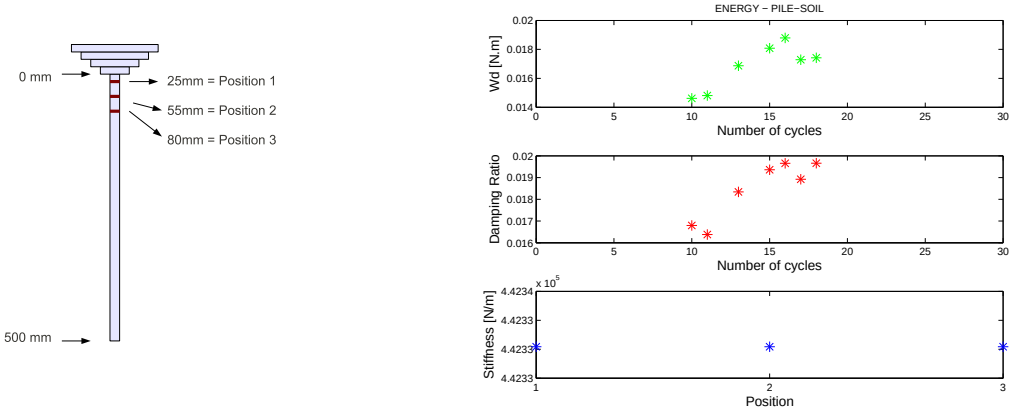

(a) (b)

Figure 7.51: LTC 5cm P-y Loop (exp LTC4)

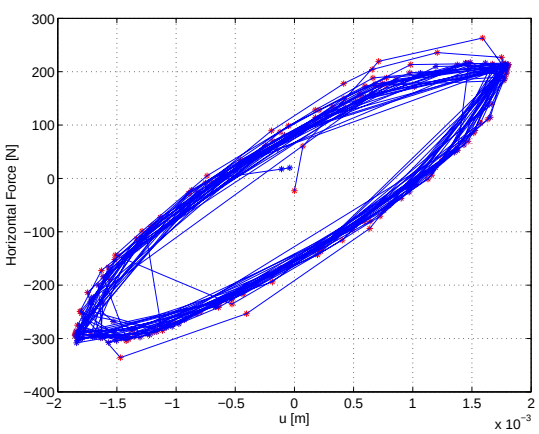

(a)

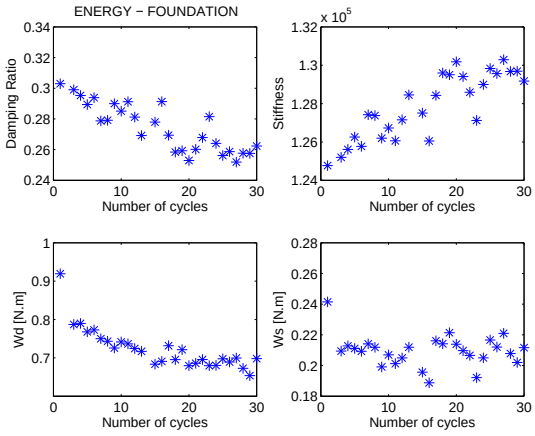

(b)

Figure 7.52: LTC 8cm H-u Loop (exp LTC6)

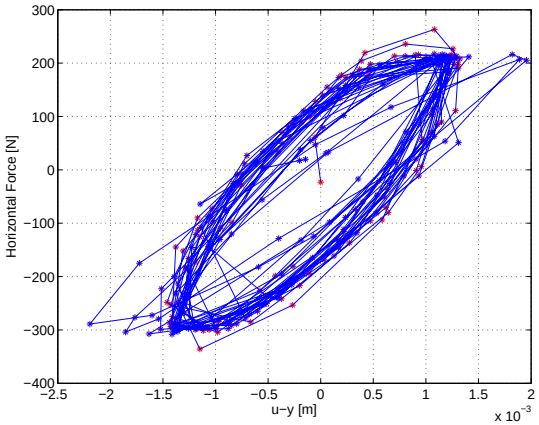

(a)

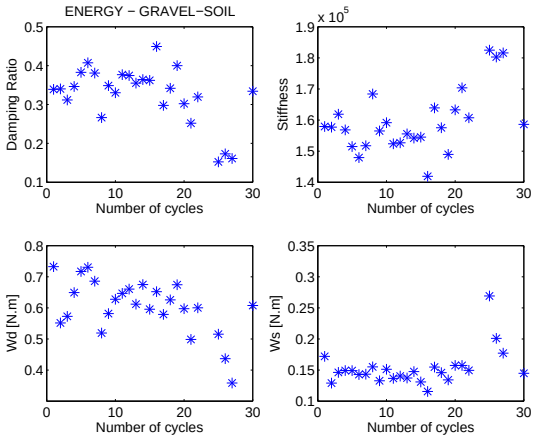

(b)

Figure 7.53: LTC 8cm H-(u-y) Loop (exp LTC6)

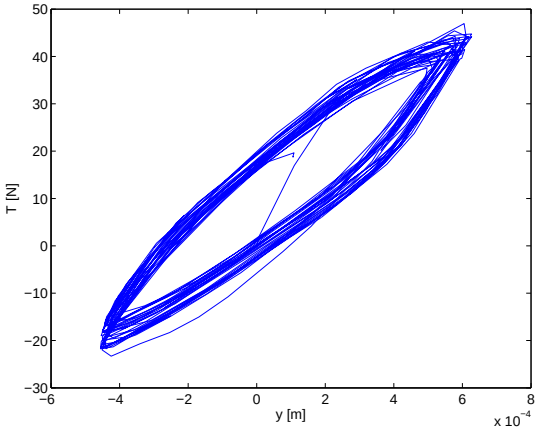

(a)

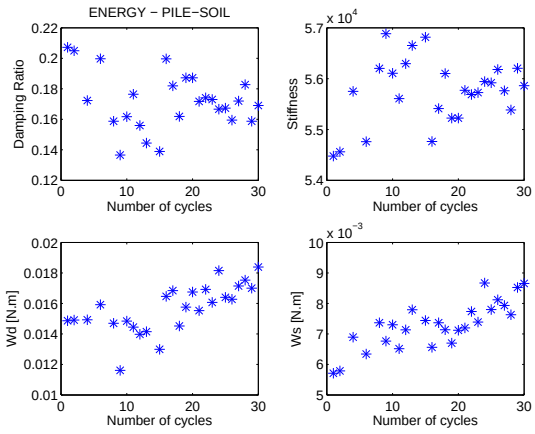

(b)

Figure 7.54: LTC 8cm T-y Loop (exp LTC6)

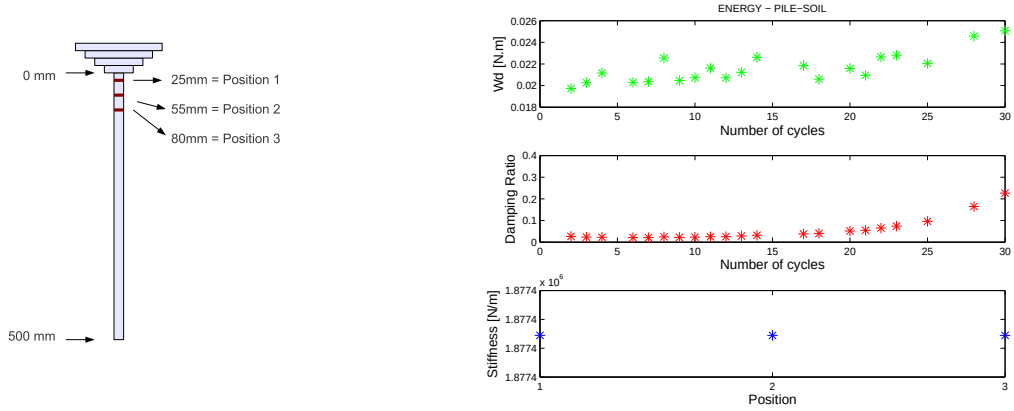

(a) (b)

Figure 7.55: LTC 8cm P-y Loop (exp LTC6)

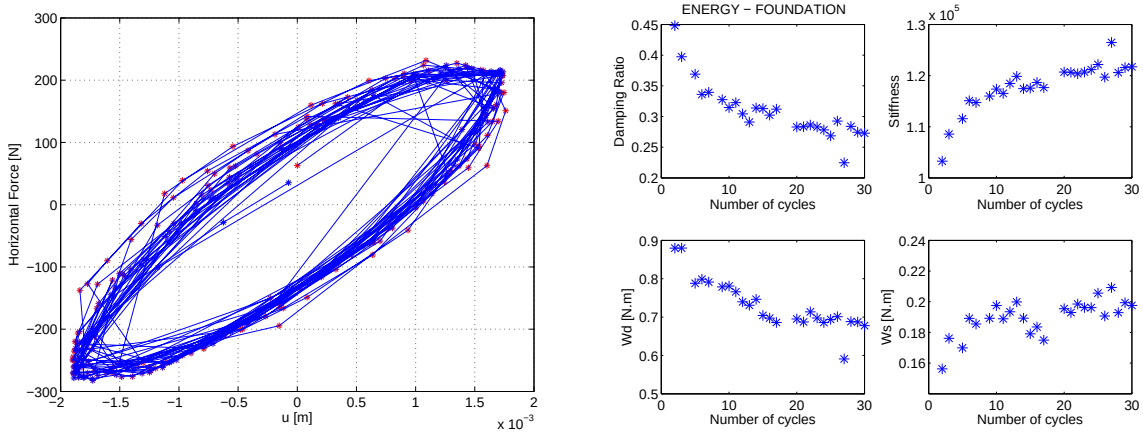

(a) (b)

Figure 7.56: LTC 8cm H-u Loop (exp LTC7)

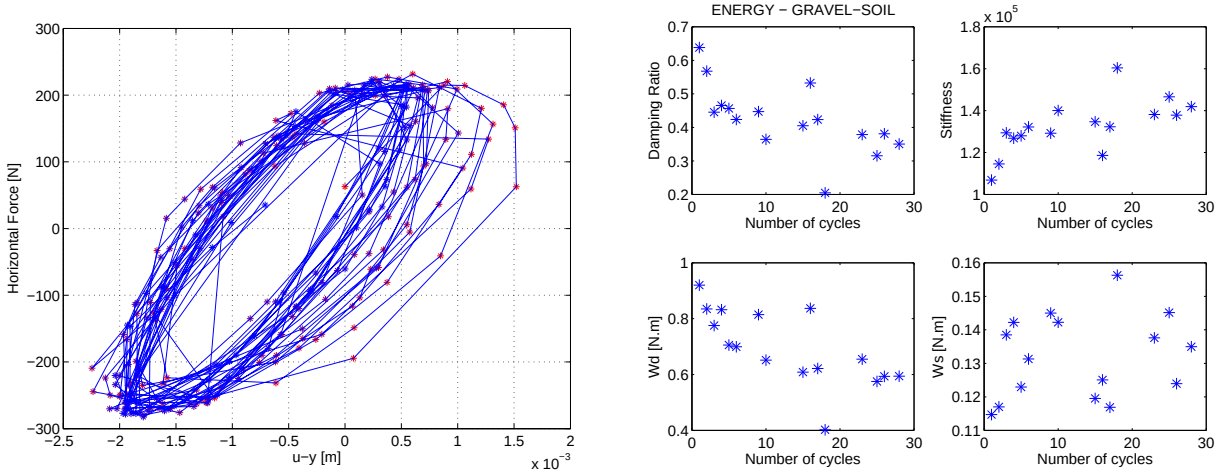

(a) (b)

Figure 7.57: LTC 8cm H-(u-y) Loop (exp LTC7)

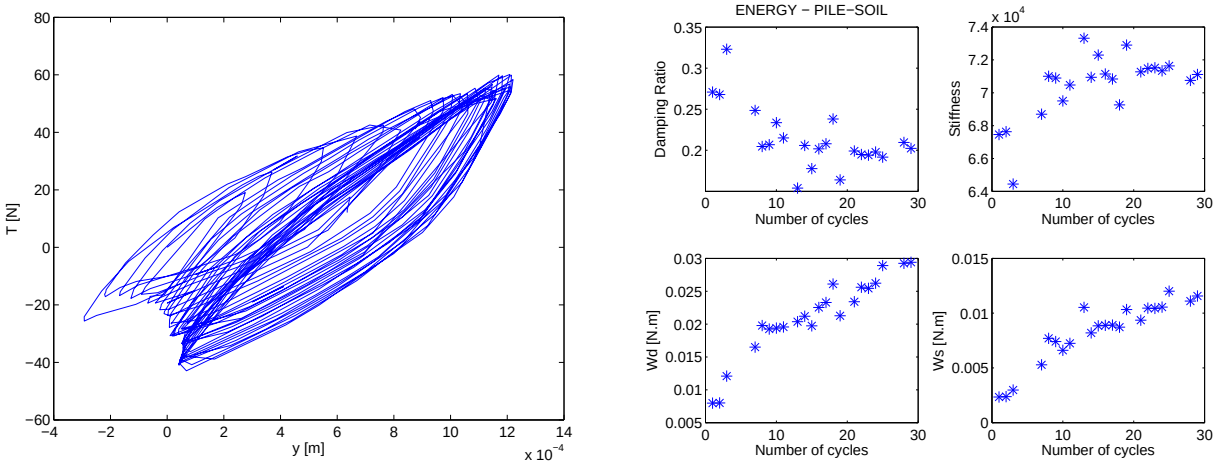

(a) (b)

Figure 7.58: LTC 8cm T-y Loop (exp LTC7)

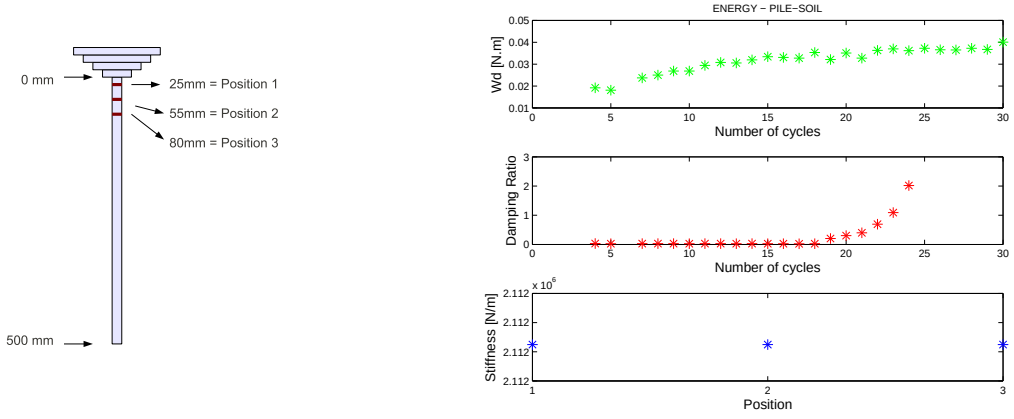

(a) (b)

Figure 7.59: LTC 8cm P-y Loop (exp LTC7)

7.5 Energy Dissipation

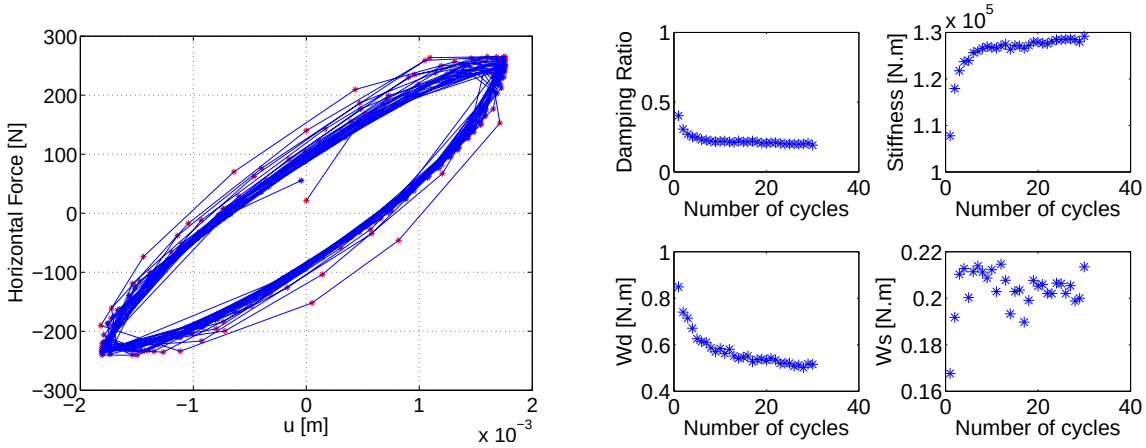

(a) (b)

Figure 7.60: LTP 5cm P-y Loop (exp LTP1)

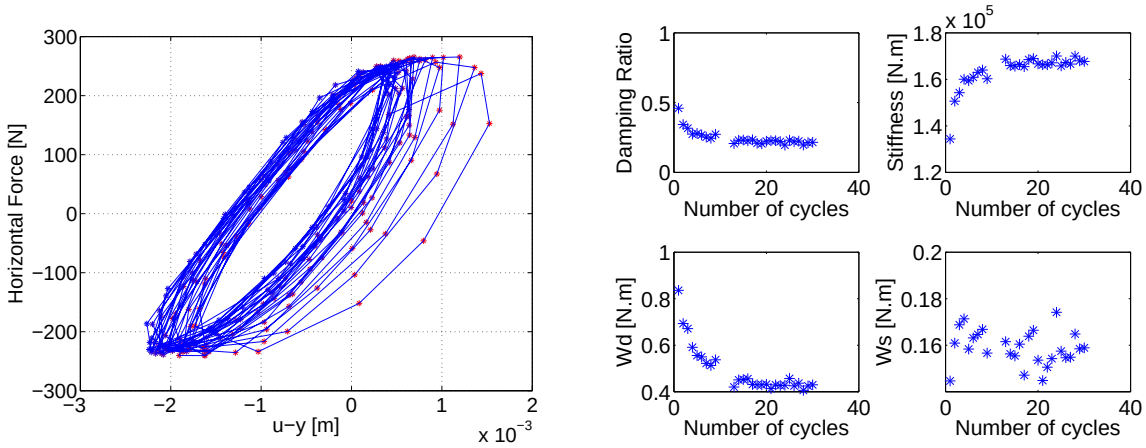

(a) (b)

Figure 7.61: LTP 5cm H-(u-y) Loop (exp LTP1)

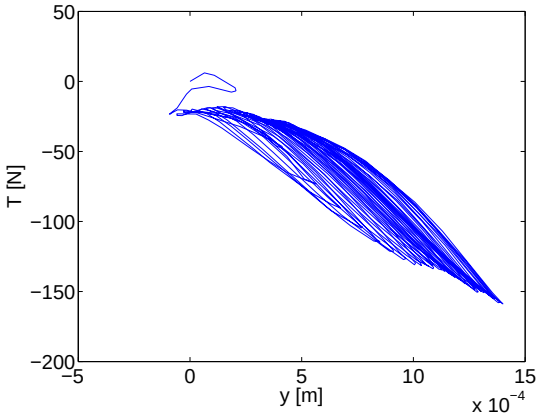

(a)

Figure 7.62: LTP 5cm T-y Loop (exp LTP1)

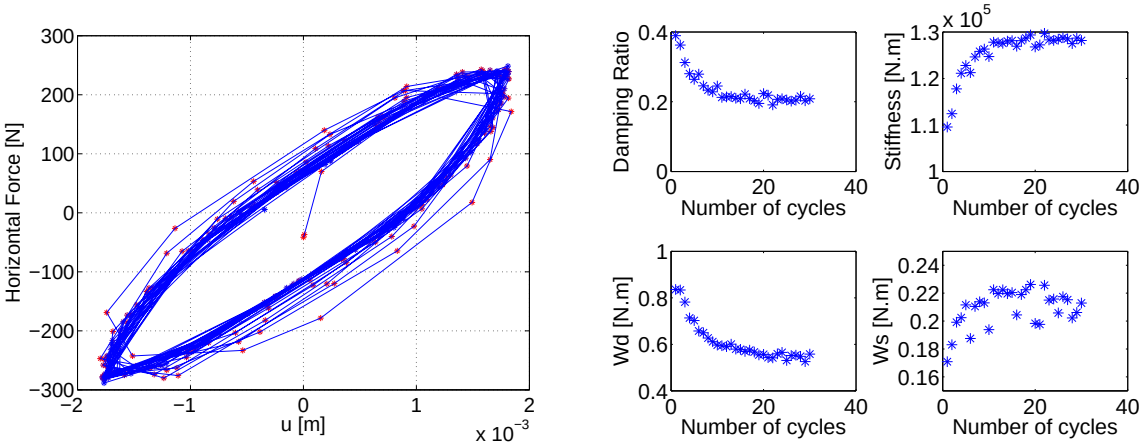

(a) (b)

Figure 7.63: LTP 8cm H-u Loop (exp LTP2)

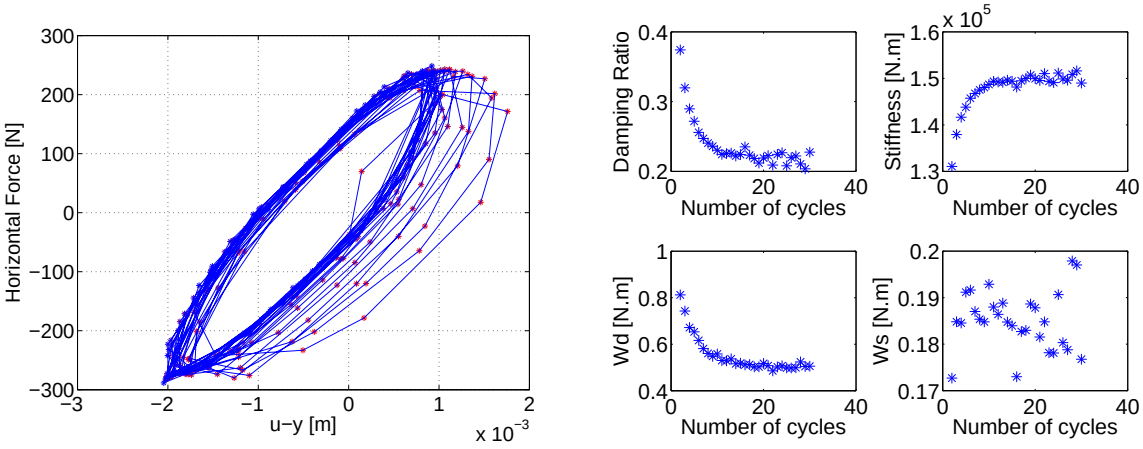

(a) (b)

Figure 7.64: LTP 8cm H-(u-y) Loop (exp LTP2)

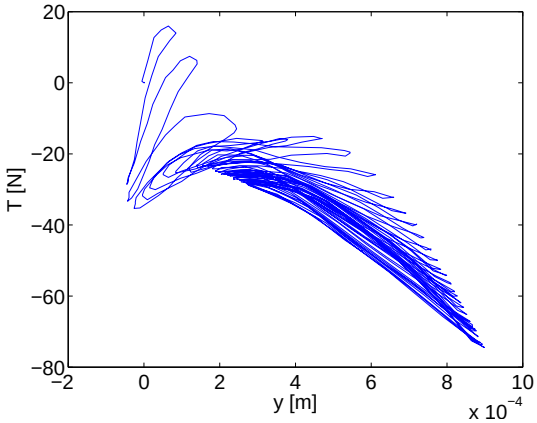

(a)

Figure 7.65: LTP 8cm T-y Loop (exp LTP2)

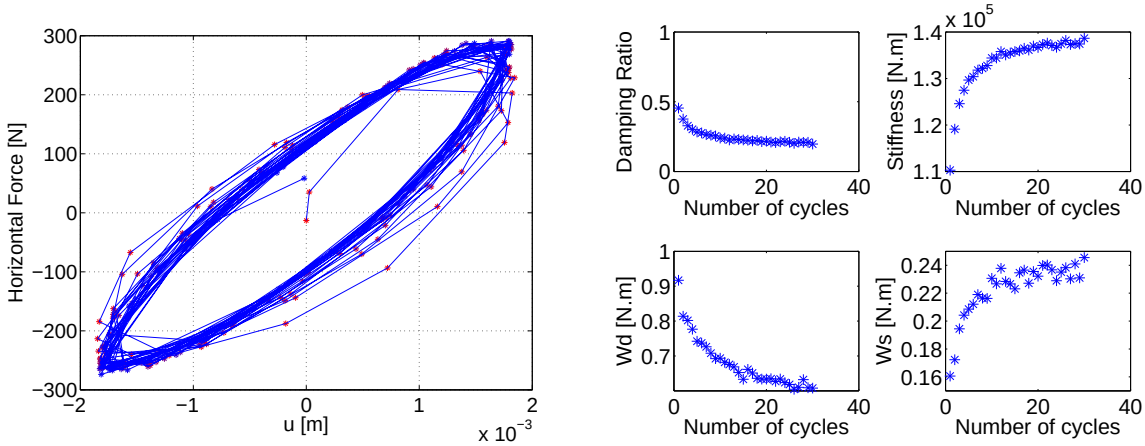

(a) (b)

Figure 7.66: LTP 10cm H-u Loop (exp LTP3)

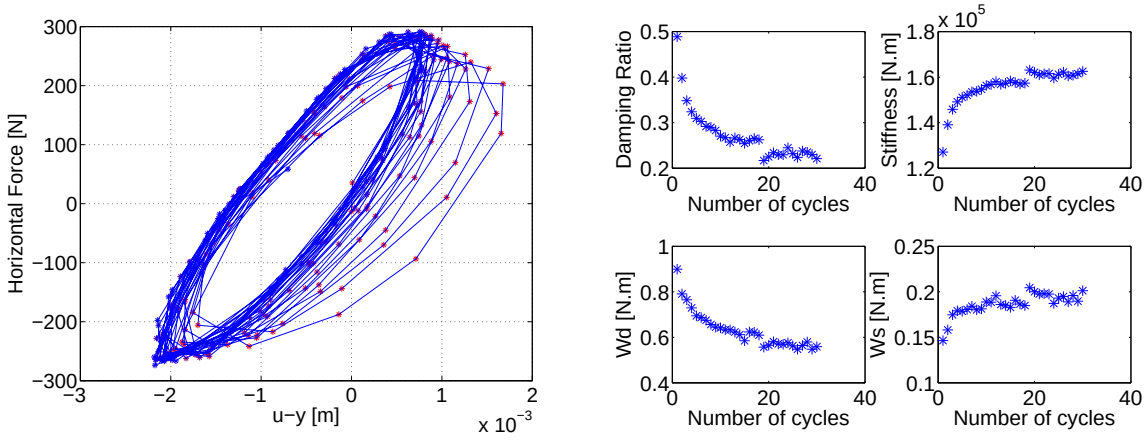

(a) (b)

Figure 7.67: LTP 10cm H-(u-y) Loop (exp LTP3)

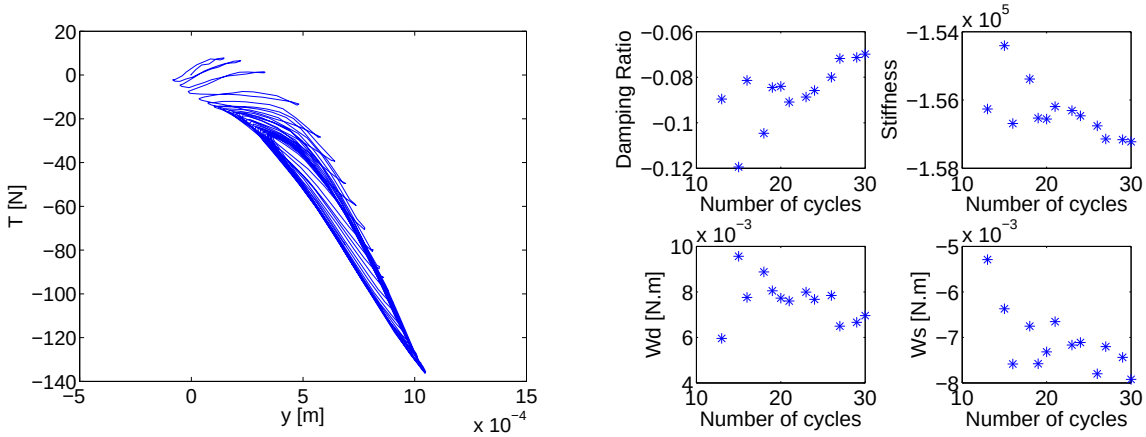

(a) (b)

Figure 7.68: LTP 10cm T-y Loop (exp LTP3)

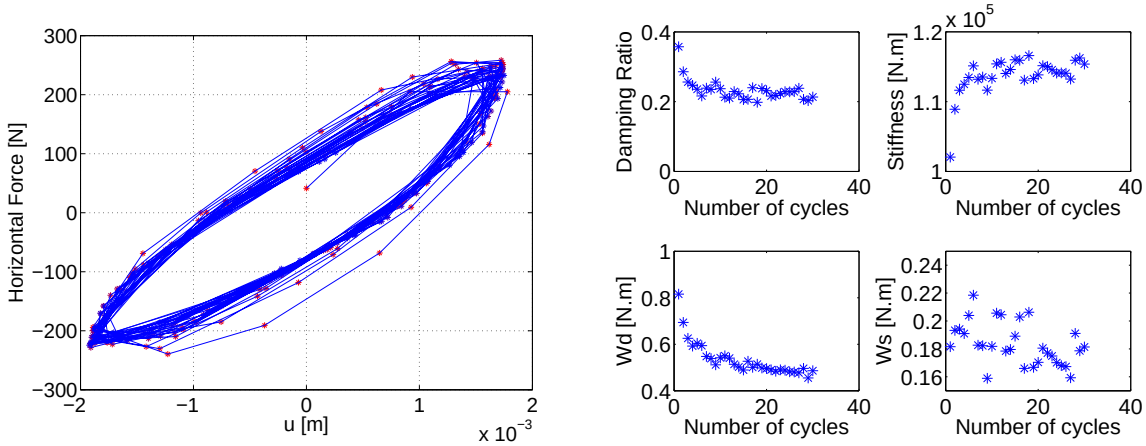

(a) (b)

Figure 7.69: LTP 5cm H-u Loop (exp LTP4)

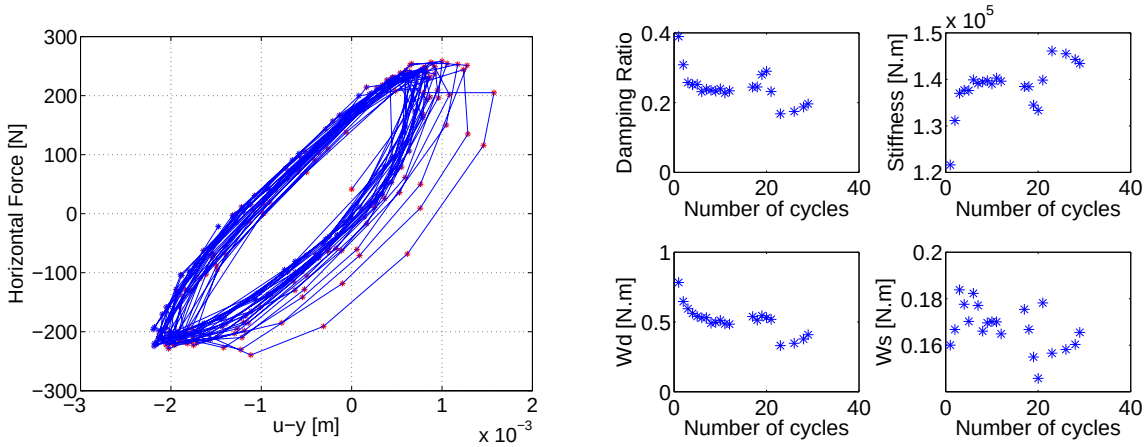

(a) (b)

Figure 7.70: LTP 5cm H-(u-y) Loop (exp LTP4)

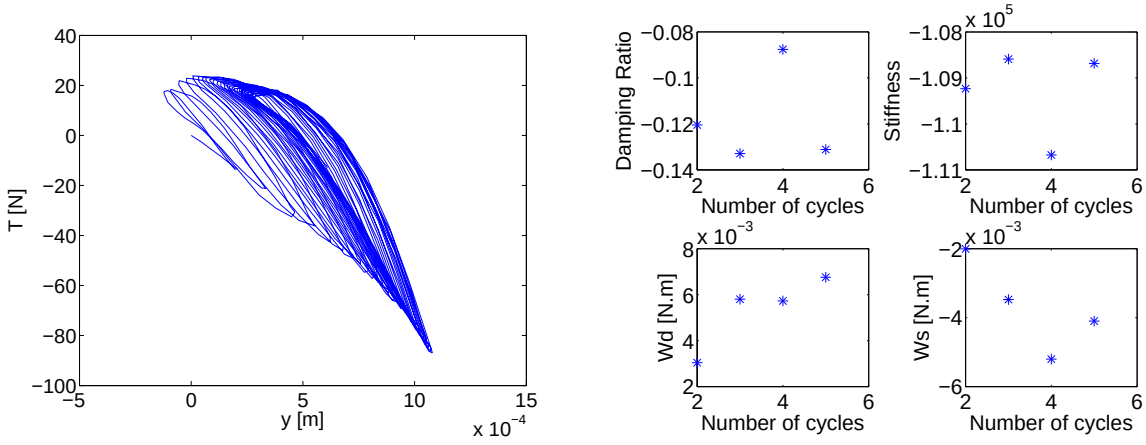

(a) (b)

Figure 7.71: LTP 5cm T-y Loop (exp LTP4)

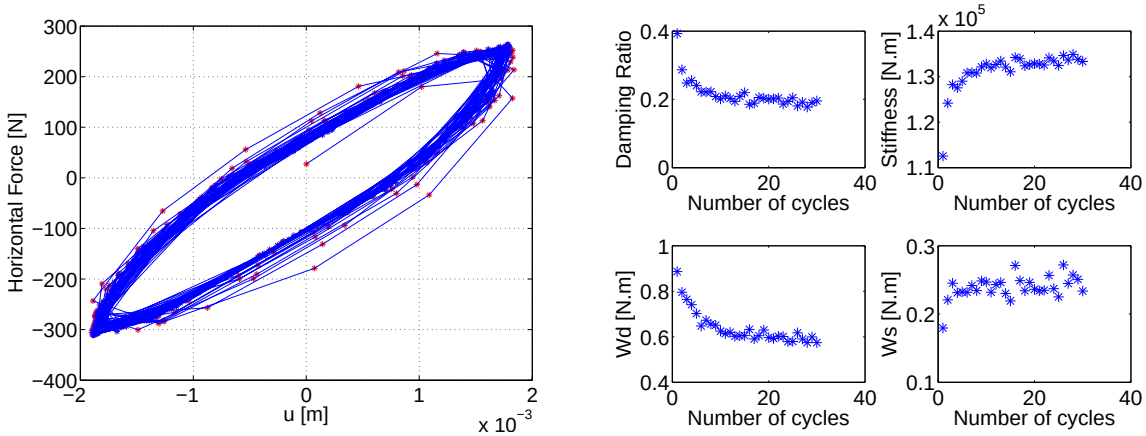

(a) (b)

Figure 7.72: LTP 8cm H-u Loop (exp LTP5)

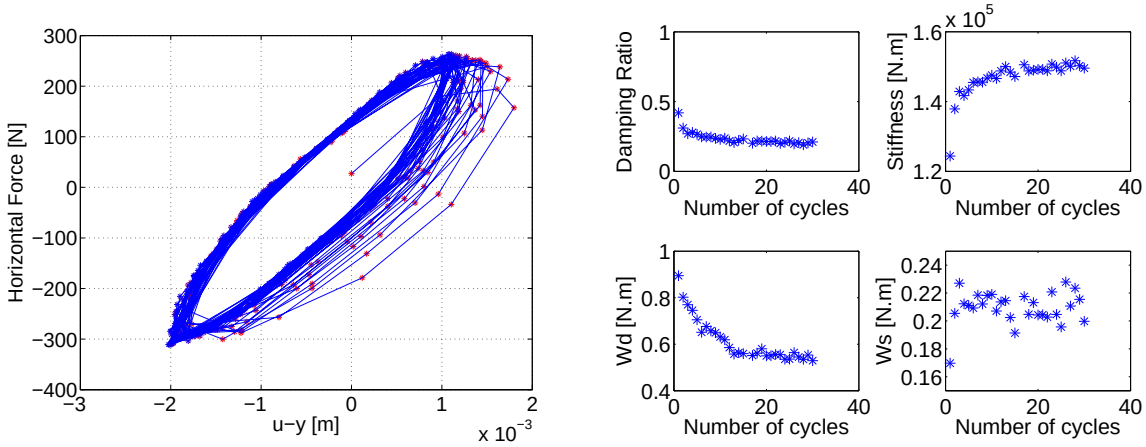

(a) (b)

Figure 7.73: LTP 8cm H-(u-y) Loop (exp LTP5)

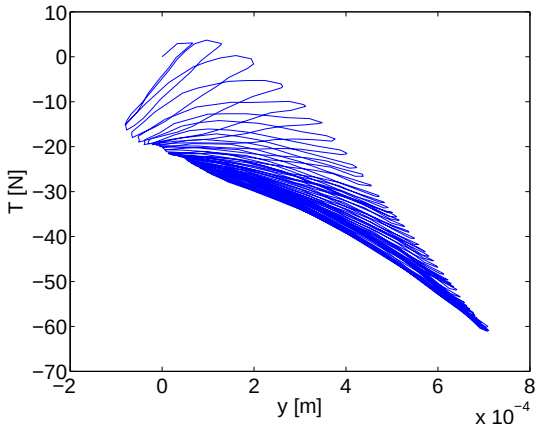

(a)

Figure 7.74: LTP 8cm T-y Loop (exp LTP5)

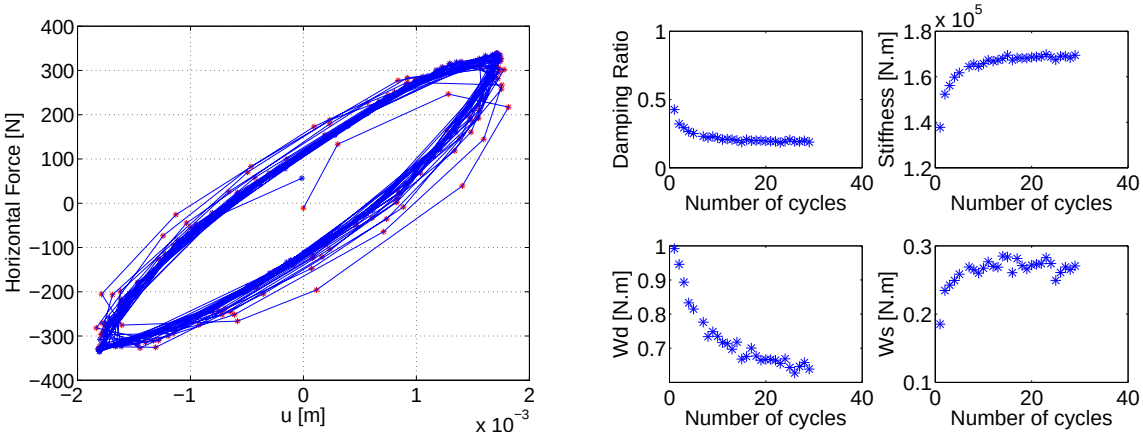

(a) (b)

Figure 7.75: LTP 10cm H-u Loop (exp LTP6)

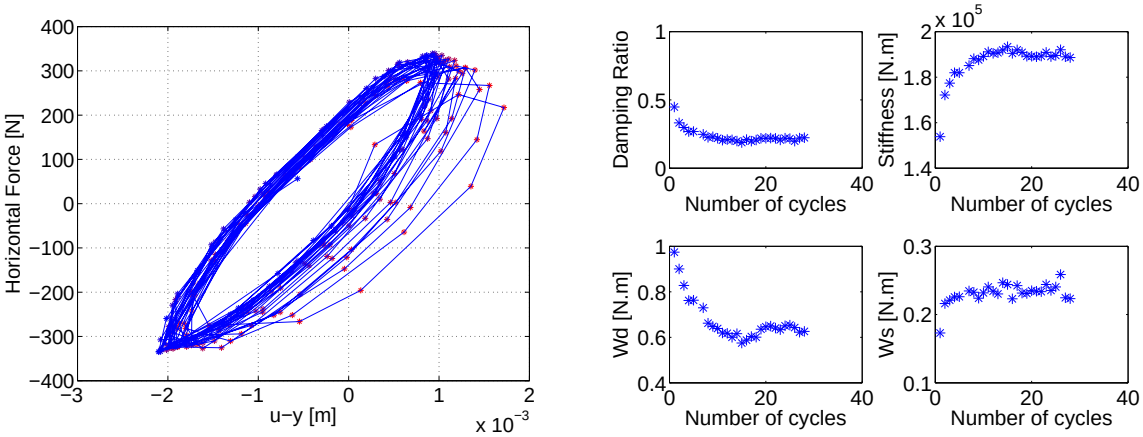

(a) (b)

Figure 7.76: LTP 10cm H-(u-y) Loop (exp LTP6)

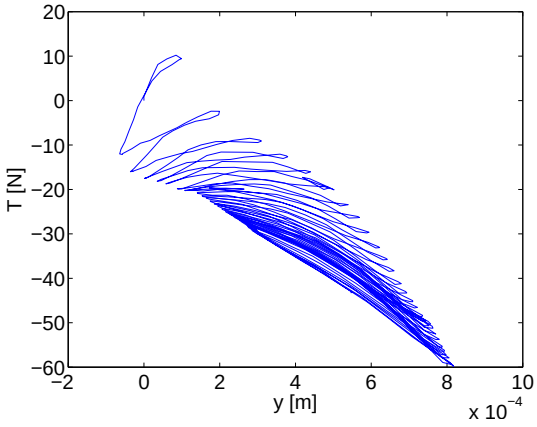

(a)

Figure 7.77: LTP 10cm T-y Loop (exp LTP6)

Bibliography

API (2000). *Recommended practice for planning, designing and constructing fixed offshore platforms-working stress design.* 21st Ed., Washington, DC.

Atkinson, J. H. (1993). *An Introduction to Mechanics of Soils and Foundations Through Critical State Soil Mechanics.* McGraw-Hill International (UK) Limited.

Baguelin, F., Jezequel, J., and Shields, D. (1978). *The pressiometer and foundation engineering.* Trans. Tech. Publications, Clausthal, R.F.A.

Baudouin, G., Rault, G., and Thorel, L. (2010). Renforcement de sol compressible par iclusions rigides sous dallage: Modelisation en centrifugeuse. pages 547–554. Journèes Nationales de Gèotechnique et de Gèologie de l'engènieur JNGG 2010.

Berthelot, P., Pezot, B., and Liausu, P. (2003). Amélioration des sols naturels ou anthropiques par colonnes semi-rigides : Le procédé cmc. In *XIIIth European Conference on Soil Mechanics and Geotechnical Engineering (ECSMGE)*. Praha, Czech Republic.

Briançon, L. (2002). Renforcement des sols par inclusions rigides - etat de làrt. In ., page . IREX.

Broms, B. B. (1964). Lateral resistance of piles in cohesive soils. *Journal of the Soil Mechanics and Foundation Division; Proceedings of the American Society of Civil Engineers*, 90:27–63.

Broms, B. B. (1965). Design of laterally loaded piles. *Journal of the Soil Mechanics and Foundation Division; Proceedings of the American Society of Civil Engineers*, 91:81–99.

Brown, D. A., Reese, L. C., and ONeil, M. (1987). Cyclic lateral loading of a large scale pile group. *Journal of Geotechnical Engineering*, 113(11):1326–1343.

Butterfield, R. and Gottardi, G. (1994). A complete three-dimensional failure envelope for shallow footings on sand. *Geotechnique*, 44:181–184.

Byrne, B. W. and Houlsby, G. T. (2001). Observations of footing behaviour on loose carbonate sands. *Gèotechnique*, 51:463–466.

Chenaf, N. (2007). *Interaction inertielle et interaction cinématique Sol-Pieu.* PhD thesis, L'école Centrale de Nantes et l'Université de Nantes, France.

Chevalier, B., Villard, P., Combe, G., and Grange, S. (2010). Transfert des charges dans les structures géotechniques renforcées par inclusions rigides. pages 547–554. Journées Nationales de Géotechnique et de Géologie d'engénieur JNGG 2010.

Cofone, A. (2010). Physical modeling of dynamic soil structure interaction in the case of stiff inclusions for the reinforcement of the soil.

CSTB, C. (2007). *Fondations profondes pour le batiment, DTU 13.2.* CSTB.

Davisson, M. T. (1970). Lateral load capacity of piles. *High. Res. Rec.*, 39:25–48.

Day, R. W. (2006). *Foundation Engineering Handbook.* McGraw-Hill Companies, Inc, USA.

Eurocode8 (2005). Eurocode 8, european norm on seismic structural calculations. *NF EN 1998-1.*

FLAC3D (2006). *Fast Lagrangian Analysis of Continua in 3 Dimensions.* Itasca Consulting Group, Inc. User's Guide, Version 3.1.

Foray, P., Bonjean, D., and Michallet, H. (2004). Influence of sand liquefaction on the self burial of a pipe submitted to wave action. In *The Proceedings of the 14th International Offshore and Polar Engineering Conference*, pages 571–578. Toulon, France.

Garnier, J. (1995). Modèles réduits en mécanique des sols. In *Les modèles réduits en Génie Civil*, pages 21–44. AUGC.

Garnier, J. and Pecker, A. (1999). Use of centrifuge tests for the validation of innovative concepts in foundation engineering. In *2nd Int. Conf. on Earthquake Geotechnical Engineering*, page 7 p. Lisabon, June.

Grange, S. (2008). *Modélisation simplifiée 3D de l'interaction sol-structure: application au génie parasismique.* PhD thesis, Institut Polytechnique de Grenoble, France.

Hatem, A. (2009). *Comportement en zone sismique des inclusions rigides -Analyse de l'interaction sol-inclusion-matelas de répartition - structure.* PhD thesis, Laboratoire de Mécanique de Lille UMR CNRS 8107, France.

Hewlett, W. and Randolph, M. (1988). Analysis of pile embankments. *Ground Engineering*, pages 12–18.

Jeanjean, P. (2009). *Re-assesment of P-Y curves for soft clays from centrifuge testing and finite element modelling.* Proceeding Offshore Technology Conference, Houston, Texas.

Jenck, O., Diaz, D., and Kastner, R. (2007). Two-dimensional physical and numerocal modeling of a pile-supported earth platform over soft soil. *Journal of Geotechnical and Geoenvironmental Engineering*, 133:295–305.

Keller (2006). *Colonnes à Module Mixte (CMM) procèdè Keller.* Cahier des Charges Colonnes à Module Mixte, France.

Khemakhem, M. (2012). *Etude experimentale de la réponse aux charges latérales monotones et cycliques d'un pieu foré dans l'argile.* PhD thesis, L'école Centrale de Nantes, France.

Kumar, J. and Rao, V. B. K. M. (2002). Seismic bearing capacity factors for spread foundations. *Géotechnique*, 52:79–88.

Matlock, H. (1970). Correlations for design in laterally loaded piles in clay. *Proc. Offshore Technology Conf., Houston*, Paper OTC1204:577–588.

Mayoral, J. M., Romo, M. P., Cirion, A., and Paulin, J. (2006). Effect of layered clay deposits on the seismic behaviour of a rigid inclusion. In *Proceedings of the symposium on rigid inclusions in difficult subsoil conditions*. ISSMGE TC36, Sociedad Mexican de Mecanica de Suelos.

Menard, L., Bourdon, G., and Gambin, M. (1969). Méthode générale de calcul d'un rideau ou d'un pieu sollicité latéralement en fonction des résultats pressiométriques. *Sols-Soils*, VI:16–29.

Orozco, M. C. (2009). *Etude de l'interaction cyclique sol-pipe dans les grands fonds marins*. PhD thesis, Institut Polytechnique de Grenoble, France.

Pecker, A. (1997). Analytical formulae for the seismic bearing capacity of shallow strip foundations. In *Seismical Behaviour of Ground and Geotechnical Structures*, pages 261–268. Seco e Pinto (ed.), Balkema, Rotterdam.

Poulos, H. and Davis, E. (1980). *Pile foundation analysis and design*. John Wiley and Sons.

Reese, L. C. and Welch, R. C. (1975). Lateral loading of deep foundations in stiff clay. *Journal of Geotechnical Engineering, Division Proceeding of American Society of Civiv Engineers*, 101(GT7):633–649.

Remaud, D. (1999). *Pieux sous charges latérales: Etude experimentale de l'effet de groupe*. PhD thesis, L'école Centrale de Nantes, France.

Richards, R., Elms, D. G., and Budhu, M. (1993). Seismic bearing capacity and settlements of foundations. *Journal of Geotechnical Engineering*, 119:662–674.

Roscoe, K. (1968). Soils and model tests. *Journal of strain analysis*, 3:57–64.

Rosquoët, F. (2004). *Pieux sous charge laterale cyclique*. PhD thesis, L'école Centrale de Nantes et l'Université de Nantes, France.

Skempton, A. W. (1951). *The Bearing Capacity of Clays*. London. Inst. Civ. Engrs.

Terzaghi, K. (1955). Evaluation of coefficients of subgrade reaction. *Géotechnique*, 5:297–326.

Zhang, C., White, D., and Randolph, M. (2011b). Centrifuge modelling of the cyclic lateral response of a rigid pile in soft clay. *Journal of Geotechnical and Geoenvironmental Engineering*, 137:717–729.

Zhang, X. (2011). *Modélisation physique et numérique des interactions sol-structure sous sollicitations dynamiques transverses*. PhD thesis, Universite de Grenoble, France.

Zhang, X., Gotteland, P., Foray, P., Grange, S., Santruckova, H., and Lambert, S. (2011). Seismic performance of mixed module columns; physical and numerical modelling of inertial interaction. In *5th International Conference on Earthquake Geotechnical Engineering*. Santiago, Chile.

Résumé en français

7.6 Objectifs du projet

L'analyse du risque sismique des structures devient de plus en plus importante du fait de l'augmentation démographique, principalement dans les zones à fort aléa sismique. La réduction de ce risque est un objectif important. Par ailleurs, l'industrie de la construction est aussi confrontée à de nombreux problèmes liés à la localisation de certains ouvrages et à la raréfaction des terrains présentant de bonnes caractéristiques. C'est pourquoi, pour des raisons économiques et environnementales, nous sommes de plus en plus amenés à construire dans des zones de terrains fortement compressibles, qui sont par nature plus vulnérables aux risques sismiques.
Les techniques d'amélioration des sols compressibles sont actuellement en plein développement. De nombreuses techniques sont proposées, en particulier le renforcement par inclusions rigides associant deux éléments de rigidité différentes : des pieux, micro pieux en partie basse, associés en partie haute en interaction avec la structure, à une zone de transfert de charge répartie (matelas - figure 7.78) ou localisée (colonnes - figure 7.79) autour des inclusions. Une zone de transition relie les deux parties. De nombreuses études ont été entreprises en statique afin de montrer les apports de ces techniques sur les capacités portantes des sols améliorés. Les potentialités d'amélioration du comportement dissipatif sous sollicitation transversale semblent très prometteuses, mais les interactions sol renforcé-structure sous chargement dynamiques et sismiques, tout particulièrement latéraux sont encore mal connues compte tenu de la complexité des interactions entre les différents éléments en présence.

La combinaison de l'aléa sismique avec la méconnaissance des caractéristiques des sols renforcés conduit donc à des dimensionnements non optimisés et à un comportement des bâtiments mal maitrisé. Une meilleure connaissance de ce complexe sol-structure semble donc indispensable. A défaut de pouvoir agir sur l'aléa, la réduction du risque sismique sur les structures passe par une meilleure analyse de l'interface entre le sol et la structure mais surtout sur l'analyse du comportement sismique de ces sols améliorés.

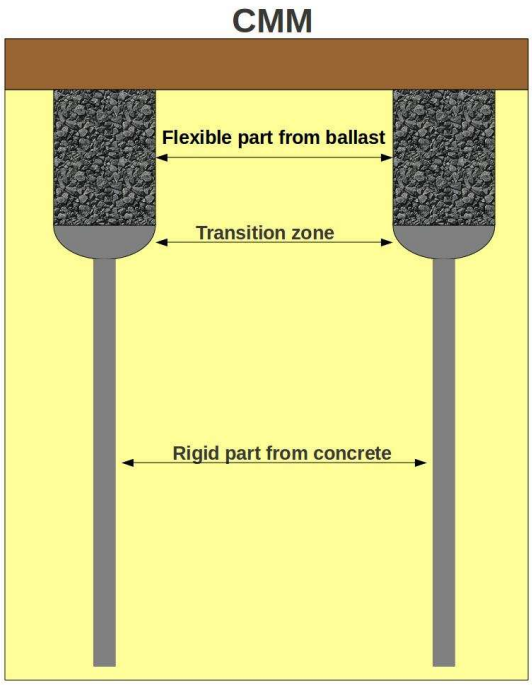

Figure 7.78: Technique d'amélioration des sols compressibles avec des inclusions rigides en partie basse et des colonnes en gravier en partie haute. Cette technique, qui s'appelle Colonne à module mixte – CMM a été introduite par KELLER Fondations Spéciales

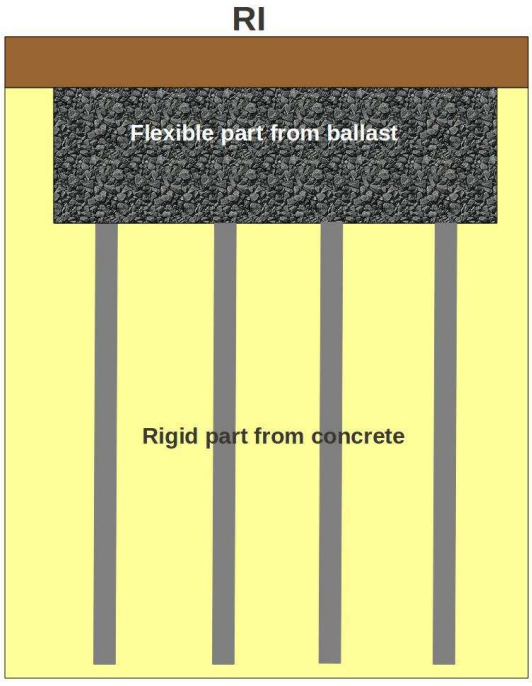

Figure 7.79: Technique d'amélioration des sols compressibles avec des inclusions rigides en partie basse et un matelas en gravier en partie haute - IR (Inclusions Rigides)

7.7 Contexte

Ce projet s'insère dans le cadre d'une étude des risques sismiques d'une construction fondée sur un sol compressible amélioré par la technique des inclusions rigides qui sont associées à une zone de transfert de charge qui est flexible. On souhaite à travers ce projet contribuer à montrer l'intérêt de ces nouvelles techniques de renforcement sur la stabilité des structures face aux risques sismiques et notamment face aux sollicitations horizontales. En effet, dans le cas de sollicitation sismique, c'est la réponse aux ondes de cisaillement S et donc aux sollicitations horizontales qui est importante. Cette étude à également pour but de comparer les techniques à zone de transfert de charge réparties (IR) avec celles localisées (CMM).

L'élément clé du dispositif est une colonne de sol ou un matelas granulaire, positionné au dessus du réseau de pieux et sous le bâtiment, ayant un rôle dissipatif et limitatif quant aux efforts horizontaux (fortement préjudiciables) transmis à la structure, puis par retour et effet inertiel, aux pieux. En effet, dans le cas d'un renforcement de sol par inclusions rigides seules, on a souvent l'obligation d'armer les inclusions par des cages d'armatures ou de les associer avec un matelas, avec toutes les sujétions d'exécution que cela suppose, afin que le sol renforcé puisse accepter des sollicitations horizontales liées essentiellement au vent et au séisme. Un des objectifs de ce projet est de montrer que tous ces inconvénients peuvent être évités grâce à la réalisation de la partie supérieure en gravier refoulé de la CMM. Cette dernière, plus déformable en interaction avec le sol en place se comporte comme une zone rotulée dissipative qui transmet moins d'énergie dans la superstructure par effet direct et moins d'énergie à la partie inférieure rigide des CMM par effet inertiel.
De nombreuses études expérimentales ont été réalisées sur les fondations superficielles reposant sur sol mou renforcé par les colonnes ballastées, par les inclusions rigides soumises à des chargements verticaux et sur les pieux soumis à des chargements verticaux et horizontaux (Rosquoët, 2004), (Chenaf, 2007), (Remaud, 1999). Par contre, peu de travaux de recherche sont répertoriés sur le comportement des sols renforcés par inclusions qu'elles soient souples, rigides ou les CMM sous sollicitation transverse horizontale correspondant à une réponse en zone sismique (Hatem, 2009).

Dans le cadre d'une collaboration avec l'entreprise Keller France, le Laboratoire 3SR s'est proposé d'effectuer une étude à la fois expérimentale et numérique sur cette thématique. C'est ce programme de recherche qui fait l'objet de ma Thèse et qui a reçu le soutien du CNRS.

7.8 Modélisation physique

Dans le cadre de ce travail, la condition de similitude rigoureuse n'est pas respectée pour le niveau de contrainte pour les modèles réduits soumis à une gravité normale ($g^* = 1$). Néanmoins, cette modélisation physique a pour objectif d'analyser d'interaction du complexe sol-renforcement-semelle sous sollicitation horizontale dynamique. Elle doit également permettre de caler un modèle numérique qui pourra ensuite être utilisé sur des ouvrages réels.

Notre étude expérimentale a été réalisée au laboratoire 3SR dans le dispositif Visucuve. Un

modèle réduit (échelle : 1/10) de massif de sol renforcé par inclusions rigides associé à une zone de transfert de charge a été réalisé et soumis à des sollicitations dynamiques horizontales. Les chargements cycliques quasi-statiques et dynamiques sont appliqués sur le modèle de fondation pour examiner l'effet inertiel. Nous avons conçu un modèle formé de quatre inclusions en aluminium implantées dans un massif d'argile, surmonté d'une partie souple.
L'avantage de ces essais est leur relative simplicité de mise en œuvre. Ils permettent d'avoir des informations importantes concernant les transferts de charges, les interactions cinématiques et inertielles.

7.8.1 Présentation des modèles physiques

Un modèle réduit d'une semelle carrée de 24cm de côté et de 2cm d'épaisseur a été réalisé. Elle repose sur un massif d'argile renforcé par 4 inclusions rigides qui sont associées à une partie supérieure qui est souple. Deux types de partie supérieure ont été modélisés:

1. un matelas en gravier - LTP (Load Transfer Platform), Figure 7.81
2. des colonnes en gravier entourées par l'argile - LTCs (Load Transfer Columns), 7.80

Pour connaitre l'influence de l'épaisseur de la plateforme de transfert sur les sollicitations dans les inclusions rigides, les épaisseurs de 5, 8 et 10 cm vont être étudiées. La semelle est encastrée dans le sol sur toute sa hauteur.

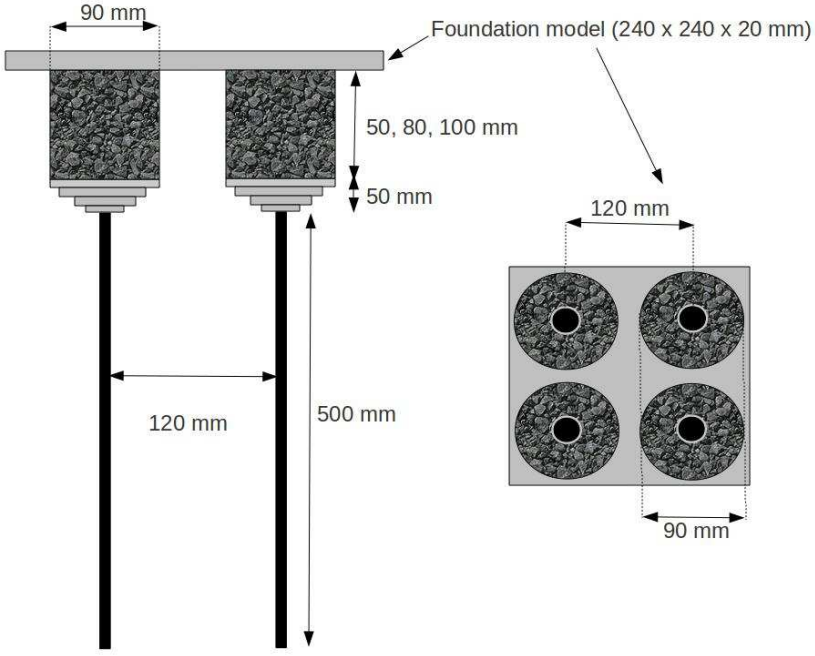

Figure 7.80: Les inclusions rigides (en partie inférieure) sont associées aux colonnes en gravier entourées par l'argile - LTCs (Load Transfer Columns)

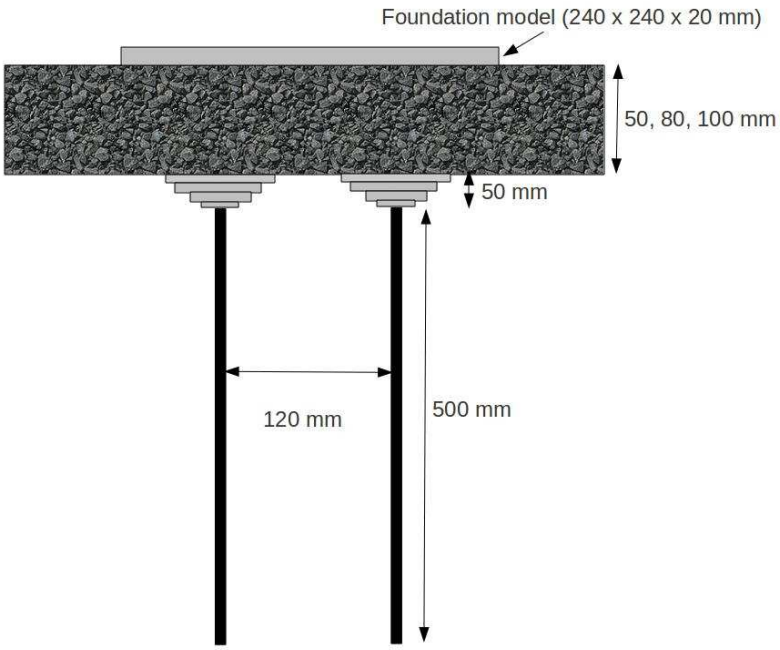

Figure 7.81: Les inclusions rigides (en partie inférieure) sont associées au matelas en gravier - LTP (Load Transfer Platform)

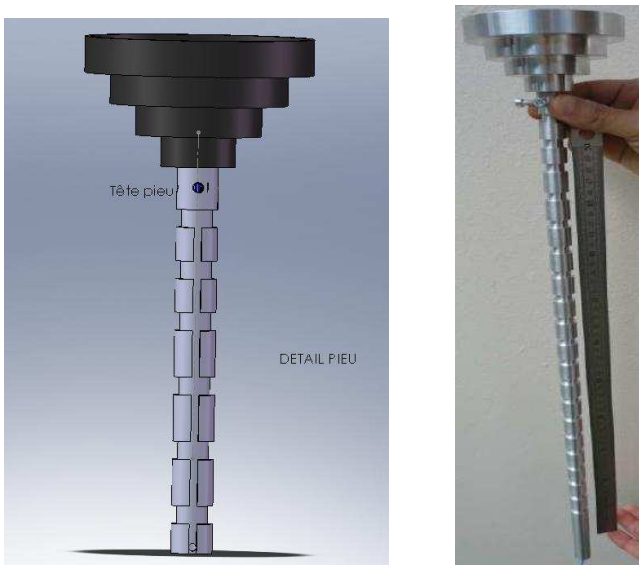

(a) (b)

Figure 7.82: Pour l'étude des sollicitations latérales de l'inclusion rigide, une inclusion est instrumentée avec 20 extensomètres répartis sur toute la hauteur de manière à représenter les profils des sollicitations de manière détaillée. Chaque pieu a été encastré dans un entonnoir en aluminium rempli par du gravier afin de simuler les zones de transition

Les quatre pieux, qui représentent la partie inférieure, sont en aluminium d'un diamètre extérieur 16mm et d'un diamètre intérieur 8mm. Une des inclusions rigides est instrumentée

de 20 jauges (figure 7.82) permettant de connaître sa déformée à chaque instant et de remonter ainsi aux efforts transmis au pieu. Les longueurs des inclusions sont de 5-10cm pour la partie supérieure et 50cm pour la partie inférieure. La partie inférieure a été rigidement encastrée dans le fond de la VisuCuve. L'entre-axe des deux LTCs est de 12cm. Les têtes de la partie rigide ont été encastrées dans quatre entonnoirs en aluminium (figure 7.82) remplis par du gravier afin de simuler les zones de transition entre partie rigide et partie souple.

7.8.2 Méthodologie expérimentale

Le dispositif expérimental est constitué d'une grande cuve (VisuCuve - figure 7.83) rigide et imperméable de 2m de long, 1m de large et 1m de profondeur. La partie supérieure de la cuve comporte deux rails de guidage sur lesquels peut se déplacer horizontalement un chariot piloté par un vérin électro-mécanique EXLAR FT35-2410-FIA-EX4-L2 avec un moteur brushless et un variateur numérique qui peut avoir une vitesse maximale de 700mm/s. Un second vérin vertical est fixé sur le chariot, l'ensemble permettant ainsi l'application de charges couplées verticales/horizontales à une structure fondée sur un massif de sol. Ce dispositif permet aussi l'application de charges horizontales rapides cycliques.

Figure 7.83: Dispositif expérimental - 'VisuCuve'

La cuve est remplie d'argile saturée. Le massif argileux a été mis en place par des blocs d'argile empilés (voir figure 7.84) en veillant à créer d'une part un massif le plus homogène possible et d'autre part un bon contact entre la partie rigide et le sol. L'argile utilisée se caractérise par une cohésion de 18 kPa et une teneur en eau de 20 %. Pour le cas des LTCs, 4 colonnes de gravier ont été installées au-dessus de la zone de transition au sein de l'argile (voir figure 7.85) et compactés par un piston pour obtenir une densité estimée à 16 kN/m3 en moyenne.

(a)

(b)

(c)

(d)

Figure 7.84: L'installation d'argile avec l'objectif de créer un massif le plus homogène possible

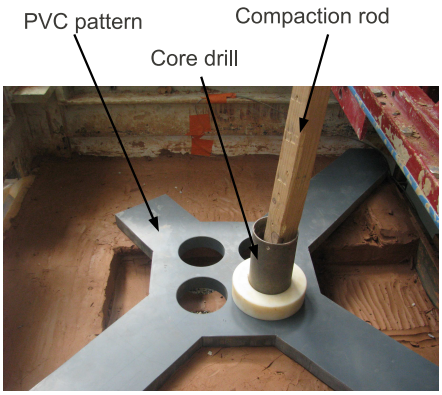

(a)

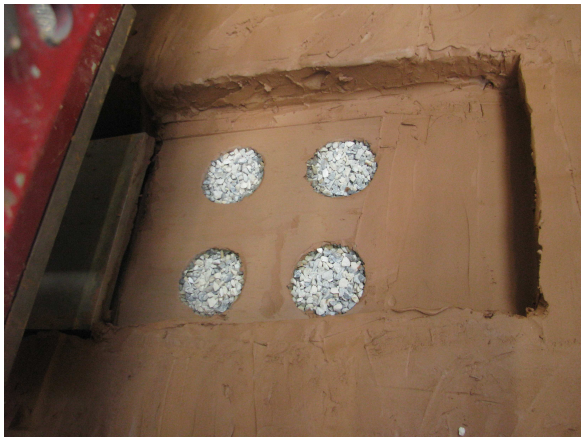

(b)

Figure 7.85: Procédure d'installation des LTC entourées d'argile

La charge verticale est appliquée sur le modèle de semelle par un vérin vertical électromagnétique Exlar IX40. Les forces horizontale et verticale sont mesurées par deux capteurs de force montés sur le chariot de chargement. Les déplacements horizontaux sont mesurés par un LVDT fixé sur le chariot. Le déplacement vertical est mesuré par un LVDT fixé sur le modèle de la fondation. Après avoir appliqué la semelle sur le sol renforcé, une charge verticale de 5 000 N est appliquée progressivement en 5 paliers réguliers. Cette charge est maintenue ensuite constante pour assurer une complète consolidation du sol. La charge verticale de 5 000 N correspond au tiers de la charge de rupture du sol renforcé. Après la phase de consolidation du sol sous la charge verticale, un chargement horizontal de 30 cycles est appliqué sous déplacements contrôlé de +/- 2 mm à une fréquence de 2,7 Hz.

7.8.3 Traitement des données

Le traitement correct des données expérimentales est essentiel pour la compréhension du phénomène. L'instrumentation de l'inclusion mesure des déformations de flexion à partir de 20 jauges. Les moments de flexion le long du pieu ont été obtenus à partir de la loi de Hooke et de l'équation de Euler-Bernoulli. La principale difficulté pour une telle analyse est une interpolation temporelle correcte du moment sur la hauteur de l'inclusion. Ceci est effectué avec une fonction polynomiale de 6 degrés. En appliquant des conditions aux limites à la base de l'inclusion (déplacement et rotation nuls), la pression latérale et le déplacement horizontal sont obtenus par :

$$P = -\frac{d^2M}{dz^2} \tag{7.1}$$

$$y = \frac{1}{EI}\int(\int M.dz).dz \tag{7.2}$$

Ces valeurs physiques et leurs dérivées sont utilisées dans cette présente étude pour analyser le comportement latéral de l'inclusion.

7.8.4 Résultats experimentaux

7.8.4.1 Chargement vertical statique

Une charge verticale a été appliquée progressivement en 5 paliers réguliers sur le modèle de semelle. Un tassement induit par ce chargement est montré dans la figure 7.86. Plusieurs hauteurs de la partie souple en gravier ont été étudiées pour connaitre leur incidence sur le comportement de la fondation.
La figure 7.86 montre que sous un chargement vertical, la fondation subit un tassement plus important quand elle est posée sur sol renforcé par les inclusions rigides associées aux LTCs que quand elle est posée sur sol renforcé par les inclusions rigides associées au LTP. Ce phénomène pourrait être dû au fait qu'il y a de l'argile présente entre les LTCs - Cette argile subit une consolidation pendant le chargement qui entraine par conséquent un tassement plus important de la fondation.

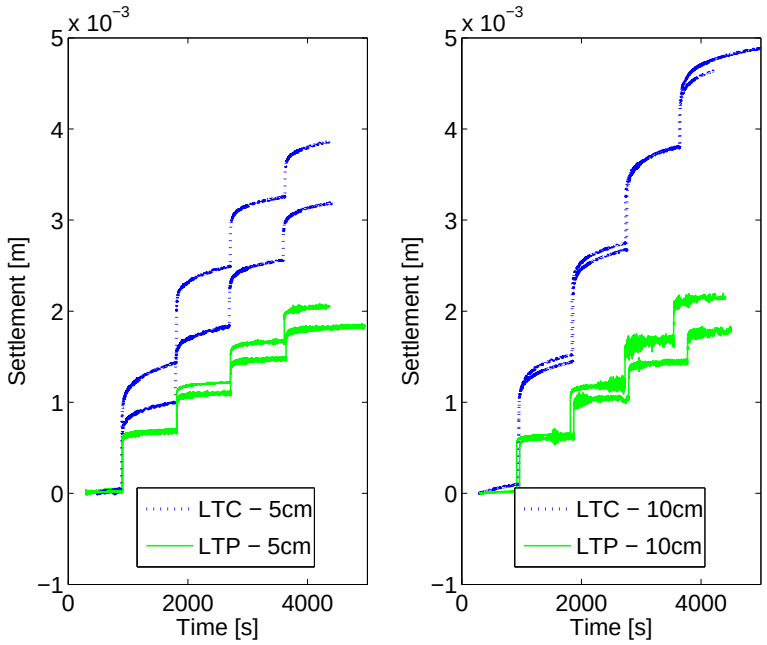

Figure 7.86: Tassement de la semelle sur sol renforcé par les inclusions rigides associées au LTP ou LTC. La hauteur de la partie souple a été variée pour connaitre son incidence sur le tassement

7.8.4.2 Chargement vertical et horizontal statique

L'objectif est de trouver la combinaison des charges limites verticale V et horizontale H qui provoque la rupture de la fondation isolée. Une courbe enveloppe de rupture est décrite par la formule analytique de Butterfield and Gottardi ((Butterfield and Gottardi, 1994)) :

$$\frac{H}{t_h} = \frac{V}{V_{max}}.(V_{max} - V) \tag{7.3}$$

Où Vmax est la charge limite verticale et th le coefficient de frottement sol/semelle. Cette courbe enveloppe de rupture peut être trouvée expérimentalement par une augmentation de la charge verticale jusqu'à sa capacité ultime, puis en appliquant une force horizontale tout en bloquant la fondation verticalement. Cette procédure est communément appelé le « swipe test ». La mesure des forces verticales et horizontales appliquées sur la fondation donne pour la semelle l'enveloppe de rupture du sol. Le « swipe test » a été effectué d'une part pour le sol non renforcé et d'autre part pour le sol renforcé par les inclusions rigides associées aux LTCs. Un comparatif de ces 2 courbes est donné sur la figure 7.87. On constate que l'enveloppe de rupture du sol renforcé est bien plus large que celle du sol non renforcé. La forme de ces deux enveloppes est homothétique avec un rapport approximatif de 4 entre les 2 courbes.

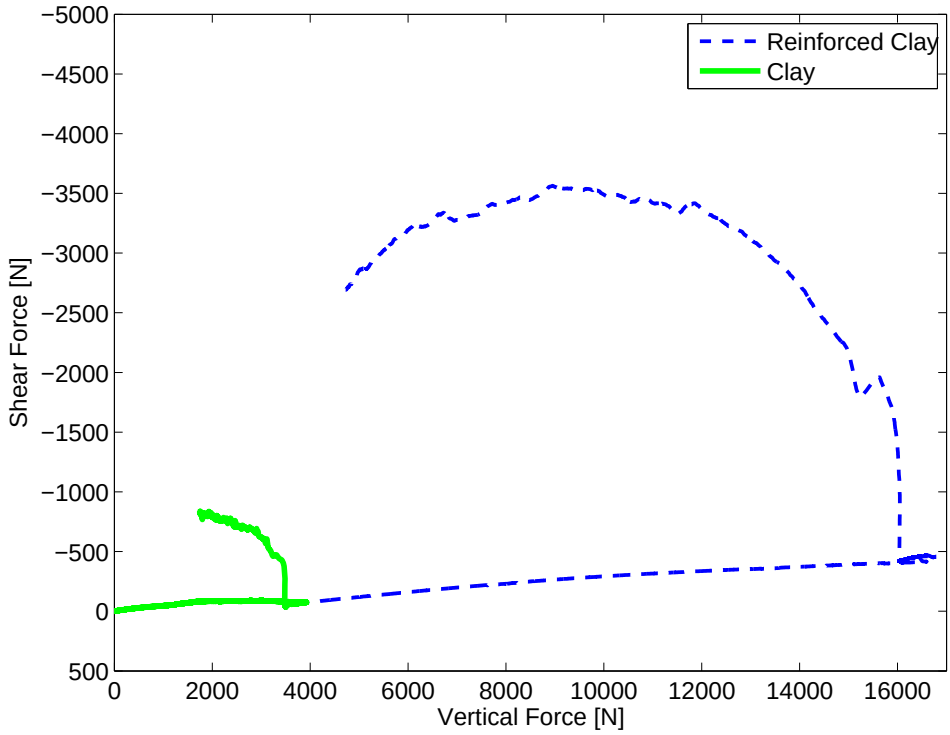

Figure 7.87: Un comparatif entre un « swipe test » effectué pour un sol non renforcé et un sol renforcé par les inclusions rigides associées aux LTCs

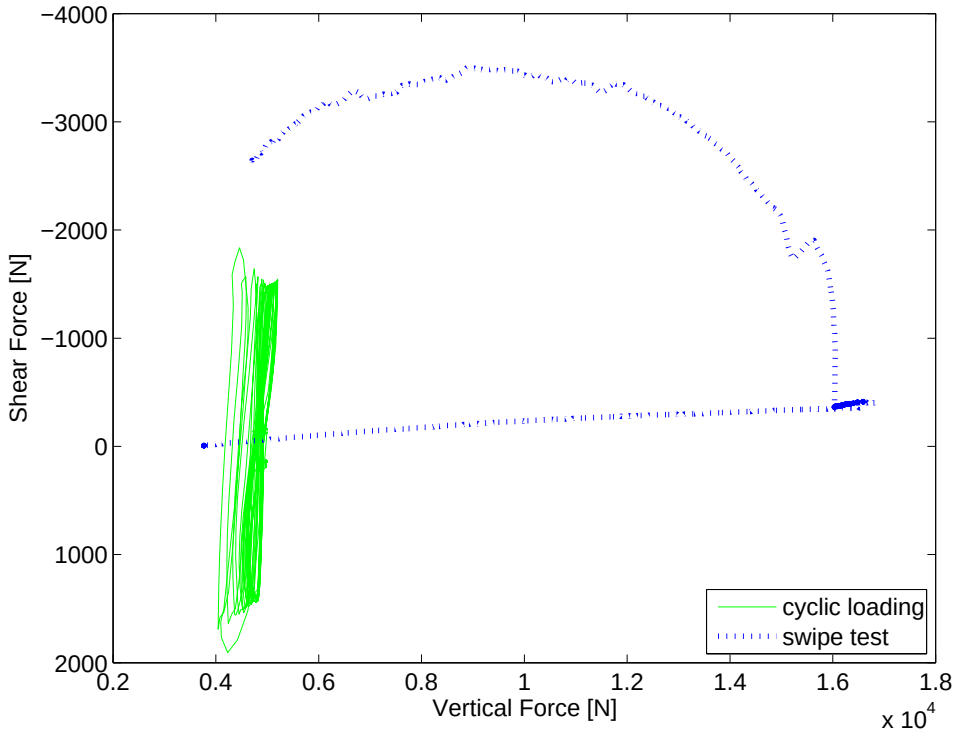

Figure 7.88: Les sollicitations cycliques exercées se situent à l'intérieur de l'enveloppe de rupture

Les swipe test a permis de vérifier que le niveau du chargement cyclique (présenté à la suite) reste suffisamment éloigné de la courbe de rupture. La figure 7.88 montre en effet que les sollicitations cycliques exercées se situent à l'intérieur de la courbe et restent éloignées d'une rupture par glissement de la semelle.

7.8.4.3 Chargement vertical statique et horizontal cyclique

Le comportement d'un sol renforcé par les inclusions rigides associées au LTP ou LTCs sous une sollicitation horizontale cyclique va cette fois-ci être étudié. La charge verticale est maintenue constante. Trente cycles de chargement horizontal avec une amplitude de +/-2mm et une fréquence de 2.7Hz sont imposés sur la fondation. Ce chargement, qui est montré dans la figure 7.89b, est contrôlé en déplacement. La direction du premier chargement de l'inclusion rigide est marquée comme 'A' (figure 7.89) - Cette direction correspond au cas où la déformation de l'inclusion instrumentée se fait vers l'extérieur du groupe formé par les quatre inclusions.
Plusieurs hauteurs de la partie souple en gravier vont être étudiées pour connaitre leur incidence sur le comportement de la fondation et de la partie rigide sousjacente.

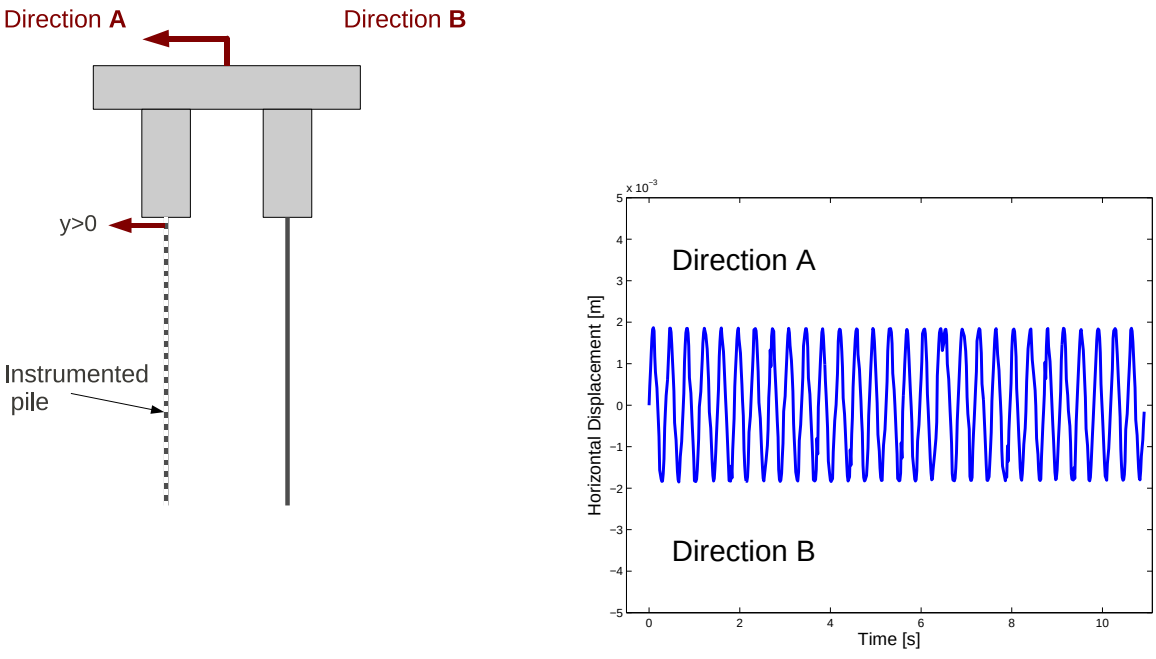

(a) (b)

Figure 7.89: Le chargement horizontal- Direction A, Direction B

Tassement de la fondation sous chargement cyclique

Après stabilisation des tassements sous chargement vertical, les valeurs de tassement ont été remises à zéro et un chargement cyclique de la fondation a débuté pour 30 cycles durant 11 s. Les résultats du tassement de la semelle posée sur un sol renforcé par les inclusions rigides associées au LTP et LTCs figurent respectivement sur les figures 7.90 et 7.91. On observe que des tassements de la fondation augmentent avec la hauteur de la partie souple. On constate que l'ordre de grandeur est le même pour les deux types de renforcement (inclusions rigides associées aux LTCs ou LTP) ce qui est consideré comme étant lié au fait que le chargement dynamique est si court que l'argile entre les LTCs n'a pas le temps de se consolider, comme dans le cas du chargement statique.

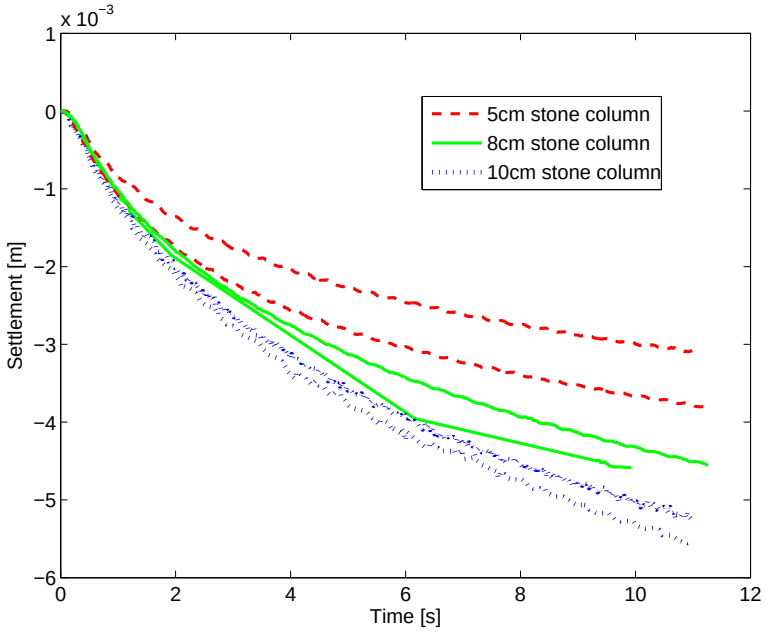

Figure 7.90: Tassements sous chargement vertical et horizontal cyclique - semelle sur sol renforcé par les inclusions rigides associées aux LTCs

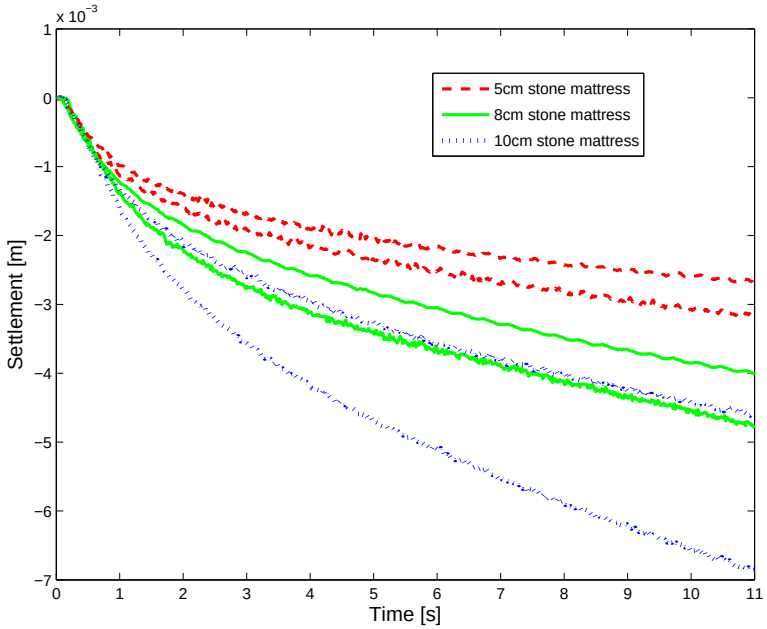

Figure 7.91: Tassements sous chargement vertical et horizontal cyclique - semelle sur sol renforcé par les inclusions rigides associées au LTP

Sollicitation horizontale de la partie rigide

Lorsque la fondation subit un déplacement cyclique horizontal (+/-2 mm dans notre cas), il se produit également un déplacement au niveau de la partie rigide des modèles. Cette déformation est enregistrée et traitée afin d'obtenir les profils du déplacement horizontal, du moment de flexion, d'effort tranchant et de la réaction latérale de sol sur la hauteur de l'inclusion rigide.
La hauteur de la partie souple (hauteurs variables de 5, 8 et 10 cm) est variée afin de d'étudier son influence sur les sollicitations horizontales de la partie rigide.

Les courbes du moment de flexion et d'effort tranchant ont été tracées pour les temps t1 à t10 correspondant à différents instants pendant les trente cycles du chargement. Les temps t1, t3, t5, t7 et t9 indiquent les maxima de la déflexion mesurée en tête de l'inclusion pour le premier, cinquième, dixième, quinzième et trentième cycle et les temps t2, t4, t6, t8 et t10 indiquent les minima de la déflexion mesurée en tête de l'inclusion pour les mêmes cycles (figure 15 à 17). Sachant qu'une seule inclusion a été instrumentée, il est possible de connaitre les sollicitations des inclusions à l'avant du groupe (sens du déplacement dans la direction 'A' - figure 7.89) pour t1, t3, t5, t7 et t9 et les sollicitations des inclusions à l'arrière du groupe pour t2, t4, t6, t8 et t10 (sens du déplacement dans la direction 'B' - figure 7.89). Les résultats sont représentés sur les figures 7.92 à 7.94 pour une inclusion qui est surmontée par une LTC et figures 7.95 à 7.97 pour une inclusion qui est surmontée par une LTP.

Les résultats obtenus indiquent que:

- Le déplacement horizontal est réversible au début du chargement puis à mesure que le nombre de cycles augmente, l'inclusion ne revient plus au-delà de sa position initiale et montre une accumulation des déplacements dans le sens positif avec le chargement dy-

namique. Ce déplacement latéral accumulé, tout en restant toujours faible par rapport au déplacement de la semelle, se développe vers l'extérieur de la fondation (c'est-à-dire dans la direction 'A') et a une tendance à se stabiliser vers la fin du chargement cyclique.

- Il est intéressant de noter que l'inclusion rigide surmontée par una LTC ou une LTP se déforme jusqu'à une profondeur de respectivement 25cm et 35cm ce qui correspond à une fois et une fois et demi la largeur de la fondation.

- La position du moment maximal descend le long de l'inclusion rigide au cours du chargement. Cette tendance a été déjà observée pour les pieux sous un chargement latéral cyclique dans l'argile (Khemakhem, 2012) et signifie une dégradation des propriétés mécaniques du sol qui entoure le pieu.

- On constate que sous le chargement horizontal cyclique appliqué au niveau de la fondation, l'inclusion rigide qui est associée à la partie souple (LTC ou LTP) de 5cm de hauteur subit des sollicitations plus importantes que l'inclusion rigide associée à la partie souple de 10cm de hauteur. Ce phénomène peut être expliqué par le fait qu'une partie souple du modèle agit comme une liaison entre la fondation et le pieu plus rigide dans le cas de 5cm de hauteur que dans le cas de 10cm de hauteur. Par conséquent, en augmentant la hauteur de LTP ou LTC, le niveau de la sollicitation du pieu diminue.

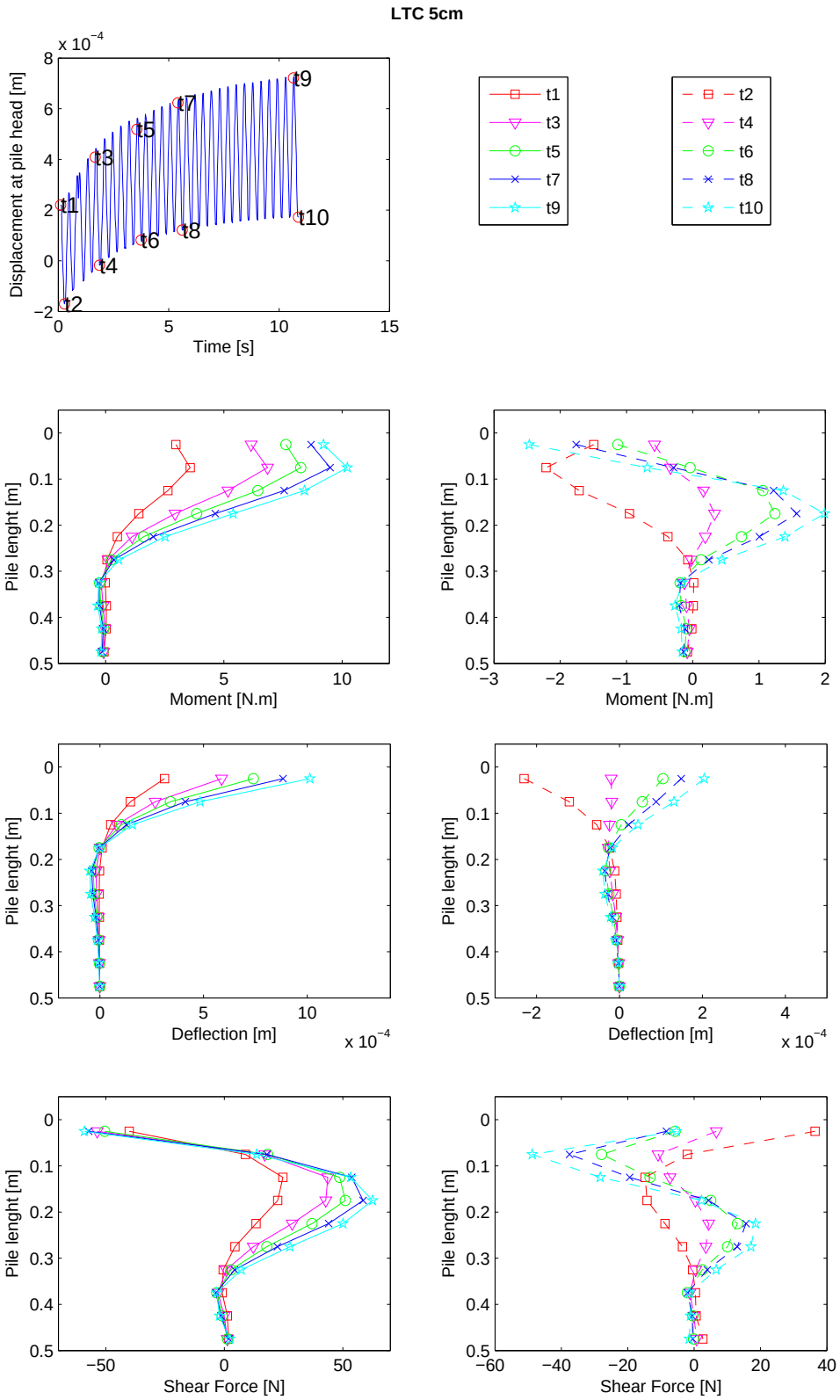

Figure 7.92: Moment fléchissant, déflexion et effort tranchant le long d'inclusion rigide associée à LTC avec 5 cm de hauteur (exp LTC9); Direction 'A' = t1,t3, t5, t7, t9; Direction 'B' = t2, t4, t6, t8, t10

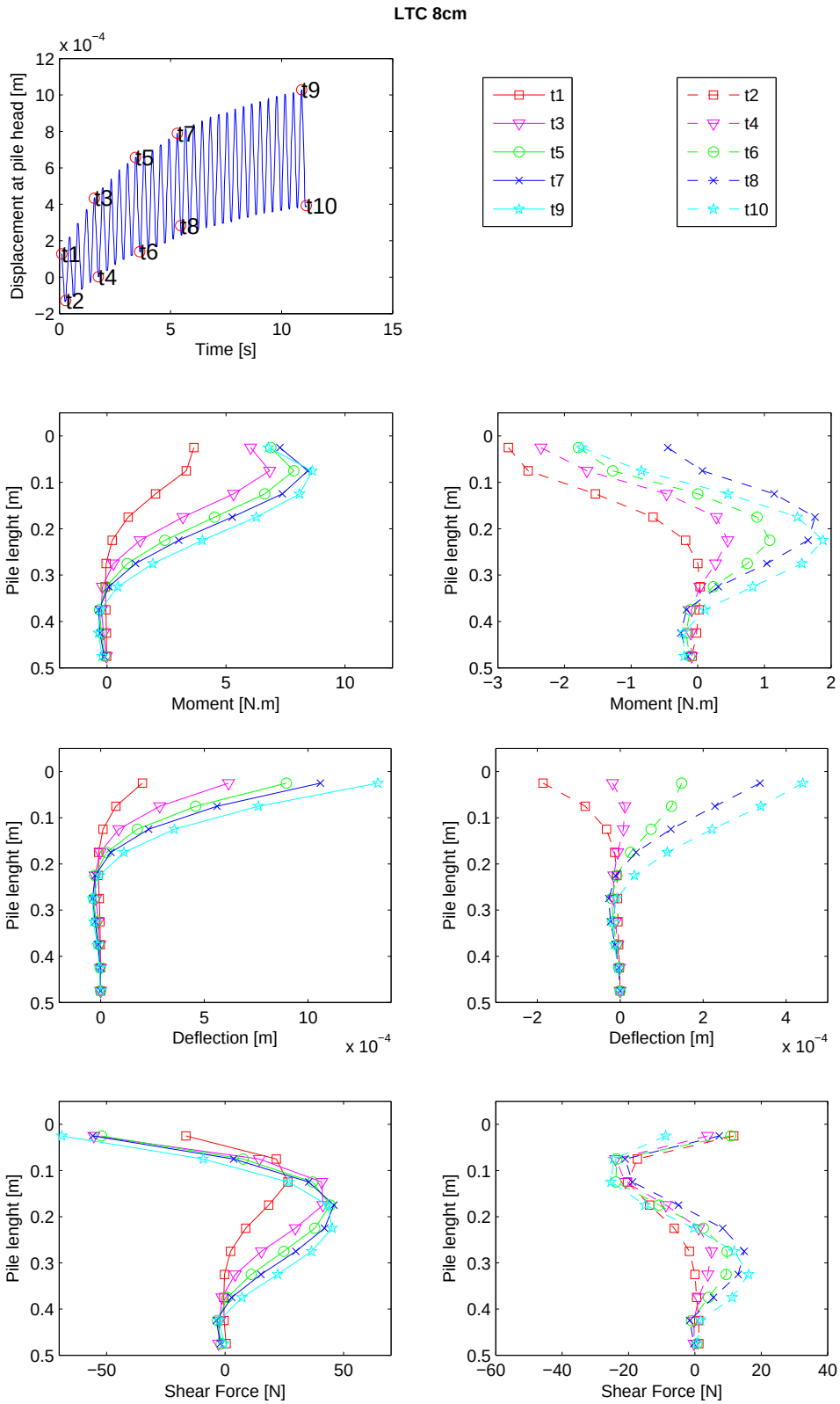

Figure 7.93: Moment fléchissant, déflexion et l'effort tranchant le long d'inclusion rigide associée à LTC avec 8 cm de hauteur (exp LTC11); Direction 'A' = t1,t3, t5, t7, t9; Direction 'B' = t2, t4, t6, t8, t10

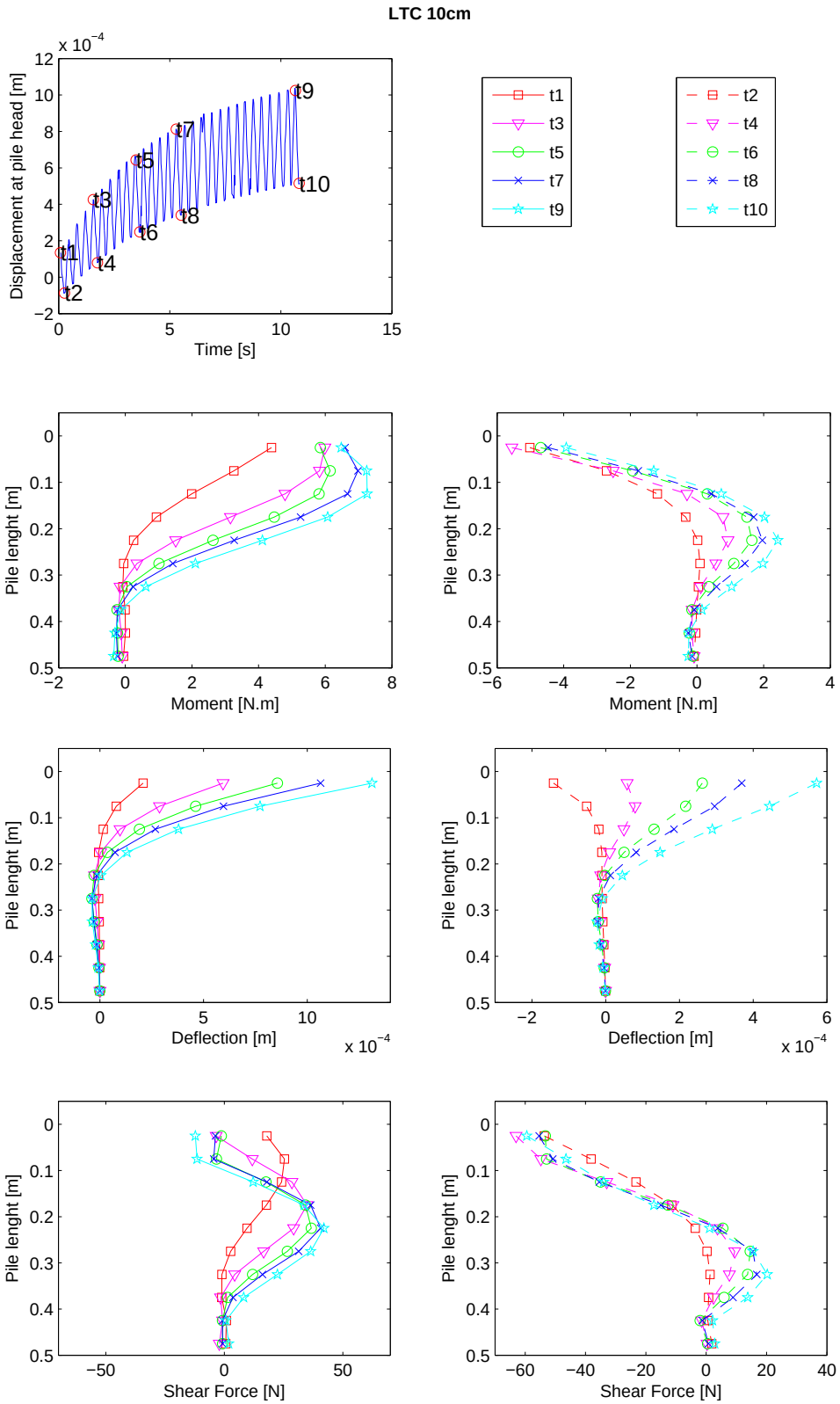

Figure 7.94: Moment fléchissant, déflexion et l'effort tranchant le long d'inclusion rigide associée à LTC avec 10 cm de hauteur (exp LTC10); Direction 'A' = t1,t3, t5, t7, t9; Direction 'B' = t2, t4, t6, t8, t10

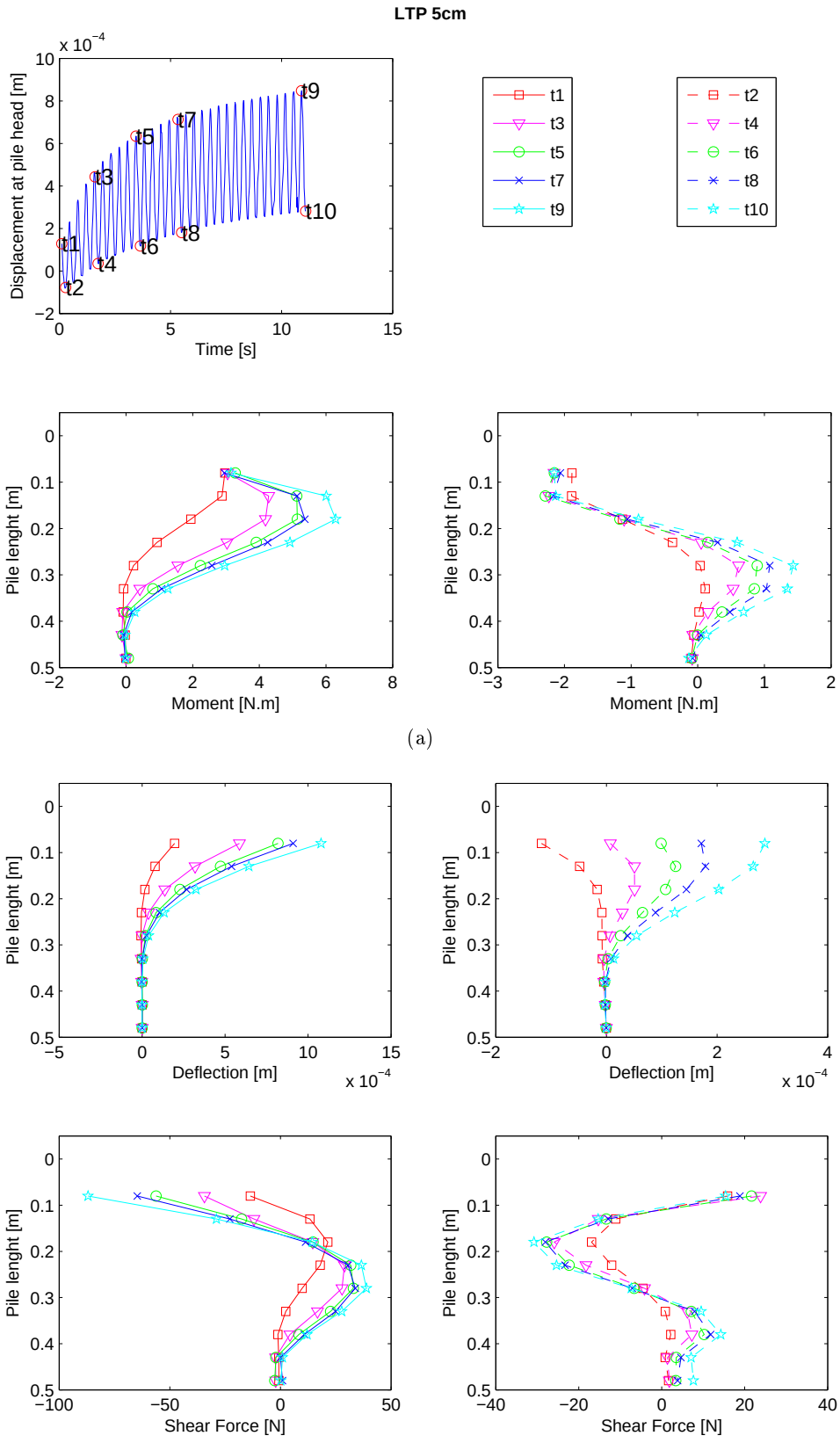

(a)

(b)

Figure 7.95: Moment fléchissant, déflexion et l'effort tranchant le long d'inclusion rigide associée à LTP avec 5 cm de hauteur (exp LTP4); Direction 'A' = t1,t3, t5, t7, t9; Direction 'B' = t2, t4, t6, t8, t10

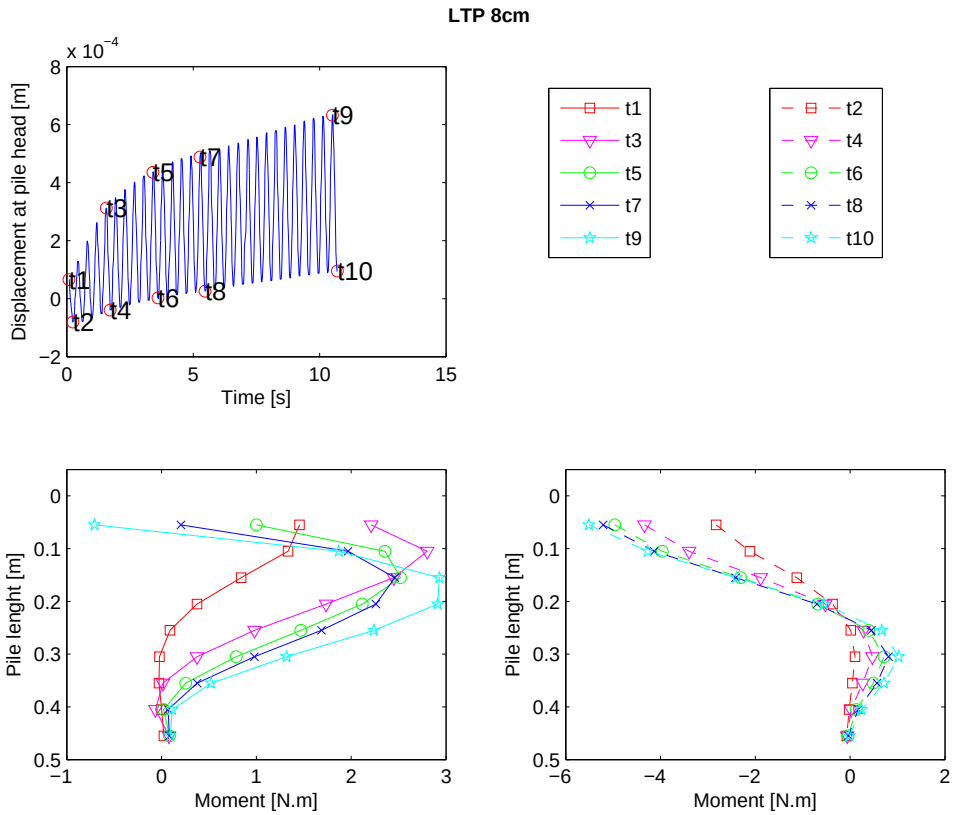

(a)

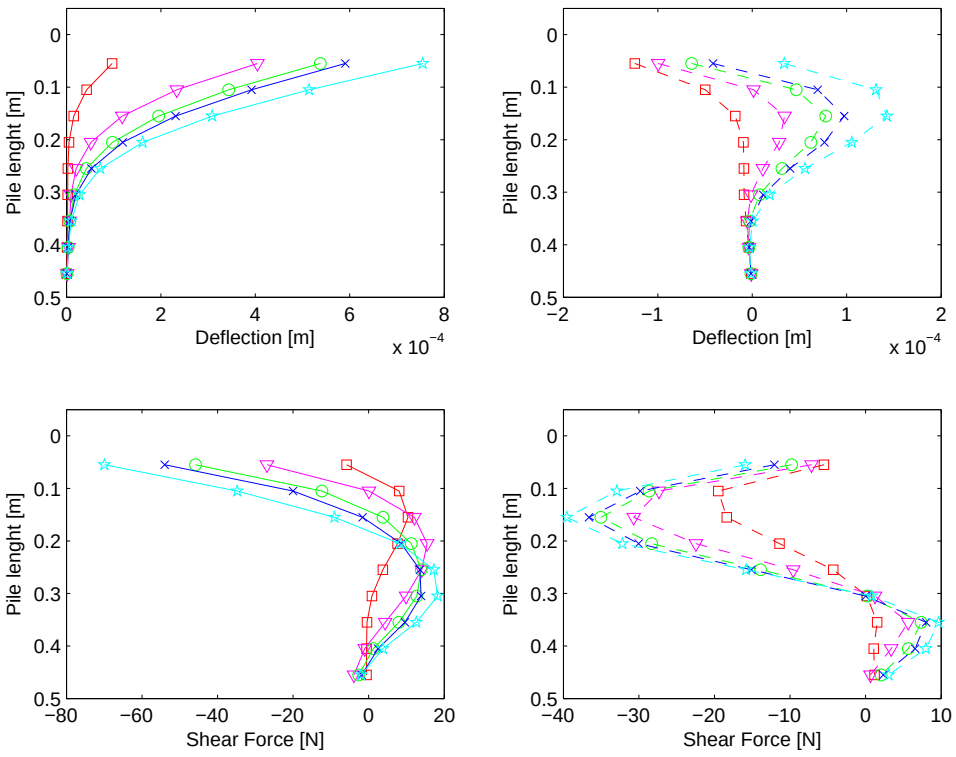

(b)

Figure 7.96: Moment fléchissant, déflexion et l'effort tranchant le long d'inclusion rigide associée à LTP avec 8 cm de hauteur (exp LTP5); Direction 'A' = t1,t3, t5, t7, t9; Direction 'B' = t2, t4, t6, t8, t10

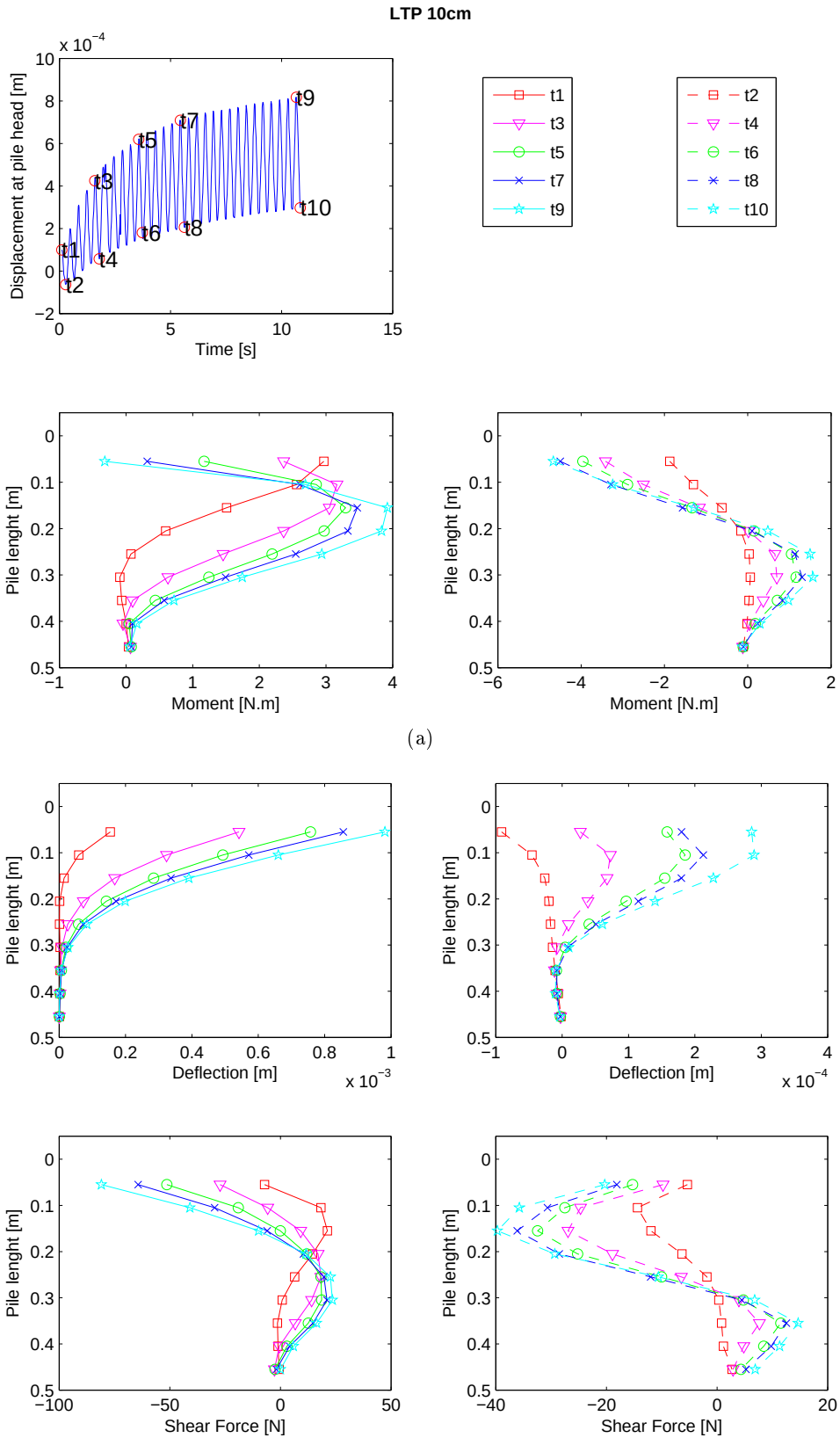

Figure 7.97: Moment fléchissant, déflexion et l'effort tranchant le long d'inclusion rigide associée à LTP avec 10 cm de hauteur (exp LTP6); Direction 'A' = t1,t3, t5, t7, t9; Direction 'B' = t2, t4, t6, t8, t10

- Le niveau de la sollicitation du pieu est du même ordre pour les LTC et LTP de 5cm de hauteur. Par contre, si la hauteur de la partie souple devient plus importante, on constate que le pieu est plus sollicité lorsqu'il est surmonté par un LTC. Une hypothèse est que ce comportement est lié à la différence dans la géométrie des deux types (LTC et LTP) de partie souple. La géométrie du modèle avec les LTCs est telle que quand la fondation applique une charge au sol renforcé, les colonnes subissent une rotation qui génère des moments en tête des pieux. Cette rotation est créée par une tendance du sol à migrer vers les zones soumises à des contraintes moins élevées, situées en dehors du sol renforcé.

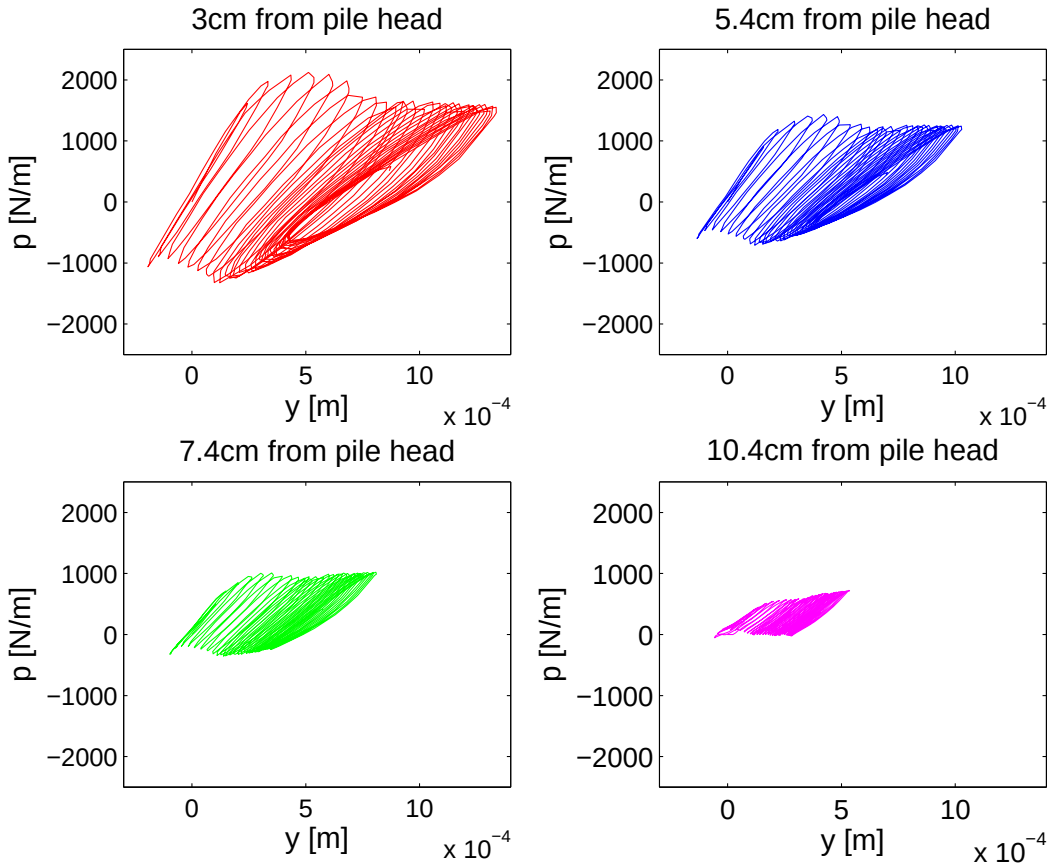

Figure 7.98: Les courbes P-y obtenues aux différentes profondeurs pendant le chargement cyclique du sol renforcé par des inclusions rigides associées aux LTCs de 8 cm de hauteur (exp LTC11)

L'influence du type et de la hauteur de la partie souple du modèle sur les sollicitations mesurées dans la partie rigide peut être évaluée par la représentation du déplacement horizontal y de la partie rigide en fonction de la pression latérale du sol P. Un exemple des boucles P-y obtenues aux différentes profondeurs pendant le chargement cyclique est montré dans la figure 7.98. Cet exemple correspond à l'essai pour lequel le sol a été renforcé par les inclusions rigides associées aux LTCs de 8cm de hauteur.

On constate que la pression latérale du sol P est plus mobilisée quand le pieu est chargé dans la direction 'A', c'est-à-dire vers l'extérieur de la fondation. Cette observation est en accord avec les résultats montrant que la déflexion du pieu n'est pas réversible sous le chargement dynamique et qu'elle évolue vers l'extérieur de la fondation (en gardant à l'esprit que la pression latérale du sol P augmente avec la déflexion du pieu y jusqu'à l'état ultime)

La raideur des boucles P-y exprime la rigidité du système sol-pieu. On observe que la raideur, et donc la rigidité, diminue avec le nombre des cycles. Cette dégradation de la rigidité du système sol-pieu avec le chargement cyclique est due à la formation d'un vide à l'arrière du pieu et a la dégradation des propriétés mécaniques d'argile.

Les figures 7.99 et 7.100 montrent l'ensemble des courbes P-y tracées pour le premier cycle de chargement. Toutes les boucles P-y sont obtenues à la même profondeur et peuvent donc être comparées entre elles. L'influence du type de partie souple sur la sollicitation du pieu est examinée. La figure 7.99 montre les résultats des expériences pour lesquelles le pieu a été associé à la LTC. On constate que ces boucles ont une surface qui est plus petite que celle des boucles mesurées lorsque le pieu a été associé à la LTP (figure 7.100). Du fait que la surface de la boucle P-y est proportionnelle à la sollicitation imposée à la tête du pieu, on peut conclure que les pieux qui sont associés à la LPT sont plus sollicités que les pieux associés aux LTCs.

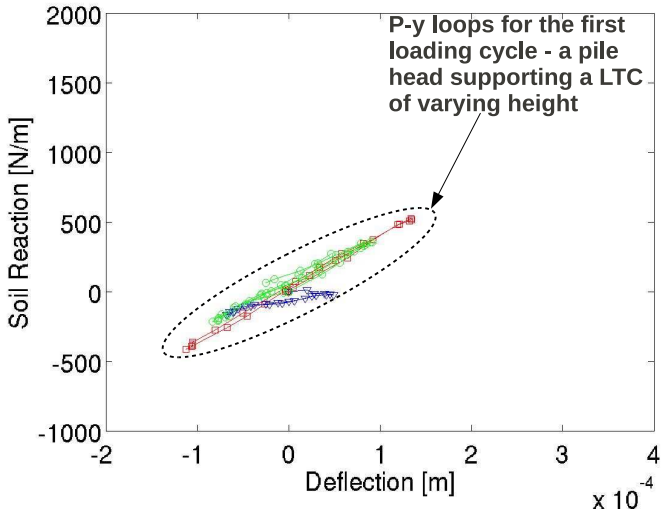

Figure 7.99: Boucles P-y tracées pour le premier cycle de chargement qui a été imposé au sol renforcé par les pieux associés aux LTCs.

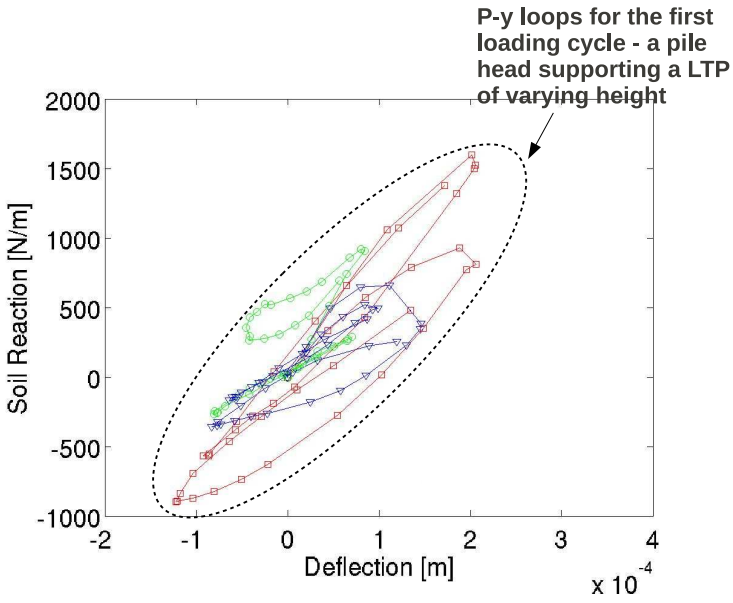

Figure 7.100: Boucles P-y tracées pour le premier cycle de chargement qui a été imposé au sol renforcé par les pieux associés au LTP.

Une étude paramétrique concernant la hauteur de la partie souple des modèles a été présentée.Le dimensionnement du renforcement par des inclusions rigides associées aux colonnes ou matelas (LTCs ou LTP) de transfert de charge vis-à-vis de la portance de la fondation devra définir la hauteur de la partie souple qui permettra d'assurer la portance de la fondation et la vérification intrinsèque de la partie rigide.

Dissipation d'énergie

La dissipation d'énergie a été analysée au niveau global (système sol renforcé-fondation) et au niveau local (partie souple du modèle et partie rigide du modèle). En traçant (au niveau local et global) les boucles d'hystérésis qui relient l'effort horizontal et le déplacement horizontal, l'énergie dissipée et la rigidité du système peuvent être obtenues (Figure 7.101).
A partir des analyses effectuées, on constate que:

- La plupart de l'énergie est dissipée dans la partie souple du modèle. En effet, les résultats montrent que 90% de l'énergie totale induite par le chargement de la fondation au sol est dissipée par les LTCs ou LTP.
- Il semble que la colonne entourée d'argile (la LTC) a plus de capacité de dissipation d'énergie que le matelas (LTP).
- Faire varier la hauteur de la partie souple n'a pas un effet important sur le niveau d'énergie dissipée.
- La rigidité globale (c'est-à-dire la rigidité obtenue au niveau de la fondation) augmente avec le nombre des cycles imposés. La rigidification du système est due au fait que

la densité du gravier augmente pendant la sollicitation dynamique horizontale de la fondation. Comme la partie souple du système devient plus rigide avec les cycles, tout le système montre une rigidité qui augmente.

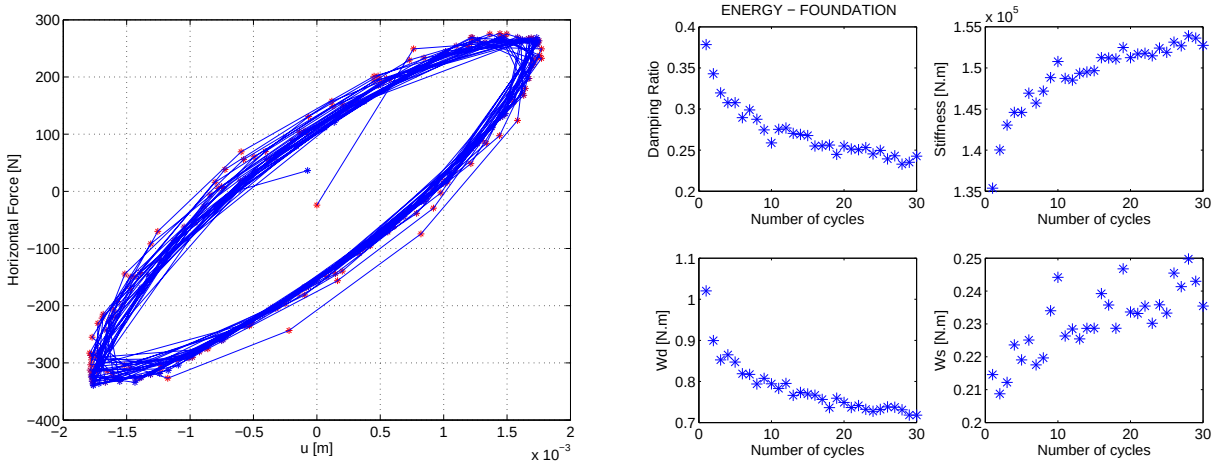

(a) (b)

Figure 7.101: Un exemple de dissipation d'énergie analysée au niveau global. Les boucles d'hystérésis qui relient l'effort horizontal et le déplacement horizontal u (figure (a)) servent pour calculer l'énergie dissipée Wd, l'énergie accumulée Ws, coefficient d'amortissement et la rigidité du système (figure (b))

7.9 Modélisation numérique

Une modélisation numérique avec le but de compléter et confirmer les résultats expérimentaux concernant le comportement du pieu et de la fondation a été effectuée. Le code FLAC3D (Fast Lagrangian Analysis of Continua in 3 Dimensions), développé par la société Itasca Consulting Group Inc a été utilisé. Ce code de calcul permet d'analyser le comportement mécanique des milieux continus tels que des géomatériaux décrits par une loi élastoplastique. La méthode des différences finies explicites pour réaliser une analyse lagrangienne est utilisée, permettant la modélisation en dynamique.

7.9.1 Les modèles numériques

Les simulations numériques ont été réalisées à l'aide de FLAC3D afin de modéliser les expériences effectuées. L'intérêt a été de confronter le comportement de la partie rigide des modèles obtenus numériquement avec les résultats expérimentaux.
Les modèles physiques à l'échelle 1/10, présentés auparavant, ont été reproduits numériquement (figures 24 et 25) avec les mêmes dimensions. Le comportement du sol est décrit par des lois de comportement avec des paramètres qui ont été calibrés à partir d'essais effectués en laboratoire (compression simple, triaxiaux, cisaillement, propagations d'ondes,...) sur les matériaux utilisés dans l'étude expérimentale. Les chargements ont été appliqués en respectant la même forme que les chargements expérimentaux - le niveau du chargement, les

amplitudes et les fréquences ont été gardés identiques.
La longueur des colonnes ballastées a été variée afin d'examiner son influence sur les réponses des inclusions rigides en partie inférieure. La partie rigide a été modélisée en 3D par les éléments «pieux» qui peuvent simuler l'interface entre l'élément de structure et le sol. Le comportement des sols (gravier et argile) a été décrit par une loi élastoplastique du type Cam-clay (pour l'argile) et Mohr-Coulomb avec la règle d'écoulement non-associée (pour le gravier). Une loi élastique linéaire a été utilisée pour les éléments de structure: la semelle, la partie rigide et les zones de transition. Le contact entre la semelle et le sol a été modélisé à partir des éléments «interface» du type Mohr-Coulomb.

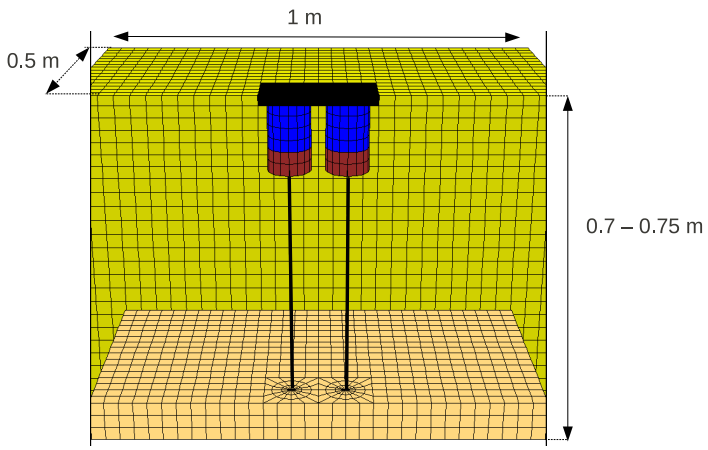

Figure 7.102: Modèle numérique du sol renforcé par les inclusions rigides associées au LTC

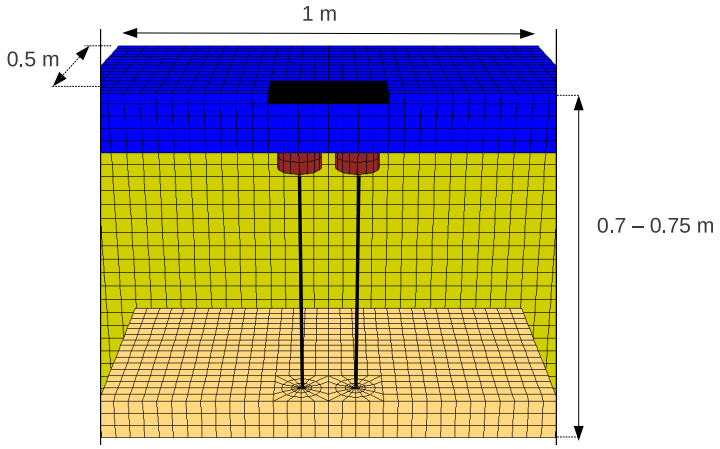

Figure 7.103: Modèle numérique du sol renforcé par les inclusions rigides associées au LTP

7.9.2 Les résultats numériques

7.9.2.1 Chargement vertical statique

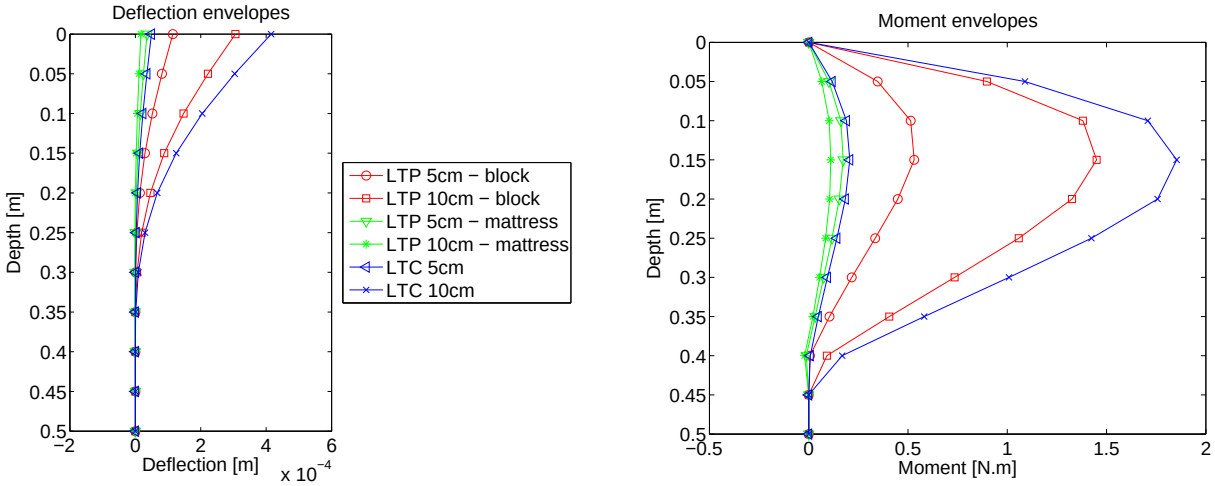

(a) (b)

Figure 7.104: Comportement latéral des pieux associées aux LTP ou LTCs sous un chargement vertical statique imposé par la fondation. Déflexion latérale le long du pieu (a); Moment fléchissant le long du pieu (b)

Les figures 7.104(a) et (b) montrent une déflexion maximale (a) et un moment maximal (b) exercé sur le pieu sous un chargement vertical statique imposé par la fondation. La partie souple du modèle a été variée afin d'étudier son effet sur la sollicitation du pieu.

On constate que le comportement latéral de la partie rigide est du même ordre si elle est associée au LTP ou à la LTC de hauteur 5cm. Par contre, en augmentant la hauteur de la partie souple, les sollicitations transmises au pieu diffèrent selon qu'il est surmonté par une LTC ou une LTP - Une LTC entourée par l'argile semble transmettre plus de déformation à la partie rigide du modèle.
Les mêmes tendances ont été observées aussi au niveau expérimental. Une hypothèse a été faite que ce comportement est lié à la différence dans la géométrie des deux types (LTC et LTP) de partie souple - La géométrie du modèle avec les LTCs est telle que quand la fondation applique une charge au sol renforcé, les colonnes subissent une rotation qui génère des moments en tête des pieux. Cette rotation est créée par une tendance du sol à migrer vers les zones soumises à des contraintes moins élevées, situées en dehors du sol renforcé.
En souhaitant confirmer cette hypothèse numériquement, des vecteurs déplacement ont été tracés pour les simulations numériques dans les figures 7.105. On peut constater que les figures confirment les tendances à la migration du sol supposées dans la partie expérimentale.

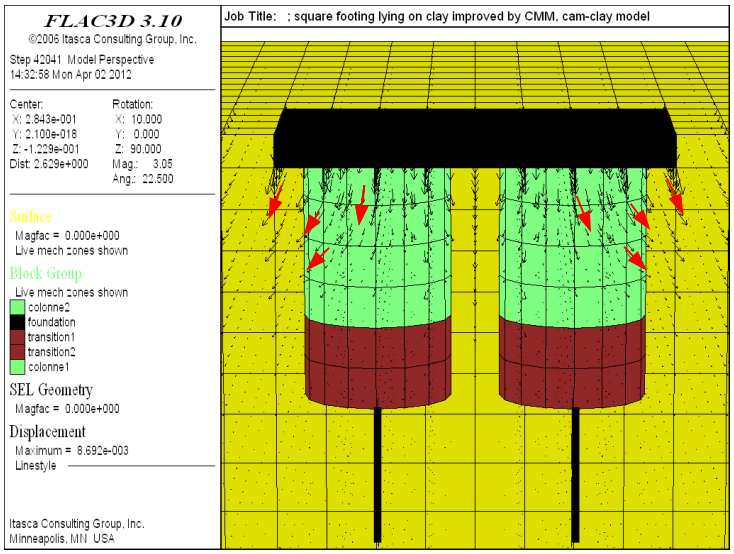

(a)

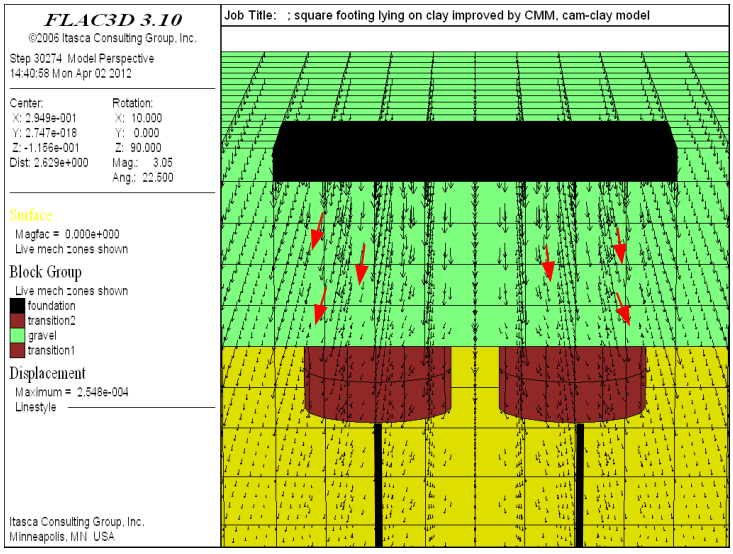

(b)

Figure 7.105: Une tendance du sol à migrer vers les zones soumises à des contraintes moins élevées, situées en dehors du sol renforcé.

7.9.2.2 Chargement vertical statique et horizontal dynamique

Après avoir appliqué une charge verticale qui a été maintenue constante, un chargement cyclique de la fondation a débuté pour 30 cycles durant 11 s. Les résultats du moment maximal et de la déflexion maximale du pieu mesurés pendant le premier cycle de chargement sont tracés dans les figures 7.106(a) et (b). Ils montrent que sous le chargement horizontal cyclique appliqué au niveau de la fondation, l'inclusion rigide qui est associée à la partie souple (LTC ou LTP) de 5cm de hauteur subit des sollicitations plus importantes que l'inclusion rigide associée à la partie souple de 10cm de hauteur. Le niveau de la sollicitation du pieu est du même ordre pour les LTC et LTP de 5cm de hauteur. Par contre, si la hauteur de la partie souple devient plus importante, on constate que le pieu est plus sollicité lorsqu'il est surmonté par une LTC. Ces résultats sont en accord avec les résultats expérimentaux, ce qui confirme les hypothèses faites auparavant.

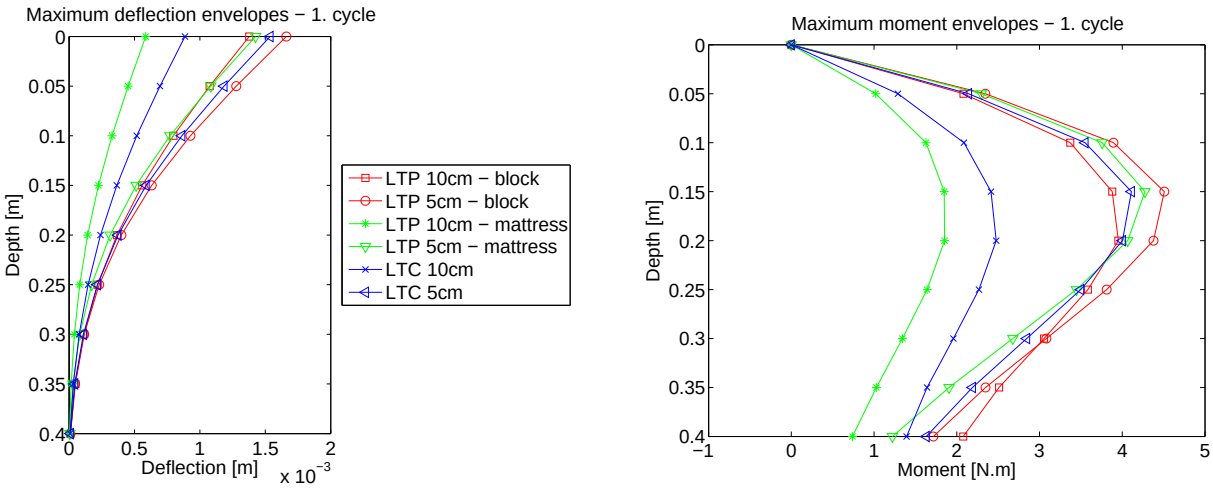

(a) (b)

Figure 7.106: Comportement latéral des pieux associés aux LTP ou LTCs sous un chargement horizontal cyclique imposé par la fondation. Déflexion latérale le long du pieu (a); Moment fléchissant le long du pieu (b)

7.9.2.3 Comparaison des résultats numériques avec les résultats expérimentaux

On constate que les résultats numériques sont généralement en accord avec les résultats expérimentaux. La déformation de la partie rigide des modèles numériques est du même ordre que celle mesurée expérimentalement (figure 7.107). Les tassements de la fondation sur le sol renforcé obtenus numériquement et expérimentalement suivent les mêmes tendances (figure 7.108).

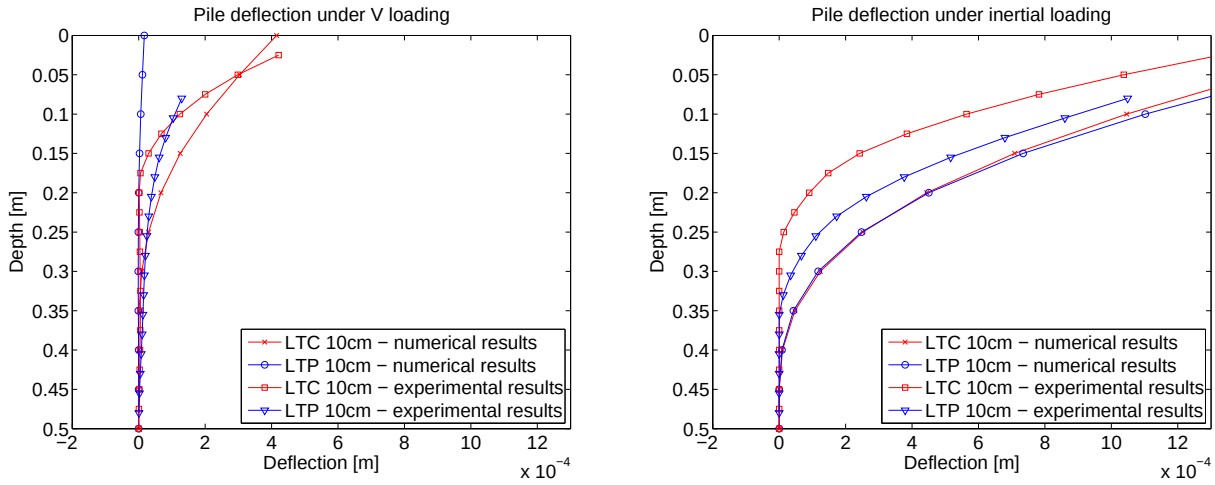

(a) (b)

Figure 7.107: Un exemple qui montre que la déflexion de la partie rigide des modèles numériques est du même ordre que celle mesurée expérimentalement - une expérience quand la partie rigide a été associée à une LTC ou LTP de 10cm.

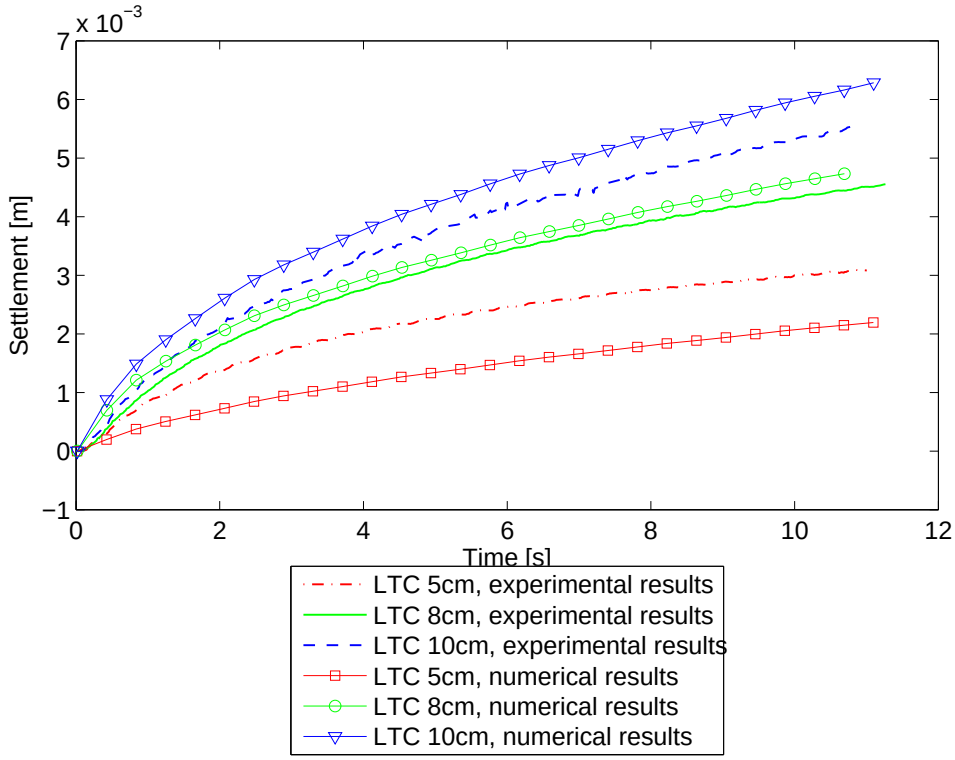

Figure 7.108: Les tassements de la fondation sur le sol renforcé obtenus numériquement et expérimentalement suivent les mêmes tendances.

7.10 Conclusions et perspectives

Le travail présenté aborde la problématique du chargement inertiel d'une fondation sur sol renforcé. Le projet a été développé en collaboration étroite avec l'entreprise KELLER, Fondations spéciales qui a cofinancé avec le CNRS (Le Centre National de la Recherche Scientifique), la bourse BDI de la thèse.

Le but de cette étude, qui est essentiellement expérimentale, est d'approfondir la connaissance du comportement sismique des sols compressibles améliorés par la technique des inclusions rigides associées à une zone de transfert de charge qui est flexible.

Une modélisation physique et numérique des inclusions rigides associées aux colonnes de transfert de charge (LTCs) a été effectuée afin de simuler une technique de renforcement de sol nommé Colonnes à module mixte (CMM). En parallèle, en associant les inclusions rigides à un matelas de transfert (LTP), une technique d'inclusions Rigides (IR) a été simulée.

Une étude paramétrique concernant la hauteur de la partie souple des modèles a été présentée.Le dimensionnement du renforcement par des inclusions rigides associées aux colonnes ou matelas (LTCs ou LTP) de transfert de charge vis-à-vis de la portance de la fondation devra définir la hauteur de la partie souple qui permettra d'assurer la portance de la fondation et la vérification intrinsèque de la partie rigide.

Les résultats présentés montrent le comportement d'une semelle sur un sol renforcé sous une sollicitation sismique. Lorsque la fondation subit un déplacement cyclique horizontal, il se produit une déformation au niveau des parties souple et rigide des modèles. Cette déformation est analysée afin de tirer des conclusions sur le comportement du système sol renforcé-structure.
L'influence du type et de la hauteur de la partie souple du modèle sur les sollicitations mesurées dans la partie rigide a été analysée. Le niveau de la sollicitation du pieu est du même ordre pour les LTC et LTP de 5cm de hauteur. Par contre, si la hauteur de la partie souple devient plus importante, on constate que le pieu est plus sollicité lorsqu'il est surmonté par un LTC. Une hypothèse est que ce comportement est lié à la différence dans la géométrie des deux types (LTC et LTP) de partie souple. La géométrie du modèle avec les LTCs est telle que quand la fondation applique une charge au sol renforcé, les colonnes subissent une rotation qui génère des moments en tête des pieux. Cette rotation est créée par une tendance du sol à migrer vers les zones soumises à des contraintes moins élevées, situées en dehors du sol renforcé.
On constate que sous le chargement horizontal cyclique appliqué au niveau de la fondation, l'inclusion rigide qui est associée à la partie souple (LTC ou LTP) de 5cm de hauteur subit des sollicitations plus importantes que l'inclusion rigide associée à la partie souple de 10cm de hauteur. Ce phénomène peut être expliqué par le fait qu'une partie souple du modèle agit comme une liaison entre la fondation et le pieu plus rigide dans le cas de 5cm de hauteur que dans le cas de 10cm de hauteur. Par conséquent, en augmentant la hauteur de LTP ou LTC, le niveau de la sollicitation du pieu diminue.

En analysant le comportement sismique du système sol renforcé-fondation, on constate que la plupart de l'énergie est dissipée dans la partie souple des modèles. En effet, les résultats montrent que 90% de l'énergie totale induite par le chargement de la fondation au sol est dissipée par les LTCs ou LTP.

Dans le cadre de ce travail, la condition de similitude rigoureuse n'est pas respectée. Néanmoins, cette modélisation physique a pour objectif d'analyser l'interaction du complexe sol-renforcement-semelle sous sollicitation horizontale dynamique. Les résultats obtenus ont une valeur qualitative, qui permet de conclure sur les mécanismes physiques qui apparaissent. La modélisation numérique menée en complément montre néanmoins que les tendances observées expérimentalement sont bien reproduites et permet d'envisager une extrapolation au niveau des ouvrages réels. Malgré cela, il est considéré comme important qu'une étude en respectant les conditions de similitude (à l'échelle réelle ou sur modèle réduit en centrifugeuse) soit effectuée afin d'obtenir des résultats qui soient aussi quantitatifs et qui puissent confirmer les conclusions de ce travail.